



UNIVERSITY OF NAIROBI

**DEVELOPMENT OF AN IMMUNOSENSOR FOR DETECTION OF LUNG
CANCER BIOMAKERS**

BY

LUCIA KATUNGWA KHIO

REG NO: I80/55014/2019

**A Thesis Submitted in Fulfillment of the Requirements for Award of the Degree of
Doctor of Philosophy in Chemistry of the University of Nairobi**

**Nov
2023**

DECLARATION

I declare that this thesis is my original work and has not been submitted elsewhere for examination, award of degree or publication. Where other people's work or my own work has been used, this has properly been acknowledged and referenced in accordance with the University of Nairobi's requirements.


	Signature	Date
Lucia K. Kiio		<u>29/11/2023</u>

Reg. No I80/55014/2019
Department of Chemistry
University of Nairobi

This thesis is submitted with our approval as research supervisors:

	Signature	Date
Dr. Damaris Mbui		<u>29/11/2023</u>

Department of Chemistry
University of Nairobi
P.O Box 30197-00100
Nairobi, Kenya.
dmbui@uonbi.ac.ke

	Signature	Date
Dr. John O. Onyatta		<u>29/11/2023</u>

Department of Chemistry
University of Nairobi
john.onyatta@uonbi.ac.ke

	Signature	Date
Dr. Peter Ndangili		<u>29/11/2023</u>

School of Chemistry and Material Science
Technical University of Kenya
Ndangili.peter@tukenya.ac.ke

DEDICATION

I dedicate this thesis to my mum Domitilla Muthio, my dad Richard Munyao my sisters and brothers for their steadfast support, financially and morally and their encouragement throughout my studies.

ACKNOWLEDGEMENTS

First and foremost, I would like to thank the Almighty God for his guidance, protection and giving me strength, good health, knowledge and patience during my studies. Second, I would like to thank my parents for their everlasting love, encouragement, patience, support and motivation in the whole time I was doing my thesis. You always believed in me that I will finish the race one day.

Greatest thanks to my supervisor Dr. Damaris Mbui, for her tireless and continuous support and encouragement for the entire period of my PhD studies, Dr. Onyatta of University of Nairobi and Dr. Ndangili of Technical University of Kenya for giving me an opportunity to complete my PhD under their excellent supervision, guidance, professional support and encouragement during this period.

I would also like to appreciate all my lecturers and technical staff in the Departments of Chemistry and Physics, the university mentor's colleagues and all who have contributed to my progress during the entire period of this study.

My greatest gratitude to you Carolina of University of Navarra. You gave me all the support, assistance and attention for the three months I worked with you. I will not have attained the heights I reached without you.

Special thanks to Dr. Chris sola, Dr. Itziar for the support you gave me when I was working in your labs, University of Navarra.

Special thanks to Professor Luis Montuenga for giving me the opportunity to work in your lab. You gave me all the necessary support I needed for the six months when I was in CIMA, Spain. Thank you for the guidance, encouragement and believing in me. I will not have achieved the heights I achieved in my thesis were it not for you.

Great thanks to Dr. Karmele of University of Navarra for the help and encouragement you gave me. Special thanks to Mirari, Miriam, Andrea Arricibita, Andrea, Sergio, Alfonso, Diego, Benat, Jeniffer, Dani you played a fundamental role in my scientific work in CIMA and I am immensely grateful for each one's contribution to my stay in solid tumors lab. I would have loved to dedicate a few lines of gratitude to each one of you.

Great thanks to Prof Oloo of Technical University of Kenya for your support. In addition to being my scientific mentor, you have been there in the personal difficult moments that have also been part of these years.

I would like to thank CIMA and the University of Navarra for giving the opportunity to carry out my research in your labs on detection of the biomarkers and for the provision of the actual samples which were used.

Special thanks to all my siblings for being there always for me especially in my dark days.

This work has been carried out with financial support from:

- Gandhi Smarak Nidhi Fund (GSNF), 2018/2019 Scholarship award
- Gandhi Smarak Nidhi Fund (GSNF), 2019/2020 Scholarship award
- Harambee Scholarship award for African Scientists (Spain) 2019/2020 for research.

ABSTRACT

Early detection of cancer (long before the tumor is perceived) greatly increases the chance of curability, and is the point of focus for many cancer researchers. The mortality rate due to lung cancer has not decreased for a number of years. This rate can be reduced by early diagnosis, for example if the serum proteins, microRNA, tumor-associated antigens, Carcinoembryonic antigen (CEA) and YES1 are detected in elevated amounts in the blood of potential lung cancer patients using a highly sensitive biosensor. In this study an innovative and ultrasensitive sandwich electrochemical multiplex immunosensor was fabricated for the simultaneous, sensitive, specific, and rapid detection of lung cancer biomarkers CEA and YES1. CEA is a paramount broad-spectrum tumor marker and YES1 (v-YES-1 Yamaguchi sarcoma viral oncogene homolog 1), a member of the SRC (proto-oncogene tyrosine-protein kinase Src) family kinases (SFKs), has been found in a significant subset of patients with lung cancer. The combination of the duplex tumor biomarkers detection was realized to be a formidable perfect tool for screening, diagnosis and monitoring of lung cancer.

Gold Nano clusters coupled with thiolated protein G provided a good conductive platform with high surface area, and provided more binding sites for both YES1 and CEA antibodies. Glutaraldehyde facilitated the cross linking of the antibodies to the electrode surface through the thiolated protein G. The Horseradish peroxidase (HRP)-functionalized Au nanoparticles served as a good conductive platform to encapsulate a large amount of redox probe and to label secondary antibodies for signal amplification, due to the bountiful reactive oxygen functional groups on its surface. Through differential pulse voltammetric (DPV) measurements, two separate signals were detected directly in a single run, which indicated the presence of YES1 and CEA. Under optimized conditions, the electrochemical immunosensor manifested good sensitivity and selectivity for the simultaneous detection of YES1 and CEA with linear ranges of 0.1–50 ng/mL. The detection limit for YES1 and CEA was found to be 0.0022 and 0.0034 ng/mL respectively. To assess the functionalization of the immunosensor for the investigation of YES1 and CEA in human samples, investigation was done in experimentally cultured cancer cell supernatants, cellular protein lysates and human plasma. The results indicated that the immunosensor was able to pick out the CEA and YES1 biomarker, and that the results correlated satisfactorily with those of enzyme linked immunosorbent assay (ELISA). This method gave an auspicious simple, sensitive and quantitative approach for the detection of NSCLC biomarkers. We recommend that that the immunosensor be further tested *in vivo* in other human sample specimens, for example bronchial lavage, urine or sputum and also that the immunosensor be miniaturized in order to develop a point of care gadget that can be used for clinical monitoring of cancer progression.

TABLE OF CONTENTS

DECLARATION.....	ii
DEDICATION.....	iii
ACKNOWLEDGEMENTS	iv
ABSTRACT.....	v
TABLE OF CONTENTS	vi
LIST OF TABLES	xi
LIST OF FIGURES	xii
LIST OF SCHEMES	xv
LIST OF ABBREVIATIONS, SYMBOLS AND ACRONYMS.....	xvi
CHAPTER ONE: INTRODUCTION	1
1.1: Background information.	1
1.2: Statement of the Problem	2
1.3 Objectives of the study	4
1.3.1 General Objective	4
1.3.2 Specific Objectives.	4
1.4 Justification and significance of the study	4
CHAPTER TWO: LITERATURE REVIEW	6
2.1 Lung Cancer	6
2.2 Histopathological classification of Lung Cancer	11
2.3 Origin and Historical Features of Lung Cancer Types	12
2.3.1: Small Cell Lung Cancer	14
2.3.2: Squamous Lung Cancer, Adenocarcinoma, Large Cell Carcinoma, Adenosquamous Carcinoma and Large Cell Neuroendocrine Carcinoma.	14
2.4: Current Methods Employed to Diagnose Lung Cancer	16
2.5: Biomarkers	17
2.5.1: Classification of Cancer Biomarkers.	17

2.5.1.1: Carcinoembryonic Antigen (CEA) biomarker.....	20
2.5.1.2: YES1 biomarker	22
2.6: Biosensor.....	22
2.6.1: Classification of Biosensors.....	25
2.6.1.1: Immunosensors	27
2.7: Electrochemical methods	28
2.7.1: Potentiometric transducers.....	29
2.7.2: Amperometric biosensors	30
2.8: Voltammetry	31
2.8.1: Linear sweep voltammetry.....	32
2.8.2: Cyclic voltammetry (CV)	34
2.8.4: Differential Pulse voltammetry (DPV)	36
2.8.5: Square wave voltammetry (SWV).....	37
2.9: Immobilization methods.....	38
2.9.1: Physical immobilization	39
2.9.2: Chemical immobilization.....	39
2.10: Cancer proteins.....	42
2.11: Glassy Carbon Electrode (GCE)	44
2.12: Gold Nanoparticles.....	44
2.13: Role of <i>Mangifera indica</i> in synthesis of gold nano particles	45
2.14: Summary of Gaps in Knowledge	47
CHAPTER THREE: MATERIALS AND METHODS	48
3.1 Experimental procedures.....	48
3.1.1 Instrumentation	48
3.1.2 Materials and Reagents.....	49
3.2. Preparation of plant extracts for biosynthesis of gold Nano particles.....	49
3.3 Preparation of Thiolated protein G	50

3.4 : Biosensor Construction	51
3.4.1: Preparation of glassy carbon electrode	51
3.4.2: Synthesis of gold nanoparticles	52
3.4.2.1: Synthesis of gold nanoparticles (AuNPs)	52
3.4.2.2: Electrodeposition of gold nanoparticles	53
3.4.3: Synthesis of secondary antibody (AB ₂)–AuNPs conjugate	53
3.4.4: Electrode surface modification	53
3.5 : Optimization procedures	57
3.5.1: pH Optimization	57
3.5.2: Antibody dilution	58
3.5.3: Incubation time	58
3.5.4: Glutaraldehyde dilution	59
3.6: Electrochemical measurements	59
3.7: Detection of lung cancer biomarkers YES1 and CEA in cell culture supernatants and cell lysates	60
3.7.1: Culture and maintenance of human cell lines	60
3.7.2: Mycoplasma testing	60
3.7.3: Sub culturing and cell counting	61
3.7.4: Freezing, thawing and protein extraction	62
3.8: Western blot	63
3.8.1: Immunoblotting	64
3.8.1.1: Protein extraction and quantification of Cell lysates	64
3.8.1.2: Protein extraction and quantification for Cell line supernatants.....	65
3.8.2: Electrophoresis and transference.	65
3.8.3: Immunodetection	67
3.9: Enzyme linked immuno sorbent assay (ELISA).....	67
3.10: Human Plasma Samples Analysis	68

3.11: Analytical Techniques.....	69
3.11.1: Cyclic Voltammetry.....	69
3.11.2: Differential Pulse Voltammetry.....	70
3.11.3: Dynamic light scattering (DLS) analysis.....	71
3.11.4: UV-VIS Spectra Analysis:.....	71
3.11.5: Fourier transform infra-red spectroscopy (FT-IR).....	71
3.12: Data Analysis	72
CHAPTER 4 :RESULTS AND DISCUSSION	73
4.1: Introduction.....	73
4.2: Characterization of gold Nano particles.....	73
4.2.1: Ultraviolet-Visible (UV-vis) spectrum analysis.....	73
4.2.2: Fourier transform Infra-red (FT-IR) spectroscopy	75
4.2.3: Dynamic light scattering (DLS) analysis.....	76
4.3: The electrodeposition process	77
4.4: Immobilization of antibodies	79
4.5: Characterization and electrochemical performance of the immunosensor	80
4.6: Optimization studies.....	84
4.7: Immunosensor Performance.....	88
4.7.1: Expression and detection of YES1 recombinant and CEA antigen.....	88
4.7.2: Analytical performance of the fabricated immunosensor.....	89
4.7.3: Determination of kinetic parameters of the immunosensor.....	92
4.7.4: Detection of YES1 and CEA in cell culture supernatants and cell lysates.....	94
4.7.5: Verification of the immunosensors.....	96
4.8: Electrochemical immunosensor detection of YES1 and CEA in human plasma.....	99
4.8.1 Detection of YES1 in human plasma.....	101
4.9: Simultaneous detection of CEA and YES1.....	105

4.9.1: Evaluation of reproducibility, stability, specificity, and cross-reactivity of the immunosensor.....	111
4.9.1.1: Reproducibility	111
4.9.1.2: Stability.....	113
4.9.1.3: Specificity	113
4.9.2: Evaluation of feasibility and cross- reactivity of the immunosensor.....	115
4.9.2.1: Evaluation of feasibility.....	115
4.9.2.2: Cross reactivity tests	117
4.9.3: Real sample analysis with the developed immunosensor and validation of the results with ELISA.....	117
CHAPTER 5: CONCLUSION AND RECOMMENDATIONS	121
5.1 Conclusion.....	121
5.2 . Recommendations	122
REFERENCES.....	123
APPENDICES.....	158
APPENDIX 1: BUFFERS USED	158
APPENDIX 2:PROTOCOL FOR PROTEIN QUANTIFICATION	160
APPENDIX 3: PROTEIN QUANTIFICATION RESULTS.....	161
APPENDIX 4: ELISA DATA AND STANDARD CURVE	163
APPENDIX 5: REPRODUCIBILITY OF CEA AND YES1 DIFFERENT ELECTRODES	165
APPENDIX 6: REPRODUCIBILITY OF CEA AND YES1 SAME ELECTRODES ...	166
APPENDIX 7: STABILITY OF CEA AND YES1	167

LIST OF TABLES

Table 2. 1: Available diagnostic tools for cancer with their advantages and disadvantages.....	10
Table 2. 2: DNA- and protein-based biomarkers in lung cancer detection (Arya and Bhansali, 2011).	19
Table 2. 3: Some biomarkers and biosensors used in detection of cancer and their detection limits.	20
Table 2. 4: Immunosensors for different cancer proteins detection	43
Table 4. 1: FTIR peaks determined in the green synthesized gold nanoparticles and Mangifera Indica.....	76
Table 4. 2: Comparison of the response characteristics of different modified electrodes	91
Table 4. 3: Summary of blood samples data obtained from Clinic Universidad de Navarra Cohort (n = 104).....	100
Table 4. 4: Multiplexed electrochemical Immunosensors	108
Table 4. 5: Assay results in ng/mLs of clinical serum samples using the fabricated immunosensor and the ELISA method.....	118
Table 4. 6: Assay results of clinical serum samples spiked with YES1 recombinant. .	119

LIST OF FIGURES

Figure 2. 1: Estimated new cases of cancer in males and females worldwide	6
Figure 2. 2: Incidence and Mortality Age-Standardized Rates in High/Very High Human Development Index (HDI) Countries Versus Low/Medium HDI Countries Among (A) Men and (B) Women in 2020.....	8
Figure 2. 3: classification of lung cancer histological types.....	12
Figure 2. 4:Histogenesis of histological types of lung cancer	12
Figure 2. 5:Classification of cancer biomarkers adapted from www. Research gate. Net. ...	18
Figure 2. 6: Schematic representation of the human CEA protein.	21
Figure 2. 7: The three components of biosensors.	23
Figure 2. 8: Biosensor classification.....	24
Figure 2. 9: Schematic representation of (A) a direct biosensor and (B) an indirect biosensor using a sandwich assay	26
Figure 2. 10: Scheme of an electrochemical immunosensor. Voltammetric signal is obtained for distinct analytes, which allows (1) simultaneous or (2) individual detection	28
Figure 2. 11: Voltage applied between working electrode and counter electrode with respect to time and the current response measured at the working electrode during LSV	32
Figure 2. 12: Voltage applied between the current and working electrodes and current response measured at the working electrode during Cyclic voltammetry	35
Figure 2. 13: Excitation signals (A) and Voltammogram for DPV experiment.	36
Figure 2. 14: Square wave voltammetry potential sweep.....	38
Figure 2. 15: Self assembled monolayers of alkanethiols.....	41
Figure 2. 16: Carbon electrode.....	44
Figure 2. 17: <i>Mangifera indica</i>) plant.....	46
Figure 3. 1: Image of Mango leaves (<i>Mangifera indica</i>) , before grinding (A) and after drying and grinding (B).	50
Figure 3. 2: A schematic representation of the electrode modification process and consequent immunosensor formation.	55
Figure 3. 3: Cell lines sub-culturing and cell counting process.....	62
Figure 3. 4: Freezing and thawing procedure of the cultured cells.....	63
Figure 3. 5: Electrophoresis (1) Transference (2) Immunodetection (3) and Visualization (4)	66

Figure 3. 6: Detection of YES1 protein using sandwich ELISA process	68
Figure 4.1: UV-Vis spectra recorded in the reaction solution for the synthesis of (A) AuNPs. Plasmonic peak assigned to metal nanoparticles is indicated by the arrow. (B) UV-Vis spectra of the plant extract and gold chloride solution (C) Color change profile of biosynthesized gold nanoparticles; I- gold chloride solution, II- Gold Nano particles solution, III- plant extract solution.....	74
Figure 4.2: FT-IR spectrum of AuNPs bio synthesized from <i>Mangifera indica</i> plant extract	75
Figure 4.3: DLS showing the intensity particle size distribution obtained for a colloidal gold sample.	77
Figure 4.4: CV plots of gold nanoparticles electrodeposition, potential range of – 0.7 V to + 0.3 V at a scan rate of 50 mV s ⁻¹	78
Figure 4.5: Characterization and assessment of the electrochemical performance of the YES1 and CEA immunosensors ; cyclic voltammetry curve (A) CEA, (B) cyclic voltammetry curve YES1, (C) DPV curve of CEA (D) DPV curve of YES1 recorded in 5mM K ₃ [Fe(CN) ₆] and 0.1 M KCl pH 7.2 at a scan rate of 50 mV s ⁻¹	82
Figure 4.6: (A) kinetic analysis of AuNPs/GCE at scan rates ranging from 10 to 100 mV s ⁻¹ in 5mM K ₃ [Fe(CN) ₆] and 0.1 M KCl pH 7.2 . (B) linear fits of the oxidation peak current (I _{pa}) and reduced peak current (I _{pc}) versus the square root of the scan rate (v ^{1/2})	84
Figure 4.7: Optimization experiments on the immunosensor, responses effect of pH on CEA (A) and YES1 (B)	85
Figure 4.8: Optimization experiments on the immunosensor: DPV responses of: Effect of incubation time of 10ng/ml CEA (A) and YES1 (B) on the immunosensor.	86
Figure 4.9: Optimization experiments on the immunosensor: DPV responses effect of CEA (A) and YES1 (B) antibody concentration on immunosensor response.	87
Figure 4. 10: Optimization of % GA concentration for cross linking antibody to thiolated protein G (A) A CV of different concentrations of GA (B) line graph.	88
Figure 4.11: Characterization of (A) YES1 recombinant and (B) CEA, SDS-PAGE showing the respective protein in lane 2 and protein molecular weight marker in lane 1	89
Figure 4.12: (A) DPV showing detection at varying YES1 concentration (0.01 -100 ng/mL) in 0.1 M PBS (pH 7.4) with 1 mM [K ₃ Fe(CN) ₆], 0.1 M KCl. Scan rate: 50 mV s ⁻¹ . (B) calibration curve showing linear relationship of the immunosensor in detection of YES1... ..	89

Figure 4.13: DPV showing dependence of YES1 antibody on antigen concentration (A); linear calibration curve showing dependence of YES1 antibody on antigen concentration(B) Each datum point represents the average analysis of triplicate values (n= 3). Error bars correspond to the standard deviation (SD) of three measurements (n=3).....92

Figure 4.14: A plot of YES1 concentration divided by peak current vs. YES1 concentration.93

Figure 4.15: Electrochemical immunosensor measured with and without analyte (A549 supernatant) by DPV (A) YES1 (B) CEA. DPV detection of varying amount of A 549cells (C) using YES1 sensor (D) using CEA sensor (E) Immunoblotting of varying cells CEA (F) Immunoblotting of varying cells YES195

Figure 4.16: DPV curves showing universal detection of biomarkers in cell culture supernatants of multiple cell lines (A and B) YES1 (C and D) CEA. Immunoblot analysis in cell culture supernatants (E) YES1 and (F) CEA. Error bars represent SD (n = 3).....97

Figure 4.17: Analysis of YES1 in cell lysates (G) DPV analysis of CEA in cell lysates (H). Immunoblot analysis in cell culture lysates (I) YES1 and (J) CEA. Error bars represent SD (n = 3).....98

Figure 4.18: DPV showing the detection of YES1 by serial dilution of human plasma (A). linear curve showing detection of YES1 by dilution of human plasma (B) Each datum point represents the average analysis of triplicate values (n= 3). Error bars correspond to the standard deviation (SD) of three measurements (n=3).100

Figure 4.19: DPV showing detection of YES1 in human plasma (A and D). Immunoblots for human plasma for samples of SET 1 (B) and SET 2 (E). Analysis of immunoblots of B using image J (C) Analysis of immunoblots of E using image J (F) 103

LIST OF SCHEMES

Scheme 3. 1: Schematic reactions illustrating protein G conjugation with glutaraldehyde covalent immobilization of primary antibodies	54
Scheme 3. 2: Schematic illustration of the stepwise electrochemical immunosensor fabrication process. (A). Electrodeposition of gold nanoparticles(AuNPs) on GCE. (B). Modification of GCE/AuNPs with thiolated protein G (TPG). (D) Incubation of GCE/AuNPs/TPG with glutaraldehyde (GA). (D) Immobilization of capture antibodies YES1 and CEA on the modified electrode and blocking with BSA. (E) incubation with the analyte containing antigen CEA and YES1. (F) Sandwiching with secondary antibody. (D) DPV analysis.....	56
Scheme 4. 1: Outline of covalent attachment of glutaraldehyde to the electrode surface through the thiolated protein G, resulting in a table bio-sensing interface	79

LIST OF ABBREVIATIONS, SYMBOLS AND ACRONYMS

APUD-system	Amine precursor uptake and decarboxylation system
18F-FDG:	18F-Fluorodeoxyglucose
Au-NPs:	Gold Nanoparticles
BSA	Bovine serum albumin
CA:	Cancer Antigen
CEA:	Carcinoembryonic Antigen
CRG	Chest radiograph
CT scans	Computed Tomography scans
CV	Cyclic voltammetry
CYFRA21-1	Cytokeratin fragment 21-1
DNA	Deoxyribonucleic acid
DPV	Differential pulse voltammetry
EGFR	Epidermal growth factor receptor
ELISA:	Enzyme-Linked Immunosorbent Assay;
ERCC	Excision repair cross-complement
FISH	Fluorescent in situ hybridization
FTIR	Fourier- Transform Infrared Spectroscopy
GCE	Glassy carbon electrode
HRP	Horseradish peroxidase
kDa	<i>Kilo Daltons</i>
KEMRI	Kenya Medical Research Institute
KRAS	Kirsten ras
LCNEC	Large cell neuroendocrine carcinoma
LDCT	Low-dose CT
L-DOPA	L-3,4-dihydroxyphenylalanine
LOD	Limit of detection
MIT	Magnetic induction tomography
MRI:	Magnetic Resonance Imaging;
NCL	Nucleolin
NSCLS	Non-small cell lung carcinoma
PBS	Phosphate buffer solution
PCR	Polymerase chain reaction

PET	Positron emission tomography
ProGRP	Pro-gastrin-releasing peptide
PSA	Prostate-specific antigen
PSGs	Pregnancy specific glycoproteins
PVDF	Poly(vinylidene difluoride)
RNA	Ribonucleic acid
RT-PCR	Reverse transcription polymerase chain reaction
SAMs	Self-assembly monolayers
SCLC	Small cell lung carcinoma
TAAAs	Tumor-associated antigens
TS	Thymidylate synthetase
TUB	Tubulin
UV-VIS	Ultraviolet–visible spectrophotometry
VEGF	Vascular endothelial growth factor
VIM	Vimentin
WHO	World Health Organization

CHAPTER ONE: INTRODUCTION

1.1: Background information.

Cancer is the abnormal and uncontrolled cell growth due to an accumulation of specific genetic and epigenetic defects. It has posed a particular threat to human health which makes it to be ranked third in Kenya as a cause of death after infectious diseases and cardiovascular diseases (Rooprai, 2021). The unregulated cell growth leads to the formation of a tumor, which after some period of time spreads beyond the site of origin and metastasizes to other body organs and systems, making it incurable.

Cancer diagnosis and treatment is of great concern due to the widespread occurrence of cancer cases, high death rate, and its recurrence after treatment. According to Melonie *et al.*, (2006) in the National Vital Statistics Reports, the rate of incidence (per 100,000 persons) of cancer in white people was 470.6, in black people 493.6, in Asians 311.1, and Hispanics 350.6, indicating that cancer is wide- spread among all races.

According to global statistics by Globocan 2021, an estimated 19.3 million new cancer cases were recorded in 2020. 18.1 million excluding non-melanoma skin cancer and nearly 10.0 million cancer deaths (9.9 million excluding nonmelanoma skin cancer) occurred in 2020. Female breast cancer has surpassed lung cancer as the most commonly diagnosed cancer, with an estimated 2.3 million new cases (11.7%), followed by lung (11.4%), colorectal (10.0 %), prostate (7.3%), and stomach (5.6%) cancers. Lung cancer remained the leading cause of cancer death, with an estimated 1.8 million deaths (18%), followed by colorectal (9.4%), liver (8.3%), stomach (7.7%), and female breast (6.9%) cancers (Sung *et al.*, 2021).

According to GLOBOCAN 2018, Lung cancer is the leading cause of cancer-related death worldwide (Bray *et al.*, 2018a). In Kenya, cancer ranks third as a cause of death after infectious diseases and cardiovascular diseases (Macharia *et al.*, 2019). It causes 7% of total national mortality every year. Although population based data does not exist in the country, it is estimated that the annual incidence of cancer is about 28,000 cases and the annual mortality is over 22,000 (Macharia *et al.*, 2019). Over 60% of those affected are below the age of 70 years. In

Kenya, the risk of getting cancer before the age of 75 years is 14% while the risk of dying of cancer is estimated at 12% (KEMRI, 2016).

Another complication about cancer, is that the symptoms can recur. According to the National Cancer Institute, cancer is greatly feared due to recurrence. Although tumors can be treated, they can return after a period of time, even after chemotherapy, surgery, or radiotherapy.

Cancer onset and progression is accompanied by mutated or aberrantly expressed proteins which would evoke immune response, resulting in the production of autoantibodies. It would be possible to detect these antibodies in cancer patient's months or years before the clinical diagnosis of cancer. Survival of a cancer patient depends heavily on early detection and thus development of sensors for detecting cancer at an early stage would be especially useful in the war against cancer.

Existing cancer screening methods include the Papanicolaou test for women to detect cervical cancer, mammography to detect breast cancer, prostate-specific antigen (PSA) level detection to detect prostate cancer, occult blood detection for colon cancer, endoscopy, Lobectomy for lung cancer, CT scans, X-ray, ultrasound imaging and Magnetic Resonance Imaging (MRI). These diagnostic methods however are not very useful for early cancer detection (Reddy *et al.*, 2011). Additionally, some of the screening methods are quite costly and not available for many people. Therefore, the development of technology that is specific, reliable and easily accessible for early detection of cancer is of utter importance.

1.2: Statement of the Problem

The social, economic and psychological wellbeing of the human person and of the society as a whole is greatly affected by the human person's state of health. Cancer is one of the leading causes of human death in the world (Tripathi *et al.*, 2016). In Kenya, cancer ranks third as a cause of death after infectious diseases and cardiovascular disease, and causes 7% of the total national mortality each year (Rooprai, 2021) Early detection and precise diagnosis upon onset of cancer is the most promising approach to accelerate the healing process or to improve survival of patients (Susana *et al.*, 2017). Clinical treatment and monitoring of disease recurrence after treatment also require continuous screening.

Lung cancer is a major health problem worldwide (WHO, 2017). Every year, approximately 1.3 million new lung cancer cases and about 1.2 million lung cancer deaths occur worldwide (Hasan *et al*; 2014; Zhang *et al*; 2013).

The five-year survival rate for lung cancer remains much lower than that of other cancers, at approximately 15% (Mulshine, 2005), despite advancements of lung cancer diagnostic methods. Some of the methods that have been used include, X-rays, computed tomography (CT) scans, chemotherapy, immunotherapy, surgery medical imaging, enzyme linked immunosorbent assay (ELISA) and tissue biopsy. However, these methods have been found to have limitations such as lacking the sensitivity or selectivity to detect the disease at a premature state (Pragati, 2013). They are also time-consuming in their measurement, hazardous to health, require highly trained personnel and are also expensive and require sophisticated instrumentation (Tibor, 2017). Furthermore, high risk of radiation exposure is a problem with current screening techniques (Henschke *et al*; 1999). A better diagnostic measure that facilitates early detection of lung cancer, thereby allowing for effective intervention, is necessary to lower lung cancer mortality rates. Various putative biomarkers have been identified from blood samples or serum, and these markers could be used to develop a non-invasive, cost effective biosensor to identify individuals who are at high risk of developing lung cancer.

Proteomics strategies have provided powerful information toward blood based biomarker discovery. Cytokeratin-19 fragments (CYFRA 21-1), carcinoembryonic antigens (CEA) and neuron-specific enolase (NSE) are among some of the lung cancer protein biomarkers that have been discovered to date. Tumor markers and biosensors have a great advantage due to their potential to reduce cancer mortality rates by facilitating diagnosis of cancers at early stages. The fabrication of a nano structured biosensor for the detection of multiple cancer biomarkers, for example, YES1 and carcinoembryonic antigen (CEA) in a single sample will largely enhance the quality of life, especially for people prone to lung cancer. YES1 is a nonreceptor tyrosine kinase in the SRC family of kinases (SFK), it controls multiple cancer signaling pathways (Garmendia *et al.*, 2022). YES1 can be used as predictive biomarker for lung cancer(Garmendia *et al.*, 2019).

1.3 Objectives of the study

1.3.1 General Objective

The general objective of this study was to fabricate a nanostructured immunosensor for lung cancer biomarker detection using YES1 and carcinoembryonic antigen (CEA).

1.3.2 Specific Objectives.

The specific objectives of this study were:

- i. To bio-synthesize and characterize gold nanoparticles.
- ii. To conjugate a GCE electrode with antibodies and characterize it.
- iii. To determine limit of detection (LOD) of the immunosensor towards CEA, YES1
- iv. To determine optimum response of the immunosensor towards CEA and YES1.
- v. To evaluate the kinetics of the immunosensor using the Michaeli's Menten model.
- vi. To determine CEA, and YES1 levels in real samples using the fabricated biosensor.

1.4 Justification and significance of the study

Human health is closely guarded, and ways to alleviate ill health earnestly sought, especially due to the fact that lack of good human health greatly destabilizes a society, as ill health is expensive and detrimental to development. Cancer, with lung cancer being the most common (Jemal *et al.*, 2011), is one of the most life-threatening diseases in the world. In 2015, 8.8 million deaths due to cancer occurred worldwide (WHO 2018). In 2018, it was noted that, the highest number of cancer deaths that occurred were from cancers of: the lung (1.69 million deaths), liver (788 000 deaths), colorectal (774 000 deaths), stomach (754 000 deaths) and breast (571 000 deaths) (WHO 2018)

According to a Kenya Medical Research Institute (KEMRI) incidence report of 2012, the annual incidence of cancer in Kenya is about 28 000 new cases with an annual mortality of 22 000 cases, that is, 78.5% of the victims do not survive (Wambalaba *et al.*, 2019).

According to the regional cancer registry at Kenya Medical Research Institute (KEMRI 2016), about 80% of the reported cancer cases in the years 2011 – 2016, were diagnosed at advanced stages and the chances of cure/survival were very slim. This was largely due to the little awareness of the signs and symptoms of cancer, inadequate screening services, inadequate diagnostic

facilities and poorly structured referral facilities. The existing diagnostic methods such as biopsies and screening are not very reliable in early cancer detection because of lack of sensitivity and precision to identify various tumor types (Lone et al., 2022).

In addition, some of the screening methods are quite costly, since samples have to be sent to central laboratories for analysis, making the process expensive and time-consuming. Procedures for taking samples can also be invasive and distressing for the patient. Furthermore, biopsies and screening lack sensitivity and selectivity to detect the disease at an early stage and are not easily accessible to many people. Therefore, the development of an immunosensor that can be used for detecting cancer at early stages will be of utmost importance.

The study is of significance since it will provide a low cost, sufficiently sensitive and selective nanostructured electro- analytical biosensor for low marker concentrations and early lung cancer stage detection. This will help in reducing mortality rate of many people, especially in developing countries, who cannot afford the existing methods of detection and treatment of lung cancer. Our goal is to make the device widely available in primary health care facilities in the future.

CHAPTER TWO: LITERATURE REVIEW

2.1 Lung Cancer

Lung cancer has the most occurrence and highest death rate in men. In 2020 Lung cancer accounted for 1.80 million deaths followed by Colon and Rectum cancer accounting for 916,000 deaths worldwide (Sung et al., 2021). Lung cancer is a major health problem worldwide (Besaratina and Pfeifer 2008). According to Bray et al. (2018), it is the most commonly occurring cancer in men and the third most commonly occurring cancer in women. There were 2 million new cases in 2018 (Figure 2.1) (Bray, *et al* 2018).

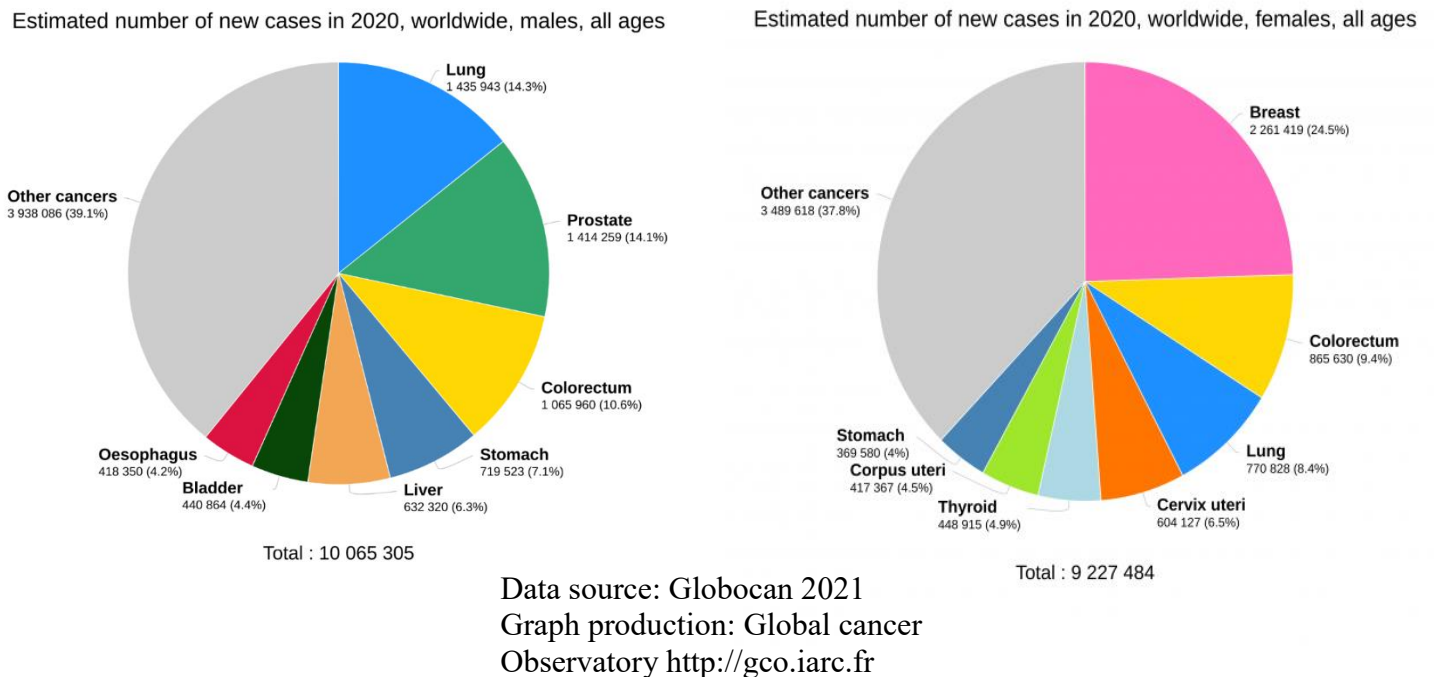
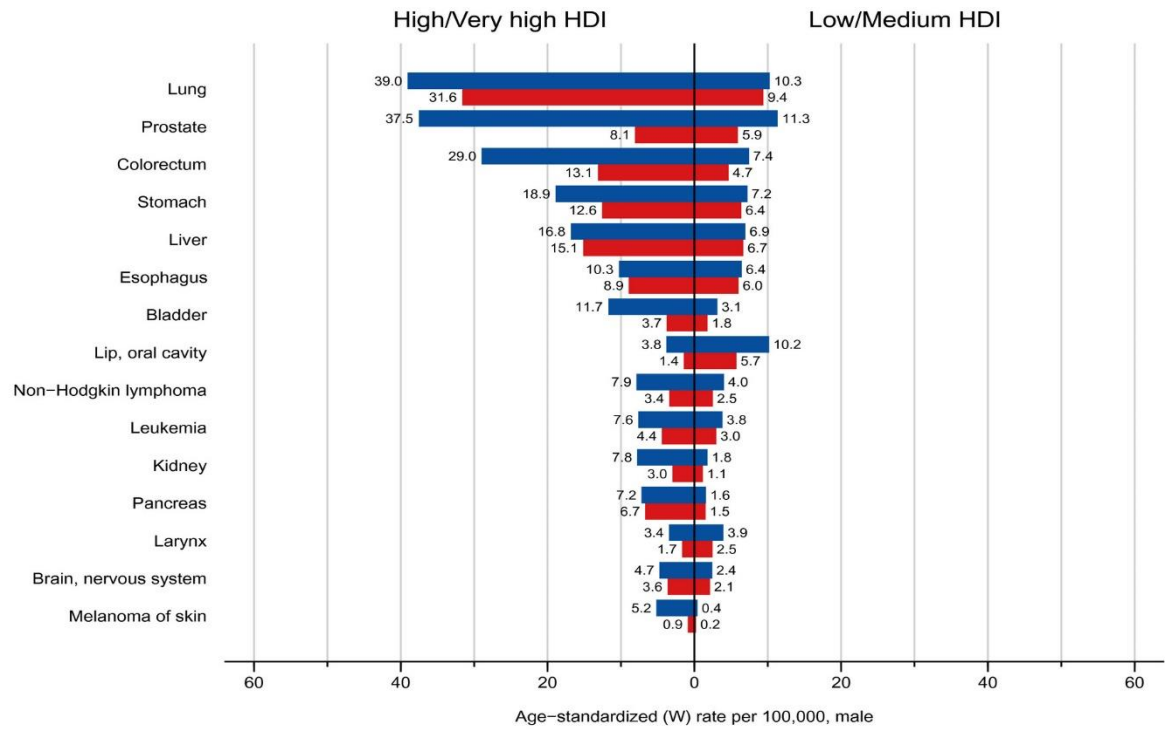


Figure 2.1: Estimated new cases of cancer in males and females worldwide

Lung cancer is the leading cause of cancer deaths, with an estimated 1.8 million deaths (18%), followed by colorectal (9.4%), liver (8.3%), stomach (7.7%), and female breast (6.9%) cancers (Sung et al., 2021). Fig 2.2 shows the incidence and mortality age-standardized rates in high/very high human development index (HDI).

A

Male



B

Female

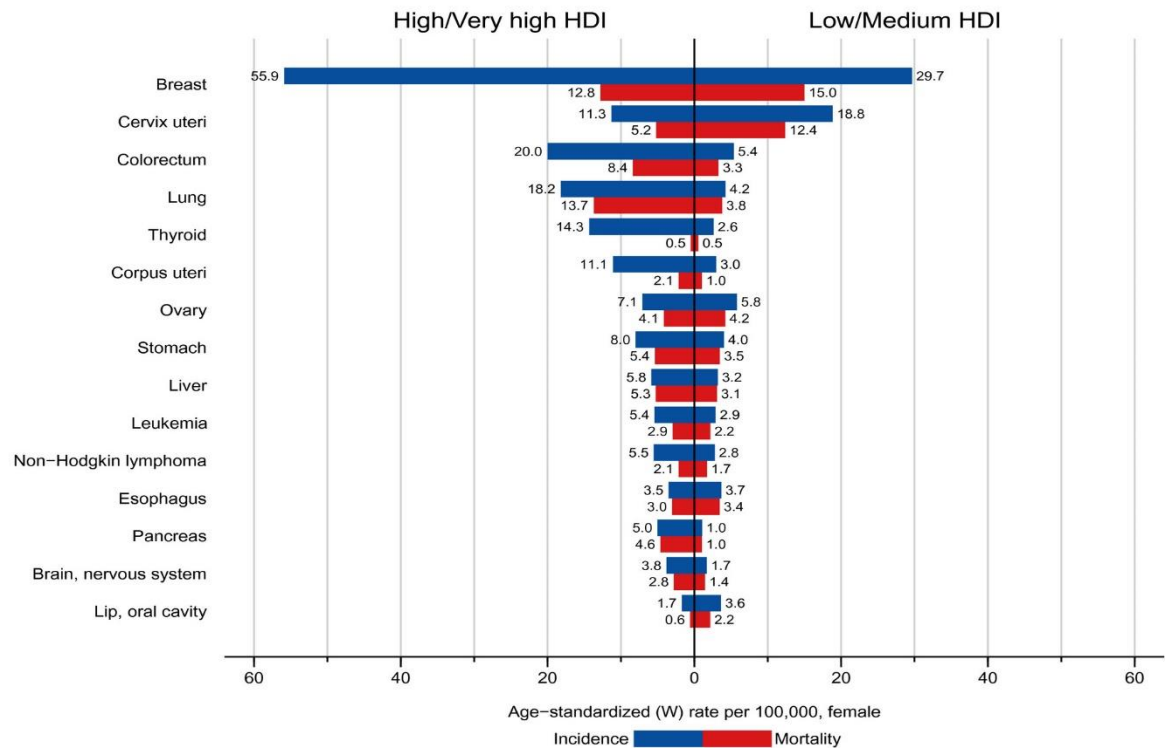


Figure 2.2: Incidence and Mortality Age-Standardized Rates in High/Very High Human Development Index (HDI) Countries Versus Low/Medium HDI Countries Among (A) Men and (B) Women in 2020.

Source: Globocan 2021.

The 15 most common cancers in the world (W) are shown in descending order of the overall age-standardized rate for both sexes combined. *Source: GLOBOCAN 2021.*

In Kenya, the Nairobi cancer registry (2013) in a report reported by Ogendo *et al.*, (2013) reported that 34 people out of 100,000 with a male to female ratio of 2:1 having been diagnosed with lung cancer. Locally, this malignancy is the seventh and tenth most common for males and females respectively (Ogendo *et al.*, 2013). Worldwide, it is the most common type of cancer with the highest mortality rate amongst cancer sufferers (Ogendo *et al.*, 2013). A 2018 report in Kenya estimated that there were 670 new cases annually with 659 deaths annually (Bray *et al.*, 2018b). The predisposing factors for lung cancer include: smoking - both active and passive - which is responsible for up to 80 – 90% of cases, asbestos exposure, family history of lung cancer, chronic lung diseases and air pollution.

Previous studies have indicated that cigarette smoking is by far the dominant global risk factor for developing lung cancer (Besaratina and Pfeifer, 2008). Environmental pollution (Alexander *et al.*, 2015), second-hand smoke (Sullivan *et al.*, 2017), industrial substances (Lee *et al.*, 2012) and genetic factors (Reed *et al.*, 2004) may also cause lung cancer. Radon is another key risk factor in lung cancer. Radon is a radioactive gas produced from the decay of natural Uranium, Radium and Thorium in rocks and soil. Inhalation of Radon can be responsible for about 3.4% of lung cancer deaths. (Cheng *et al.*, 2021). Compared to some other common cancers such as breast cancer, lung cancer continues to have a much lower survival rate (Chiang *et al.*, 2008). Chemotherapy and radiation therapies are commonly applied for small cell lung carcinoma (SCLS) (Stamatis *et al.*, 2004), while surgical treatments are normally provided for non-small cell lung carcinoma (NSCLS)

Some lung cancer screening methods, for example chest radiograph (CRG), computed tomography (CT), low-dose CT (LDCT), magnetic resonance imaging (MRI), and positron emission tomography (PET) have been studied extensively. These techniques have some drawbacks, such as being expensive and having low sensitivity for identifying cancer cells at early stages. Annual

CRG was reported as not helpful in reducing the mortality of lung cancer (Journy *et al.*, 2015). CT has been considered as the gold standard lung cancer screening tool, which offers information on tumor features such as size, characterization and tumor growth. 3D CT image offered assessment of the chest wall, diaphragm, and mediastinum invasion, in addition to staging the tumor. Radiations produced from CT, however, increased the cancer risk (Church *et al.*, 2013). To solve this limitation, LDCT was applied for lung imaging and it reduced 20% of lung cancer mortality (Asselin *et al.*, 2012). However, LDCT continues to have a high false positive rate (up to 96.4%) (Chicklore *et al.*, 2013). 18F-Fluorodeoxyglucose PET/CT was applied in oncological imaging but produced inaccurate results (Ippolito *et al.*, 2013 and Griffiths, 2011). Magnetic induction tomography (MIT) has been recently proposed for early disease detection with advantage of high-sensitivity (Cheng 2016) but disadvantage of high costs.

Apart from imaging approaches, biopsy is another common way to identify lung cancer; however, it is expensive and requires trained physicians (Zhong *et al.*, 2006).

The major limitations of the existing diagnostic methods include being time-consuming, expensive, and having low-sensitivity for low cancer cell concentrations (Nooreldeen and Bach, 2021). Therefore, it is necessary to develop a rapid, low-cost and high-sensitive method for early diagnosis of lung cancer. Biomarker-based techniques for early diagnosis of tumor markers have attracted much attention (Wang 2017). Autoantibodies can detect lung cancer cells about five years earlier than autoradiography because tumor growth is associated with gene and protein changes (Wang, 2017).

Such methylation or point mutation of DNA, RNA and mutated or aberrantly expressed proteins, carbohydrates, cytokines and chemokines, as well as volatile organic compounds from the peroxidation of the cell membrane species (Peng *et al.*, 2010) could be detected months or years prior to clinical diagnosis and are able to act as cancer biomarkers. According to Zhong *et al.* (2006), tumor-associated autoantibodies for NSCLC could be detected 5 years before it could be detected using autoradiography.

The most frequent method to test serum Tumor associated antigen (TAAs) is ELISA and solution hybridization detection method for miRNA. To detect TAAs, monoclonal antibodies and aptamers are usually used as capture agents while for miRNA, capture agents used are usually the corresponding single- stranded DNA (ssDNA). These methods are time consuming, expensive, and are not sufficiently sensitive for the low marker concentrations at early cancer stages (Tohill,

2009). Some of the tools that have been used for diagnosis of cancer with their advantages and disadvantages are presented in Table 2.1

Table 2. 1: Available diagnostic tools for cancer with their advantages and disadvantages.

Diagnostic method	Advantage	Disadvantage	Reference
Biopsy	Fast and easy	Inflammation, painful, invasive	(Woolner and McDonald.,1952)
Sputum cytology	easy and noninvasive	Degradation of biomarkers due to enzymes in sputum, false positive results	(Palmisano <i>et al.</i> ,2000)
Chest X-ray	Quite reliable	Use of radiation, false negative response, high cost	(De González and Darby, 2004)
Magnetic resonance imaging	Quite reliable	Use of magnetic field, high cost, not suitable for all patients that have other complications	(Leach <i>et al.</i> ,2005, (Beets-Tan RG <i>et al.</i> , 2001)
Computed tomography	Quite reliable	High cost, false negative scans, use of radiation	(Watt <i>et al.</i> ,1989)
Positron emission tomography	Quite reliable	Need for radioactive substance and sophisticated instrument, not suitable for all patients who have other complications, high cost	(Lardinois <i>et al.</i> ,2003)

Early diagnosis of lung cancer with suitable treatment significantly improves the five-year survival rate (Hara *et al.*, 1986). Fabrication of a Nano-structured electro-analytical biosensor for early detection of lung cancer could effectively reduce mortality rate due to lung cancer. In this project, a biosensor for a potential biomarker for early diagnosis of lung cancer was fabricated with an emphasis on serum biomarker detection. Monoclonal antibodies were used as capture agents.

2.2 Histopathological classification of Lung Cancer

Lung cancer is a malignant lung tumor that may stem from bronchial epithelium, bronchioles, alveoli, or bronchial mucous glands (Schnabel and Junker, 2015). It is characterized by post-treatment relapses, metastasis, and a variety of histological types (Travis 2012). Accurate classification of lung cancer is significant for the clinical management of the patient. In 2015, the new World Health Organization (WHO) classified lung tumors into two (Schnabel and Junker, 2015), namely the small-cell lung carcinoma (SCLC) and non-small-cell lung carcinoma (NSCLC) (Figure 2.3). Approximately 80% of lung cancer cases which have diverse molecular-biological features and clinical course forms of the disease are NSCLC. NSCLC is classified into adenocarcinoma, adenosquamous carcinoma, squamous cell carcinoma, large cell carcinoma, and large cell neuroendocrine carcinoma (Travis 2012).

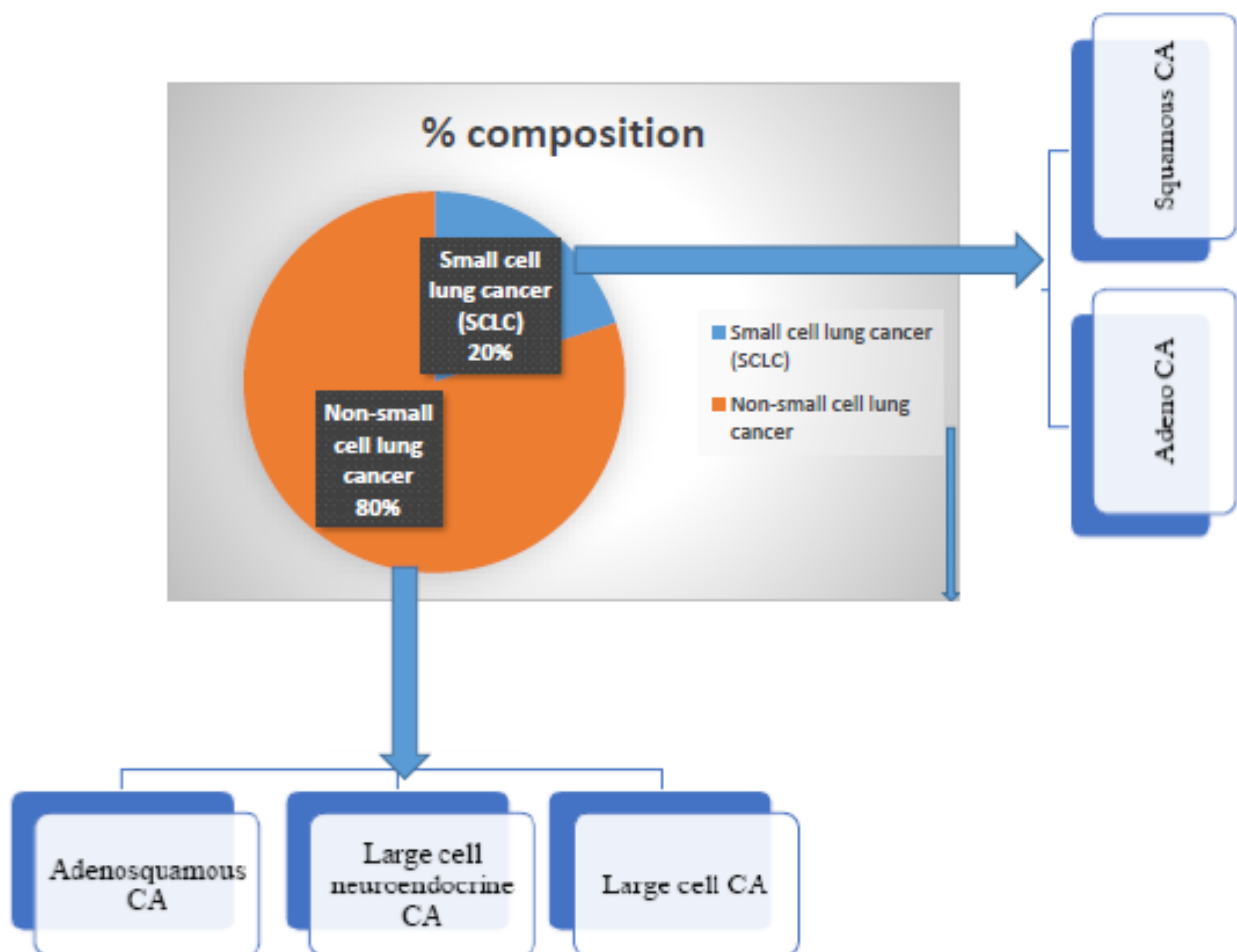


Figure 2.3: classification of lung cancer histological types.

(Schnabel and Junker, 2015)

2.3 Origin and Historical Features of Lung Cancer Types

Currently, there are two view points on the origin of Small-cell lung cancer (SCLC). According to the first hypothesis, SCLC arises from cells of the diffuse endocrine system, i.e., the Amine precursor uptake decarboxylation (APUD)-system (Figure 2.4), the second suggests that this type of lung cancer originates from the endoderm bronchial lining layer (Weynants *et al*; 1990)

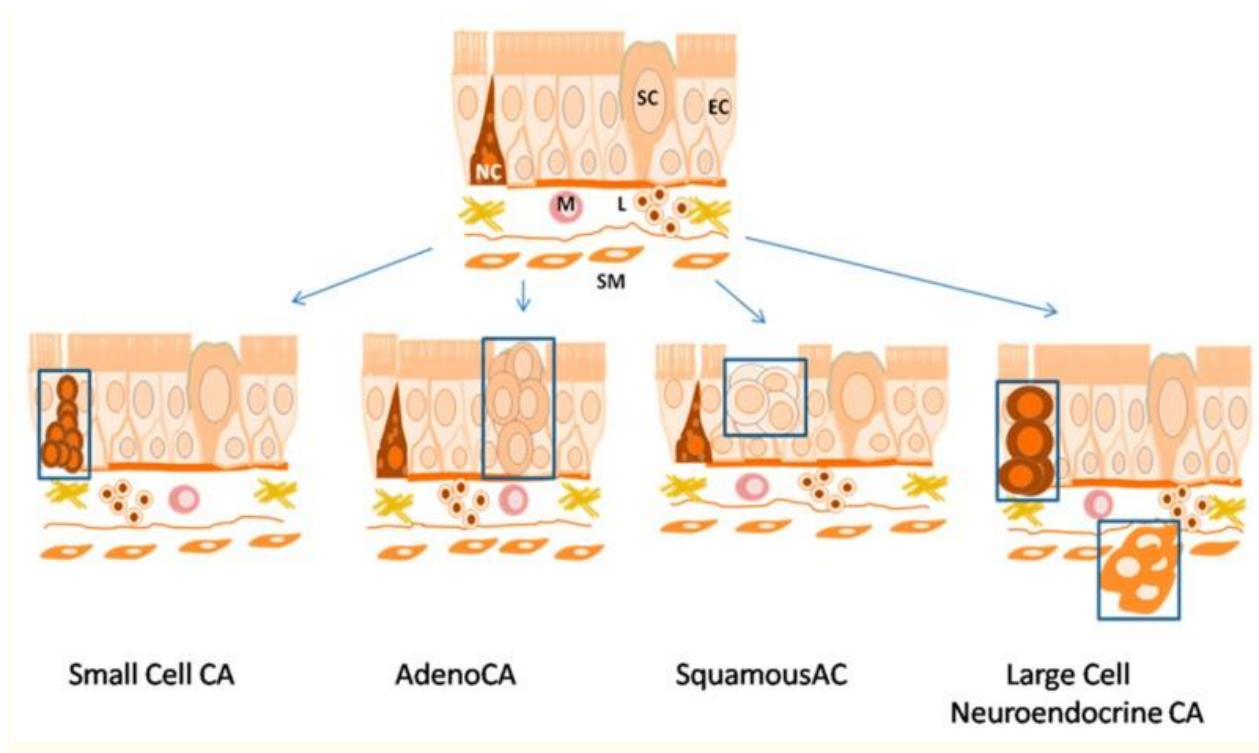


Figure 2. 4:Histogenesis of histological types of lung cancer

(Muller 1984).

SM—Smooth Muscle; M—Macrophage; L—Lymphocyte; NC—Neuroendocrine Cell; EC—Epithelial Cell; SC—Secretory Cell.

Small-cell lung cancer (SCLC) is characterized by small size cells, absence of differentiation, fast tumor growth, metastasis at early stages, and release of specific biomarkers and hormones.

As can be seen in Figure 2.4, among the other subtypes of non-small-cell lung carcinoma (NSCLC), adenocarcinoma originates from glandular cells of bronchial mucosa and represents the dominant histological subtype among the other lung cancer types. Squamous lung cancer arises from the modified bronchial epithelial cells and is characterized by keratinization, keratin pearl formation, or the presence of intercellular bridges.

Adenosquamous carcinoma is a type of cancer that contains two types of cells: squamous cells (thin, flat cells that line certain organs) and gland-like cells (Travis, 2012). Large cell neuroendocrine carcinoma is a malignant epithelial tumor, which is comprised of large polygonal cells that do not show any obvious evidence of histological differentiation. The cases include large cell neuroendocrine carcinoma, basaloid carcinoma, lymphoepithelioma-like carcinoma, and clear cell carcinoma. The tumor arises from neuroendocrine cells of the respiratory tract lining layer or smooth muscle cells of its wall (Figure 2.4). Large-cell carcinoma is a heterogeneous group of undifferentiated malignant neoplasms that lack the cytologic and architectural features of small cell carcinoma and glandular or squamous differentiation. Large-cell carcinoma is categorized as a subtype of NSCLC that arises from epithelial cells of the lung (Muller 1984).

It is well known that a unique combination of exogenous and endogenous factors influences the occurrence and development of lung cancer in each individual, hence, lung cancer, like any other oncological diseases, is heterogeneous. Thus, in addition to various histological types, this disease has many molecular and pathological subtypes characterized by heterogeneous cellular genetic and epigenetic changes and a different combination of protein biomarkers. However, at present, data on protein signatures of molecular subtypes of histological types of lung cancer is extremely limited, but a large number of genetic studies reflecting the probability of certain mutations in genes are presented. In particular, mutations of the epidermal growth factor receptor (EGFR) in lung adenocarcinoma have been well studied. It was found that in patients with lung adenocarcinoma, the probability of EGFR mutations increases linearly from patients aged 18–30 years (3.7%), 31–40 years (5.1 %), 41–50 years (6.5 %), 51–60 years (10.8 %), 61–70 years: (13.7 %), 71–80 years, (17.1 %) and 81–100 years (18.5 %). In female non-smokers, the probability of mutations is higher than in men (Imyanitov *et al.*, 2016). In male non-smokers, the probability of EGFR mutation is much higher than in smokers (Dogan *et al.*, 2012)

Identification of the correct histological type of lung cancer and their molecular subtypes is necessary due to different treatment strategies. Tumor cells of each histological type release certain protein biomarkers into the bloodstream and therefore play a key role in cancer genesis. The use of blood plasma to determine the origin and nature of the malignant cells for diagnosis requires knowledge about expression of protein biomarkers, their specificity, sensitivity, and their release by different types of lung cancer cells. (Capelozzi 2009, Vazquez *et al.*, 2007)

2.3.1: Small Cell Lung Cancer

SCLC originates from neuroendocrine cells of the APUD-system (amine precursor uptake and decarboxylation system) (Stovold *et al.*, 2012). SCLC has two of the main biological features of these cells which include: production of L-3,4-dihydroxyphenylalaninedecarboxylase (L-DOPA-decarboxylase) and NSE. L-DOPA decarboxylase is the gene encoding for the enzyme that catalyzes the biosynthesis of dopamine in humans (Papadopoulos *et al.*, 2015). NSE is a glycolytic neuron specific enzyme of enolase with two almost identical 39-kDa polypeptides produced in the central and peripheral neurons and malignant tumors of neuro ectodermal origin. NSE is specific only for SCLC. (Yu *et al.*, 2014). Adrenocorticotrophic hormone, serotonin, antidiuretic hormone, calcitonin, growth hormone, melanocyte-stimulating hormone, and estrogen are also produced in SCLC.

The other well-known biomarker of SCLC is pro-gastrin-releasing peptide (ProGRP). High levels of ProGRP were found in the blood of patients with SCLC and medullary thyroid cancer (>200 pgmL^{-1}). Blood plasma of healthy people and patients with benign diseases have ProGRP concentrations of 35 pgmL^{-1} and 4.5×10^3 pgmL^{-1} respectively. ProGRP has organ specificity and does not correlate with the stage of lung cancer. Although ProGRP is more specific than NSE, its use in biosensors is complicated due to its instability and difficulty of identification. Sensitivity and specificity of ProGRP was 80% and 90%, respectively, while that for NSE was 64% and 43%. However, 27% of patients with SCLC had increased levels of NSE and normal levels of ProGRP (Montani *et al.*, 2015).

2.3.2: Squamous Lung Cancer, Adenocarcinoma, Large Cell Carcinoma, Adenosquamous Carcinoma and Large Cell Neuroendocrine Carcinoma.

Squamous lung cancer originates from modified bronchial epithelial cells. One of the most distinctive features of squamous lung cancer is high levels of fragmented cytokeratin CK-19

subunit, CYFRA 21-1. CK-19 is a protein component of intermediate fibers of epithelial cells (Stieber *et al.*, 1993). The level of CYFRA 21-1 is increased during the malignization process of normal epithelial cells. CYFRA 21-1 is highly expressed in serum of patients with a metastatic form of squamous lung cancer (Okamura *et al.*, 2013, Wang *et al.*, 2010).

The other specific protein for squamous lung cancer is squamous cell carcinoma antigen (SCCA), a 48-kDa protein which is found in increased levels in squamous lung cancer (Wang *et al.*, 2010, Lakshmanan *et al.*, 2015). Squamous cell carcinoma antigen (SCCA) is an inhibitor of serine proteases such as human chymotrypsin -like elastase (CELA), calpain 1 (CAPN1), and cathepsin L (CTSL) (Wang *et al.*, 2022). It also inhibits apoptosis of tumor cells and stimulates invasion and metastasis (Suminami *et al.*, 1998).

Adenocarcinoma is another type of lung cancer which arises from glandular cells of bronchial mucosa and expresses several protein markers. Diagnosis of adenocarcinoma is often based on identification of molecular markers of mutations, in particular EGFR, Excision repair cross-complement (ERCC), ribonucleoside-diphosphate reductase (RRM 1), KRAS proto-oncogene (KRAS), thymidylate synthetase (TS), and echinoderm microtubule-associated protein-like 4 gene fused to anaplastic lymphoma kinase receptor tyrosine kinase (EML4-Alk) (Sholl 2015). Recently, protein PSF3 (DNA replication complex GINS) has become popular as a biomarker of adenocarcinoma (Tauchi *et al.*, 2016, Hokka *et al.*, 2013). PSF3 is a member of the heterotetrameric complex GINS (“go-ichi-ni-san” complex, from the first letters of the Japanese numbers 5-1-2-3) comprising Systemic RNA interference defective protein 5 (SLD5), GINS complex subunit 1 (PSF1), GINS complex subunit 2 (PSF2), and GINS complex subunit 3 (PSF3). This complex associates with proteins, which in turn regulate both the initiation and the progression of DNA replication (Bermudez *et al.*, 2011). To date, an overexpression of PSF3 in adenocarcinoma has been clearly established, which leads us to conclude that its level should be higher in blood plasma. However, data on the level of PSF3 in blood is yet to be reported. In addition to these biomarkers, several novel lung adenocarcinomas associated proteins have been found using aptamers, such as lamin (LMN) and vimentin (VIM) (Indovina *et al.*, 2011), neutrophil defensin (DEF) and tubulin (TUB) (Zamay, *et al.*, 2015), cytoplasmic actin (ACT), cathepsin D (CTSD), clusterin (CLU), nucleolin (NCL), and mucin-1 (MUC1) (Zamay *et al.*, 2016, (Kikuchi *et al.*, 2012). According to recent studies, identification of such proteins would improve the diagnosis of adenocarcinoma.

Large cell carcinoma is a malignant epithelial tumor that comprises of large polygonal cells showing no obvious evidence of histological differentiation. Large cell carcinoma is characterized by small, scattered groups of large non-differentiated, polymorphic, and often dual- or multi-core cells (Muller 1984). Adenosquamous carcinoma is characterized by the features of squamous cell carcinoma and adenocarcinoma simultaneously. Therefore, it has a protein biomarker of both histotypes. (Lakshmanan *et al.*, 2015)

Large cell neuroendocrine carcinoma (LCNEC) is extremely rare. There are difficulties related to its diagnosis and treatment. LCNEC shows overexpression of topoisomerases somatostatin precursor (TOP SST), and excision repair 1, endonuclease non-catalytic subunit (ERCC1) (Makino *et al.*, 2016)

2.4: Current Methods Employed to Diagnose Lung Cancer

Currently, lung cancer is detected mostly in the late stages with such symptoms as coughing, including coughing up blood, shortness of breath, and chest pain. The early stages of this disease are often detected by accident (Midthun, 2016). Chest radiography and computer tomography are the most commonly used methods for lung cancer diagnosis (Marshall *et al.*, 2013).

In addition, recent developments in genomics have been used to define high-risk populations, making them more suitable for lung cancer screening for early diagnosis (Ye *et al.*, 2019). Other commonly used procedures in diagnosing lung cancer include fiber optic bronchoscopy with or without trans bronchial needle aspiration, endobronchial ultrasonography, image-guided trans-thoracic needle aspiration, mediastinoscopy, pleural fluid analysis (thoracentesis), thoracoscopy, and surgical approaches (Nooreldeen & Bach, 2021). These procedures are costly, prone to complications, may need more samples (Kennedy *et al.*, 2000) and can only identify visible and, in many cases, irreversible changes in the lung. In order to enable and facilitate cure of lung cancer, there is a need for methods for early diagnosis, for example highly sensitive, and specific biomarkers.

2.5: Biomarkers

Biomarkers can be defined as molecules that represent the biological homeostasis and thus make it possible to detect changes in physiology (Eissa and Shoman, 1998). More specifically in the case of cancer, tumor markers indicate the presence of malignant cell growth when they are measured in higher concentrations than usual (Eissa and Shoman, 1998; Sung and Cho, 2008).

2.5.1: Classification of Cancer Biomarkers.

Biomarkers can be classified into four types based on the disease state (Figure 2.5). The first type is the diagnostic or screening biomarkers. These are used to detect and identify an explicit type of cancer. To be effective, this sort of biomarker should be very specific and sensitive (Hamdan 2007). Second, there are prognostic biomarkers, which are utilized once the disease status has been determined, to foresee the expected evolution of the cancer. The third type is the predictive or stratification biomarkers. These are applied to predict the response to a treatment. These biomarkers allow clinicians to select a set of chemotherapeutic agents which will work best for an individual patient (Hamdan 2007). Finally, there are the detection biomarkers they are used at all stages of a cancer to screen people, predict prognosis, and monitor for disease recurrence (Khailany et al., 2020).

Biomarkers are also classified based on biomolecules and other criteria such as imaging, pathological and silico biomarkers as shown in Figure 2.5. Biomarkers can also be classified based on the different areas they work in. For instance, a distinction can be made between genetic, epigenetic, proteomic, metabolic and microRNA-related biomarkers. The growth of a tumor is associated with both genetic alterations and the release of proteins, metabolites, nucleic acids and other biomolecules.

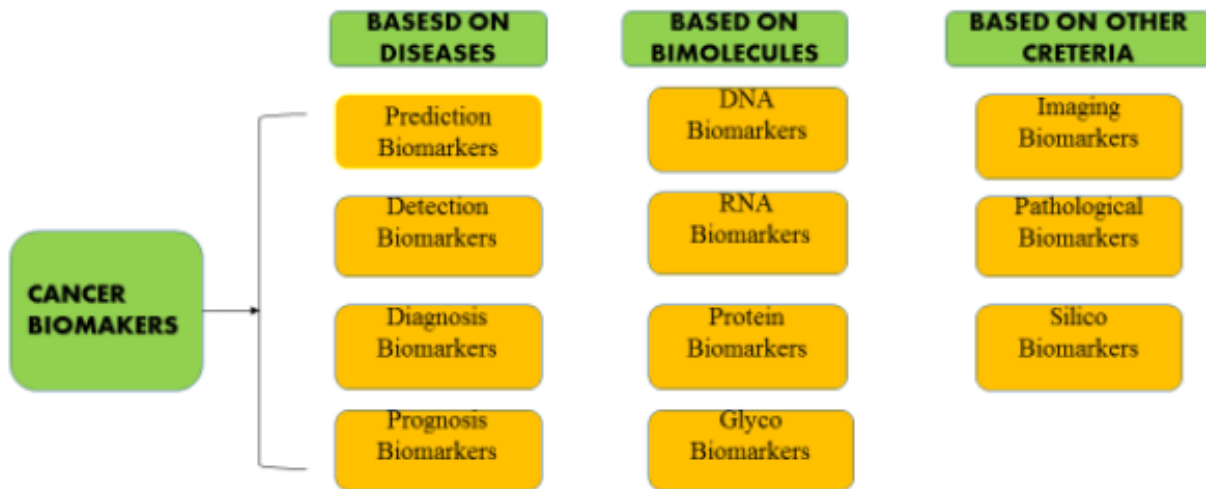


Figure 2.5: Classification of cancer biomarkers.

(Adapted from [www. Research gate. Net](http://www.researchgate.net))

Genetic-based biomarkers are detected using DNA arrays, polymerase chain reactions (PCR), reverse transcription polymerase chain reactions (RT-PCR), DNA sequencing or fluorescent *in situ* hybridization (FISH). For the determination of the levels of certain protein biomarkers, proteomic techniques are applied. These include mass spectrometry, enzyme-linked immunosorbent assay and immunohistochemistry. Metabolites are generally detected using liquid chromatography (Nna *et al.*, 2010; Arya and Bhansali 2011; Ponomaryova *et al.*, 2011).

A number of important biomarkers investigated for lung cancer diagnosis are listed in Table 2.2. Some of them are already in use, while others have shown considerable potential and are still being studied. The most broadly applied division is the one between DNA- or genetic-based biomarkers and protein or proteomic-based biomarkers. Examples of DNA and protein based biomarkers are as shown in Table 2.2.

Table 2. 2: DNA- and protein-based biomarkers in lung cancer detection (Arya and Bhansali, 2011).

Genetic biomarkers	RAR- β mRNA, COX2, DAPK, RASSF1A, IL-8 mRNA, FHIT, K-ras mutant, p53 mutant, EGFR
Protein biomarkers	CEA, CYFRA21-1, TPA, tumour M2-pyruvatekinase, haptoglobin- α 2, APOA1, KLK B1, ProGRP, α -enolase(NSE), α -1-acidglycoprotein, chromogranin A, bombesin-like gastrin-releasing peptide, CK-BB, cytokeratin-7, CA 19-9, CA125, plasma kallikrein B1, VEGF, nitrated ceruloplasmin, annexin II, CD59 glycoprotein, transthyretin (TTR), GM2AP

For lung cancer diagnosis, both genetic and protein markers are examined. However, none of the DNA tumor markers investigated so far seem to be sensitive and selective enough to be broadly used as a diagnostic tool. One of the reasons for this challenge is that the mRNA levels are not linked directly to the protein levels. The advantage of protein tumor markers is that they can be more specific to the cancer type and status because they show more variety. Diversity is created for example by post-translational modifications (such as acetylations, glycosylations, phosphorylations and methylations), protease cleavages or alternative splicing (Sung and Cho, 2008; Ponomaryova *et al.*, 2011).

The level of protein biomarkers can be determined in several body fluids, such as blood, serum, sputum, cerebral spinal fluid and urine. The fact that much information can be obtained non-invasively is a big asset of proteomics. In genetics, on the other hand, the DNA usually has to be extracted from the cells before analysis is possible. Often, extra enrichment is necessary because the concentration of the markers is generally very low. Tests have also been performed on the determination of certain oncomarkers in exhaled breath (Tothill 2009; Simon 2010; Arya and Bhansali, 2011; Bohunicky and Mousa, 2011).

In this study, CEA and YES1 biomarkers will be used for early detection of lung cancer. Table 2.3 shows some biomarkers and biosensors used in detection of cancer and their detection limits.

Table 2. 3: Some biomarkers and biosensors used in detection of cancer and their detection limits.

Biomarker	Biosensor	Surface Ligand	Detection Limit	Reference
AFP	Electrochemical*	Microfluidic immunosensor	1 to 10103 ng/mL	(Maeng <i>et al.</i> ,2008)
		Graphene and thionin nanocomposit film	5.66 pg to 2 ng/mL	(Wei <i>et al.</i> ,2010a)
		Antibody	50pg to 500ng/mL	(Tang <i>et al.</i> , 2011)
CA15-3	Electrochemical*	Antibody	10 U/mL	(Altintas <i>et al.</i> , 2014b)
CA19-9	SPR	Antibody	66.7U/mL	(Chung <i>et al.</i> , 2006)
CEA	Electrochemical*	Antibody	0.1 pg to 500 ng/mL	(Altintas <i>et al.</i> , 2014b)
	SPR*	Antibody	Up to 3 ng/mL	(Ladd <i>et al.</i> , 2009)
	SPR			
CRP and TNF	Electrochemical*	Antibody	3.2 to 10.4 µg/mL	(Lee <i>et al.</i> , 2010)
			25 pg to 25 ng/mL	(Qureshi <i>et al.</i> ,2009)
CRP	QCM*	Antibody	0.1 pM to 0.53 nM	(Kim <i>et al.</i> , 2010)
			0.3 ng to 0.5 mg/mL	(Kim <i>et al.</i> , 2010)
DNA mutations	SPR*	ssDNA	50 nM	(Ladd <i>et al.</i> , 2009)
EGFR	Optical*	Aptamer	-	(Ilyas <i>et al.</i> ,2012)
	Lab-on-a-chip*	Antibody		(Kallempudi <i>et al.</i> ,2012)
K-ras point mutation	SPR	PNA	-	(Sato <i>et al.</i> ,2003)
PSA	Electrochemical*	Antibody	1 pg to 35 ng/mL	(Triroj <i>et al.</i> ,2011)
		Nanoparticle-antibody	5 pg to 10 ng/mL	(Wei <i>et al.</i> ,2010)
		Nanoparticle-antibody	0.005 to 50 ng/mL	(Li <i>et al.</i> ,2011)
	SPR*	Antibody	0.02-2.3 ng/mL	(Li <i>et al.</i> ,2011)
p53 gene	SPR	Antibody and dsDNA	1.06 and 10.6 pM	(Wang <i>et al.</i> 2017)
p53 point mutation	SPR and QCM	ssDNA	0.03 µM	(Altintas <i>et al.</i> , 2013)

*Serum; AFP: Alpha-Fetoprotein; CA: Cancer Antigen; CEA: Carcinoembryonic Antigen; CRP: C-Reactive Protein; dsDNA: Double-Stranded DNA; EGFR: Epidermal Growth Factor Receptor; PNA: Peptide Nucleic Acid; PSA: Prostate-Specific Antigen; SPR: Surface Plasmon Resonance; ssDNA: Single-Stranded DNA; TNF: Tumor Necrosis Factor; QCM: Quartz Crystal Microbalan

2.5.1.1: Carcinoembryonic Antigen (CEA) biomarker.

Carcinoembryonic antigen is a serum protein that can be used as a diagnostic or therapeutic tumor marker in different types of cancer. It is a glycoprotein, belonging to the immunoglobulin super family. The human CEA is encoded by a gene located on chromosome 19 and has a molecular weight of about 70 kD, that can run up to 200 kD through glycosylation. The CEA protein consists of an *N*-terminal sequence, three repeated disulphide-linked domains comprising 178 amino acids

each and a C-terminal region. Every repeated domain can be split into two subdomains, which show sequence similarities. The C-terminus is hydrophobic and is associated to the cell membrane, differentiating CEA from other members of the CEA family, such as the secreted PSGs (pregnancy specific glycoproteins). The structure of the CEA protein is illustrated in Figure 2.6 (Hammarström 1999; Kaufman *et al.*, 2000).

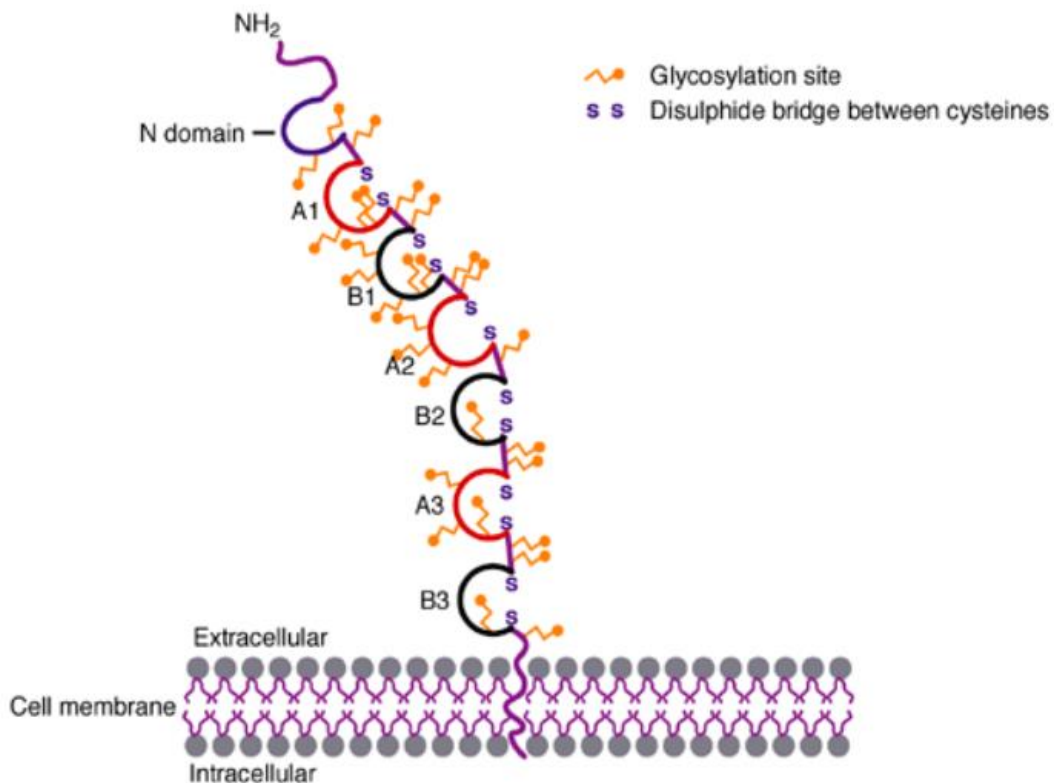


Figure 2.6: Schematic representation of the human CEA protein.

(Kaufman *et al.*, 2000).

CEA was first mentioned as a tumor-related antigen by Gold and Freedman in 1965. In the past decades, many clinical assays have been performed on this potential tumor marker. In contrast to what was believed earlier, it is now clear that CEA is not only expressed in fetuses and cancer patients, but also in healthy adults. A normal adult who does not smoke generally has levels of CEA that are below 2.5 ng/mL. The concentration is higher in smokers, but is commonly less than 5.0 ng/mL, while in cancer patients, it can rise to above 100 ng/mL. Elevated levels of the oncofoetal glycoprotein are mainly seen in the serum of people with colorectal, breast and lung carcinomas (Hammarström *et al.*, 1999; Su *et al.*, 2008).

Since an increased level of CEA can be an indication of the growth or recurrence of a tumor, the detection of the elevated amount of CEA in the serum could be of use in the diagnosis of cancer. However, one of the main restrictions for the application of CEA as a diagnostic screening tool for lung cancer is that the expression of this glycoprotein is also increased in other, non-malignant diseases, such as bronchitis, cirrhosis, hepatitis, inflammatory bowel disease, pancreatitis etc. The levels of CEA in benign conditions normally do not exceed 10 ng/mL though (Kaufman *et al.*, 2000; Laborla *et al.*, 2010; Altintas *et al.*, 2011). Research has also been done on the determination of tumor markers in pleural effusions. Radjenovi-Petkovic *et al* (2009) noted that the levels of CEA are significantly higher in patients with lung cancer than in people with benign pleural effusions.

2.5.1.2: YES1 biomarker

YES1 is a member of the Src kinase family of proteins. The YES1 protein is an important NSCLC tumor marker expression associated with high numbers of Regulatory T (**Tregs**) cells in patients with NSCLC (Redin *et al.*, 2021). Studies by Redin *et al.* (2021) showed that high YES1 levels are significantly associated with shorter overall survival in patients with NSCLC. Garmendia *et al* (2019) and Redin *et al.* (2021) have shown that YES1 levels can be a good companion biomarker for predicting the tumor response to the Dasatinib, a Src kinase inhibitor or to more specific YES1 inhibitors. The sensitive detection of low levels of YES1 in serum would be of great clinical significance in assessing tumor status and therapeutic efficiency, as well as in the early clinical diagnosis of the tumor.

YES1 has, therefore, been identified as an important biomarker for clinical diagnosis of Lung cancer. Immunohistochemistry (Cha *et al.*, 2021), western blotting (Takeda *et al.*, 2017), flow cytometry and quantitative real-time polymerase chain reaction (QRTPCR) (Redin *et al.*, 2021) are some of the molecular techniques which have been employed to detect YES1.

2.6: Biosensor

Turner *et al.* (1987) define biosensors as "analytical devices incorporating a biological material (e.g. tissue, microorganisms, organelles, cell receptors, enzymes, antibodies, nucleic acids, etc.), a biologically derived material (e.g. recombinant antibodies, aptamers, etc.) or a biomimic (e.g.

synthetic receptors, combinatorial ligands, imprinted polymers, etc.) intimately associated with/or integrated within a physicochemical transducer, which may be optical, electrochemical, thermometric, piezoelectric, magnetic or micromechanical. The principal parts of biosensors are outlined in Figure 2.7

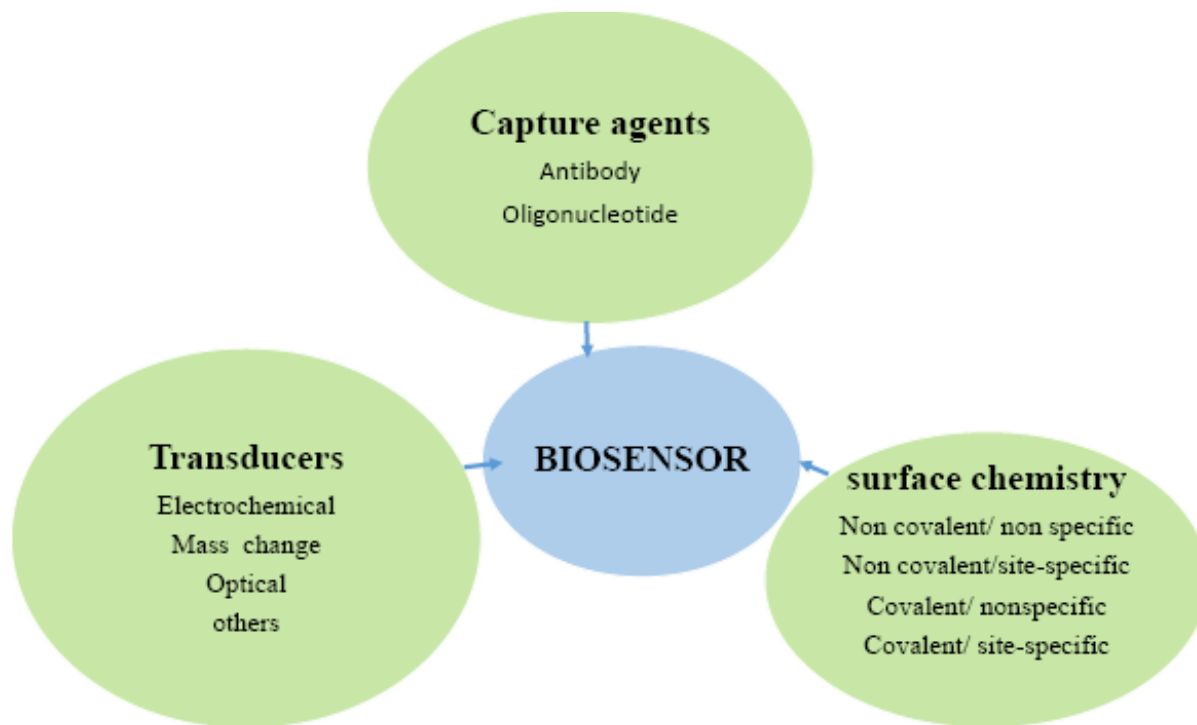


Figure 2. 7: The three components of biosensors.

(Gerard *et al.*, 2002)

When constructing a biosensor, three components should be considered, a bio-recognition element for selective recognition of an analyte also known as bio receptor, an immobilization matrix for the immobilization of a recognition biomolecule and a transducer for conversion of biochemical response into a measurable signal (Gerard *et al.*, 2002). Bio-receptors and transducers are together referred to as a bio sensing membrane.

To detect cancer antigens, monoclonal antibodies and aptamers are often used as capture agents and capture micro Ribonucleic acids (miRNAs) corresponding to single stranded Deoxyribonucleic acid (ssDNA). A transducer is a device that converts the molecular recognition signal to an electrical signal. The transducer may be electrochemical (by Potentiometry, amperometry, conductometry / impedimetry), optical (fluorescence, luminescence, colorimetric

and interferometry), calorimetric (thermistor) or based on mass changes (piezoelectric / acoustic waves). Such classification of biosensors can be summarized as in Figure 2.8.

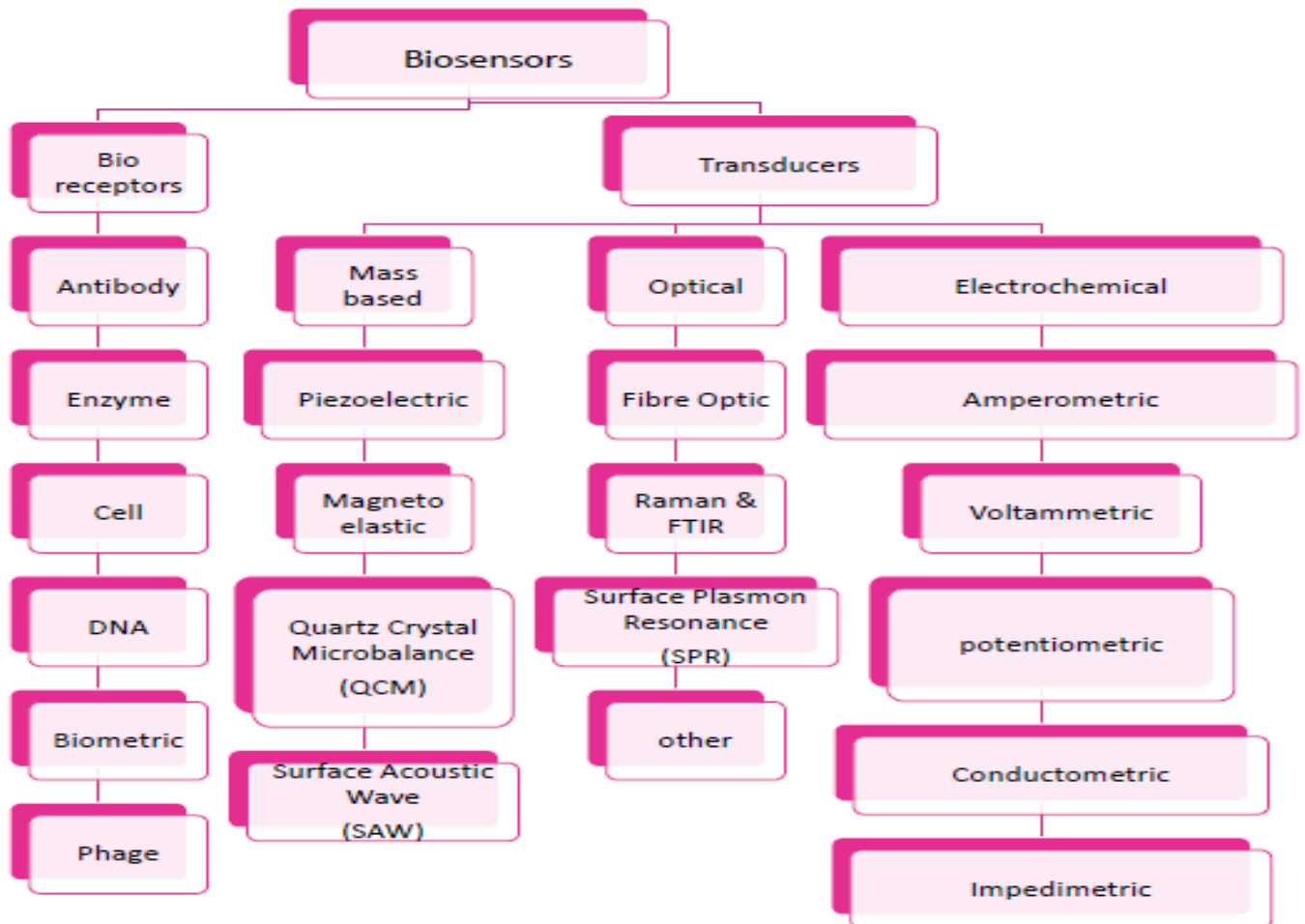


Figure 2.8: Biosensor classification.

Adapted from (Velusamy *et al.*, 2009)

Biosensors have a number of potential advantages over other methods of cancer diagnosis such as reduced assay time, portability, high sensitivity and selectivity, simplicity, miniaturization and flexibility. Biosensor-based diagnostics can assist cancer screening and improve the rates of earlier diagnosis and attendant improved forecast. This technology can be particularly useful for enhanced healthcare delivery in the public setting and to underserved diasporas. Biosensors have potential for multi-target analyses, automation, and cost effective testing (Chapman *et al.*, 2007). A successful biosensor must have most of the following significant features:

- i) The response of the biosensor should be precise, reproducible, accurate and linear over a relevant analytical range, without dilution or concentration. The signal to noise ratio of the biosensor should be high (Thévenot et al., 2001).
- ii) The reaction between the bio-recognition element and analyte of interest should be independent of physical parameters such as stirring, pH and temperature. This would allow the analysis of samples to be conducted with minimal pretreatment (Thévenot et al., 2001).
- iii) The bio-recognition element must be highly specific for the purpose of the analysis, and be stable under normal storage conditions (Thévenot et al., 2001).
- iv) There should be a market for the biosensor. There is no benefit to developing a biosensor if other factors (e.g. government subsidies, the continued employment of skilled analysts, or poor customer perception) encourage the use of traditional methods and discourage the decentralization of laboratory testing.
- v) The complete biosensor should be cheap, small, portable and capable of being used by semi-skilled operators.
- vi) If the biosensor is to be used for in-vivo monitoring in clinical situations, the probe must be tiny and biocompatible, having no toxic or antigenic effects. If the sensor is reusable then it should be able to withstand standard sterilization procedures (Thévenot et al., 2001)

2.6.1: Classification of Biosensors

There are different ways of classifying biosensors. First, based on the method of signal transduction, biosensors may be classified into six basic groups, i.e. optical, mass, micromechanical, electrochemical, magnetic and thermal sensors (Ivnitski *et al.*, 1999). Among the various biosensors, electrochemical biosensors have received special attention as they allow high sensitivity, lower detection limits, automation, inexpensive testing, and development of disposable devices and methodologies capable of working with very small sample volumes.

In this study electrochemical biosensors were used for early detection of lung cancer.

Biosensors can also be classified according to the type of recognition material applied. First, a distinction can be made between enzymatic or bio catalytic and affinity biosensors. An enzyme biosensor is derived from a combination of a transducer with a thin enzymatic layer, which normally measures the concentration of a substrate (Wang 2006a). The enzymatic reaction

transforms the substrate into a reaction product that is detectable by the electrode. The concentration of any substance can be measured provided that its presence affects the rate of an enzymatic reaction which is especially true for enzyme inhibitors. The signal, that is the current or potential measured, is proportional to the rate-limiting step in the overall reaction (Kimmel *et al.*, 2012). Bio catalytic sensors use enzymes, cells or tissues as bio receptors. In affinity-based biosensors antibodies, receptor proteins, nucleic acids or bio mimetics are utilized as recognition elements (Wang 2006; Simon 2010). Affinity biosensors can be further differentiated into direct or indirect sensors.

The classification shown in Figure 2.9 depends on whether or not the presence of a labeled element is needed for the generation of the sensor signal.

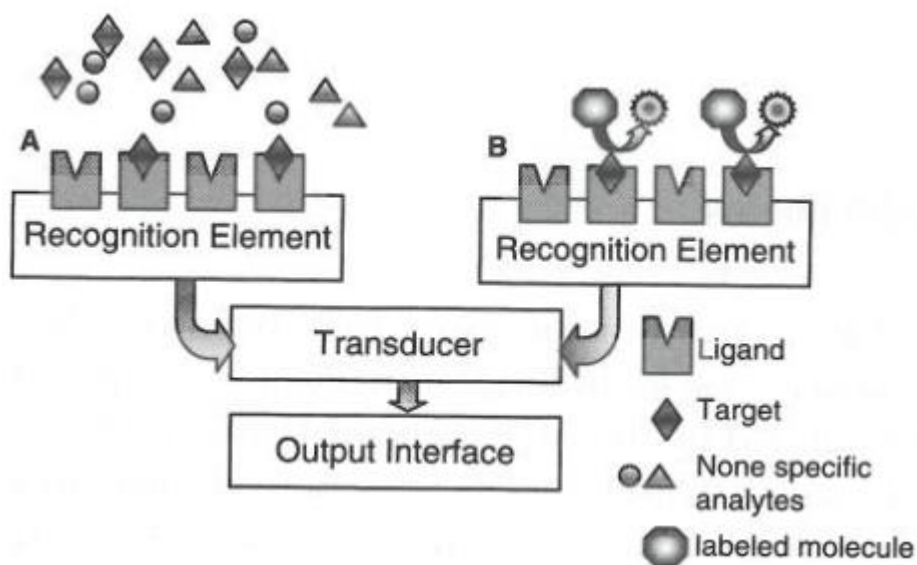


Figure 2.9: Schematic representation of (A) a direct biosensor and (B) an indirect biosensor using a sandwich assay. (Rasooly and Herold, 2008)

The preference goes to label-free or direct biosensors because they make real-time measurements possible, are less expensive and there is no need for extensive sample preparation. In labeled or indirect biosensor formats, the signal is not generated by the analyte receptor complex itself, but by a secondary element, the label bound to the complex. This kind of biosensor is derived from

immunoassays for example, sandwich complexes (Berggren *et al.*, 2001; Rasooly and Herold, 2008; Parker *et al.*, 2009; Simon 2010; Heurich *et al.*, 2011)

2.6.1.1: Immunosensors

An electrochemical immunosensor is a compact analytical tool that allows the detection of an antigen, for example a cancer protein biomarker, in which the antigen-antibody interaction can be detected using a transducer that can convert the biochemical reaction into a measurable electrical signal that is then recorded and displayed (Felix and Angnes, 2018). When the recognition element or target analyte consists of an antibody or antigen as receptor, the event is then termed as an immunosensing strategy. When an electrode is used to transduce the immunosensing strategy, it can be classified as electrochemical immunosensor.

The molecular recognition element must be able to detect low concentrations of the target molecule in a mixed population, so there is need for high specificity and sensitivity. To address these requirements, antibodies are often used. According to Bohunicky and Mousa (2011), antigen- and antibody-based recognition elements are not only very specific, which leads to low detection limits, but the detection system is also very fast. Both polyclonal and monoclonal antibodies have proved to be successful. However, monoclonal antibodies tend to be more specific. Polyclonal antibodies are generally cheaper, but show varying affinities. Extensive research is being done to replace the antibodies by synthetic recognition elements, such as peptides, aptamers, nanomaterials and molecular imprinted polymers. This will increase the stability and reproducibility of the biosensor (Soper *et al.*, 2006; Tothill 2009; Simon 2010; Bohunicky and Mousa 2011; Tothill 2011).

Figure 2.10 shows the schematic representation of an electrochemical immunosensor, the transducer connection and the signal processor.

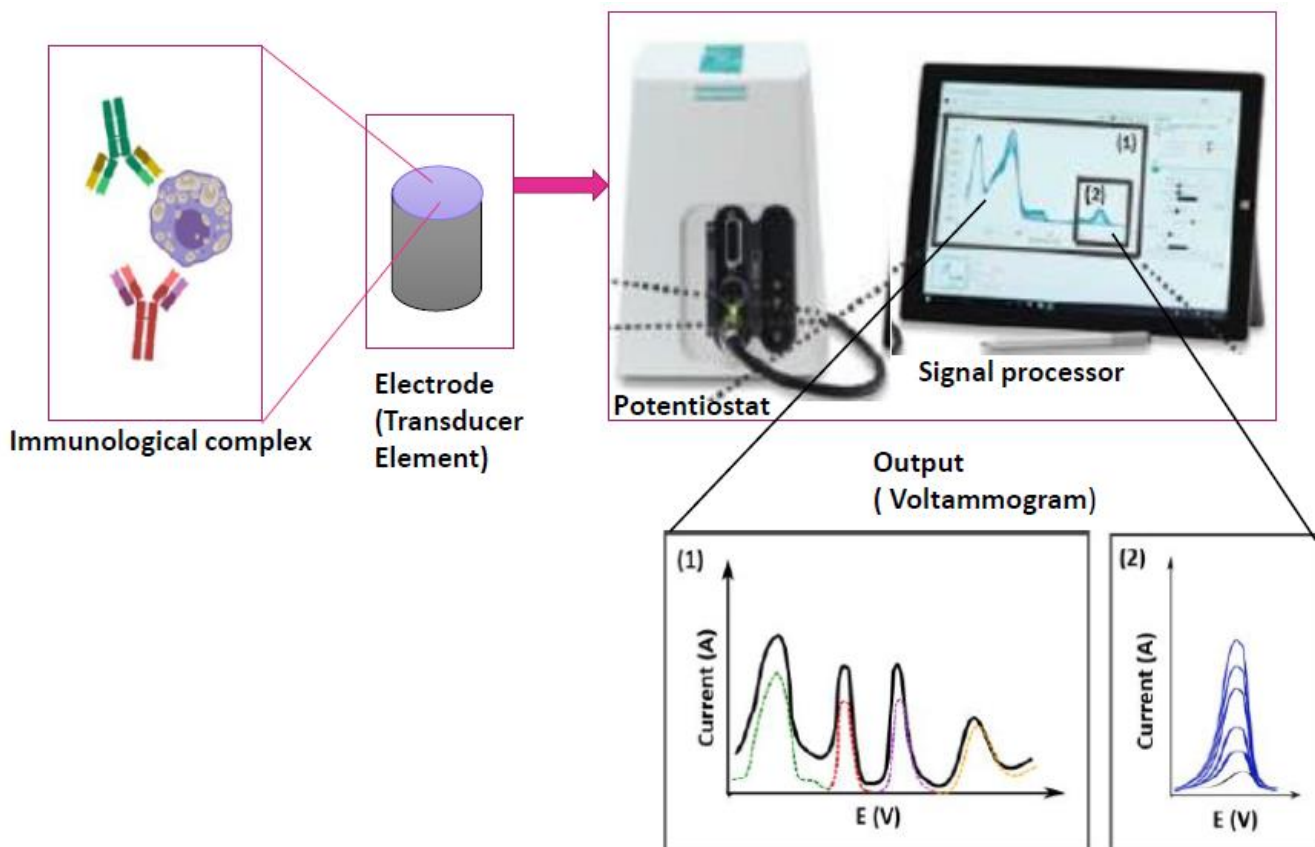


Figure 2.10: Scheme of an electrochemical immunosensor. Voltammetric signal is obtained for distinct analytes, which allows (1) simultaneous or (2) individual detection

In this study, sandwich assay was used in the fabrication of biosensor (as in Figure 2.9 (B)). The analyte contained antigens that bound with the antibodies. One of the antibodies was immobilized onto the surface of the electrode as the capture antibody and it was used to recognize the target molecule. The second antibody, which was enzyme-labelled was also immobilized onto the surface of the electrode and bound to the antigen as the detection antibody. This led to the generation of an electro active product which could be detected. This type of enzyme immunosensor was applied because of its ability to amplify the response signal fast. In this work horseradish peroxidase (HRP) was used as the label enzyme to amplify the signal of the immunosensor for the detection of CEA.

2.7: Electrochemical methods

Electrochemical methods have been commonly used towards the development of numerous biosensors, the most common of which is the glucose biosensor. Electrochemical analysis entails

the measurement of current, potential or charge. The concentration and properties of the analyte, or the properties of the material used to make the electrode can be reflected by these measurements. Basic electrochemical methods involve voltammetry and amperometry. Variations of methods such as cyclic voltammetry, linear sweep voltammetry, square wave voltammetry and constant potential amperometry are selected to suit the specific application.

An electrochemical biosensor is an analytical device that is fabricated by modifying the surface of electrode with biomolecules, such as enzymes, antibodies, and DNA (Khalil *et al.*, 2016). This biosensor is based on electrochemical techniques in which analyte sensing is made by measuring the electrical response as an analyte reacts electrochemically with the surface of the working electrode of the sensor (Tiwari *et al.*, 2016). Ideally, such a device is capable of responding continuously and reversibly and does not perturb the sample. Electrochemical biosensors combine the analytical power of electrochemical techniques and the specificity of biological recognition processes. Electrochemical biosensors were preferred as opposed to other biosensors because they are easy to miniaturize, they have sensitivity, selectivity, real-time detection, ease of use, affordability they offer broad detection limits even with small volumes of analyte. Furthermore, electrochemical biosensors can be used to analyze bio fluids with high turbidity and optically absorbing and fluorescing compounds (Kulkarni *et al.*, 2022)

2.7.1: Potentiometric transducers

Potentiometric transducers make use of ion-selective electrodes in order to transduce the biological response or biochemical reaction into a potential electrical signal. In the simplest terms this comprises of an immobilized enzyme membrane surrounding the probe from a pH-meter, where the catalyzed reaction generates or absorbs hydrogen ions. The reaction occurring next to the thin sensing glass membrane causes a change in pH, which may be read directly from the pH-meter's display. Typical of the use of such electrodes is that the electrical potential is resolved at very high impedance allowing effectively zero current flow and causing no intrusion with the reaction. The foundation of this type of biosensor is the Nernst equation that relates the electrode potential (E) to the concentration of the electroactive species present in buffer solution. For the reaction: $aA + ne^- \leftrightarrow bB$, the Nernst equation is described by equation 2.1

$$E = E^0 + \frac{RT}{nF} \frac{C_A^a}{C_B^b} \quad \text{Equation 2.1}$$

Where E^0 is the standard redox potential, R is the gas constant, T is the absolute temperature, F is Faraday's constant, n is the number of electrons exchanged in the reaction, and C_A and C_B are the concentrations of the oxidized and reduced species. A particular application of potentiometric sensors was developed to measure glucose (Kauffmann and Guilbault, 1991). Glucose has minimal effect on pH, but the enzymatically formed product of glucose and glucose oxidase immobilized on the sensor outer surface of a pH electrode causes acidification and thus results in a signal change. Semiconductor based physio-chemical transducers are commonly used in ion selective field effect transistors (ISFETs) and light addressable potentiometric sensor (LAPS) (Yoshinobu *et al.*, 2005). The working principle of the ISFET sensor is related to a local potential generated at the surface of the sensor by ions from solution. Potentiometric sensors using semiconductor sensors have been successfully developed for the detection of glycoalkaloids (Korpan *et al.*, 2006), herbicide atrazine (D'Agostino *et al.*, 2006), creatinine (Erden *et al.*, 2006), neurotransmitter serotonin (Kitade *et al.*, 2004), and organophosphate pesticides (Timur & Telefoncu, 2004). The LAPS biosensor has been used for the detection of as low as 10 cells/ml of *Escherichia coli* and has been commercialized for an automated 8-channel device for detection of biological agents (Ercole *et al.*, 2002).

2.7.2: Amperometric biosensors

Amperometric biosensors on the other hand monitor the current generated against applied constant potential by the reduction or oxidation of the electro active species involved in the bio recognition process (Wang 1999). The enhanced sensitivity, specificity, simplicity, and inherent miniaturization of modern electrochemical bioassays allow them to compete with the most advanced optical protocols (Wang 2006)

Amperometric sensors can work in a two- or three-electrode configuration based on the application. The first scenario consists of the working (contains bio-recognition element) and reference electrodes. The main challenge of the two-electrode configuration is the short linear range obtained due to limited control of the potential on the working electrode surface with higher currents (Fort *et al.*, 2007). A third auxiliary electrode is employed to solve this problem. Therefore, in the three-electrode configuration voltage is applied between the reference and the working electrodes, and current flows between the working and the auxiliary electrodes. Using amperometric sensors in the 3-electrode configuration, currents as low as 10^{-9} to 10^{-6} A can be easily measured. The resulting current is directly correlated to the bulk concentration of the electroactive species or its

production or consumption rate within the adjacent bio catalytic layer. Amperometric sensors have often been used on a large scale for detection of analytes such as glucose, lactates (Ohnuki *et al.*, 2007) and salicylic acid (Marzouk *et al.*, 2007). Detection of cancer marker genes like BRAC₁ and BRAC₂ from breast tissue has been achieved by the catalytic oxidation of guanine nucleobase (Tansil *et al.*, 2005). Biosensors using enzymes such as butyrylcholinesterase and acetylcholinesterase have been employed for the rapid detection of organophosphates and carbanates (Rajangam *et al.*, 2017) and (Štěpánková and Vorčáková, 2016). Amperometric and potentiometric transducers have been used commonly for biosensor development, but much attention in recent years has been devoted towards impedance based transducers as they can accomplish label-free analysis. Conductometric biosensors follow the changes in conductance or impedance of a solution as a result of the bio recognition component using a noble element working electrode. Thus the expression of impedance or its inverse conductance is as follows, where Z is impedance, R is component resistance, C is component capacitance:

$$Z^2 = R^2 + \frac{1}{(2FC)^2} \quad \text{Equation 2.2}$$

Conductometric biosensors include two electrodes with applied alternating voltage, amplitudes from a few to 100 mV have been used (Jaffrezic-Renault and Dzyadevych, 2008). Biosensors based on the Conductometric principle present a number of advantages such as: (i) The transducers are not light sensitive. (ii) The thin-film electrodes which are suitable for miniaturization and large scale production use inexpensive technology (Gs *et al.*, 2014). (iii) They do not require any reference electrode (Nikolelis *et al.*, 2013). (iv) The driving voltage can be sufficiently low to decrease significantly the power consumption and large spectrum of compounds of different nature can be determined on the basis of various reactions and mechanisms (Nikolelis *et al.*, 2013).

2.8: Voltammetry

The chief characteristic of all voltammetric techniques is that they involve the application of a potential (E) to an electrode and the monitoring of the resulting current (I) flowing through the electrochemical cell. In many cases the applied potential is varied or the current is monitored over a period of time (t) (Scholz, 2015). Thus, all voltammetric techniques can be described as some function of E, I, and t. They are considered active techniques (as opposed to passive techniques such as potentiometry) because the applied potential forces a change in the concentration of an

electroactive species at the electrode surface by electrochemically reducing or oxidizing it. The analytical advantages of the several voltammetric techniques include excellent sensitivity with a very large useful linear concentration range for both inorganic and organic species (10^{-12} to 10^{-1} M), a large number of useful solvents and electrolytes, a broad range of temperatures, fast analysis times (seconds), simultaneous determination of several analytes, the ability to determine kinetic and mechanistic parameters, a well-developed theory and thus the ability to reasonably estimate the values of unknown parameters, and the ease with which different potential waveforms can be generated and small currents measured. (Scholz, 2015)

2.8.1: Linear sweep voltammetry

In linear sweep voltammetry (LSV) a fixed potential range is employed, much like potential step measurements, and the voltage is scanned from the lower limit to the upper limit as shown in Figure 2.11

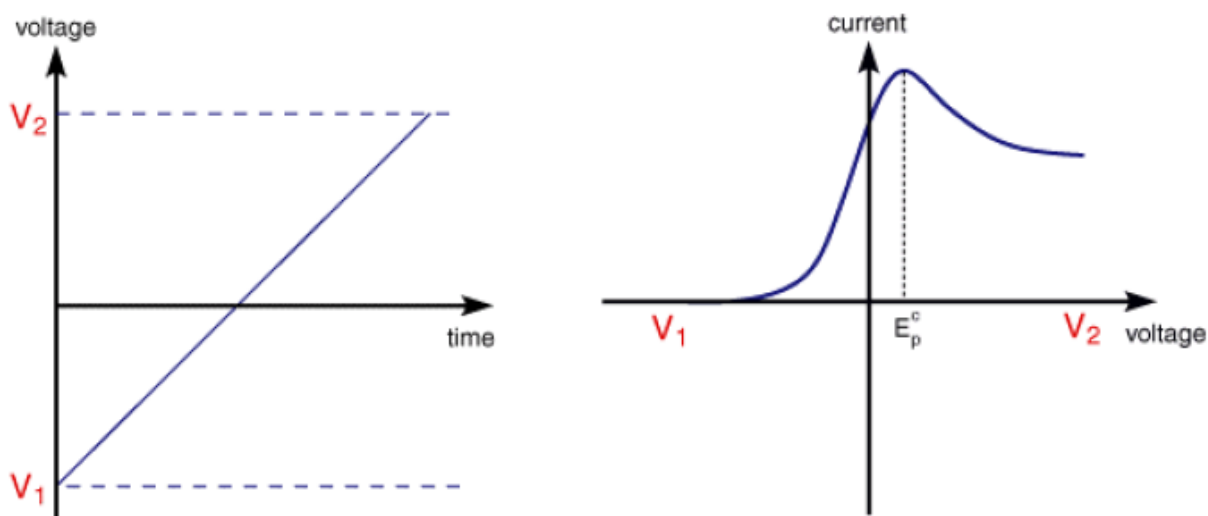


Figure 2.11: Voltage applied between working electrode and counter electrode with respect to time and the current response measured at the working electrode during LSV

Characteristics of the linear sweep voltammogram depend on several factors such as (i) The chemical reactivity of the electroactive species, (ii) The rate of the electron transfer reactions and (iii) The voltage scan rate (Administrator, 2013). In LSV measurements the current response is plotted as a function of voltage rather than time, unlike potential step measurements. The scan

starts from the left hand side of the current/voltage plot where no current flows. As the voltage is swept further to the right (to more reductive values) a current start to flow and finally reaches a peak before dropping. To rationalize this behavior, we need to consider the influence of voltage on the equilibrium established at the electrode surface. Here the rate of electron transfer is fast in comparison to the voltage sweep rate. Thus, at the electrode surface equilibrium is established similar to that predicted by thermodynamics. The exact form of the voltammogram can be rationalized by considering the voltage and mass transport effects. As the voltage is initially swept from V_1 the equilibrium at the surface begins to change and the current begins to flow. In LSV, the current increases as the voltage is swept further from its initial value as the equilibrium position is moved further to the right hand side, thereby converting more reactant. The peak occurs, since at some point the diffusion layer has grown sufficiently above the electrode so that the flux of reactant to the electrode is not fast enough to satisfy that required by the Nernst equation. In this situation the current begins to drop just as it did in the potential step measurements. Actually the drop in current follows the same behavior as that predicted by the Cottrell equation (Equation 2.3) which describes the change in electric current with respect to time in a controlled potential experiment. (Macero & Rulfs, 1959)

$$i = \frac{nFA C_0 \sqrt{D_0}}{\sqrt{\pi t}} \quad \text{Equation 2.3}$$

Where

n = number of electrons

F = Faraday's constant, 96,500 coulombs/mole

A = area of the (planar) electrode in units cm^2

C_0 = initial concentration of the reducible analyte (unit molarity)

D_0 = diffusion coefficient for species in units cm^2/s

t = time in s

In LSV the voltammogram is recorded at a single scan rate. If the scan rate is altered the current response also changes. Each curve has the same form but it is apparent that the total current increases with increasing scan rate. This can be rationalized by considering the size of the diffusion layer and the time taken to record the scan. Clearly the linear sweep voltammogram will take longer to record as the scan rate is decreased. Therefore, the size of the diffusion layer above the

electrode surface will be different depending upon the voltage scan rate used. In a slow voltage scan the diffusion layer will grow much further from the electrode in comparison to a fast scan. Consequently, the flux to the electrode surface is considerably smaller at slow scan rates than it is at faster rates. As the current is proportional to the flux towards the electrode the magnitude of the current will be lower at slow scan rates and higher at high rates.

2.8.2: Cyclic voltammetry (CV)

Cyclic voltammetry (CV) is very similar to LSV. In this case the voltage is swept between two values at a fixed rate but when the voltage reaches V_2 the scan is reversed and the voltage is swept back to V_1 . A typical cyclic voltammogram recorded for a reversible single electrode transfer reaction is shown in Figure 2.12. In this Figure, the solution contains only a single electrochemical reactant. The forward sweep produces an identical response to that seen for the LSV experiment (Wang 2006). When the scan is reversed we simply move back through the equilibrium positions gradually converting the electrolysis product (e.g. Fe^{2+} back to reactant Fe^{3+}). The current flow is now from the solution species back to the electrode and so occurs in the opposite sense to the forward sweep but otherwise the behavior can be explained in an identical manner. Cyclic voltammetry plays a major role in the study of electrode kinetics. The generated cyclic voltammogram is applied in electrochemistry to rapidly locate the redox potentials of electro active species. (Bard and Faulkner, 2001; Wang 2006; Compton and Banks, 2011). For a reversible electrochemical reaction, the CV recorded has certain well defined characteristics which include the following: (Scholz, 2015)

- i. The voltage separation between the peaks should be ± 59 mV
- ii. The positions of peak voltage don't change as a function of voltage scan rate.
- iii. The ratio of the peak currents is equal to one
- iv. The peak currents are proportional to the square root of the scan rate.

The Randles-Sevcik equation (equation 2.4) can be used to predict the peak current obtained from a reversible redox reaction (Lether and Wenston, 1987).

$$i_p = (2.69 \times 10^5) n^{\frac{3}{2}} A C \sqrt{D} \sqrt{v} \quad \text{Equation 2.4}$$

where:

i_p is current maximum in amperes,

n = number of electrons transferred in the redox event,

A = electrode area in cm^2

F = Faraday's Constant in C mol^{-1}

D = diffusion coefficient in cm^2/s ,

C = concentration in mole/cm^3

v = scan rate in V/s .

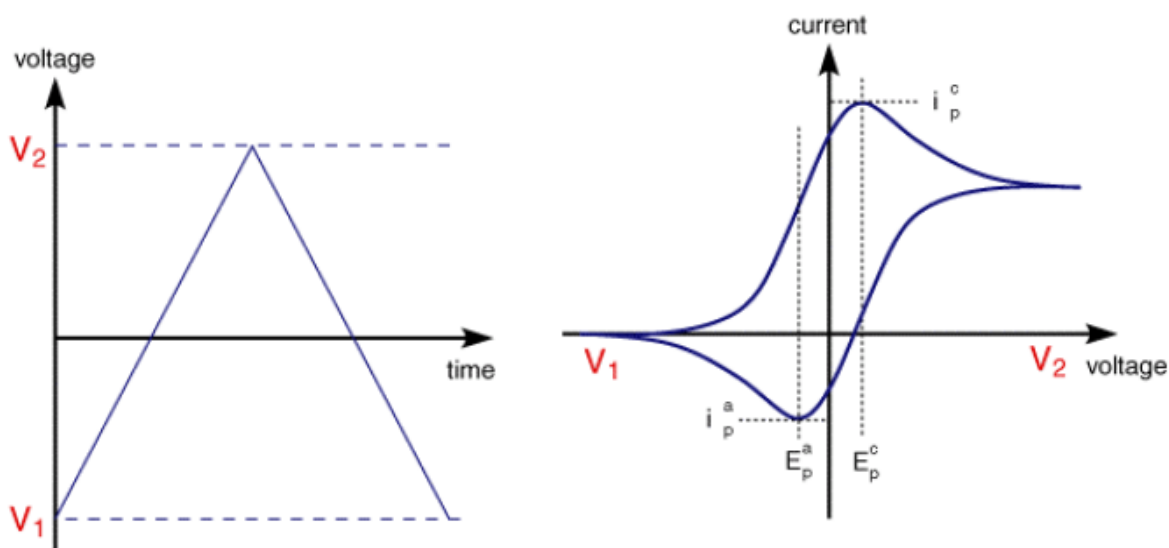


Figure 2.12: Voltage applied between the current and working electrodes and current response measured at the working electrode during Cyclic voltammetry

2.8.3: Constant potential Amperometry (CPA)

This is an electrochemical technique in which a constant potential is applied to a sensor (working electrode) and the faradaic current is measured. The current is generated by the reduction or oxidation of a chemical substance on the electrode surface. The advantage of this technique is that the time resolution is limited only by the data collection frequency of the instrument (Kile *et al.*, 2012). On the other hand, the main limitation is the low chemical selectivity (Kile *et al.*, 2012).

For example, all species with oxidation potentials below the applied voltage will be oxidized and contribute to the current

2.8.4: Differential Pulse voltammetry (DPV)

Differential Pulse voltammetry (DPV) is a voltammetric technique where the potential perturbation, that consists of small pulses, is superimposed upon a staircase waveform. In this case the instrumentation has been developed in such a way that current measurements and potential pulses are performed at very short time intervals (Scholz, 2015). More specifically, the current is sampled twice (before and after the pulse application) and the first current is subtracted from the second. The current difference is plotted versus the applied potential (Figure 2.13). DPV has become a widely used voltammetric technique and is useful to determine trace concentrations (Scholz, 2015)

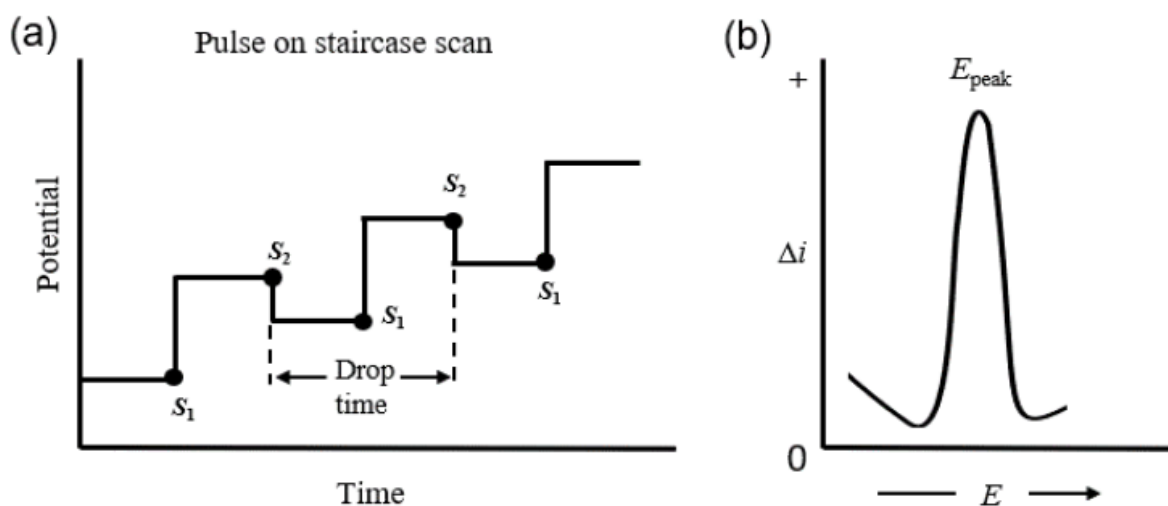


Figure 2. 13: Excitation signals (a) and Voltammogram (b) for DPV experiment.

Adapted from (Brett and Brett, 1993)

A common technique used for pre concentration purposes is anodic stripping voltammetry, usually employed for trace metal ion determination. In this technique the pre-concentration step consists of the application of a constant potential for the electrodeposition of the electroactive species (Daniele, 2005). This step is followed by an equilibration time and a determination step. The latter consists of stripping the previously electrodeposited species back in the solution. (Daniele, 2005).

A good example is cadmium ion determination. Initially, the electrode potential is adjusted to a negative enough value to reduce cadmium ions to metallic cadmium, which is electrodeposited onto the electrode. In the next step the potential is scanned to more positive (anodic) values, and the cadmium is oxidized and re-dissolved into the solution. When cadmium re-oxidation occurs, the current will vary and the obtained i_p value is proportional to the cadmium concentration in the sample solution (Wang *et al.*, 2022). The pre-concentration (electrochemical deposition) is a key step to achieving a higher analytical signal related to the concentration of the analyte in the solution, which also explains the increased sensitivity of the technique (Kile *et al.*, 2012).

2.8.5: Square wave voltammetry (SWV)

The excitation signal in SWV consists of a symmetrical square-wave pulse superimposed on a staircase waveform of step height E , where the forward pulse of the square wave coincides with the staircase step. The net current is obtained by taking the difference between the forward and reverse currents and is centered on the redox potential (Ramaley and Krause, 1969). The peak height is directly proportional to the concentration of the electroactive species and direct detection limits as low as 10^{-7} M are possible. SWV has several advantages. Among these are its excellent sensitivity, rejection of background currents and speed of analysis (Simões and Xavier, 2017). This speed, coupled with computer control and signal averaging, allows for experiments to be performed repetitively and increases the signal to noise ratio. Applications of SWV include the study of electrode kinetics with regard to preceding, following, or catalytic homogeneous chemical reactions, determination of some species at trace levels, and its use with electrochemical detection in HPLC (Soriano, 2014).

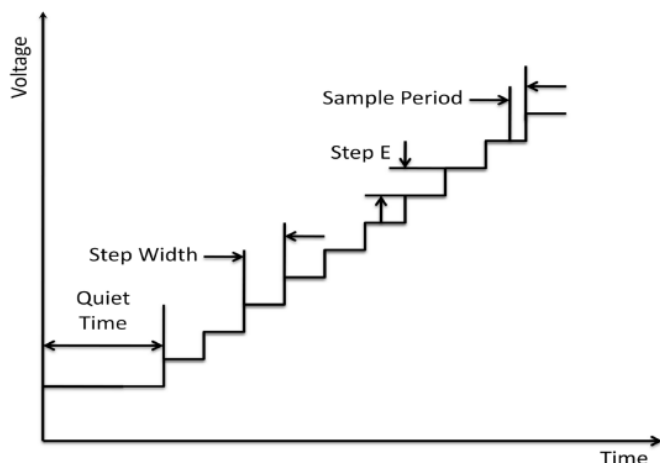


Figure 2. 14: Square wave voltammetry potential sweep.

Adapted from(Brett and Brett, 1993)

In conclusion, there are a number of voltammetric techniques all of which have a variety of characteristics of interest that can be used in the development of biosensors.

2.9: Immobilization methods

Immunosensor characteristics such as sensitivity, specificity, selectivity, stability, reproducibility and response time are dependent, to a great extent, on the antibodies/antigens used for the immobilization. Maintenance of the native protein structure, biological activity and a good orientation are some key parameters that need to be optimized in order to obtain efficient immunosensors with good performance. The immobilizations method not only affects the stability of biomolecules, but also affects the immune-recognition event of antibodies towards antigens, making the immobilization process a crucial step for the immunosensor construction (Sassolas et al., 2011).

Assemblies of immunosensors are classified into physical and chemical methods. Physical methods involve adsorption and entrapment while chemical methods include cross-linking, affinity and covalent attachment. It is also possible to use a combination of them, or to include nanomaterials, such as nanoparticles, to improve the general properties of the immunosensors (Ronkainen & Okon, 2014).

2.9.1: Physical immobilization

Physical methods are usually performed with biocompatible materials and solutions, in order to avoid damage of antibodies/antigens. The principal problems of these methods are related with the stability of biomolecules, blocking the immunorecognition active sites of antibodies/antigens and non-specific adsorption. (Shen *et al.*, 2017)

Direct adsorption of antibodies/antigens on solid supports remains the easiest method to construct functional immunosensors. The adsorption phenomenon is controlled by electrostatic and hydrophobic interactions and van der Waal's forces, Adsorption is commonly done using a fixed amount of antibodies/antigens in contact with solid surfaces and then washing away unadsorbed molecules (Rao *et al.*, 1998). Associated problems could occur, because these biomolecules may desorb with physical or chemical changes, and are easily affected by the non-specific adsorption of other proteins (Schramm *et al.*, 1993).

In immunosensor construction, entrapment of biomolecules represents a more stable alternative than simple adsorption. Physical entrapment of antibodies/antigens inside micro-pores of polymers, three dimensional matrices or carbon pastes could be used, and these are similar to some enzymatic biosensors. However, the active sites of antibodies/antigens need to be available to perform the immunorecognition event. This methodology can diminish the number of available sites or completely block them. Some strategies have overcome those problems and are used for the detection of enterotoxins (Sun *et al.*, 2011;(Susmel *et al.*, 2005) and pesticides (Sun *et al.*, 2011).

2.9.2: Chemical immobilization

Chemical immobilization methods involve the use of chemical reactions to attach antibodies/antigens on solid supports, or the chemical modification of these biomolecules in solution and their posterior immobilization (Schramm *et al.*, 1993). Chemical methods present inherent risks to antibodies/antigens, due to a possible and irreversible cross-linking between them, complete modification of their properties, or complete denaturation due to the presence of harsh chemicals and/or conditions. Despite these associated problems, they present an excellent alternative to physical methods, because they offer more control, stability and sometimes the ability to orient the immobilization through specific groups present in the biomolecules (Schramm

et al., 1993).

Cross-linking is a straightforward method that entails the formation of covalent bonds, either by cross-linking of antibodies/antigens or with the addition of inert proteins such as BSA (Simons *et al.*, 2002), (Macieira-Coelho and Avrameas, 1973) This method is achieved by incorporating bifunctional agents such as glutaraldehyde or gloxal, either directly onto the surface or after the adsorption of the antibodies/antigens. An alternative is to perform this method in solution, depositing the cross-linked biomolecules after. Some examples can be found using modified screen printed electrodes with chitosan and glutaraldehyde (Bonel *et al.*, 2010) .

Physical methods are usually performed with biocompatible materials and solutions, in order to avoid damage to antibodies/antigens. Principal problems of these methods are related with the stability of biomolecules, blocking the immunorecognition active sites of antibodies/antigens and non-specific adsorption.

Direct adsorption of antibodies/antigens on solid supports remains the easiest method to construct functional immunosensors. The adsorption phenomenon is controlled by electrostatic, hydrophobic interactions and van der Waal's forces. However, adsorption is commonly done using a fixed amount of antibodies/antigens in contact with solid surfaces, washing away unadsorbed molecules. Associated problems could occur, because these biomolecules may desorb with physical or chemical changes, and are easily affected by the non-specific adsorption of other proteins.

Entrapment of biomolecules represents a more stable alternative than simple adsorption in the immunosensor construction. Physical entrapment of antibodies/antigens inside micro-pores of polymers, three dimensional matrices or carbon pastes could be used. This physical entrapment is similar to some enzymatic biosensors used. However, the active sites of antibodies/antigens need to be available to perform the immunorecognition event. This methodology can diminish the number of available sites or completely block them. Some strategies have overcome those problems and are used for the detection of enterotoxins (Sun *et al.*, 2011 and Susmel *et al.* 2005) and pesticides (Sun *et al.*, 2011).

In affinity immobilization the oriented and site specific method uses immobilized active molecules e.g. avidin, lectin, etc., Site orientation is achieved using antibodies/antigens with active groups, such as biotin, carbohydrates, etc., that specifically bind the active molecules. Detection of a toxin using a biotin-BSA-gold nanoparticles approach has been studied for the detection of a mycotoxin

(Sojinrin *et al.*, 2019), another study used biotinylated antibodies for the detection of the sex hormone, estradiol (Ojeda *et al.*, 2012).

Covalent attachment is a prominent and frequently used immobilization method, where surfaces are first activated using reagents and afterwards antibodies/antigens are joined covalently through a specific chemical group existent in them. For this method, it is possible to also use pre-activated surfaces. Several approaches can be used in order to assemble an immunosensor, for example immobilization on functionalized controlled pore glass beads(Lates *et al.*, 2012), or using an iridium oxide conducting matrix and immobilization through the generated aldehyde groups (Wilson, 2005).

Self-assembled monolayers are of exceptional importance because of their inherent properties for formation of immunosensors, not only by the formation of well-ordered and closely packed structures on metal surfaces, but also because of the presence of functional groups that can be linked easily to antibodies/antigens through a covalent linkage. Self-assembled monolayers of alkanethiols are shown in Figure 2.15. A diluted solution of thiol is used for the formation of well-ordered self-assembled monolayers of Sulphur groups which are chemisorbed, forming a very strong bond. Sulphur-gold bonds are attained not only by alkyl sulfides but also from similar structures, such as disulfides or related organosulfur compounds (Ghorai & Glotzer, 2007) .

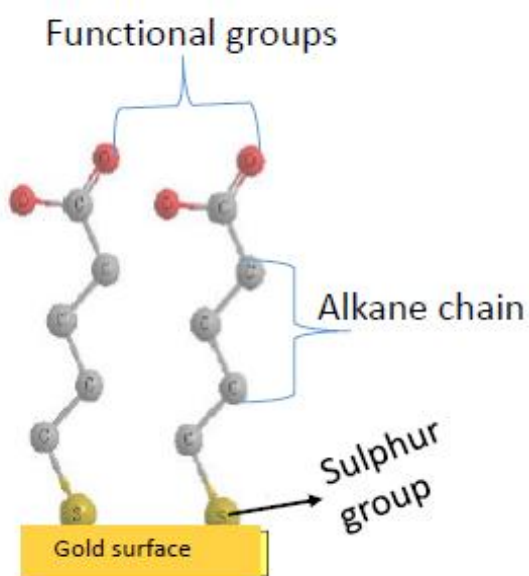


Figure 2.15: Self assembled monolayers of alkanethiols

In this study, chemical immobilization of antibodies was used using glutaldehyde as a cross linker of the antibodies and thiolated protein G.

2.10: Cancer proteins

The elevated presence of some proteins can establish the presence or recurrence of cancer in a person. Although only few proteins are very specific, routine clinical diagnosis of tumor markers has been studied extensively and can be associated directly as predictive factors. An example is the carcinoembryonic antigen (CEA), a glycoprotein used as a part of annual medical checkups in many countries. Detection methods of some proteins are presented in Table 2.4.

Table 2. 4: Immunosensors for detection of some cancer proteins

Tumour marker	Immobilisation	LOD, assay time	Linear range	Reference
PSA & IL-6	Adsorption on SPCEs modified with gold nanoparticles	0.23 pg/mL for PSA 0.30 pg/mL for IL-6 40 min for both	0.23 to 5 pg/mL for PSA 0.30 to 20 pg/mL for IL-6	(Chikkaveeraiah et al., 2012)
AFP	Adsorption on SPCEs modified with gold nanoparticles and a sulfhydryl viologen	0.23 ng/mL	1.25 to 200 ng/mL	(Liang et al., 2022)
CEA	Covalent attachment to a SAM of a dithiol	0.2 ng/mL, in 90 min	0 to 200 ng/mL	(Laboria et al., 2010)
AFP	Entrapped in a chitosan matrix	0.74 ng/mL in 35 min	0 to 20 ng/mL and 20 to 150 ng/mL	(Yu et al., 2004)
CEA	Adsorption on a porous organometallic material	0.18 ng/mL	0.25 to 160.0 ng/mL	(Zhuo et al., 2008)
CEA & AFP	Using microchip capillary electrophoresis and amperometric detection	CEA 0.25 ng/mL AFP 0.13 ng/mL In 15 min	0.5 to 66.0 ng/mL for CEA 0.5 to 80.0 ng/mL for AFP	(Costa et al., 2021)

2.11: Glassy Carbon Electrode (GCE)

GCEs are inert both chemically and electrochemically. They have the advantage of being easy to produce, inexpensive, disposable, portable and highly reproducible. The electrode GCE can be modified using different substances and this improves its sensitivity and selectivity (Serp, 2013). Considering the physical and chemical properties, glassy carbon has become an interesting and broadly applied electrode material (Dekanski et al., 2001). It exhibits a low oxidation rate and a high chemical inertness which, together with very small pore sizes and a small gas and liquid permeability makes it a very convenient electrode (Van der Linden and Dieker, 1980). The goal in lung cancer diagnosis using CEA, and YES1 as biomarkers is to rapidly analyze the level of the tumor marker *in situ*.



Figure 2. 16: Carbon electrode

2.12: Gold Nanoparticles

Gold nanoparticles (AuNPs) play an important role in biomedical applications. AuNPs have been commonly employed for diagnostics, and have seen increasing use in the field of therapeutics. Gold nanoparticles (AuNPs) have been broadly employed in bio nanotechnology based on their distinctive properties and several surface functionalities. The ease of AuNP functionalization provides a multifaceted platform for Nano biological assemblies with antibodies (Mukherjee et al., 2007) and proteins (You et al., 2006). Bio conjugates of AuNPs have also become promising candidates in the configuration of novel biomaterials for the exploration of biological systems (Moyano and Rotello, 2011)

The adaptability of AuNPs has provided beneficial materials for diversity of biomedical applications. In diagnostics, the binding event between the analytes and the AuNPs can modify the physicochemical properties of AuNPs like conductivity, surface plasmon resonance, and redox behavior, resulting to detectable signals (Uehara, 2010). AuNPs also constitute practical

platforms for therapeutic agents, with their high surface area allowing a dense presentation of multidisciplinary moieties such as drugs (Brown et al., 2010) and targeting agents (Khan et al., 2011).

Electrochemical Glassy carbon electrode (GCE) sensors can be coupled with gold nanoparticles (Au-NP) to improve their sensitivity and extend stability of the bio-element. The small size of the nanoparticles allows a high surface area to volume ratio and resulting in unique optical, electronic and catalytic properties that show promising prospects for bio sensing applications (Tothill 2011).

In the immobilization of biomolecules such as antibodies, Au-NPs not only show high affinity for proteins, but also allow prolonged stability of the bio element. Gold nanoparticles also show excellent conductivity leading to enhanced electron transfer between the redox center of the proteins and the electrode surface (Yuan *et al.*, 2009; Arya and Bhansali 2011; Bohunicky and Mousa, 2011; Sassolas *et al.*, 2012) When comparing the various methods like physical, chemical, enzymatic, and biological methods that are used in the synthesis of AuNPs, biological methods using plant extracts have gathered substantial interest because of use of environmentally friendly materials (Chandran et al., 2006)

2.13: Role of *Mangifera indica* in synthesis of gold nano particles

The mango (*Mangifera indica*) plant is a large and leafy tropical all weather tree that yields the mango fruit, in most cases once a year (Figure 2.17).



Figure 2.17: *Mangifera indica* plant

It is well known for its juicy and vitamin C - rich fruit. Its leaves are pinkish amber, or pale green-colored when young and become dark green at maturity. These leaves have manifested various properties, especially as antimicrobials, antioxidants, efficient in the management of diabetes and for prevention of cancer (Vimalraj et al., 2018). Extracts of *Mangifera indica* leaves have also been used in resolving vascular problems and eye complaints associated with diabetes (Muralikrishna et al., 2014a). *Mangifera indica* leaves contain organic compounds such as 3β - taraxerol and ethyl acetate. 3β - taraxerol with insulin, activates GLUT4 and stimulates the synthesis of glycogen, so that it reduces the symptoms of hyperglycemia (Muralikrishna et al., 2014b). *Mangifera indica* leaves can also be used to treat diarrhoea, fever, insomnia and hypertension (Shah et al., 2010), lower high blood pressure (Shah et al., 2010), treat coughs, especially whooping cough and play a key role in treatment of asthma, bronchitis, colds and other respiratory conditions (Shah et al., 2010). The burnt ashes of *Mangifera indica* leaves also make an excellent herbal mouthwash for gum problems (Sharma et al., 2014), reducing pain and bringing relief to the mouth.

The bio reductive potential of the *Mangifera Indica* is responsible for metal Nano particle production (Jacob et al., 2011). Prior studies have been reported that the phytochemicals present in the plant extracts act as reductants in the preparation of metal nanoparticles when treated with

metal salts (Jacob et al., 2011). In this study, leaves extract of *Mangifera indica* was used as a reducing and stabilizing agent of gold (III) chloride trihydrate.

2.14: Summary of Gaps in Knowledge

Diagnosis of lung cancer has already been done using traditional assay methods such as enzyme-linked immunosorbent assay (Butler 2000) radioimmunoassay (Goldsmith 1975), electrophoretic immunoassay (Schmalzing and Nashabeh, 1997), mass spectrometric immunoassay (Diamandis and van der Merwe, 2005) and immune fluorimetric immune-polymerase chain reaction (PCR) assay (Widjoatmodjo *et al.*, 1992), chemotherapy and tissue biopsy. These methods have, however, been found to have some challenges such as, being time-consuming (Palmirota et al., 2018), hazardous to health, and requiring highly trained operators and requiring expensive (Palmirota et al., 2018) and sophisticated instrumentation. They also lack the sensitivity and/or selectivity required in order to detect the disease at an early stage (Castro-Giner et al., 2018).

In addition, while the use of biosensors for detection of lung cancer using electrochemical methods has been done, the focus has been on the detection of a single biomarker in the human serum using screen printed electrodes. This approach has faced some draw backs, for example, low sensitivity and selectivity of the biosensor especially in the detection of lung cancer in the early stages.

This study focused on fabrication of a Nano structured biosensor using glassy carbon electrode modified with thiolated protein G, Glutaraldehyde, gold Nano particles and Horseradish peroxidase enzyme. The biosensor was used for early detection of two biomarkers CEA and YES1 simultaneously in artificial antigens, supernatant of NSCLC cultured cells, cell lysates and Human plasma, and yielded satisfactory results.

CHAPTER THREE: MATERIALS AND METHODS

3.1 Experimental procedures

The experimental procedures used in this study are described in the following sections and subsections.

Briefly, in this work, the fabrication of an immunosensor was done by electrodeposition of gold nanoparticles onto a carbon graphite electrode, incubation of the modified electrode with thiolated protein G and crosslinking antibodies with glutaraldehyde. The resulting immunosensor was characterized both spectroscopically and electrochemically using cyclic and differential pulse voltammetric methods. Gold Nano particles used for labelling secondary antibodies were biosynthesized and characterized using UV VIS, FTIR and Dynamic Light Scattering (DLS).

3.1.1 Instrumentation

Fourier transform infrared spectroscopy (FT-IR) measurements were made on a FT-IR Spectrofluorometer Jasco FP- 6300, Germany. HITACHI Micro ultracentrifuge, CS 150 NX (Hitachi, Tokyo, Japan), SPECTROstar, Nano (BMB LABTECH) was used for BCA analysis, ODYSSY FC was used for imaging and UV Vis analysis was done using UV Vis Jasco- V6300 Spectrofluorometer. All electrochemical measurements (cyclic voltammetry and DPV) were carried out using a potentiostat–galvanostat Auto lab (Metrohm, Netherlands) with the general-purpose electrochemical software equipped with a conventional three electrode system which used a saturated Ag/AgCl (3 M KCl) electrode as the reference electrode, a platinum electrode as the auxiliary electrode, and GCE or modified GCE as the working electrode. Electrochemical results were analyzed using the NOVA software (version 1.11.0) and the origin 9.1 software. Enzyme linked immunosorbent assay (ELISA) measurements were performed using SPECTROstar, Nano (BMB LABTECH) (Multiscan GO, Thermo Fisher Scientific, USA). A mettler Toledo Sven Excellence pH meter with in Lab routine proISM combined pH electrode was used to measure pH. Mycoplasma in cell cultures was tested using Lumat LB 9507, BERTHOLD Technologies. Cell culture supernatant was concentrated using Amicons of MWCO (3,000 and 10,000 kDa size) purchased from Millipore Corporation (Bedford, MA). Electrophoresis was done using Sodium dodecyl-sulfate polyacrylamide gel electrophoresis (SDS-PAGE). Dynamic light scattering (DLS) analysis was done using a Nicomp 380 ZLS.

3.1.2 Materials and Reagents

For the Electrochemical cells, the materials employed include: Working Electrodes (Platinum microelectrode, Glassy Carbon electrode), Ag/AgCl reference electrode and Platinum wire (1.0 mm) as the counter electrode. Other materials included: a pH meter, Magnetic stirrer, Stirring bars, Eppendorf Micropipettes (10, 20,50, 100 and 1000 μ L), Micropipette tips, Desiccator, Vials, 0-5 μ L syringes and 0-100 μ L syringes, emery paper. Microtiter plate reader equipped with a 405 nm filter. Microtiter plate (Nunc C bottom immunoplate 96 well, 446612)

All chemicals and solvents were of analytical grade. Sulphuric acid (H_2SO_4), potassium ferricyanide ($K_3Fe(CN)_6$, (99%), Gold (III) chloride trihydrate (99.9%) ($HAuCl_4 \cdot 3H_2O$), sodium hydroxide, (NaOH) and Hydrochloric acid (HCl) were purchased from Sigma-Aldrich and used without further purification. All solutions were prepared in deionized water (18 WM). A 7.4 pH phosphate-buffered saline (PBS) potassium dihydrogen phosphate (KH_2PO_4), disodium hydrogen phosphate ($Na_2HPO_4 \cdot 7H_2O$), Potassium chloride (KCl), glutaraldehyde, L Cysteine Tween X 10, RPMI-1640 medium, 10% fetal bovine serum (FBS), 5% penicillin-streptomycin (Thermo fisher scientific), Polyclonal YES1 primary antibody purchased from Cell Signaling Technology, secondary HRP conjugated anti-rabbit and anti-mouse, from Thermo scientific, bovine serum albumin (BSA), protein G and 3,3',5,5'-tetramethylbenzidine (TMB) were procured from Sigma-Aldrich. Western blot substrate (Luminol enhancer and peroxidase) were procured from Thermo fisher scientific. Human NSCLC cell lines A549, H2009, H2170, H23 were obtained from CIMA, Navarre, Spain.

3.2. Preparation of plant extracts for biosynthesis of gold Nano particles

Leaves of *Mangifera Indica* were washed with tap water and distilled water then dried under a shade for one week. The dried leaves were ground into coarse powder by a mechanical grinder. As shown in Figure 3.1 B.



Figure 3. 1: Image of Mango leaves (*Mangifera indica*) , before grinding (A) and after drying and grinding (B).

The coarse powder was then passed through different sieves to obtain a fine powder of grain size ≤ 0.5 mm. Ten (10) g of the fine powder was added to de-ionized water (100 mL) and heated for 30 min at 60°C. The residue was then removed by filtration to obtain an aqueous *Mangifera indica* extract. The extract was centrifuged for 15 min at 5000rpm, and the supernatant collected, filtered and stored at -80 °C

The filtrate was used as both a reducing and stabilizing agent. Gold (III) chloride hydrate (HAuCl_4) was purchased from Sigma and used without further purification. De-ionized water was used throughout the experiments.

3.3 Preparation of Thiolated protein G

Thiolated protein G was prepared according to the procedure by Fowler et al (2007) with few modifications. 60 μL of protein G was added to 20 mM of L- cysteine which had been prepared by dissolution in degassed Phosphate-buffered saline (PBS) for 30 min at 4 °C. The excess L- cysteine was immediately removed by centrifugal filtration at 3500rpm for 20 minutes and the protein was concentrated to 100 $\mu\text{g/L}$ using PBS (Fowler et al., 2007).

3.4 : Biosensor Construction

3.4.1: Preparation of glassy carbon electrode

A glassy carbon electrode (GCE, diameter 3 mm) was polished using 0.3 μM alumina slurry and cleaned using an ultrasonic cleaner with HNO_3 (1:1), acetone, anhydrous ethanol, and double distilled water. The GCE was then rinsed in an ultrasonic bath using doubly distilled water and absolute ethanol for 5 min and soaked in a solution containing a 7:3 v/v sulfuric acid to peroxide ratio ($\text{H}_2\text{SO}_4:\text{H}_2\text{O}_2 = 7:3$ v/v) for 15 min.

The electrode was then electrochemically treated in a 3-electrode cell by cycling the potential between -0.4V and $+1.0\text{ V}$ in $0.1\text{ M H}_2\text{SO}_4$ to ensure no interference with organic compounds. Finally, the electrode was rinsed with double distilled water, dried at room temperature free from dust in readiness for use.

The performance and reproducibility of the electrode was done using calculations based on the Laviron's equation to estimate αn and k_s values as follows:

$$E_p = E^0 + (RT/\alpha nF) [\ln (RTk_s/\alpha nF) - \ln v] \quad \text{Equation 3.1}$$

Where:

α is the electron transfer coefficient

K_s is the standard rate constant of the surface reaction

v is the scan rate

n is the electron transfer numbers

E^0 is the formal potential.

K_s and αn values can be obtained from the intercept and slope of the linear plot of E_p with respect to $\ln v$, if the value of E^0 is known. (Laviron 1979)

After determination of the maximum current in the cyclic voltammogram, the electron transfer coefficient, (α) number of electron transferred (n) and the standard rate constant of the surface reaction (K_s) were calculated from this equation. The ratio of the active area to the theoretical area

gave a percentage that is a measure of the performance and reproducibility of the Glassy Carbon Electrode. These experiments were performed at room temperature.

About 80 mL solution comprising of 0.1 M PBS with 1 mM $[K_3Fe(CN)_6]$, 0.1 M KCl solution was pipetted into the 3-electrode cell, and covered the surface of the electrodes. Briefly, all electrochemical measurements (cyclic voltammetry and DPV) were carried out with potentiostat–galvanostat AUTLAB71016 Potentiostat electrochemical workstation (PGSTAT 12 Netherlands) using a conventional three electrode system with saturated Ag/AgCl (3 M KCl) electrode as the reference electrode, platinum electrode as the auxiliary electrode, and modified GCE as the working electrode. Electrochemical results were analyzed using the NOVA software (version 1.11.0) and the Origin® 9.1 software. A scan rate of 0.05 V/s with a step potential of 0.001 V was done. The current was determined in four cycles from -0.4 V to 1.0 V. This was repeated on several sensors to evaluate the reproducibility of the signal (Wang 2006).

3.4.2: Synthesis of gold nanoparticles

3.4.2.1: Synthesis of gold nanoparticles (AuNPs)

Synthesis of gold nanoparticles (AuNPs) was done to obtain the nano particles that would be used for labelling the CEA secondary antibody. The aim of labeling the secondary antibodies was to distinguish between the CEA and YES1 signals during the simultaneous detection of the biomarkers. The nano particles were also used for signal amplification (Chiang et al., 2019) .

The *Mangifera indica* filtrate obtained in section 3.2 above was thawed and 200 μ L of the filtrate was added dropwise to 10 mL of HAuCl₄ (1 mM) at 70 °C and stirred at 200 rpm for 15 minutes. The color change from orange to red wine signaled the bio reduction process, and confirmed the formation of AuNPs (Xin Lee et al., 2016). The biosynthesized Au NPs were ultra-centrifuged at 20,000 rpm for 15 min and the pellets were washed with distilled water. The centrifuging and re-dispersing process was repeated three times. The pellets were re dispersed in distilled water forming a gold nano particles mixture which was pink in color. The mixture was kept in the dark at room temperature to prevent any further reduction of gold ions. UV-visible spectrometric measurements of the mixture were run between 300–700 nm, and the spectra analyzed. The AuNPs size were also analyzed using Dynamic light scattering (DLS) (Malvern, UK). Fourier transform infrared (FT-IR) spectra were recorded on a spectrum RX 1-one instrument in the diffuse reflectance mode at a resolution of 4 cm^{-1}

3.4.2.2: Electrodeposition of gold nanoparticles

The fabrication of the gold nanoparticles (AuNPs) layer on the glassy carbon electrode (3 mm dia.) was done using electrochemical deposition (Wang et al., 2009) and (Zhao et al., 2009). The mechanism and kinetics of electrodeposition of Au nanoparticles on bare glassy carbon (GC) was investigated in the system GC/1 mM $\text{HAuCl}_4 \cdot 3\text{H}_2\text{O}$ in 0.1 M HCl. The Au- nanoparticles were formed on the electrode surface using cyclic voltammetry for 25 cycles in a potential range of -0.4 V and 1.0 V in 1 mM $\text{HAuCl}_4 \cdot 3\text{H}_2\text{O}$ in 0.1 M HCl which had been deaerated using nitrogen gas. The choice of 25 cycles was done after optimization. Gold nano particles were used for electrode modification due to their unique properties, such as good biocompatibility, excellent conductivity, effective catalysis, high density, and high surface-to-volume ratio (Chiang et al., 2019). Thus AuNPs were used to provide a platform for increased protein loading so as to efficiently improve the charge transfer between analyte and the electrode surface (Chiang et al., 2019).

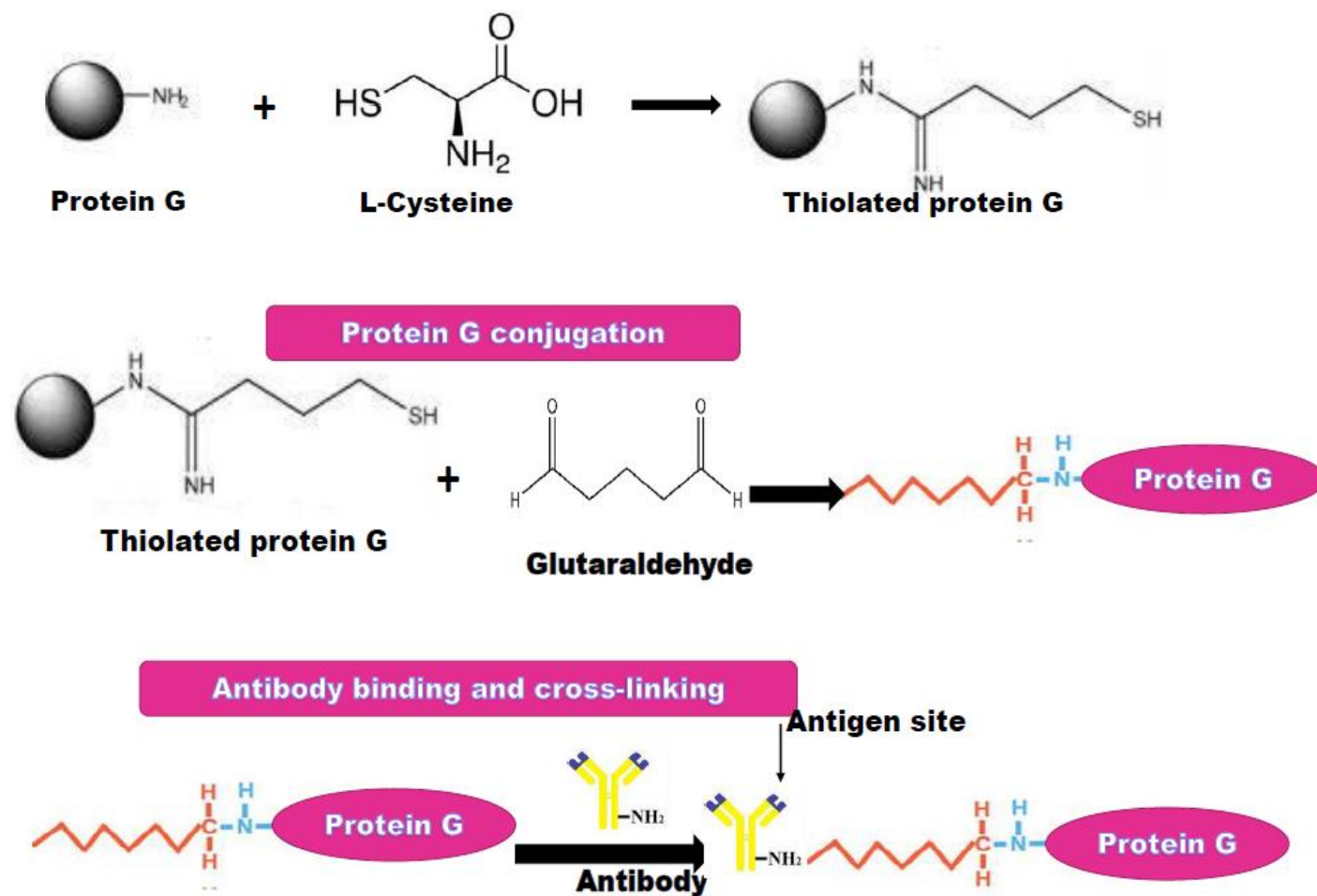
3.4.3: Synthesis of secondary antibody (AB_2)–AuNPs conjugate

A 3.0 mL sample of the synthesized gold nanoparticles obtained from section 3.4.2.2 was thoroughly mixed with AB_2 (AB_2 12 $\mu\text{g}/\text{mL}$ in 1 mL of BSA) and the mixture stirred for 24 h at 4 °C using a magnetic stirrer in an orbital shaker and in dark. 1% BSA was, then, added in order to block the remaining active sites of the gold nanoparticles. Centrifugation was carried out at 7000 rpm for 15 minutes and the resulting AB_2 -HRP/AuNPs bio conjugate was dispersed in 1 mL PBS solution and stored at 4 °C. The bio conjugate was immobilized on the working electrode and was used to label CEA antibodies during simultaneous detection of YES1 and CEA biomarkers.

3.4.4: Electrode surface modification

After electrodeposition of AuNPs (section 3.4.2.1) the electrode was washed with ultrapure water. 15 μL of 20 mM thiolated protein G was incubated on the electrode (i.e. AuNp/GCE) for 4 hours at 4 °C, whereby the thiol sites of the L-cysteine were chemisorbed onto the surface of the AuNp/GCE. This was termed as the PTG/AuNp/GCE electrode. After another washing with ultrapure water, the PTG/AuNp/ GCE was incubated for 1 hour by placing it in 15 μL of 4% glutaraldehyde (GA) at room temperature for the purpose of crosslinking the antibody with the thiolated Protein G (PTG). This electrode was termed as the GA/PTG/AuNp/GCE.

The GA/PTG/AuNp/GCE was, then, thoroughly washed with sterile deionized water to remove any loosely bound glutaraldehyde. Subsequently, 10 μL each of the polyclonal rabbit YES1 and CEA antibodies were drop casted onto the surface of the GA /PTG /AuNp/ GCE and the electrode incubated overnight at 4 $^{\circ}\text{C}$. This electrode was referred to as the CEA/YES1Ab1/GA/PTG/AuNp/GCE. This reaction was based on formation of a bond between the aldehyde group in glutaraldehyde and the amine group in thiolated protein G. The glutaraldehyde then formed a bond with the YES1 and CEA antibodies which were prepared in 5% BSA solution. The antibodies attached to the glutaraldehyde layer through their non-antigenic regions, leaving the antigen binding sites for binding of the target analyte and antibody immobilization process using PTG/GA as shown in Scheme 3.1.



Scheme 3. 1: Schematic reactions illustrating protein G conjugation with glutaraldehyde covalent immobilization of primary antibodies

The surface of the modified electrode was rinsed repeatedly with tween buffer to remove any unbound antibodies from the surface.

The summarized procedure for electrode modification is illustrated in Figure 3.2 below.

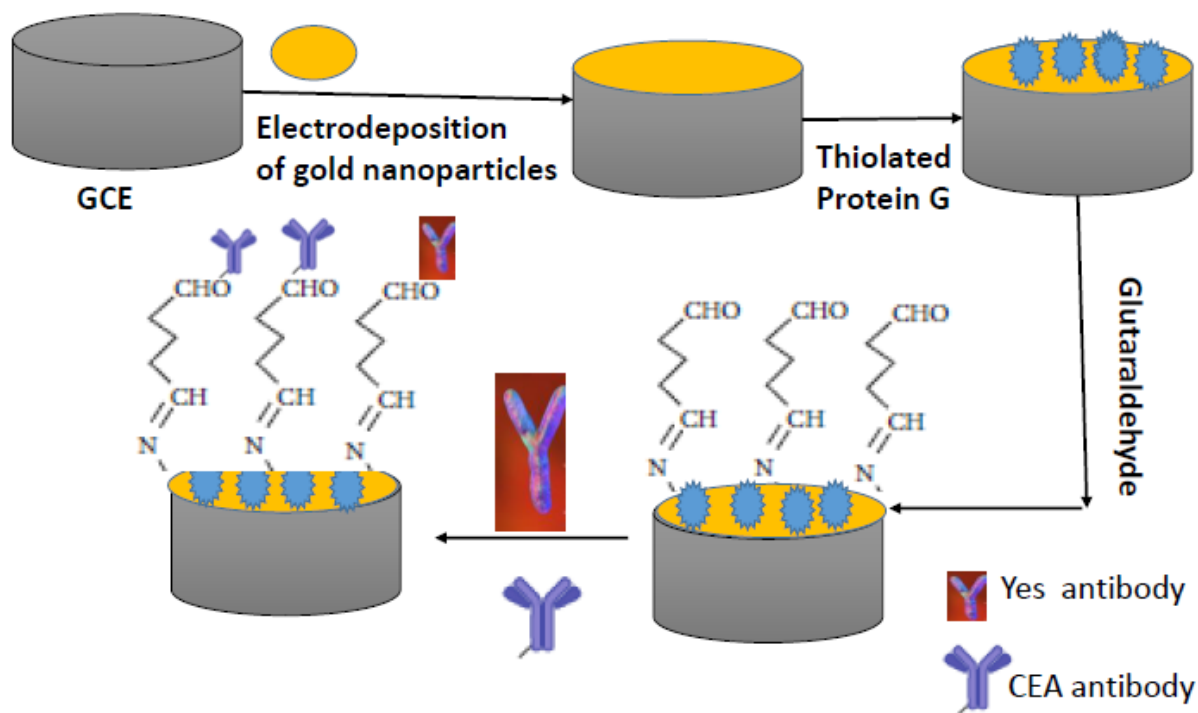
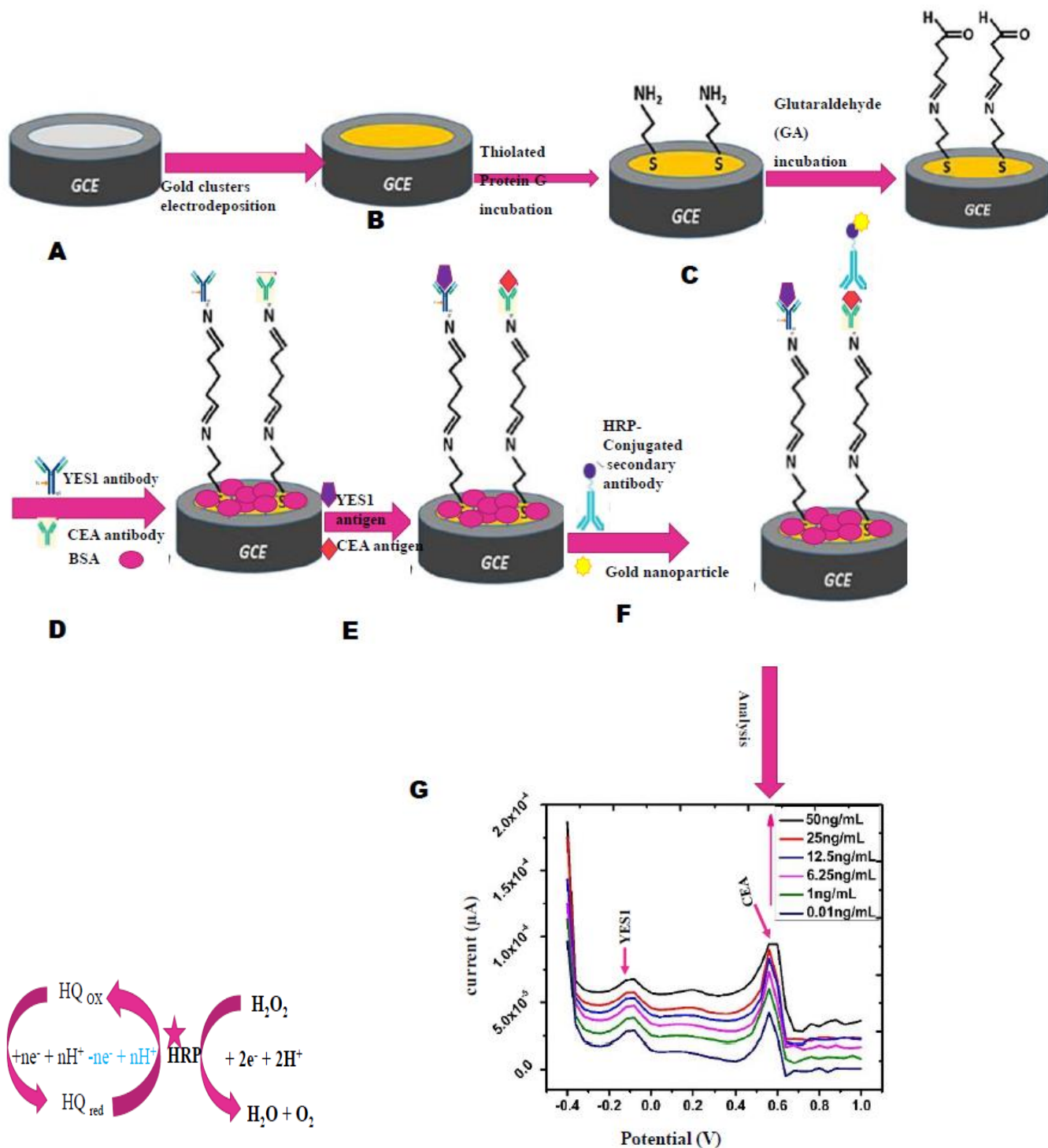


Figure 3. 2: A schematic representation of the electrode modification process and consequent immunosensor formation.

The modified electrode, BSA/CEA/YES1Ab 1 /GA/PTG/Au/ GCE, was then blocked using 10 μL of 3% of BSA to prevent nonspecific binding. This was the immunosensor. The immunosensor was stored at 4⁰C in PBS pH 7.4 when not in use. Scheme 3.2 shows the complete schematic illustration of the stepwise electrochemical immunosensor fabrication process.



Scheme 3. 2: Schematic illustration of the stepwise electrochemical immunosensor fabrication process. (A). Electrodeposition of gold nanoparticles(AuNPs) on GCE. (B). Modification of GCE/AuNPs with thiolated protein G (TPG). (D) Incubation of GCE/AuNPs/TPG with glutaraldehyde (GA). (D) Immobilization of capture antibodies YES1 and CEA on the modified electrode and blocking with BSA. (E) incubation with the analyte containing antigen CEA and YES1. (F) Sandwiching with secondary antibody. (D) DPV analysis

For the measurement procedures, a classical sandwich immunoassay was used for determination of CEA and YES1 protein. First, the BSA /CEA/YES1Ab 1 /GA/PTG/Au/ GCE was incubated with 10 μ L of a certain concentration of CEA and YES1 standard antigen (Ags) for 30 min at 37 $^{\circ}$ C, followed by a washing step with 1% Tween-20 and 0.1 MPBS solution. Subsequently, the modified electrode (Ags/BSA /CEA/YES1Ab 1 /GA/PTG/Au/ GCE) was incubated with 10 μ L each of YES1Ab2- HRP and CEA Ab2-HRP-AuNps solutions for 30 min at 37 $^{\circ}$ C. These were used as labels for CEA. The electrode was then washed with 1% Tween-20 and 0.1 MPBS solutions. Finally, the electrochemical detection was performed under nitrogen atmosphere in PBS which had been deaerated with nitrogen gas for 15 min.

The electrochemical characterization of the immunosensor was done using the Differential Pulse Voltammetry (DPV) to confirm the activity and affinity of the antibodies and their detection limits. These experiments were repeated with other CEA and YES1 concentration. To optimize the electrochemical readings from the biosensors, several parameters, for example pH, antibody dilution and incubation temperature, were optimized. The developed electrochemical biosensor was used to detect lung cancer bio markers in artificial antigens and human plasma. The experiments were conducted at room temperature.

3.5 : Optimization procedures

Parameters involved in the preparation of an immunosensor play a significant role in its voltammetric response. Hence, the immunosensor was optimized in order to obtain a maximum voltammetric response, by optimizing key parameters such as amount of antibody immobilized on the electrode surface, antibody dilution, incubation time of the analyte and the pH of the solution towards the immunosensor. A cyclic differential wave E-field was applied in order to accelerate the movement of antibodies towards the electrode surface which resulted in faster immobilization time.

3.5.1: pH Optimization

In order to determine the optimum pH of the immunosensor, a series of electrolytes comprising of in 0.1 M PBS with 1mM $[K_3Fe(CN)_6]$, 0.1 M KCl and 4mM H_2O_2 were prepared. A Mettler Toledo Sven Excellence pH meter with In Lab routine proISM combined pH electrode was used to

measure pH. The pH range was 6.0 to 7.8. pH of solution and was adjusted using 1M HCl and 1M NaOH solution. The optimum pH was determined by observing the DPV oxidation peak current for both CEA and YES1. The pH solution with the highest oxidation peak current was considered to be the optimum pH.

3.5.2: Antibody dilution

To determine the best antibody dilution for the immunosensor, a series of antibody dilutions for CEA and YES1 were done. The antibody dilution was done using 5 % BSA solution. The dilution ratios investigated were 1:200, 1:500, 1:1000, 1:1500 and 1:2000 for both CEA and YES1. After dilution, 15 μ L of CEA and YES1 were immobilized onto the modified glassy carbon electrodes with gold Nano particles, thiolated protein G and glutaldehyde. The immobilization of the antibodies for CEA and YES1 were done on different electrodes so as to determine the best dilution ratio for each antibody. The modified electrodes with the different concentrations of antibodies were kept at 4⁰C overnight, they were washed with tween buffer three times to remove any unbound antibody. The immunosensors were then incubated with 15 μ L of 3% BSA solution used as a blocking solution to prevent nonspecific binding of the antigens, this was done at room temperature. The immunosensor was then incubated with the analyte for 30 minutes at 37 $^{\circ}$ C, this was done to allow antigen antibody reaction. The immunosensor was rinsed again with tween buffer and the DPV oxidation peak current determined using 0.1 M PBS with 1 mM K₃Fe(CN)₆, 0.1 M KCl as electrolyte. Differential Pulse Voltammetry oxidation peak current was determined and recorded for all the antibody dilutions. The antibody dilution that gave the highest DPV oxidation peak current was taken as the optimum dilution for the immunosensor and used throughout the study.

3.5.3: Incubation time

The influence of the incubation time of CEA and YES1 immunosensors was investigated. The immunosensor was incubated in CEA and YES1 solution separately for 10, 20, 30, 40, 50 and 60 minutes at 37 $^{\circ}$ C. After each time of incubation, DPV oxidation peak currents were analyzed. The incubation time which gave the highest oxidation peak current was taken as the optimum incubation time for the immunosensor. This incubation time was used throughout the studies for both CEA and YES1.

3.5.4: Glutaraldehyde dilution

The glutaraldehyde concentration used for crosslinking of CEA and YES1 antibody loaded on the electrode surface were optimized for fabrication of CEA and YES1 immunosensors. The effect of glutaraldehyde concentration was investigated by incubating AuNp, thiolated protein G modified electrodes (GCE/AuNp, Thiolated PTG) with 10 μL of different % dilutions of glutaraldehyde (3%, 3.5%, 4%, and 5%) at room temperature for 2 hours. This glutaraldehyde modified electrodes were further modified with 15 μL of CEA and YES1 antibody separately and finally with 15 μL of 5% BSA. The best % dilution for the glutaraldehyde was determined by observing and recording the DPV oxidation peak currents. The glutaraldehyde (GA) % dilution with the highest DPV peak current was taken as the optimum GA % dilution.

3.6: Electrochemical measurements

After fabrication of the immunosensor, CEA and YES1 antibodies were first used for detection of CEA and YES1 biomarker in artificial antigens, then in cultured cell supernatants and finally in real human plasma samples. Secondly a multiplex immunosensor was fabricated for detection of both YES1 and CEA. The detection was first done in artificial antigens, then in cultured cell supernatants and finally in human plasma samples. Distinct antibodies were used for detection of YES1 and CEA. The antibodies used in the developed immunosensor had two-fold functions:

First, Antibodies captured/bound YES1/ CEA molecules to the sensor surface which decreased the electron tunneling distance between the sensor surface and the YES1 and CEA molecules. The decrease in the tunneling distance allowed electrons generated due to the oxidation of YES1/ CEA to travel to the sensor surface during DPV and generate a current signal. Therefore, lower quantities of YES1 / CEA can also generate a measurable signal and improve sensor performance.

Second, the Antibodies enabled highly specific detection of YES1 and CEA.

In this work DPV for the oxidation of YES1 / CEA was performed so that the magnitude of the resultant oxidation peak could be related to the amount of YES1 / CEA captured by the specific antibodies onto the electrode surface.

3.7: Detection of lung cancer biomarkers YES1 and CEA in cell culture supernatants and cell lysates

Detection of lung cancer biomarkers was done using the fabricated immunosensor. Lung cancer biomarkers (CEA and YES1) were detected using the fabricated immunosensor in cultured NSCLC cultured cell supernatants, cell lysates, artificial antigens and in human plasma. The optimized immunosensor was assessed for its ability to quantify YES1 and CEA in cell culture supernatant of A549, cell line using DPV. The detection was done in 5 mM $K_3[Fe(CN)_6]$ and 0.1 M KCl supporting electrolyte at a scan rate of 50 mV s⁻¹.

To investigate the validity of the use of the oxidation peak in the assessment of CEA and YES1 concentration in the cultured cell supernatant, varying amounts of A549 cells were incubated for 48 hours in serum free medium. The supernatant that was obtained was centrifuged at 1200 rpm for 5 minutes to remove dead cells and then concentrated using amicon 3 kDa. 20 μ L of the supernatant of YES1 and CEA were separately incubated with the immunosensors for 30 minutes at 37 °C. The amount of YES1 and CEA released in the supernatant was then detected using DPV.

3.7.1: Culture and maintenance of human cell lines

Human cell lines, H2009, A549, H23 and H2170 cells were grown in RPMI-1640 medium (Gibco). All media was supplemented with 10% FBS (Gibco) and 5% penicillin-streptomycin (Lonza). Cells were grown in a humidified atmosphere at 5% CO₂ and 37 °C. Cells were seeded in six-well plates for immunoblotting and in T 25 and T 75 flasks for further analysis.

3.7.2: Mycoplasma testing

All cell lines were tested and were found to be free of mycoplasma contamination (MycoAlert Mycoplasma Detection Kit, Lonza, LT07-418).

Approximately 1.5 mL cell culture medium was collected from a fairly confluent cell medium and then centrifuged for 5 minutes at 2000 rpm to remove any dead cells. The supernatant was transferred into cytometry tubes and 50 μ L of the supernatant and 50 μ L of the positive control was added to the cytometry tubes. A 50 μ L volume of the MycoAlert reagent was added to the supernatant and incubated for 5 minutes. Absorbance was measured using Lumat LB 9507 BERTHOLD Technologies to obtain the 1st reading. 50 μ L of the MycoAlert substrate was then added, and the mixture incubated for 10 minutes. Absorbance was measured again to obtain the 2nd reading. To establish the level of mycoplasma in the cultured cells, the 2nd reading was divided

by the 1st reading. If the ratio obtained was less than one unit (<1) then the culture was considered to be mycoplasma-free and if it was greater than one unit (>1), the culture was considered to be contaminated. If the results obtained were between 0.9 and 1.1 the testing was repeated after two days.

3.7.3: Sub culturing and cell counting

Sub culturing of the cells was done using the trypsinization procedure for adherent cells as indicated by Sigma Aldrich protocols after attaining 80–90% confluence. Medium of adherent cells was aspirated and the cells washed with phosphate buffer saline (Lonza) without calcium and magnesium ions. Trypsin EDTA X1 (Gibco) was added to the cells and the mixture incubated at 37 °C for 5 minutes to allow the cells to detach from the culturing flask. Culture medium was added to neutralize the trypsin and the total volume was centrifuged at 1200 rpm for 5 minutes. The supernatant was discarded and the pelleted cells were re-suspended in fresh medium for subsequent procedures.

Viable cells were counted using a hemocytometer and Trypan blue for experiments which required specific number of cells. A summary of the procedure is presented in Figure 3.3.

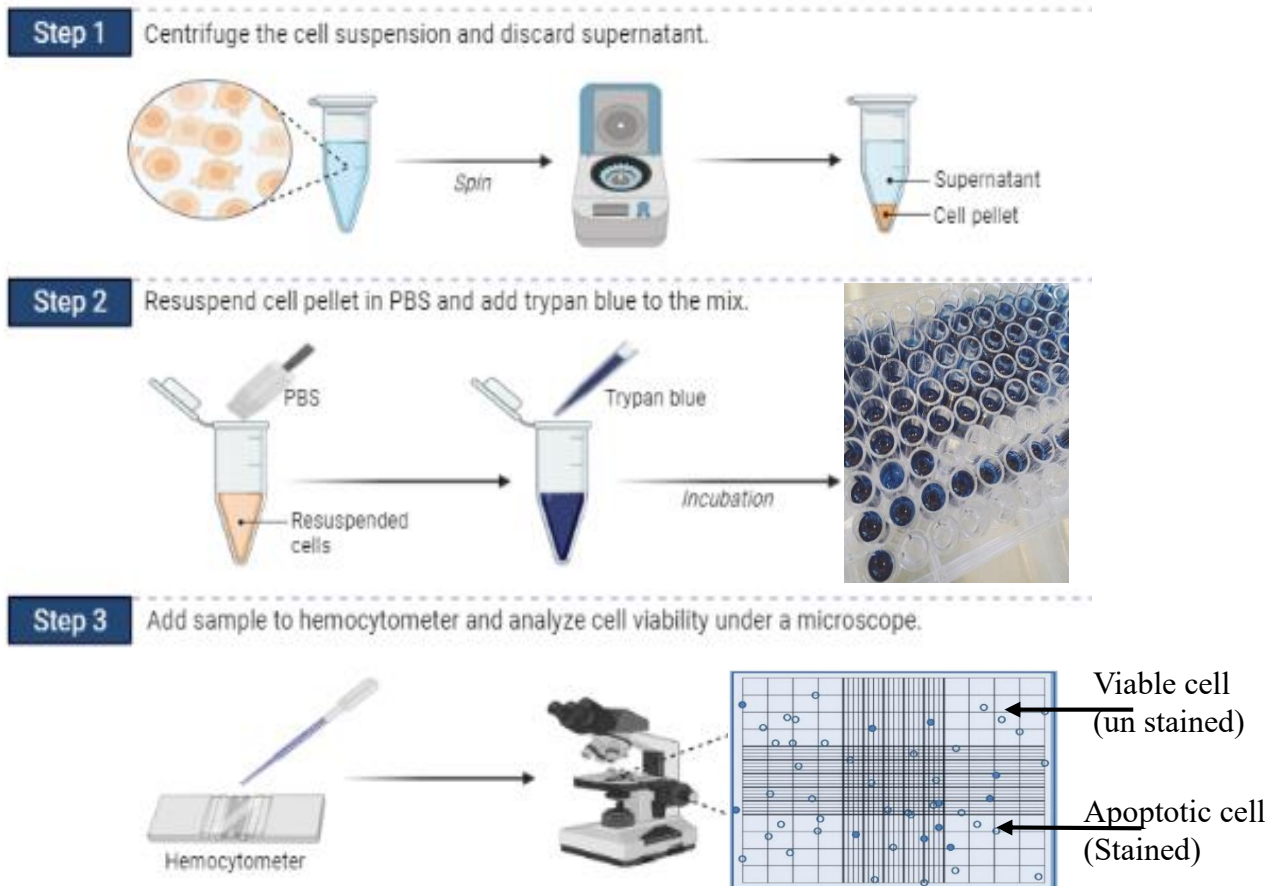


Figure 3. 3: Cell lines sub-culturing and cell counting process

3.7.4: Freezing, thawing and protein extraction

After the trypsinization process, the cell pellets were suspended in freezing medium (10% dimethyl sulfoxide (DMSO), 10% FBS and 80% culture), aliquoted into cryovials (Nunc), stored for 2 hours at $-20\text{ }^{\circ}\text{C}$ and then transferred to a freezer at $-80\text{ }^{\circ}\text{C}$.

Cell thawing was done by brief incubation of cryovials at $37\text{ }^{\circ}\text{C}$ after which the cells were transferred to 25 cm^3 culture flasks with 5 mL fresh culture medium. After 24 hours, the medium was aspirated to eliminate the DMSO and the dead cells, and then fresh medium was added and the cells incubated in a humidified atmosphere at 5% CO_2 and $37\text{ }^{\circ}\text{C}$ (Figure 3.4)

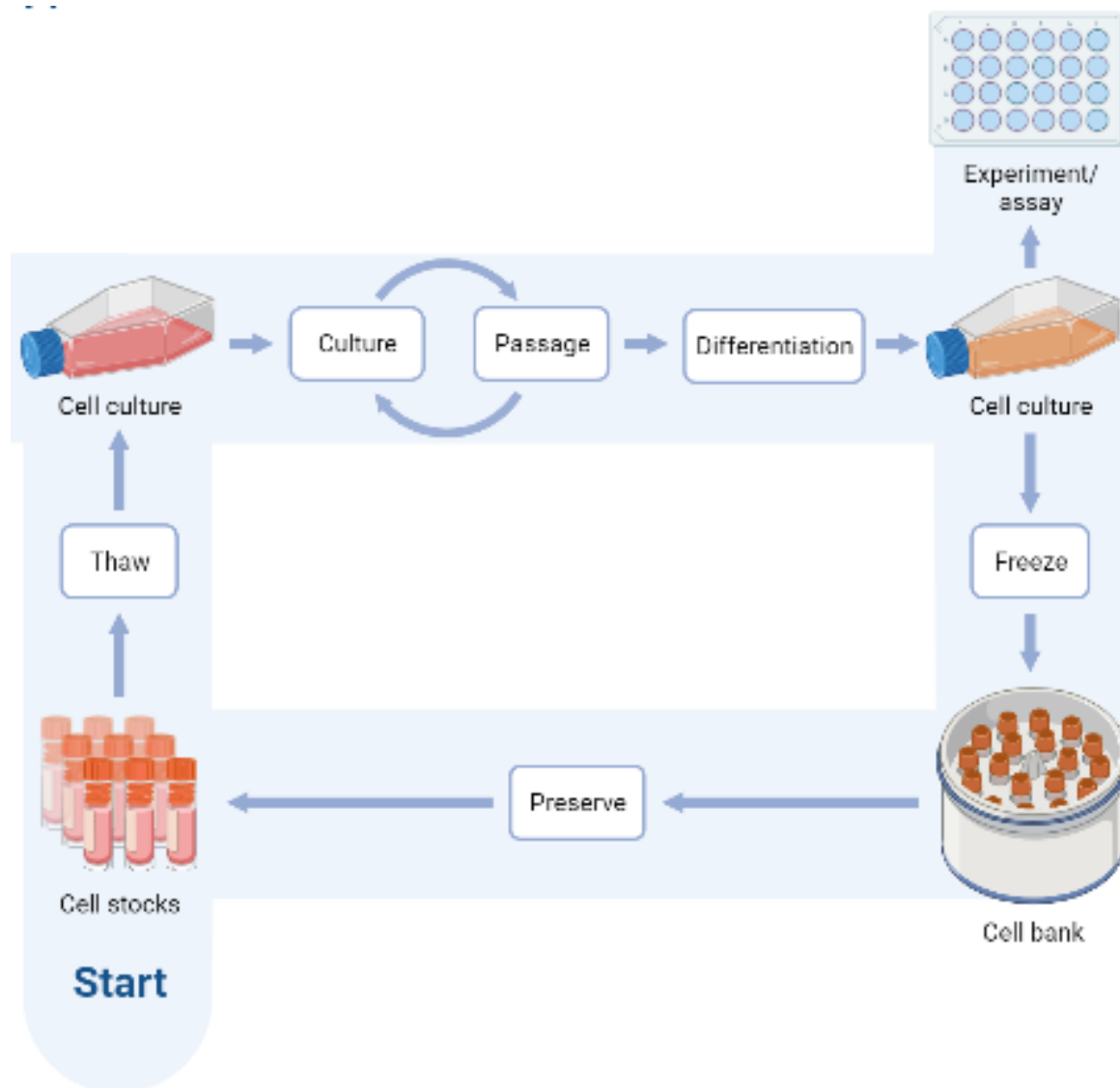


Figure 3. 4: Freezing and thawing procedure of the cultured cells

The protein was extracted using RIPA (Radio immunoprecipitation assay) buffer containing 50 mM Tris-Cl (pH 7.5), 50 mM NaCl, 1% Triton X- 100, 0.1% SDS, protease inhibitor (1 mM PMSF), phosphatase inhibitor (50 mM sodium fluoride and 1 mM sodium orthovanadate). The cell lysate was obtained by centrifugation and stored at -80°C for further use.

3.8: Western blot

Expression of recombinant human YES1(rYES1) and CEA expression in H2009, A549, H23 and H2170 cell lines in lysate and supernatants were detected using immunoblotting. YES1, CEA and H2009, A549, H23 and H2170 cell lines lysate and supernatants were loaded in each well in

Sodium dodecyl-sulfate polyacrylamide gel electrophoresis(SDS-PAGE). Polyclonal Rabbit anti-YES1 antibody of 1: 1000 dilutions was used to probe the blots. Anti-Rabbit HRP conjugated antibody of 1: 2000 dilutions were used for the secondary antibody. Blots were developed using chemi luminescence western blot substrate. Serum-free supernatants and cell lysates were resolved separately on sodium dodecyl sulphate polyacrylamide gel electrophoresis gels and transferred onto polyvinylidene difluoride membranes. Membranes were blocked with BSA for 1 hour, followed by incubation with primary antibodies in 5% BSA at 4 °C overnight with slight shaking. After removing excess primary antibodies by washing the membranes in Tris-buffered saline containing 0.1% Tween-20 (TBST, 3 × 5 minutes each), secondary anti-Rabbit antibodies conjugated with horseradish peroxidase were incubated with the membranes for 1 hour at room temperature. Membranes were then washed in TBST, three times for 5 minutes each and visualized with enhanced chemiluminescence detection reagent (Thermo Fisher Scientific).

3.8.1: Immunoblotting

For studying changes and protein levels in cell lines and cell lysates, the western blot technique was used. In order to prepare materials for western blotting, protein extraction and quantification was done for both cell culture supernatant and cell lysates for cancerous cells in four cell lines.

3.8.1.1: Protein extraction and quantification of Cell lysates

Four cell lines A549, H2009, H23 and H2170 were cultured using T75 flasks until they reached confluency of approximately 80%. They were washed with PBS, trypsinized, centrifuged at 1200rpm for 5 minutes then washed again with PBS and pelleted. The cells were then lysed using Radio immunoprecipitation assay (RIPA) buffer, Protease inhibitor 1X and Phosphate inhibitor 1X which had been previously chilled at 4 °C. The RIPA buffer had the following composition;

- 1% Triton X-100 (Sigma)
- 0.1% sodium dodecyl sulfate (SDS) (Sigma)
- 10 mM Tris- HCl (Sigma), pH 4
- 150 mM NaCl (Sigma)

The lysate was incubated on ice for 30 minutes and then centrifuged at 13,200 rpm for 30 minutes at 4 °C. The supernatant was obtained and used immediately or stored at -80°C for later experiments.

3.8.1.2: Protein extraction and quantification for Cell line supernatants

The four cell lines were cultured in T75 flasks with serum free medium for 72 hours. The supernatant was centrifuged at 1200 rpm for 5 minutes to remove any cell debris. The supernatant was concentrated using Amicons of molecular weight cut-off (MWCO) of 3 and 10 kDa size for maximum sample recovery. Ultra-4 Amicon was filled with up to 4 mL media volume ensuring that the screw closure was fully sealed. The supernatant was centrifuged for 30 minutes at 4000 rpm at 4 °C using a swing bucket centrifuge type. The filtrate container was emptied, the concentrator tube refilled with additional sample and the centrifuge process repeated until all the sample was loaded. Finally, the concentrate was recovered from the insert tube with a pipette. The supernatant obtained was used immediately or stored at – 80 °C.

Protein quantification was done using the Bicinchoninic Acid Assay (BCA) protein Assay kit (Pierce). The calorimetric kit is based on the fact that, in the presence of proteins, Cu^{2+} in an alkaline medium is reduced to Cu^+ (Biuret reaction). Cu^{2+} reacts with BCA, giving a purple colour. The absorbance obtained is directly proportional to the amount of protein present in the well. Plate reads were done at 562 nm in the plate reader SPECTROstar Nano (BMG LABTECH) with the MARS Data analysis software. The sample's protein concentration was determined by interpolating the absorbance value in a standard curve, which was constructed from known concentrations of Bovine Serum Albumin (BSA) protein (Pierce). All protein quantification processes were done in triplicate.

3.8.2: Electrophoresis and transference.

To investigate Electrophoresis and transference, 30 μL of the protein sample containing YES1 and CEA was mixed with 5 μL NuPage LSD sample buffer (Invitrogen). A 1.5 μL of β -mercaptoethanol (Sigma) was added to the mixture. The mixture was diluted to make up to 30 μL with sterile Braun water. Samples were denatured at 95°C for 10 minutes.

Electrophoresis was done in a commercial 12% NuPage Bis- Tris polyacrylamide gel (Thermo Fisher) along with a protein molecular marker (Precision Plus Protein Standards Dual colour; Bio-Rad) in order to determine the protein size. Electrophoresis was carried out using Mops running buffer (Thermo Fisher) for approximately 2 hours at a constant voltage of 130 V.

Once the proteins were separated according to molecular weight, they were transferred to a nitrocellulose membrane (0.22 μm pore diameter, Bio- Rad). Wet transference was done using

transfer buffer consisting of 10% Tris-Glycine Buffer 10X (25mM Trizma base, pH 7.4), 20% Methanol and 70% deionized water.

A constant voltage of 100 V was applied for one hour after which the membranes were stained with a Ponceau red solution(Sigma) in order to access the presence of the proteins in the membrane. Finally, the membranes were washed with TBS- Tween buffer (20mM Trizma base and 150mM NaCl, pH 7.4, supplemented with 0.1% Tween 20 (Thermo Fisher) (Figure 3.5).

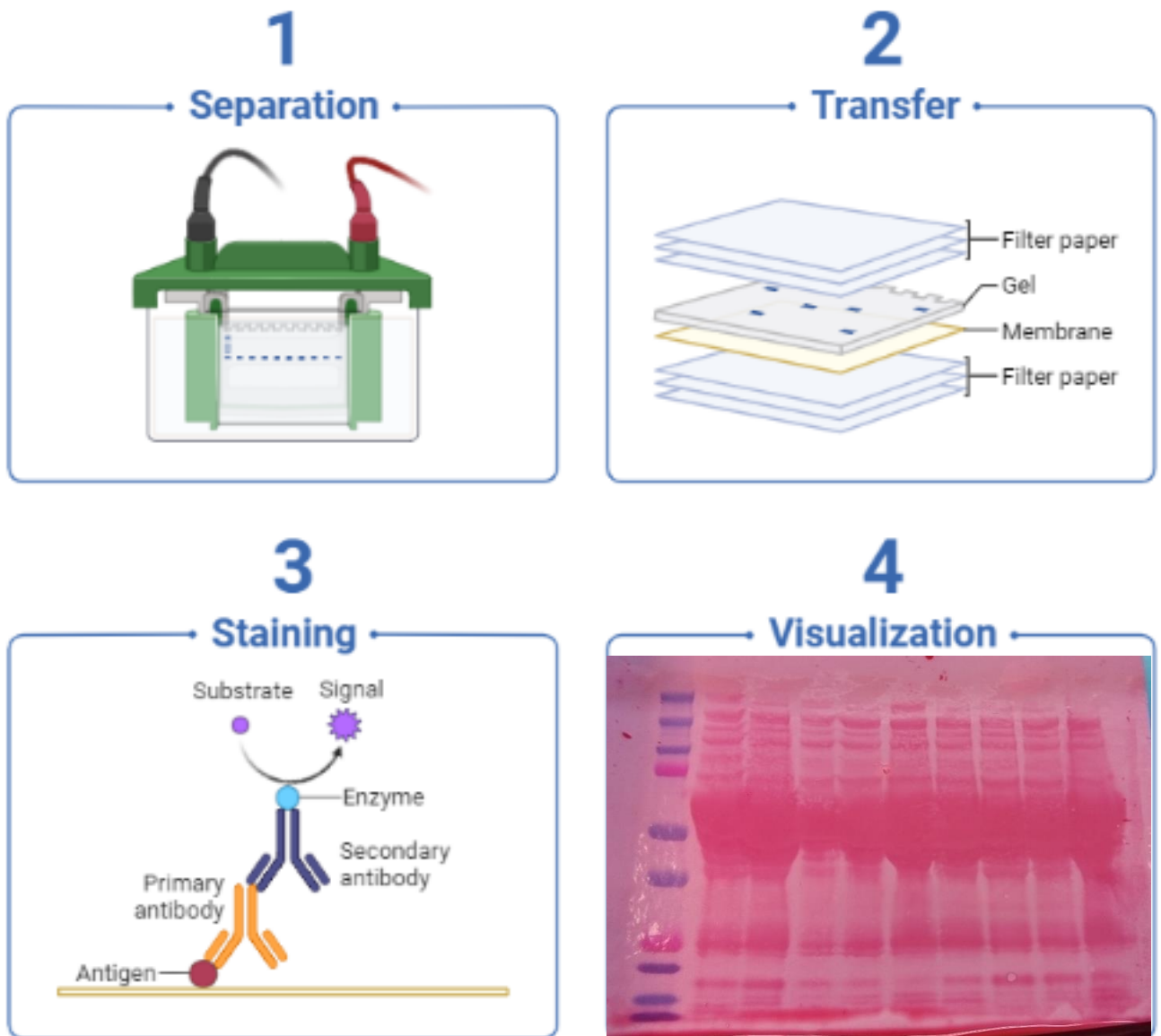


Figure 3. 5: Electrophoresis (1) Transference (2) Immunodetection (3) and Visualization (4)

3.8.3: Immunodetection

In the Immunodetection experiments, membranes were blocked using 5% BSA prepared in tween buffer to prevent antibody unspecific binding. The blocked membranes were placed in the agitator for 1 hour at room temperature. The membranes were then incubated with a primary antibody diluted in the same blocking solution at 4 °C overnight with slight agitation.

The membranes were then washed three times with TBS- Tween and incubated with HRP-conjugated secondary antibody diluted in BSA 1: 2000 for 1 hour at room temperature. The membrane was washed three more times using TBS- Tween, after which peroxidase activity was detected by incubating with Lumi-Light Plus Western blotting substrate Kit (Thermo Fisher) following the manufacturer's instructions.

Luminescent signal was captured using the Odyssey Fc Imaging System and images were processed and analyzed using the software Image Studio™ Lite v. 5.2. β -actin was used as a loading control.

3.9: Enzyme linked immuno sorbent assay (ELISA)

Enzyme linked immuno sorbent assay (ELISA) was performed to check the binding of the purified protein and its corresponding antibody. A hundred micro litres (100 μ L) YES1 cell signaling Capture antibody 1:1000 dilution was added to 96 well plate and incubated overnight at 4 °C in humidified conditions with shaking. The plate was washed three times using phosphate-buffered saline (PBS) containing 0.1% (v/v) Tween X 1. One hundred (100) μ L 3% BSA was added to each well to block the unbound sites and the resultant mixture incubated for 1 hour at room temperature. A hundred micro litres (100 μ L) of different concentrations of recombinant YES1 protein (0.078 ng/mL to 5 ng/mL) in 5 % bovine serum albumin (BSA) solution were added to the 96 well plate and incubated for 1 hour at room temperature with gentle shaking. The plate was washed three times using PBS containing 0.1% (v/v) Tween X1. One hundred micro litres (100 μ L) Polyclonal rabbit YES1, Abcam antibody of 1:1000 dilution was added to each well and incubated for 1 hour at room temperature. The plate was then washed thrice using PBS containing 0.1% (v/v) Tween X1. 100 μ L of anti-rabbit horseradish peroxidase (HRP) conjugated secondary antibody of 1:1000 dilution was added to each well followed by incubation at room temperature for 1 hour with gentle shaking. The plate was washed thrice using PBS (0.1 M, pH 7.4) containing 0.1% Tween X1. Fifty micro litres (50 μ L) of ELISA substrate, comprising of 3,30,5,50-

tetramethylbenzidine (TMB) was added to the well. The plate was incubated in the dark for 30 minutes at room temperature with gentle shaking. Finally, 50 μl of 2 M H_2SO_4 was added as stop solution. Optical density (OD) was measured at 450 nm (Figure 3.6).

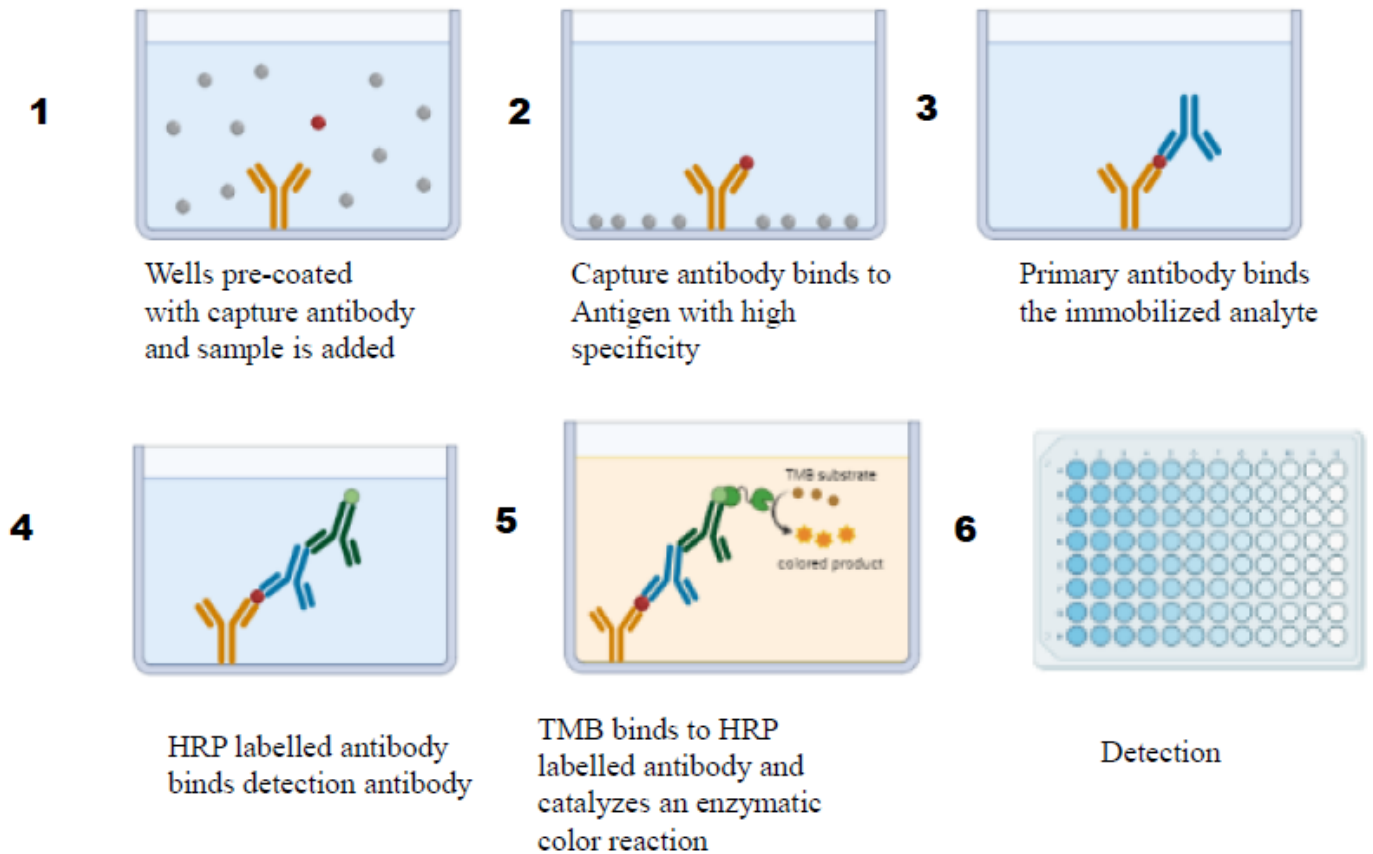


Figure 3. 6: Detection of YES1 protein using sandwich ELISA process

3.10: Human Plasma Samples Analysis

The plasma samples were retrieved from the biorepository of the Clinica Universidad de Navarre, they were diluted twenty times using PBS and used without further processing. The samples obtained were categorized according to YES1 expression in solid tumors (that is patients with high expression of YES1 and low expression of YES1). Evaluation of YES1 expression in solid tumors was performed using the H-score system by immunophenotyping and immunohistochemistry. Briefly, H-score was calculated by adding the products of each intensity and the corresponding area from densitometry obtained by immunophenotyping. The range of possible scores were from

0 to 300, and expression level was categorized as low and high using the upper tertile of the H-score (Garmendia *et al.*, 2019).

The surgical plasma samples were obtained from a cohort of 104 individuals with NSCLC with primary lung cancer from University Clinic of Navarra (CUN) (Pamplona, Spain). Eighteen (18) Samples of healthy controls were also included. The samples were obtained from patients within the age of 23 years to 85 years. Among the samples analyzed, 15 were from female patients and 89 from male patients. Furthermore, out of these samples, 61 were from former smokers, 14 samples were from current smokers while 11 samples were obtained from patients who never smoked at all. The samples obtained were from patients who were in different stages of NSCLC. Forty-two (42) samples were from patients with stage I NSCLC, 22 with stage II, 18 with stage III and 4 with stage IV.

To assess the concentration of YES1 in the human plasma samples, the fabricated immunosensor was incubated with 20 μ L of the sample for 30 minutes at 37⁰C. The immunosensor was then rinsed with tween buffer to remove any unbound YES1 antigen. It was then incubated again with polyclonal anti-Rabbit secondary antibody conjugated with horseradish peroxidase (HRP) for 10 minutes at 37⁰C. The immunosensor was then rinsed with tween buffer X1 to remove any unbound antibodies. Electrochemical measurement was then carried out in 0.1 M PBS (pH 7.4) with 5mM [K₃Fe(CN)₆,] 0.1 M KCl and 4mM H₂O₂.

3.11: Analytical Techniques

The analytical techniques that were employed in this study included: Cyclic Voltammetry (CV), Differential Pulse Voltammetry (DPV) and linear sweep Voltammetry (LSV); Spectroscopic techniques that were used included: Ultra Violet-Visible spectroscopy (UV-Vis), Fourier transform infrared spectroscopy (FT-IR) and Dynamic light scattering (DLS).

3.11.1: Cyclic Voltammetry

The Cyclic Voltammetry (CV) measurement started at an initial voltage V_1 , - 0.5V at which the current flow usually was negligible. Subsequently, the voltage was switched in a linear manner to V_2 , + 0.3V at a time t . After reaching V_2 , the direction of the scan was inverted and the voltage was swept back, usually to V_1 . This cyclic process of sweeping between V_1 and V_2 was repeated several times. V_1 and V_2 was selected so that the interval (V_2-V_1) contained an oxidation and

reduction process. If O is considered the oxidized and R the reduced form of a reversible redox couple, then the reaction that occurred during the potential sweep can be written as:

$O + ne^- \leftrightarrow R$ or in this case:



Initially, only the oxidized form O of the couple $[\text{Fe}(\text{CN})_6]^{3-}$ in this assay was present. With rising voltage, the current flow was increasing, since the redox potential was approached and the oxidized form of the redox couple was converted into the reduced form. A cathodic current peak was spotted. At the cathodic point, the oxidized form O was reduced to R or $[\text{Fe}(\text{CN})_6]^{4-}$. When sweeping back, the product was reoxidised, and $[\text{Fe}(\text{CN})_6]^{3-}$ was regenerated, leading to an anodic peak current (Wang 2006b). The cyclic voltammogram of a reversible electrochemical reaction showed some few well-defined characteristics.

First, the ratio of the anodic peak current to the cathodic peak current $i_{p,a}/i_{p,c}$ was equal to 1. This ratio can be affected by chemical reactions coupled to the redox process. Second, the voltage separation between the current peaks was given by equation 3.3

$$\Delta E_p = E_{p,a} - E_{p,c} = \frac{0.059}{nV} \quad \text{Equation 3.3}$$

with ΔE_p : separation between peak potentials (V)

$E_{p,a}$: anodic peak potential (V)

$E_{p,c}$: cathodic peak potential (V)

n : number of electrons transferred

Based on this equation, the peak separation was applied to determine the number of electrons transferred in a redox process. It is also a criterion for Nernstian behavior. Ideally, a fast one-electron process, for instance, has a ΔE_p of about 59 mV. The position of the peaks was independent of the scan rate (Wang 2006b).

3.11.2: Differential Pulse Voltammetry

Differential pulse voltammetry (DPV) is comparable to normal pulse voltammetry (NPV) in the sense that the potential is scanned with a series of pulses. DPV differs from NPV in that in DPV, each potential pulse is fixed, has a small amplitude (10 to 100 mV), and is superimposed on a slowly changing base potential (Shahrokhian and Saeed, 2007). In this study, the three electrode system was used for the electrochemical measurements, in which current was measured at two points for each pulse, the first point, just before the application of the pulse and the second at the

end of the pulse. The two points were selected to allow for the decay of the charging current. The difference between current measurements at these points for each pulse were determined and plotted against the base potential.

3.11.3: Dynamic light scattering (DLS) analysis

In order to determine the size of the obtained AuNPs, the nanoparticles were purified by centrifugation at 15,000 rpm for 10 minutes in a Hitachi CS 150NX-350 micro ultra-centrifuge (Malvern Panalytical). The size by intensity of the AuNPs was determined by dynamic light scattering (DLS), using a Nicomp 380 ZLS particle sizing system equipped with a green laser excitation source operating at 465 nm/50 mW. A frequency of the photon counting was set at 200 kHz, while a scattering angle was fixed at 90°. The temperature of the measured media was 25 °C. Disposable poly (methyl methacrylate) (PMMA) square cuvettes (ID of 1.0 cm) were used. The equilibration time was set at 200 s and the number of runs was 11 for DLS.

3.11.4: UV-VIS Spectra Analysis:

The reduction of pure Au³⁺ to nanoparticle was monitored by measuring the UV-vis spectrum the most confirmatory tool for the detection of surface Plasmon resonance property (SPR) of AuNPs (Sett *et al.*, 2016). This was achieved by diluting a small aliquot (3mL) of the sample in (7mL) distilled water. The reduction of gold ions was assessed using a double beam UV–VIS spectrophotometer (Model; Jasco –V 6300, Perkin Elmer, Singapore) and this was done at a wavelength range of 300-700 nm using a 10 mL quartz cell. The resolution of the UV–VIS spectrophotometer was 1 nm. The UV–VIS spectra of the resulting solution were recorded.

3.11.5: Fourier transform infra-red spectroscopy (FT-IR)

Functional bio-molecules associated with Au NPs after reduction of the gold ions into Au NPs using the *Mangifera indica* plant extract were confirmed by FTIR. Biosynthesized Au NPs were centrifuged at 13,000 rpm for 15 minutes and the pellets were washed with distilled water. The centrifuging and re-dispersing process was repeated to three times, after which the samples were dried and analyzed at a wave region of 400 – 4500 cm⁻¹ (Sett *et al.*, 2016).

3.12: Data Analysis

Origin pro9.1 version software (Microcal Software Inc., Northampton, MA, USA) was used for curve-fitting and data analysis. Data was obtained from a minimum of 3 independent experiments.

Electrochemical results were analyzed using the NOVA software (version 1.11.0)

Image J software was used for analysis of immunoblot images. Luminescent signal for Western blot was captured with Odyssey Fc Imaging System and images were processed and analyzed using the software Image Studio™ Lite v. 5.2

CHAPTER 4 :RESULTS AND DISCUSSION

4.1: Introduction

In this study we report the development of a real-time immunosensor which can perform highly sensitive YES1 and CEA lung cancer biomarker measurements. The general molecular architecture and working principle of the immunosensor is shown in Figure 3.1. DPV was used to get the output, and the results obtained are highlighted and discussed in this section.

4.2: Characterization of gold Nano particles

The results for characterization of gold nanoparticles using various techniques are presented in the following subsections.

4.2.1: Ultraviolet-Visible (UV–vis) spectrum analysis

A visual observation of AuNPs indicated that there was a color change in the reaction mixture of gold chloride and plant extract from light yellow to red wine, which is the characteristic color of gold Nano particles (Sengani and Devi, 2017). This indicated formation of nanoparticles as shown in Figure 4.1 (C II). The color change occurred within 15 minutes and remained unchanged, which confirmed the stability of Au NPs. The color change in the reaction mixture could be attributed to the excitation of surface Plasmon vibrations that are characteristic of the synthesized nanoparticles (Song et al., 2011).

The results further showed that the *Mangifera indica* plant extract was successfully used in the fabrication of Au NPs. The plant extract acted as both a reducing and a stabilizing agent in the conversion of gold ions to Au NPs. The results were similar to other studies reported by Sengani and Devi (2017), Kalpana *et al.* (2016) and Song *et al.* (2009).

Reduction of Au³⁺ to Au⁰ by plant extracts was characterized by UV-VIS spectroscopy. The results obtained are shown in Figures 4.1 (A, B and C)

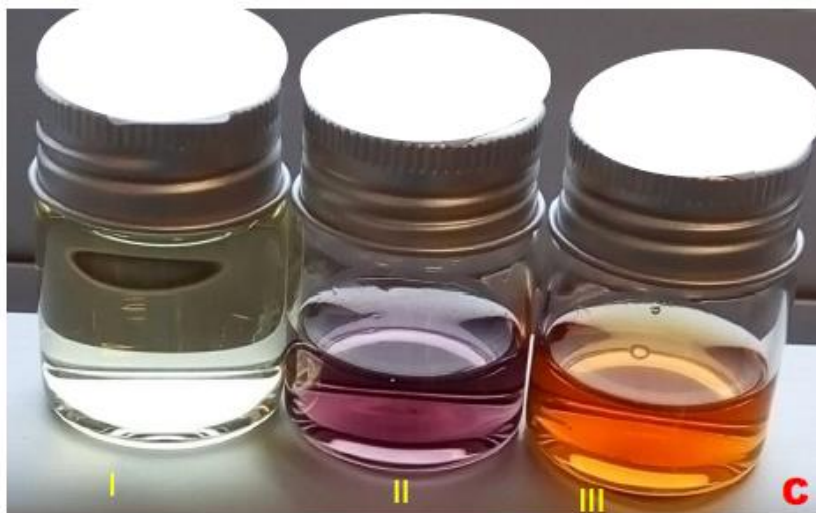
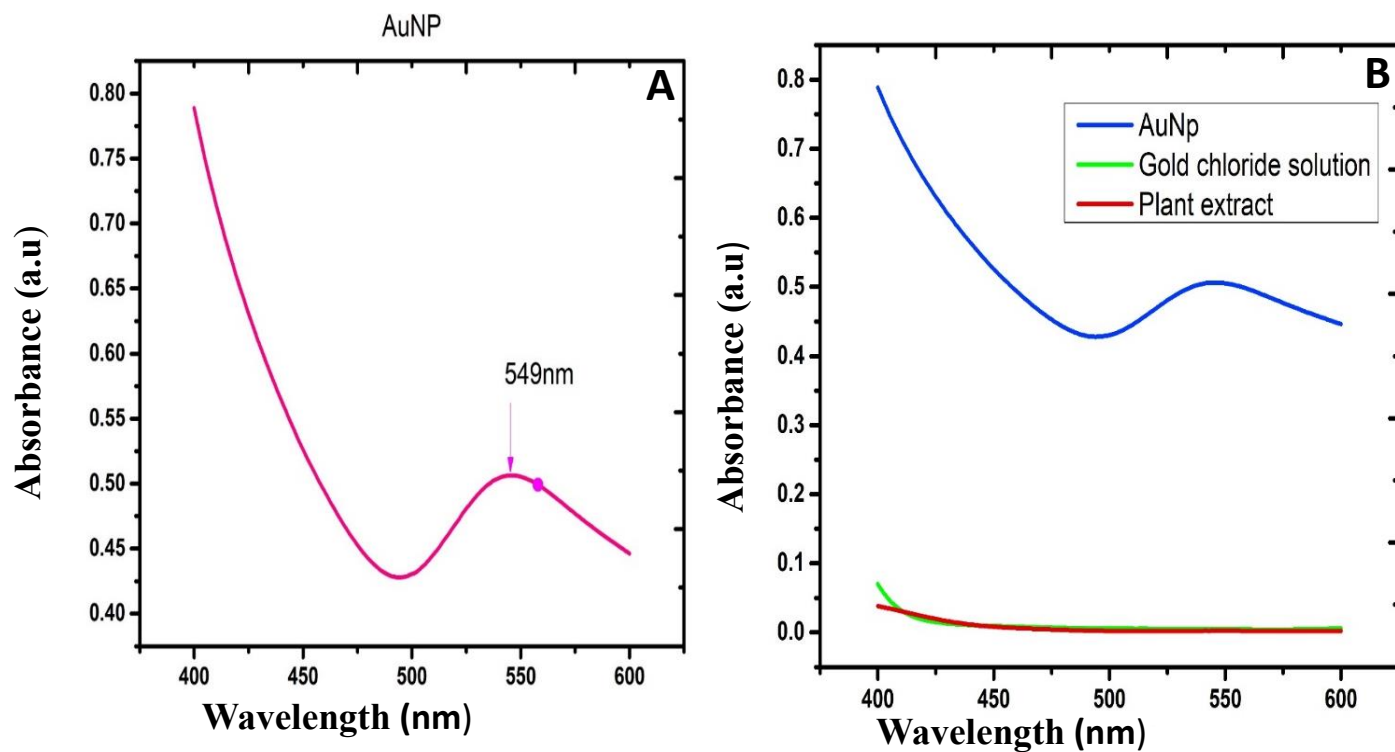


Figure 4.1: UV-Vis spectra recorded in the reaction solution for the synthesis of (A) AuNPs. Plasmonic peak assigned to metal nanoparticles is indicated by the arrow. (B) UV-Vis spectra of the plant extract and gold chloride solution (C) Color change profile of biosynthesized gold nanoparticles; I- gold chloride solution, II- Gold Nano particles solution, III- plant extract solution

Legend: Plasmonic peaks assigned to metal nanoparticles are indicated by the arrow.

The formation of Au NPs in the final reaction mixture was further confirmed by UV–VIS absorbance measurement which shows a Surface Plasmon resonance band (SPR). The results of UV–VIS spectra (Figure. 4.1 A and B) showed a sharp localized surface Plasmon resonance band at 549 nm, which is a characteristic peak for Nano gold UV–VIS spectra (Nagalingam *et al.*, 2018).

This single peak indicates the formation of monodispersed Au NPs (Daniel and Astruc, 2004) The peak, resembles previously obtained peak by some authors such as Nagalingam .M. *et al.*, (2018) and Ankamwar (2010) from spherical nanoparticles, in which case, we can conclude that the NPs formed assumed a similar topography.

4.2.2: Fourier transform Infra-red (FT-IR) spectroscopy

The functional bio-molecules that were involved in the reduction of gold ions to AuNPs were confirmed by FT-IR. The samples were analyzed at a wave region of 400 – 4500 cm^{-1} . The results are shown in Figure 4.2

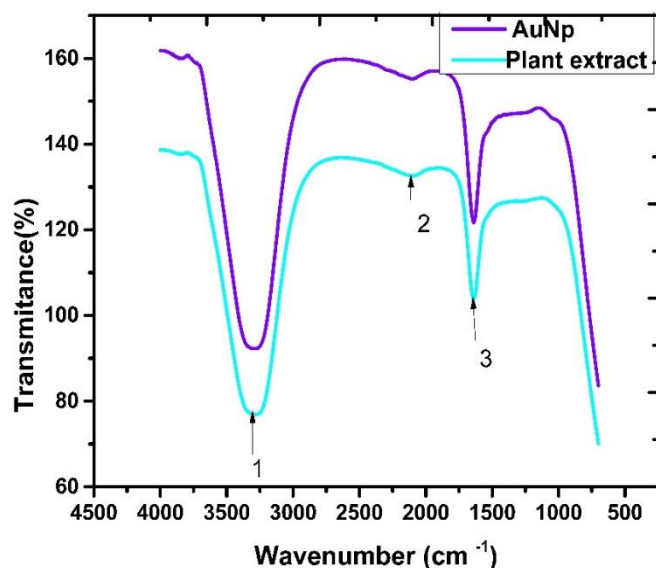


Figure 4.2: FT-IR spectrum of AuNPs bio synthesized from *Mangifera indica* plant extract

From Figure 4.2, the dispersion band for the synthesized AuNPs (around 3400 cm^{-1} (peak 1) was smaller than the one for the extract which suggested that hydroxyl groups had been oxidized to carbonyl groups (Park *et al.*, 2019). This indicated that the OH groups present in the extract were the main compounds involved in the reduction of Au ions. The FT-IR spectrum for the *Mangifera*

indica extract showed weak bands in 2922 cm^{-1} (peak 2) , before and after the Au ions reduction (Figure 4.2), which corresponded to CH_2 stretching vibrations (Ismail *et al.*, 2018)

The absorption peak measured at 1590 cm^{-1} (peak 3) was probably due to free NH groups present in the proteins (Rodríguez-León *et al.*, 2019). The reduction of the intensity of this band after the formation of AuNPs indicated that the proteins in the extract were also used for capping AuNPs, improving its stability (Foo *et al.*, 2017). The alliance of phytochemical compounds associated with the biosynthesis and stabilization of AuNPs were evaluated using FT-IR.

From these results, the role of chemical compounds found in the *Mangifera indica* extract in reducing Au^{+3} and stabilizing AuNPs are observed. The FTIR spectra results also confirmed the idea that biosynthesized nanoparticles are surrounded by a thin layer of phytomolecules including polyphenols, such as flavonoids and tannins, in addition to terpenoids and proteins (Azri *et al.*, 2019). The main peaks in the FTIR spectra of *Mangifera Indica* extract as well as those in the AuNPs are summarized in Table 4.1.

Table 4.1: FTIR peaks observed in the green synthesized gold nanoparticles and *Mangifera Indica*

Peak	Bands cm^{-1}		Possible functional groups	Reference
	Extract	AuNPs		
1	3400	3400	Free O–H	(Azri et al., 2019)
2	2922	2922	CH_2 stretching	(Ismail et al., 2018)
3	1590	1590	free NH groups	(Rodríguez-León et al., 2019)

4.2.3: Dynamic light scattering (DLS) analysis

Figure 4.3 shows the intensity of particle size distribution obtained for a colloidal gold sample measured on a Zetasizer Nano Sampler. The plot shows the relative percentage intensity of light

scattered by particles (on the Y-axis) in various size classes (on the X-axis). The diameters of the gold nanoparticles obtained from the biosynthesis were 8.765 nm, 40.09 nm and 370.9 nm. Freshly prepared gold nanoparticles were used for the preparation of secondary antibody conjugate for CEA antibody labeling whose size was 8.765 nm. The procedure for the preparation of the secondary antibody conjugate is discussed in section 3.4.3. The 370.9 nm particles obtained implied that there were significant aggregates present in this sample which could have been associated with the storage time of the Nano particles, where the Nanoparticles were kept for more than one month before analysis was done.

	Size (d.n...	% Intensity:	St Dev (d.n...
Z-Average (d.nm): 217,8	Peak 1: 370,9	57,7	86,41
Pdl: 0,410	Peak 2: 8,765	26,5	1,878
Intercept: 0,898	Peak 3: 40,09	15,8	10,26

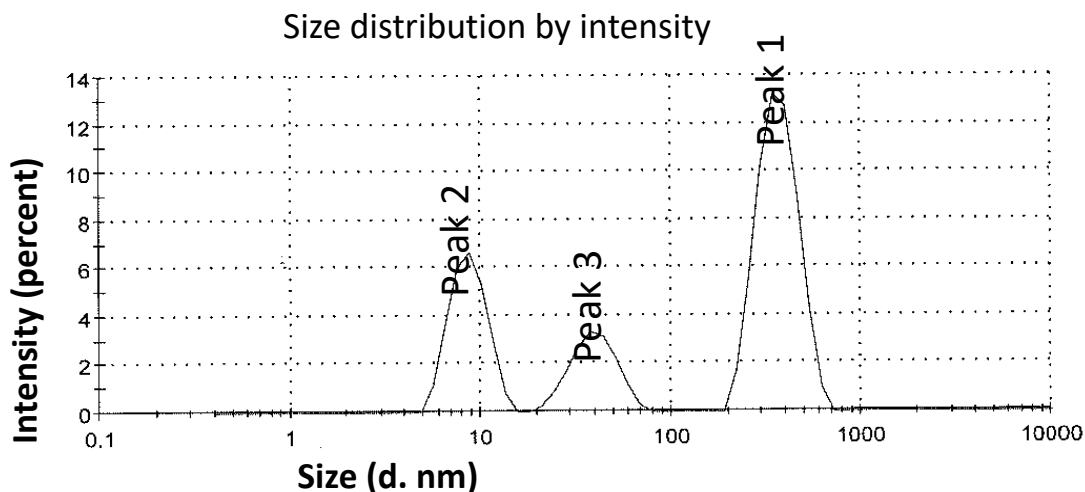


Figure 4.3: DLS showing the intensity particle size distribution obtained for a colloidal gold sample.

4.3: The electrodeposition process

Figure 4.4 shows the mechanism of electrodeposition of the AuNPs. It was confirmed that free gold (III) ions from solution were attached to the surface of the electrode through electrostatic interaction first and then the application of potential to the electrode promoted the reduction of the gold (III) ion (Mohanty, 2011). The quantity and size of the AuNPs electrodeposited on the

electrode surface relied on the gold (III) ion deposition time. The concentration of HAuCl_4 , acidity of the solution media, scan cycles and scan rate also had great effect on the size and film thickness of AuNPs deposited. In this study, we electrodeposited AuNPs films onto electrodes by cyclic voltammetry, and controlled the growth of nanoparticles size and film thickness with the mentioned different parameters. Figure 4.4 shows the CV plots of the electrodeposition of the AuNPs within scan range of -0.7 V to $+0.3 \text{ V}$.

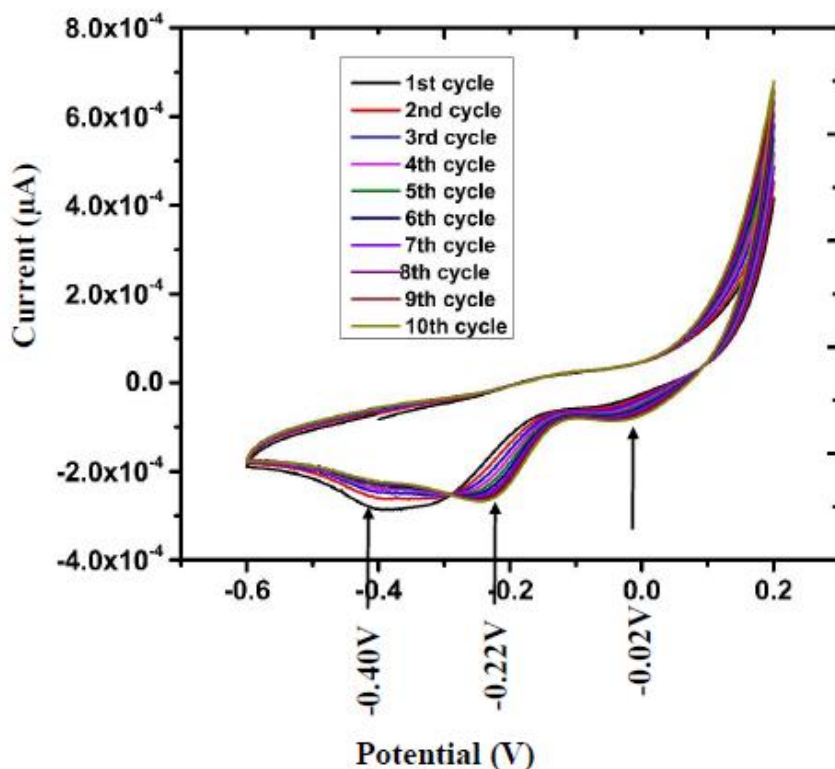
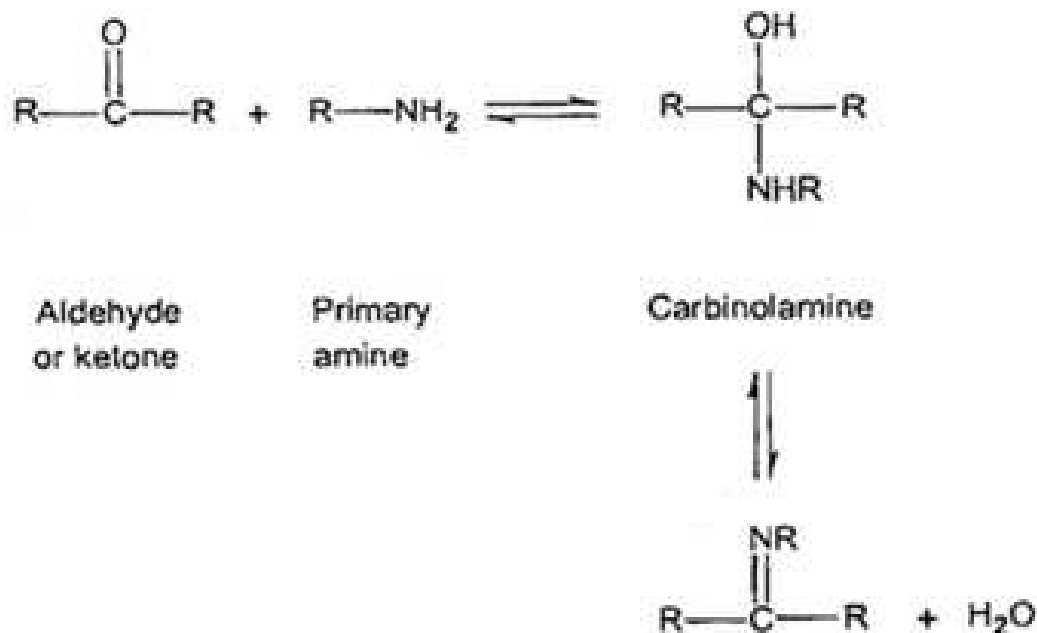


Figure 4.4: CV plots of gold nanoparticles electrodeposition, potential range of -0.7 V to $+0.3 \text{ V}$ at a scan rate of 50 mV s^{-1} .

The cathodic peak that appeared at around ca. -0.4 V in Figure 4.4 was due to reduction of gold (III) to gold. This peak in the 3rd cycle shifted to more positive potential (ca -0.22 V), which meant easier electrodeposition of gold on the existing gold particles (Chiang et al., 2019). Another peak that appeared at a potential -0.02 V was attributed to the reduction of water, resulting in the formation of hydrogen gas (Moulton et al., 2003). On the anodic scan, a small peak that appeared at around ca. -0.15 V was attributed to the surface oxidation of the electrodeposited gold.

4.4: Immobilization of antibodies

The CEA and YES1 antibody that were immobilized on a glassy carbon electrode (GCE) in a mixed ratio of 1:1 protein G/glutaraldehyde (PTG/GA) are outlined by scheme 4.1.



Scheme 4. 1: Outline of covalent attachment of glutaraldehyde to the electrode surface through the thiolated protein G, resulting in a table bio-sensing interface

Incubation of GCE working electrode with a solution of thiolated protein G and L- cysteine (0.03512 g L- cysteine was prepared in degassed 0.1 M of 10 mL PBS) for 4 hours at 4°C lead to conversion of amine groups from lysine residues in protein G to thiol groups by L- cysteine (Lee et al., 2007).

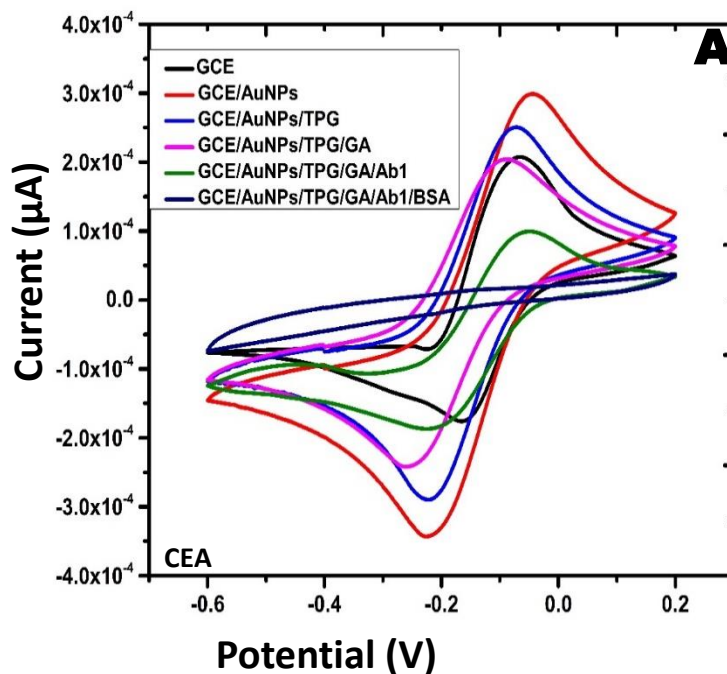
This could be attributed to the high affinity of thiols for the electrodeposited gold nanoparticles which facilitated the direct formation of a self-assembled protein G layer. A covalent bond was formed through conjugation between the AuNPs, due to their high affinity towards the Sulphur atom of the thiols and also the amine functional groups that formed a bond. (Mallesha *et al.*, 2018) The PTG-modified electrode was then incubated with GA (4% wt. in deionized water) for 1 hour. In so doing, the L- cysteine monolayer was chemisorbed onto the AuNPs through the thiol moiety and the amino groups projected away from the AuNPs surface. The exposed arrays of amino groups, then reacted with aldehyde groups of glutaraldehyde through the Schiff base reaction (Scheme 4.1) (Burcham and Pyke, 2006).

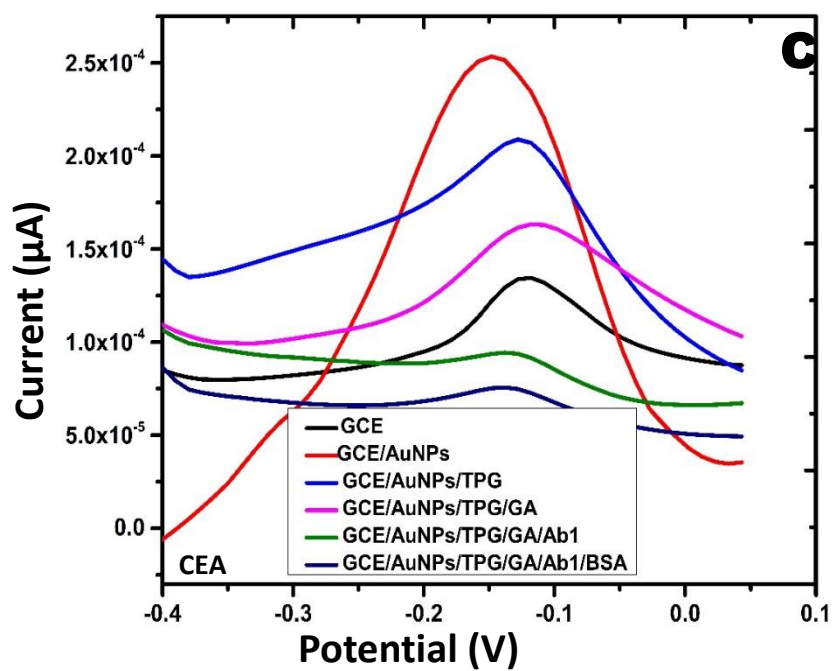
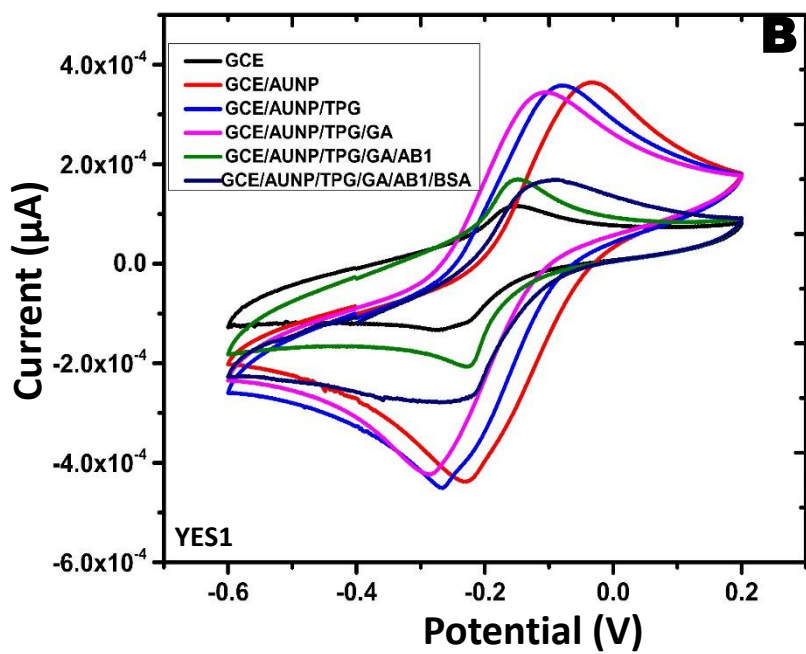
Then, CEA and YES1 antibody that had been prepared in 5% BSA were immobilized on the modified electrode with AuNPs and TPG overnight at 4 °C. The glutaraldehyde cross linked protein G to CEA and YES1 antibodies through the formation of imine bonds (C=N bonds) between -CHO groups and -NH₂ groups as shown in scheme 4.1. Lastly, the BSA (3% wt./vol. in tween buffer X 1) was deposited

onto the modified electrode for 1 hour to block unbound sites. After each modified step, the immunosensor was rinsed with PBS to remove unbound molecules. The immunosensor was stored in a refrigerator at 4 °C in PBS for further use.

4.5: Characterization and electrochemical performance of the immunosensor

The characterization and the assessment results of the performance of the immunosensor using CV and DPV are provided in Figures 4.5 A, B, C and D. The cyclic voltammograms of the YES1 and CEA electrodes were carried out in 5mM K₃[Fe(CN)₆] and 0.1M KCl solution at a scan rate of 50 mV s⁻¹





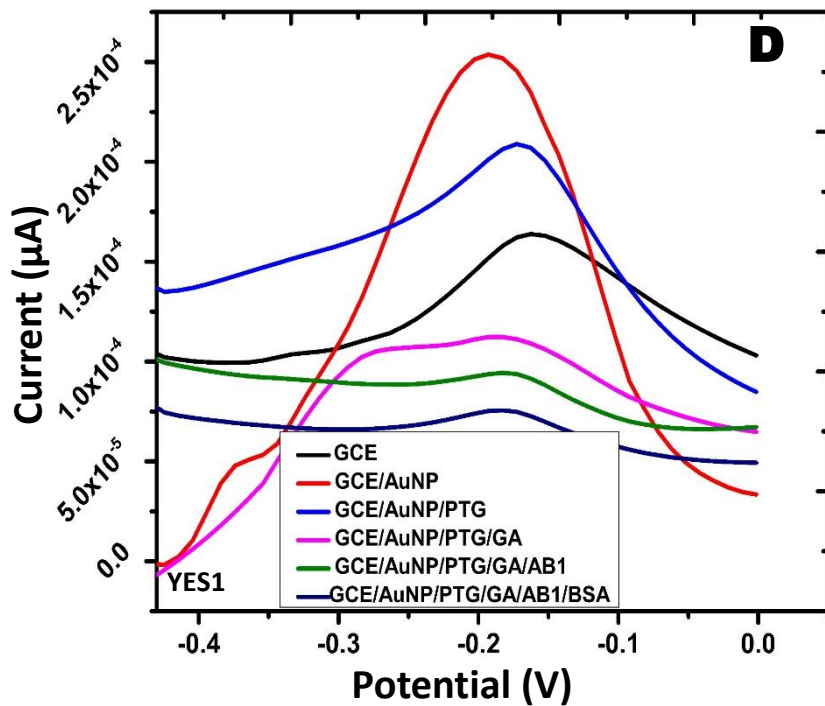


Figure 4.5: Characterization and assessment of the electrochemical performance of the YES1 and CEA immunosensors ; cyclic voltammety curve (A) CEA, (B) cyclic voltammety curve YES1, (C) DPV curve of CEA (D) DPV curve of YES1 recorded in 5mM $K_3[Fe(CN)_6]$ and 0.1 M KCl pH 7.2 at a scan rate of 50 mV s^{-1}

After the Au-Nano particles were electrodeposited onto the bare glassy carbon electrode (GCE), the peak heights of the redox couple were observed to increase considerably, owing to the enlarged surface area of the electrode and the improved rate of electron transfer (Figure 4.5 A - D). The peak heights of the redox couple also increased after the incubation of thiolated protein G on the Au/GCE due to the electrostatic interaction and attraction between the $[Fe(CN)_6]^{3-}$ and the amine terminals of the TPG / AuNPs /GCE. The peak heights decreased when glutaraldehyde (GA), YES1 antibody (Ab 1) and BSA were modified onto the PTG / AuNPs /GCE. This was attributed to the non-conductivity of GA, Ab1 and BSA. The modification of these insulative molecules on the electrode surface hindered electron transfer, which resulted in a decrease in the redox peak currents.

The electroactive surface area of electrode was determined by recording CVs of bare GCE, GCE-PTG and AuNPs- PTG modified GCE in 5 mM $[Fe(CN)_6]^{3-}$ with 0.1 M KCl at 50 mVs-1 (Figure 4.5 A). Randles- Sevcik equation was used to calculate the electroactive surface area of the electrode (Randles, 1947) and (Ševčík, 1948).

$$I_p = 2.69 \times 10^5 \times A \times D^{\frac{1}{2}} \times n^{\frac{3}{2}} \times v^{\frac{1}{2}} \times C \quad \text{Equation 4.1}$$

Where (A) is the area of the electrode (cm^2), (D) is diffusion coefficient of the molecule (cm^2/s), (n) is number of electron transferred in the redox reaction, (v) is scan rate (V/s) and (C) is concentration of the analyte solution (mM), respectively. In the $\text{Fe}(\text{CN})_6^{4-/3-}$ redox system, the value of D is equal to 6.7×10^{-6} , n is equal to 1, v is equal to 0.05 and C is equal to 5 mM. The electroactive surface area of bare GCE, GCE-PTG and AuNPs-PTG modified GCE was calculated as 0.01438 cm^2 , 0.02659 cm^2 , and 0.0664 cm^2 , respectively and the results showed improved electrochemical activity of GCE-PTG and AuNPs-PTG over the bare GCE. The results also showed that the modified nanomaterial enhanced the conductivity and sensitivity of the electrode. The kinetics of the modified electrode was investigated by analyzing the effects of the scan rate on the redox current. The electrochemical performance of AuNPs/GCE was examined in a 5 mM potassium ferricyanide solution and 0.1 M KCl scan rates ranging from 10 to 100 mV s^{-1} . Maximal current values of the redox reaction increased linearly with increasing Square root of scan rate. In addition, the distance between redox peaks grew further and further apart (Figure. 4.6A). Based on these results, we performed a linear fit of the oxidation peak (I_{pa}) and reduction (I_{pc}) peak currents relative to the square root of the scan rate ($v^{1/2}$). The ultimate linear equations were determined to be $I_{pa} = 1.533 \times 10^{-5} x + 3.162 \times 10^{-5}$ and $I_{pc} = 1.2339 x - 4 \times 10^{-5}$ (Figure.4.6B). The results from these calculations demonstrated that the electrochemical signal was due to diffusion-controlled surface reaction (Randles, 1947) and (Ševčík, 1948).

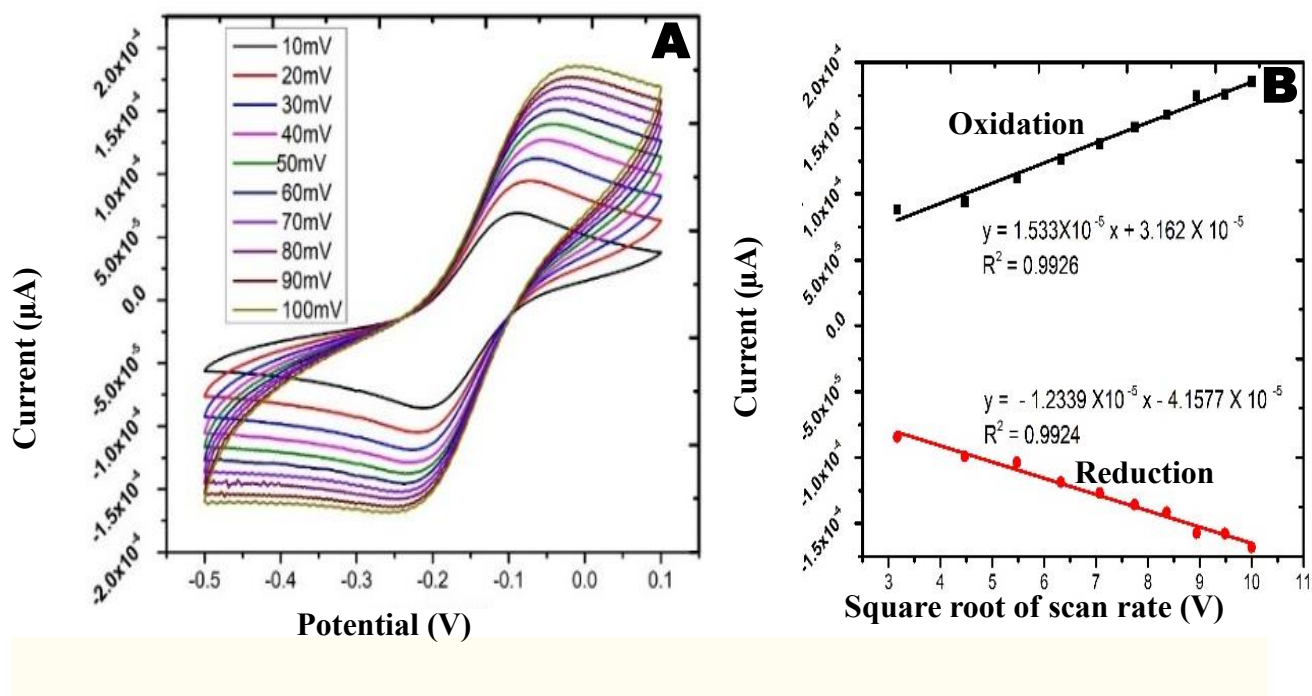


Figure 4.6: (A) kinetic analysis of AuNPs/GCE at scan rates ranging from 10 to 100 mV s^{-1} in 5mM $\text{K}_3[\text{Fe}(\text{CN})_6]$ and 0.1 M KCl pH 7.2 . (B) linear fits of the oxidation peak current (I_{pa}) and reduced peak current (I_{pc}) versus the square root of the scan rate ($v^{1/2}$)

4.6: Optimization studies

The study showed that the electrochemical performance of the immunosensor was affected by several factors such as pH, temperature and substrate concentration

To ensure that the immunosensor provided the best possible output, these factors needed to be optimized. The pH of the solution is one of the important factors in fabrication of an immunosensor. Unsuitable pH can, not only change antibodies activity, but also influence the immunosensor's electrochemical performance (Xu *et al.*, 2015). The activity of the immobilized proteins for instance, may be influenced by the acidity of the solution (Katz and Willner, 2005).

In this study, analysis was done in solutions with pH values ranging from 6.0 to 7.8 and the optimal pH determined. The results obtained are highlighted in Figures 4.7 A and 4.7 B.

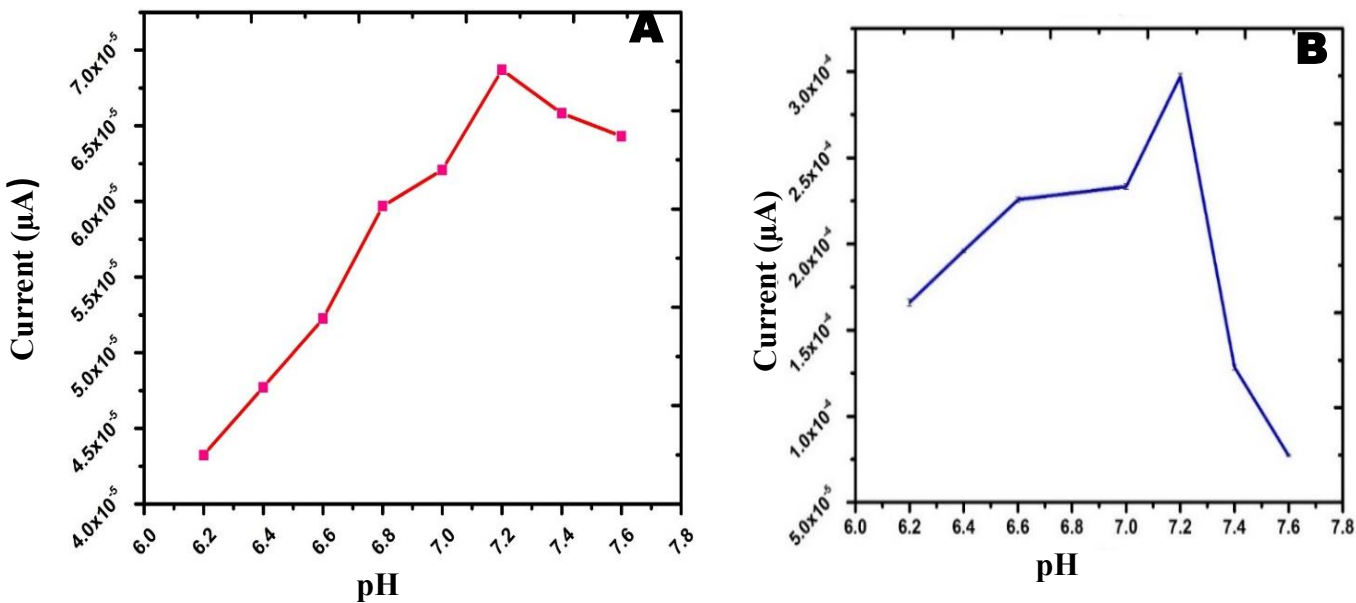


Figure 4.7: Optimization experiments on the immunosensor, responses effect of pH on CEA (A) and YES1 (B)

The results showed that the current increased as pH increased from 6.0 to 7.2 pH and decreased at higher pH conditions. The response indicated that the high pH conditions affected the activity of the antibody and caused the binding between the antibody and immunosensor to be weakened. Therefore, pH of 7.2 was taken to be the optimal pH in the detection of both CEA and YES1.

Incubation time was another parameter that was optimized in the immunosensor. The effect of incubation time for both CEA and YES1 was investigated in the time range of 0– 50 minutes with 10 ng/mL of CEA and 0- 60 min with 10 ng/mL of YES1. The results for these experiments are highlighted in Figure 4.8 A and B

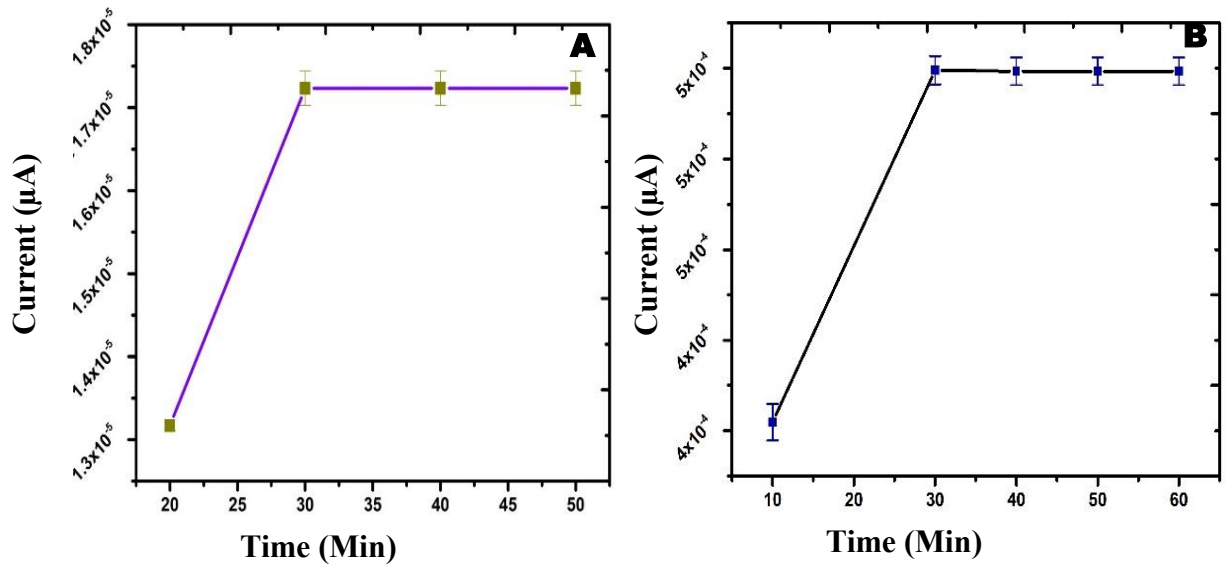


Figure 4.8: Optimization experiments on the immunosensor: DPV responses of: Effect of incubation time of 10ng/ml CEA (A) and YES1 (B) on the immunosensor.

Figures 4.8 A and B showed that the current response rapidly increased within the first 30 minutes and then leveled off due to the formation of an antigen-antibody complex which saturated the binding sites of the antibodies. Thus, the optimal incubation time was set at 30 minutes for both CEA and YES1.

The concentration of CEA- antibody and YES1 anti-body immobilized on the surface of the electrode was considered as one of the key factors that could affect the performance of the sensor and thus their concentrations were optimized.

When the antibody dilution increased from 1: 200- 1:2000 for both CEA and YES1, the sensor oxidation current increased with increasing dilution ratio up to the 1:500 dilution ratio, whereat the current decreased (Figure 4.9 A and B).

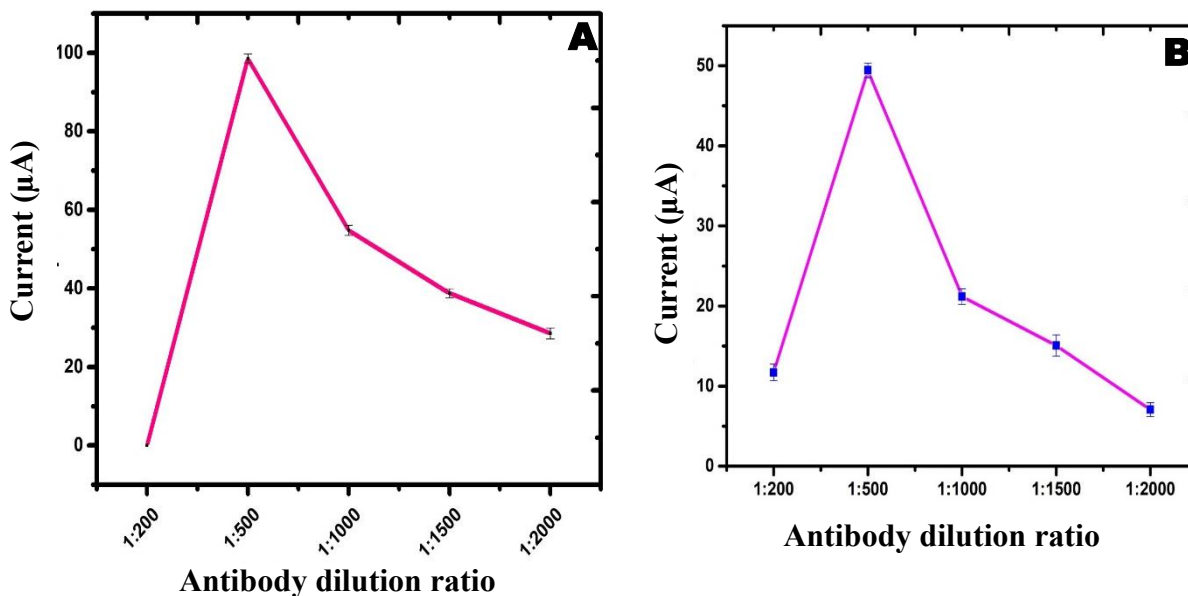


Figure 4.9: Optimization experiments on the immunosensor: DPV responses effect of CEA (A) and YES1 (B) antibody concentration on immunosensor response.

This indicated that the amount of CEA and YES1 antibodies immobilized on the sensor had reached saturation at this dilution ratio. Based on these results, the dilution ratio of 1 :500 was selected as the optimum dilution ratio of both CEA and YES1 and was used in subsequent experiments.

Glutaraldehyde (GA) concentration used for crosslinking the antibody was also optimized in the fabrication of the immunosensor. The effect of GA concentration was investigated by incubating Au Np modified electrode with different % concentration of GA at room temperature for 3 hours (3% to 5%). The 3% concentration of GA gave a weak response of immunosensor towards CEA and YES1, while 4% and 5% gave reliable responses with highest peak current. 4% was taken to be the optimum GA dilution (Figure. 4.10 A and B)

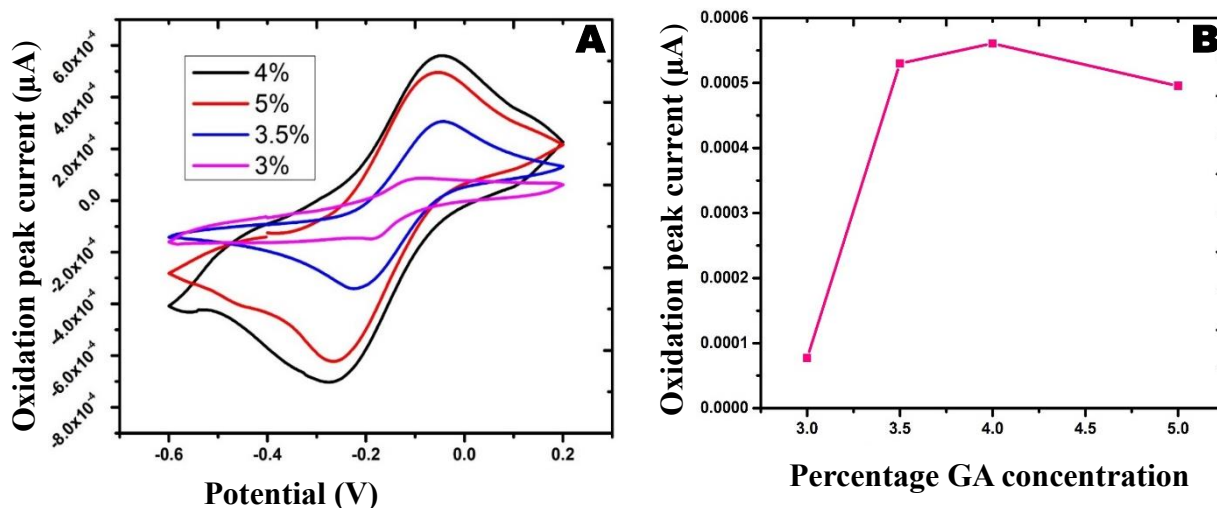


Figure 4. 10: Optimization of % GA concentration for cross linking antibody to thiolated protein G (A) A CV of different concentrations of GA (B) line graph.

4.7: Immunosensor Performance

The performance of immunosensor was assessed and the results are discussed in the following sections

4.7.1: Expression and detection of YES1 recombinant and CEA antigen

The expression of YES1 recombinant and CEA antigen, 2 ng/mL of the two biomarkers were resolved by using Sodium dodecyl-sulfate polyacrylamide gel electrophoresis (SDSPAGE) and detected using immunoblotting as shown in Figure 4.11 A and B. The molecular weight of YES1 and CEA proteins were found to be at 60 kDa and 180 kDa respectively

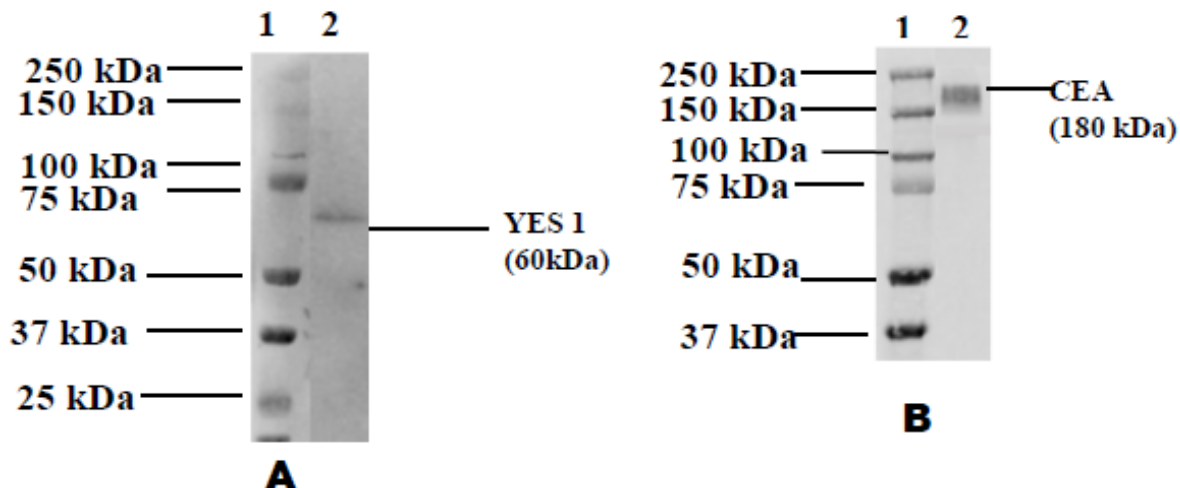


Figure 4.11: Characterization of (A) YES1 recombinant and (B) CEA, SDS-PAGE showing the respective protein in lane 2 and protein molecular weight marker in lane 1

The western blot results obtained in Figures 4.11 A and B was a confirmation of presence of YES1 and CEA in the artificial antigen used with the immunosensor.

4.7.2: Analytical performance of the fabricated immunosensor

The analytical performance of the proposed immunosensor was first evaluated at the protein level using DPV measurements which showed that the oxidation peak height signal of the protein increased with increase in concentration of the YES1 (Figure. 4.12A).

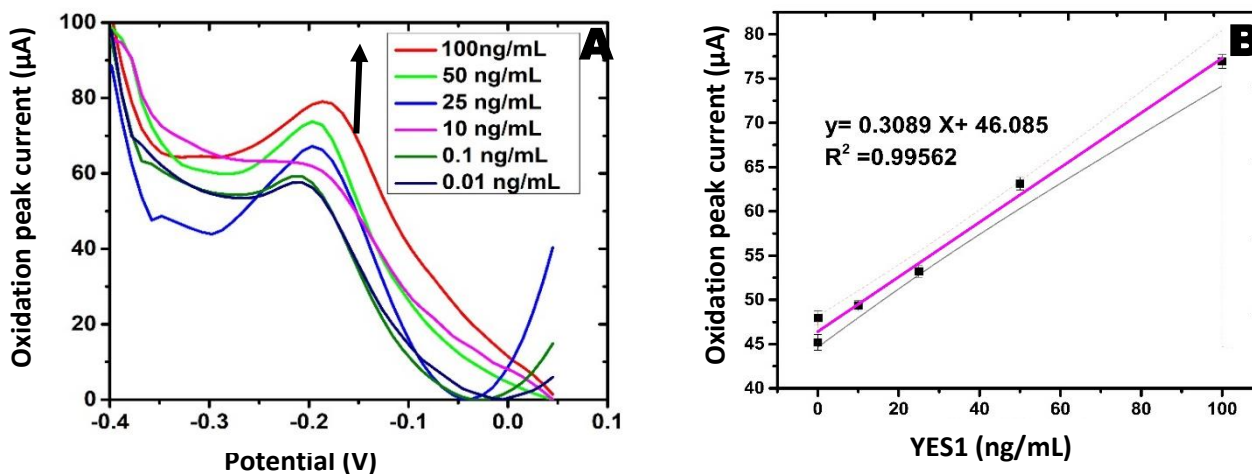


Figure 4.12: (A) DPV showing detection at varying YES1 concentration (0.01 -100 ng/mL) in 0.1 M PBS (pH 7.4) with 1 mM $[K_3Fe(CN)_6]$, 0.1 M KCl. Scan rate: 50 mV s^{-1} . (B) calibration curve showing linear relationship of the immunosensor in detection of YES1.

The increase in current could be attributed to the enhanced reaction of the antigen-antibody interaction. The proposed biosensor exhibited clear linearity with antigen concentration range of 0.01 to 100 ng /mL, and the linear regression equation was calculated as $y = 0.3089x + 46.085$ (Figure 4.12 B). In Figure 4.12 B, each datum point represented the average analysis of triplicate values ($n= 3$) and the dotted lines represented the 95% confidence interval of each datum point. The error bars corresponded to the standard deviation (SD) of three measurements ($n=3$).

The immunosensor response was precise, as indicated by the small error bars Figure 4.12 B. The limit of detection (LOD) and limit of quantification (LOQ) of the immunosensor were calculated from the expressions $LOD = (3X SD/m)$ and $LOQ = (10X SD/m)$ (Armbruster and Pry, 2008), where **SD** is the estimated standard deviation from the points used to construct the calibration curve and **m** is the slope. The LOD and LOQ of the fabricated immunosensor obtained were 0.001408 ng/mL and 0.00469 ng/mL respectively.

The detection limit obtained with the fabricated immunosensor was lower than the reported immunosensors for many other cancer biomarkers (Table 4.2).

Table 4.2: Comparison of the response characteristics of different modified electrodes

Electrode	Target biomarker	Detection range	Detection limit	Method	Ref
GCE/Au/Prot G/ GA/Ab	YES 1	0.001 -100 ng/mL	0.001408 ng/mL	DPV	This work
FTO/SWCNTs/den-Au/prob	miR-21	0.01 fM L ⁻¹ - 1 μM L ⁻¹	0.01 fM L ⁻¹	DPV	(Sabahi et al., 2020)
GCE/G2Fc/Ab	IgG	5.0–50 ng/mL	2.0 ng/mL	DPV	(Khanmohammadi et al., 2020)
Dye labeled DNA probe	CA15-3	0.01–1 U/mL	0.0039 U/mL	A.C impedance	(Zhao et al., 2020)
Self-assembled ferrocenecored poly (amido amine) dendrimers	BRCA1	1.3–20 nM	0.38 nM		(Senel et al., 2019)
ERBB2c modified probe CD24c DNA modified probe	HER2	0.37–10 nM	0.16 nM 0.23 nM	Electrochemical impedance spectroscopy	(Saeed et al., 2017)
ssDNA modified prob	CYFRA21-1	10 fM – 100 nM	1.0 × 10 ⁻¹⁴ M	DPV	(M. Chen et al., 2018)
Fe ₂ N NPs@rGOS/prob	4-NQO	0.05– 574.2 μM	9.24 nM		(T.-W. Chen et al., 2020)
p53-Ab2-tGO-AuNPs	p53	20 - 1000 fg/ml	4 fg/ml	electrochemical impedance spectroscopy (EIS)	(Aydın & Sezgintürk, 2017)
ssDNA λ-exo modified prob	EGFR exon 21	0.1 μM–3 μM	120 nM	DPV	(Shoja et al., 2018)

The obtained results showed that the fabricated immunosensor has an acceptable analytical performance and also that it is responsive to YES1 even in very low concentrations. The Gold Nano particles aided electrochemical signal enhancement by providing a lower detection limit of the immunosensor.

4.7.3: Determination of kinetic parameters of the immunosensor

Determination of the kinetic parameters of the immunosensor was done and the results obtained are as shown in Figure 4.13 (A and B). It was observed that, the electrode current increased with the increase in antigen concentration in the analyte and the linearity region was between 0.01 and 100 ng/mL. The oxidation peaks current remained constant beyond antigen concentration of 100 ng/mL (Figure 4.13 B)

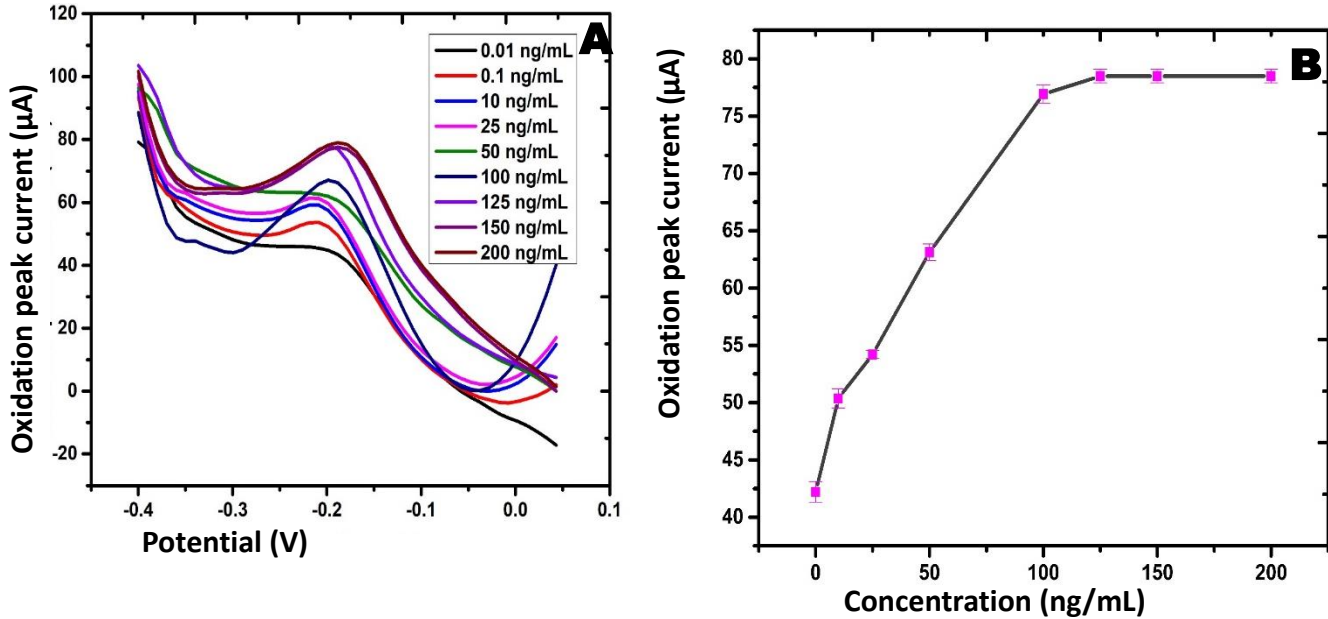


Figure 4.13: DPV showing dependence of YES1 antibody on antigen concentration (A); linear calibration curve showing dependence of YES1 antibody on antigen concentration (B). Each datum point represents the average analysis of triplicate values ($n=3$). Error bars correspond to the standard deviation (SD) of three measurements ($n=3$).

There is dependence of the peak current on analyte concentration for enzyme kinetics which was observed in this study for antibodies and antigen as the substrate. It was assumed that the antibodies had been uniformly immobilized into sensor surface for lower antigen concentration, the reaction occurred on the sensor surface, corresponding to the linearity region in Figure 4.14.

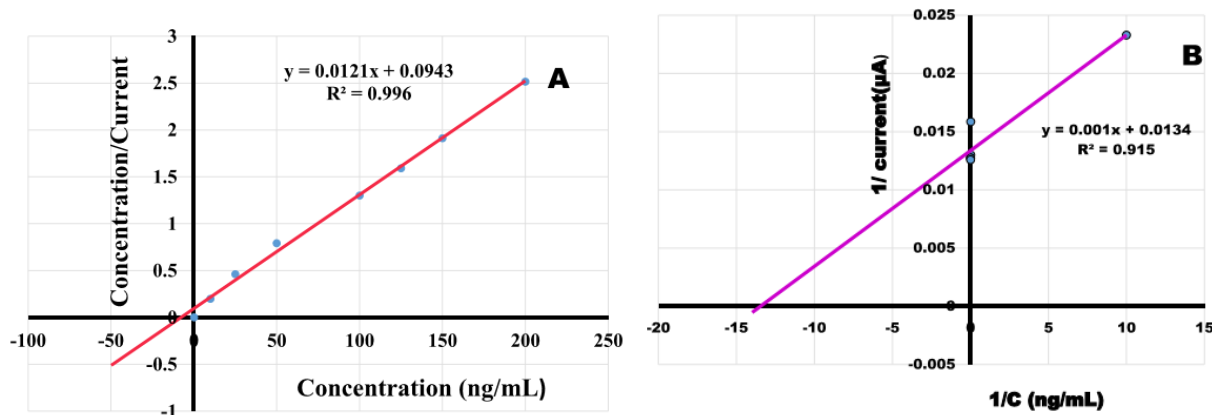


Figure 4.14 A: Hanes Woolf plot of YES1 concentration divided by peak current vs. YES1 concentration. B: Line Weaver- Burk plot of 1/ current vs 1/ Concentration.

For higher antigen concentrations, delay on the response time could be due to diffusion limitation (Figure 4.13 B). Further increase in antigen concentration resulted into constant peak current. Linearization of potential dependence on antigen concentration is given in Figure 4.14 which was used in the estimation of the apparent Michaelis-Menten kinetics parameters.

Maximum reaction rate (V_{Max}) was determined by dividing one by gradient from Figure 4.14A, and it was 82.64. Apparent Michaelis-Menten constant, K_m value, was obtained by getting $-X$ intercept from Figure 4.14A, it was 7.79 ng/mL.

The values for V_{Max} and K_m obtained compared very well with those obtained using Line Weaver Burk plot as shown in Figure 4.14 B. That value is significantly lower than results from studies such as for gold nanoparticles and glucose oxidase (K_m was 12.1mM)(Wang *et al.*, 2008) while the ZnO nanotubes have a calculated K_m of 19mM (Kong *et al.*, 2009). Michaeli's Menten constant, K_m , values are, an indication on the extent to which the protein binds onto the substrate. Generally, the lower the K_m value, the more strongly the enzyme binds to the substrate. Therefore, the K_m value obtained in this study (7.79 ng/mL) indicates that YES1 binds strongly onto the modified electrodes, and that YES1 is a suitable antibody for fabrication of the immunosensor. The low value obtained for the apparent Michaelis-Menten constant was probably as a result of good covalent conjugation of antibodies to the gold nanoparticles by thiolated protein G and also

cross linking of antibodies by glutaraldehyde. This prevented diffusion limitations and allowed favorable orientation of bound antibodies thus high accessibility to substrate.

4.7.4: Detection of YES1 and CEA in cell culture supernatants and cell lysates

Figure 4.15. shows the voltammetric response obtained after the incubation of the immunosensor with solutions containing equal concentrations of YES1 and CEA. The potential was scanned between -0.4 to +0.1 V for YES1 and -0.4 to + 0.9 V for CEA. The scans provided well-defined oxidation peaks at -0.188 V for YES1 and $+0.65$ V for CEA (Figure 4.15 A and B). The electrochemical detection that was performed with A549 cells showed that the specific electrochemical signals to the probe that appeared at -0.188 V and $+0.065$ V were related to YES1 and CEA respectively. The signals for scans without the cells did not show any peak at all (Figure 4.15 A and B). The oxidation current was observed almost instantaneously in the experiments, which could mean that equilibrium was attained very fast, resulting in the formation of the peak. The experiments were carried out at room temperature.

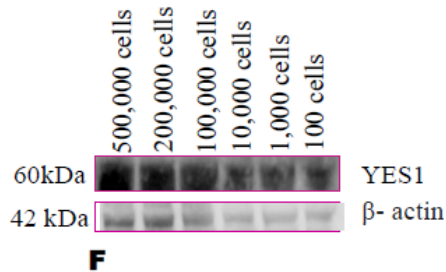
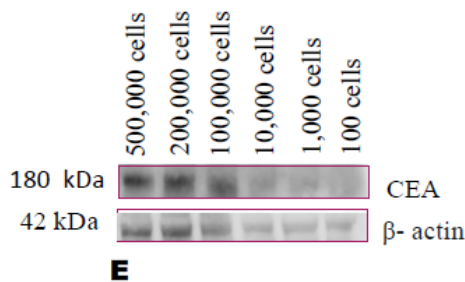
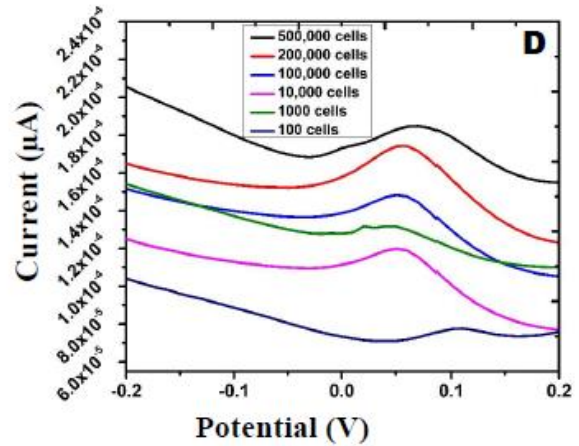
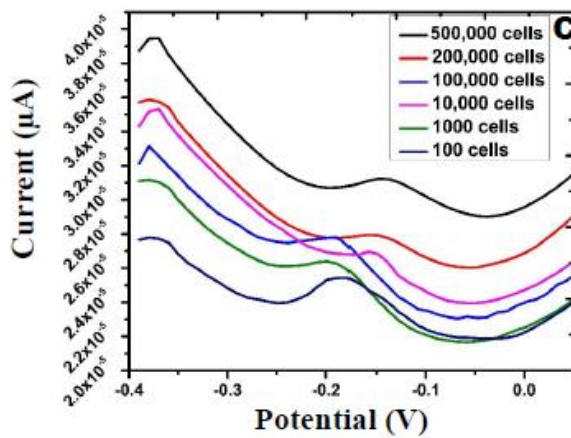
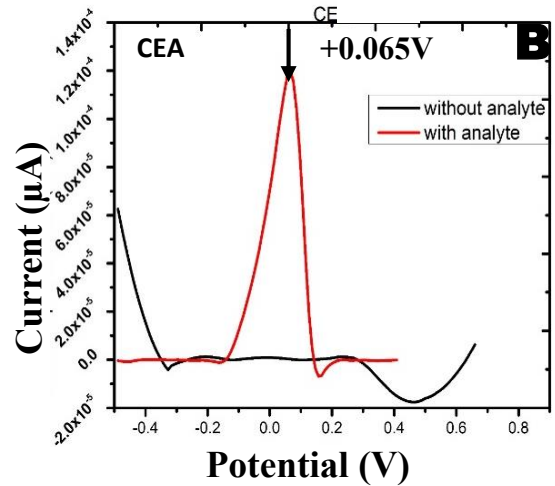
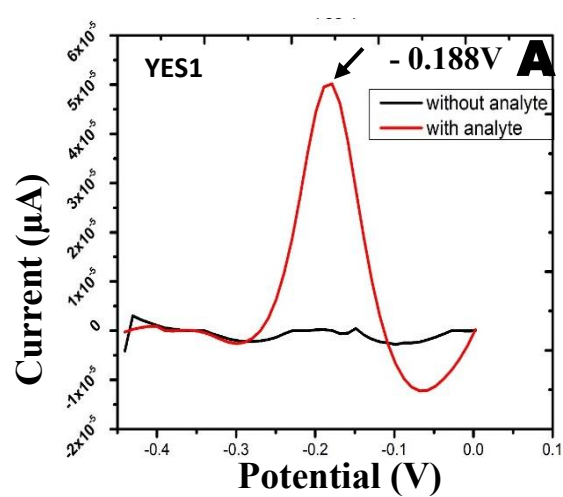


Figure 4.15: Electrochemical immunosensor measured with and without analyte (A549 supernatant) by DPV (A) YES1 (B) CEA. DPV detection of varying amount of A 549cells (C) using YES1 sensor (D) using CEA sensor (E) Immunoblotting of varying cells CEA (F) Immunoblotting of varying cells YES1

Figures 4.15 (C- F) show how the validity of the use of the oxidation peak in CEA and YES1 concentration in the cultured cell supernatant, varying amounts of A549 cells was assessed. The results obtained showed that, the oxidation peak current peak obtained significantly increased with increasing number of cells from 100 to 500,000, thereby suggesting that the immunosensor could detect less than 100 cells in the cell supernatant. These results indicate that the proposed sensing system could be used to detect CEA and YES1 in cell culture supernatants.

Comparison of the results obtained by DPV Figures 4.15 (C and D) and those obtained by immunoblotting for both CEA and YES1 Figures 4.15 (E and F) was done. The results obtained indicated that the quantity of the proteins detected in the immunoblots corresponded to the results obtained by the immunosensor (Figure 4.15 (E and F)). β - actin was used as a loading control to ensure equal volumes of proteins were loaded in all the wells of SDS PAGE.

4.7.5: Verification of the immunosensors

In the study for verification of the immunosensors, it was clear that the sensor could be used to detect YES1 and CEA biomarkers in cell culture supernatants Figures 4.16 A – F). The preparation of the cell culture supernatants was done as explained in section 3.8.1.2.

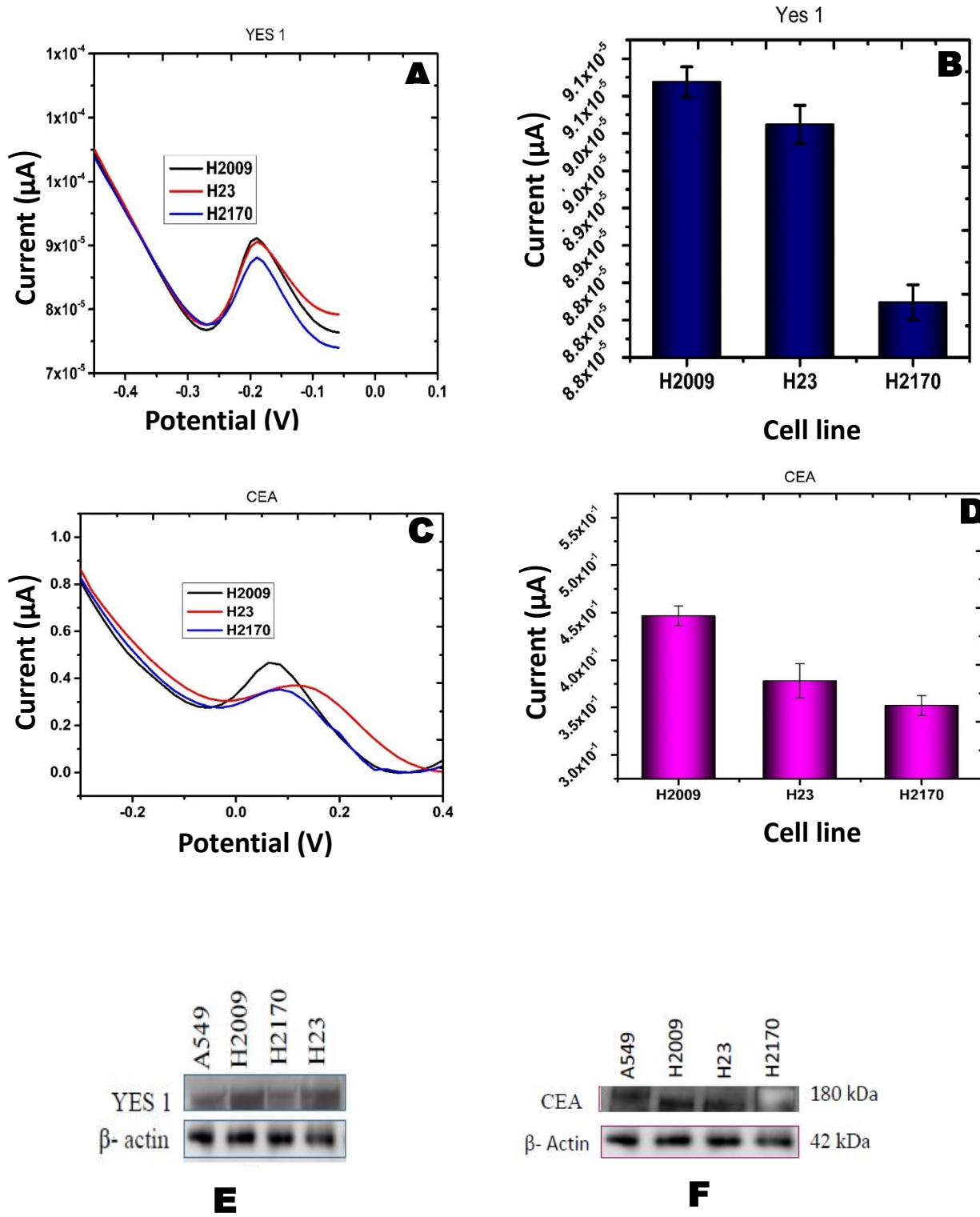


Figure 4.16: DPV curves showing universal detection of biomarkers in cell culture supernatants of multiple cell lines (A and B) YES1 (C and D) CEA. Immunoblot analysis in cell culture supernatants (E) YES1 and (F) CEA. Error bars represent SD (n = 3).

In these results, the amount of YES1 and CEA biomarker in H2009 released to the culture supernatant was higher than that released in the H23 and H2170 cancer cell lines. This could be attributed to the fact that H2009 NSCLC cell line had a higher rate of multiplication compared to H23 and H 2170, with the latter being the slowest. This was depicted by higher oxidation peak current in cancer cell line H2009 for the culture supernatant for both CEA and YES1. The results obtained by the immunosensors were also comparable to those obtained using immunoblotting as shown by the intensity of the bands (Figure. 4.16 E and F). β - actin was used as a loading control to ensure that equal volumes of proteins were loaded in all the wells of SDS PAGE.

Similar results to the one obtained using cell culture supernatants were observed when cell culture lysates of multiple cancer cell lines of Non-Small Cell Lung Cancer (NSCLC) cell lines (H2170, H23 and H2009) were analyzed, A549 was not included in the CV analysis of cell culture supernatants since it was used for the analysis of different cells (Figures 4.16 A – D).

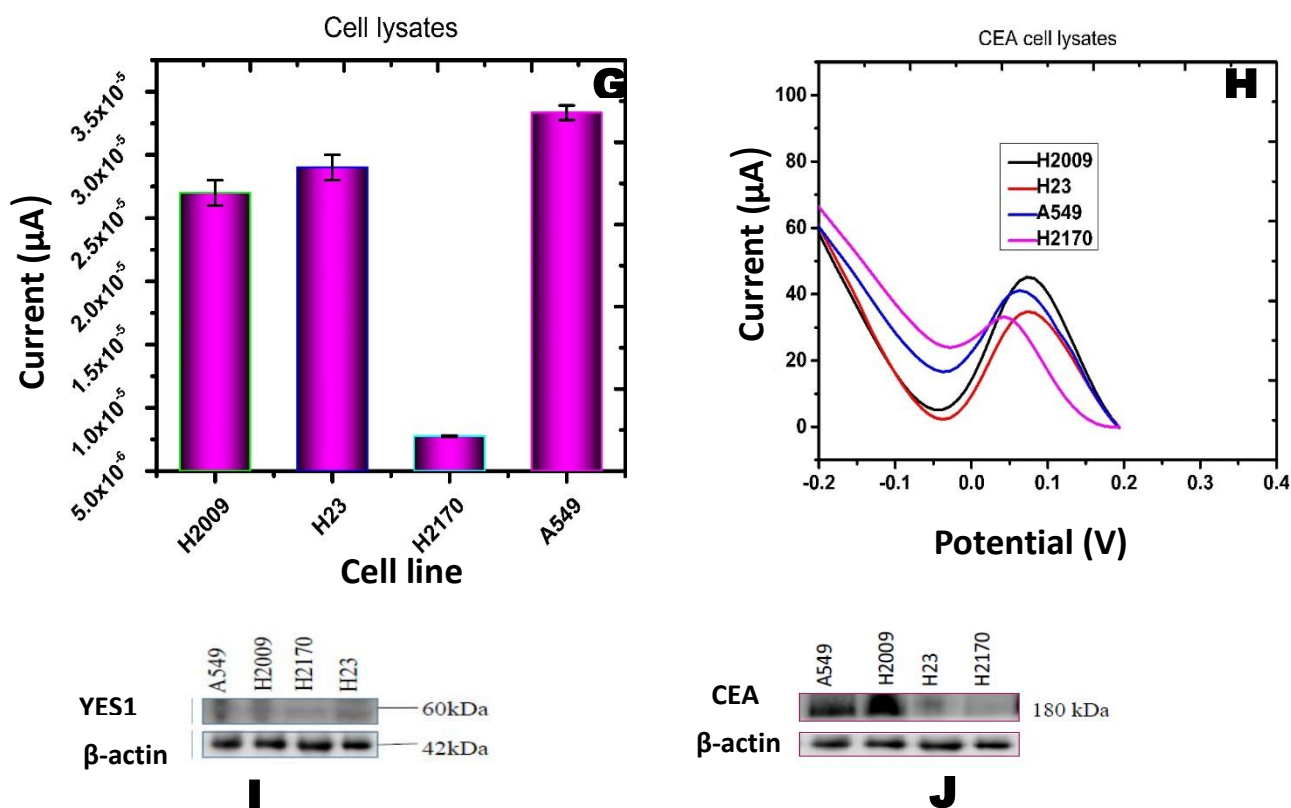


Figure 4.17: Analysis of YES1 in cell lysates (G) DPV analysis of CEA in cell lysates (H). Immunoblot analysis in cell culture lysates (I) YES1 and (J) CEA. Error bars represent SD (n = 3).

The preparation of the cell lysates from cultured cells was done as explained in section 3.8.1.1. The results showed that cancer cell line H2170 had the lowest oxidation peak current (Figure 4.17 G and H) had the weakest immunoblot band due to the fact that the cancer cells had the lowest rate of cell growth (Figure 4.17 I and J). Thus low amounts of CEA and YES1 were detected using the immunosensor and also immunoblotting. Cancer cell line A549 showed high expression for CEA when detected with the immunosensor (Figure 4.17 G). The results were in agreement with the results obtained by immunoblotting (Figure 4.17 I). Cancer cell line A549 had a high rate of cell multiplication and this higher concentration of CEA biomarker in the cell lysates. The results obtained implied that the immunosensor fabricated was able to detect different concentrations of CEA and YES1 in different cancer cell lines. Thus the results show universal use of the fabricated immunosensor in detection of different levels of CEA and YES1 cancer biomarkers in other cancer cell lines other than A549 cell line.

4.8: Electrochemical immunosensor detection of YES1 and CEA in human plasma

The study investigated whether the immunosensor could detect the presence of YES1 and CEA in human plasma samples obtained from the Clinic Universidad de Navarra in Spain.

Table 4.3 shows a summary of clinical and pathological information of the cohort of 104 samples of the human plasma analyzed. The gender from which the samples were obtained was taken into consideration as well as the range of age of the patients as shown in Table 4.3. Cancer stage and also the smoking status of the patient's plasma was also put into consideration (Table 4.3). The samples were assessed for the presence of YES1 and CEA biomarkers using the immunosensor, immunoblotting and image J.

Table 4. 3: Summary of blood samples data obtained from Clinic Universidad de Navarra Cohort (n = 104)

	N (%)
Gender	
Male	89 (86)
female	15 (14)
Age range	23-85 years
Cancer stage	
I	42 (49)
II	22 (26)
III	18 (17)
IV	4 (5)
Smoking status	
Former smokers	61 (71)
Current smokers	14 (14)
Non- smokers	11(13)

First, optimization studies were carried out to find out the optimal dilution ratio of the human plasma. Figures 4.18 A and B showed the DPV results and linear curve representation respectively obtained when a serial dilution of the plasma samples was done using phosphate buffer solution PBS (Lonza) to determine the optimum concentration for the immunosensor.

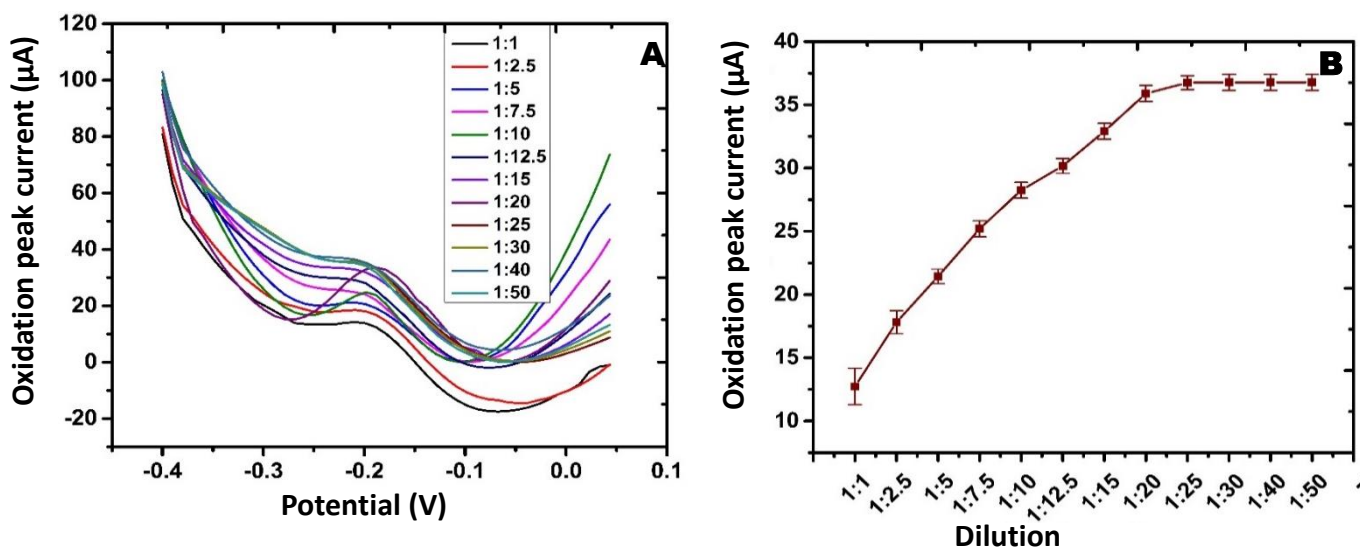


Figure 4.18: DPV showing the detection of YES1 by serial dilution of human plasma (A). linear curve showing detection of YES1 by dilution of human plasma (B) Each datum point represents the average analysis of triplicate values (n= 3). Error bars correspond to the standard deviation (SD) of three measurements (n=3).

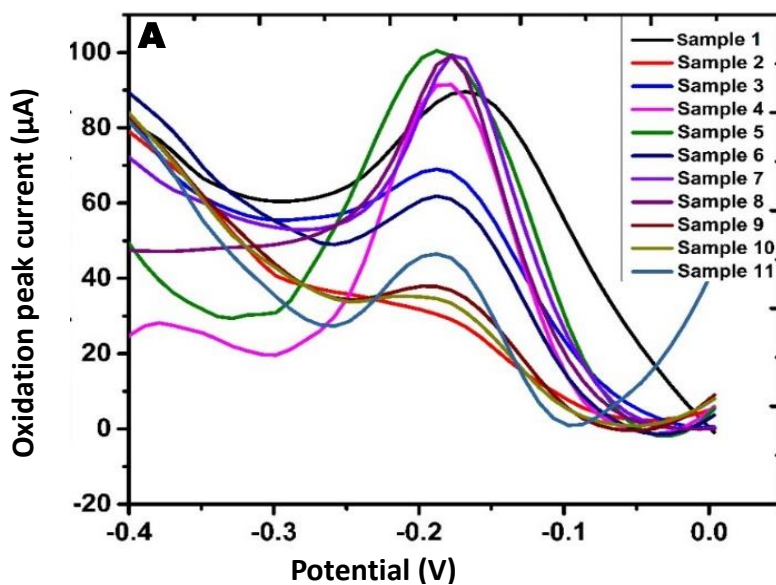
The oxidation peaks current increased with increase in concentration from dilution of 1: 1 up to dilution of 1: 20 then the potential remained constant. Dilution of 1: 20 was found to be the optimum dilution ratio for the immunosensor as shown in Figures 4.18 A and B. The obtained dilution ratio was used throughout for all immunosensor detections of blood plasma samples.

4.8.1 Detection of YES1 in human plasma

Detection of YES1 biomarker in 104 samples of human plasma was done using the fabricated immunosensor. The results reported in this study is a representation of only a few samples.

Results obtained in Figure 4.19 (A and D) showed that the oxidation peak current increased with increase in concentration of YES1 protein in the plasma. Further increase in protein concentration in the plasma led to no increase in the peak height of DPV. The reason for this could have been that increasing the amount of the immuno-complex hindered more electron transfer on the modified electrode surface.

SET1



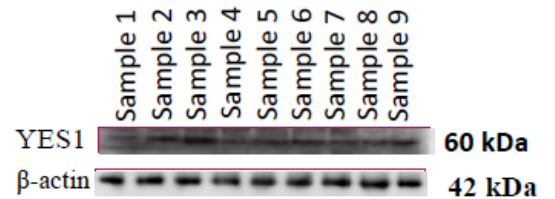
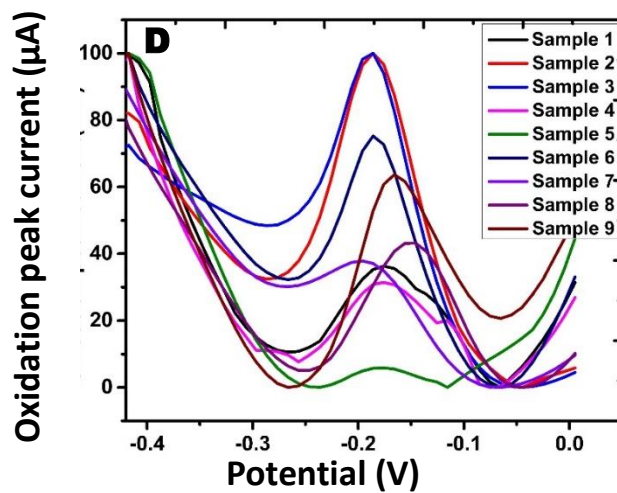


B

Sample	1	2	3	4	5	6	7	8	9	10	11
Amount of YES1 protein in tumor	207	16	200	218	Amp	195	225	243	170	60	98
Amount of YES1 analyzed using image J (a.u)	1461.84	19.74	1206.66	1670.49	2074.79	994.72	1687.57	1914.12	843.06	596.92	917.49
Peak height obtained using immunosensor (μ A)	30.74	No peak	28.93	61.80	75.76	27.30	60.85	62.52	11.94	9.38	31.10

C

SET 2



E

Sample	1	2	3	4	5	6	7	8	9
Amount of YES1 analyzed using image J (a.u)	2109.88	6998.48	7043.40	2003.20	531.54	3032.26	2438.17	2695.99	2935.36
Peak height obtained using immunosensor (μ A)	44.84	78.39	78.41	41.80	15.23	61.42	55.85	58.37	59.22

F

Figure 4.19: DPV showing detection of YES1 in human plasma (A and D). Immunoblots for human plasma for samples of SET 1 (B) and SET 2 (E). Analysis of immunoblots of B using image J (C) Analysis of immunoblots of E using image J (F)

The results obtained were verified by using immunoblotting (Figures 4.19 B and E). The immunoblots were further analyzed quantitatively using the image J software to give the densitometry of the biomarkers in human plasma (Figures 4.19 C and F). In Figure 4.19 A, sample 2 had the lowest YES1 expression and recorded no oxidation peak current. This results were verified using immunoblotting where the immunoblot band was very weak as shown in Figure 4.19 B. Further analysis was done using image J to show the densitometry of the biomarkers in human plasma (Figure 4.19 C). The results obtained showed that sample 2 in set 1 had the lowest value of 19.74 indicating that the sample had low concentration of YES1. The results obtained had a reliable correlation with those obtained using immunoblotting and image J.

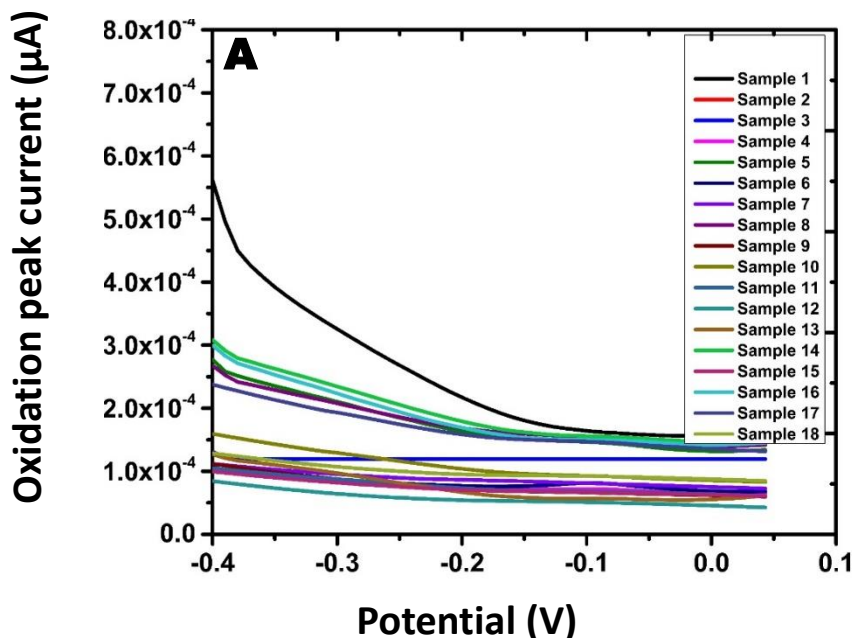
In set 2, Figure 4.19D, sample 5 had the lowest peak current showing low YES1 concentration. This results were verified using immunoblotting (Figure 4.19 E) where a weak band was observed. Analysis using image J (Figure 4.19 F) recorded a value of 531.54. In set 1, Figure 4.19 A, sample 5 had the highest peak current indicating highest YES1 expression with densitometry values of 2074.79 (Figure 4.19 C). This results were supported by the strong immunoblotting band obtained as shown in Figure 4.19B.

In set 2, Figure 4.19 D, sample 3 had the highest peak current showing highest expression of YES1 concentration. This results were verified using immunoblotting (Figure 4.19 E) which had the strongest immunoblot band. Analysis with image J showed the densitometry value of the immunoblot band was also the highest with a value of 7043.40 units.

Results obtained (Figures 4.19 A to F) showed that increase in concentration of YES1 biomarker in human plasma led to increase in the DPV oxidation peak current. This results were supported by immunoblots and image J analysis where High YES1 expression in human plasma led to strong immunoblot band and high densitometry value respectively.

β -actin was used as the loading control to ensure equal volumes of proteins were loaded in each well of Sodium dodecyl-sulfate polyacrylamide gel electrophoresis (SDS-PAGE) for immunoblotting. The results obtained showed that the fabricated immunosensor was able to detect high YES1 expression in the plasma samples of patients with cancer stage II-IV. All the results obtained have illuminated the applicability of the proposed immunosensor in real human samples such as human plasma.

When control studies were conducted using plasma obtained from healthy individuals whose gender and age was known, no peaks were observed from the immunosensor (Figure 4.20).



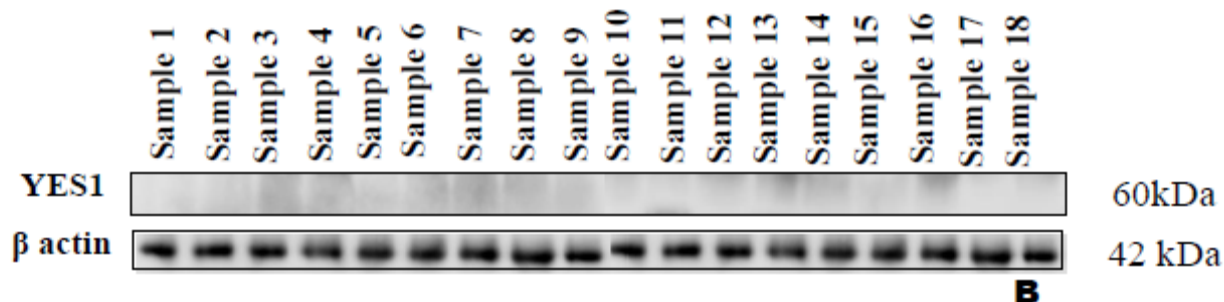


Figure 4.20: DPV showing detection of YES1 in human plasma samples from healthy individuals (A) Immunoblots for human plasma for samples of A (B).

The results obtained by immunosensor showed a co relation to those obtained by immunoblotting as shown in Figure 4.21 B where no immunoblot bands were observed in the samples obtained from healthy patients. β - Actin was used as a loading control to ensure equal volumes of proteins were loaded in each well of Sodium dodecyl-sulfate polyacrylamide gel electrophoresis (SDS-PAGE) for immunoblotting. The results obtained showed that the fabricated immunosensor could be used to differentiate human plasma from individuals with and without NSCLC

4.9: Simultaneous detection of CEA and YES1

When the performance of the fabricated multiplexed immunosensor was evaluated under optimized conditions using known concentrations of CEA and YES1, the DPV oxidation currents of the immunosensor increased with the concentrations of YES1 and CEA as shown in Figure 4.21A.

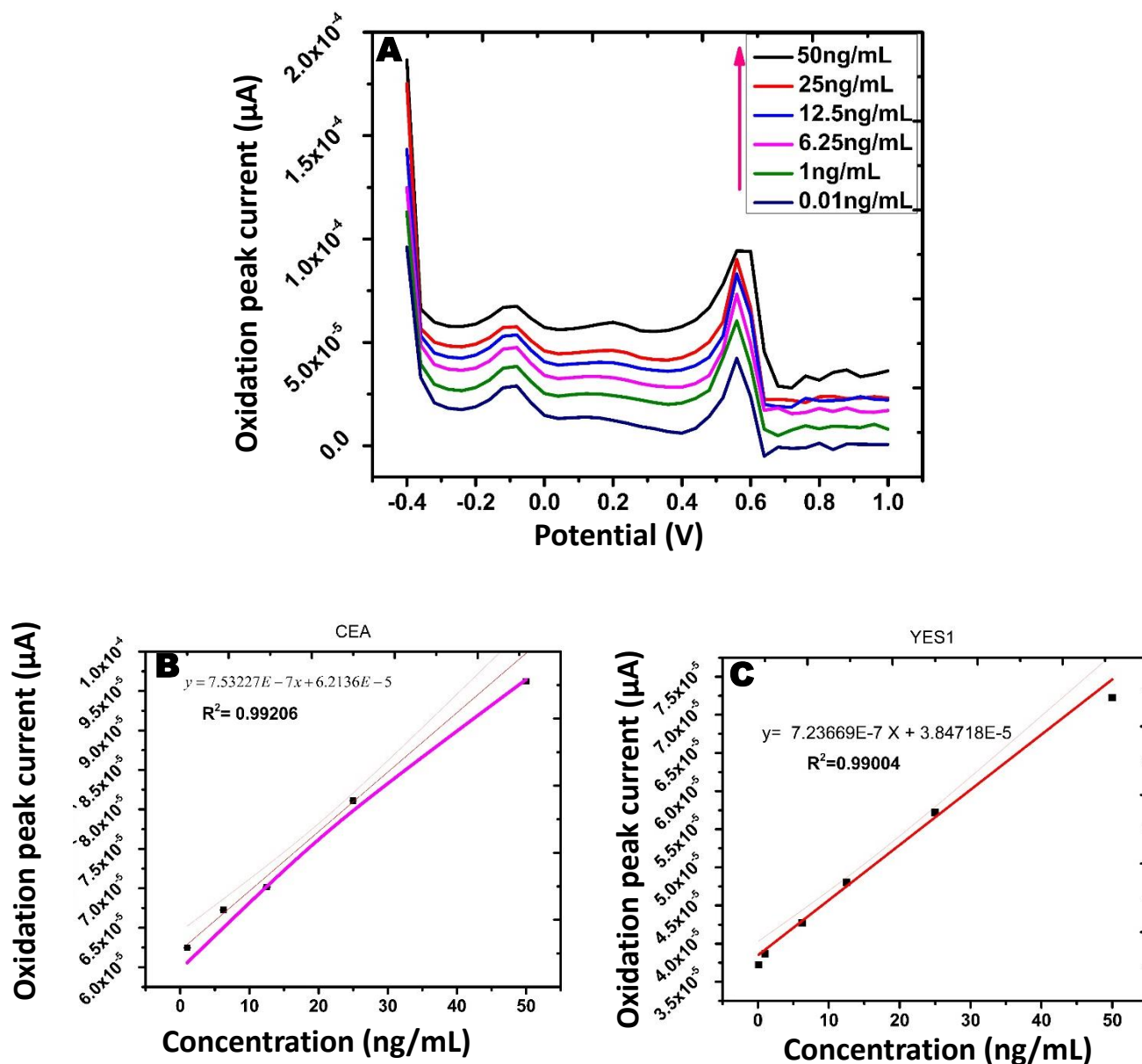


Figure 4.21: DPV responses of the proposed immunosensor after incubation with different concentrations of YES1 and CEA (A); Calibration curves of the multiplexed immunoassay toward CEA (B) and YES1 (C) in 0.1 M PBS (pH 7.4) with 1mM $\text{K}_3\text{Fe}(\text{CN})_6$, 0.1 M KCl.

The oxidation peaks at -0.18 V and $+0.53$ V represented the existence of YES1 and CEA biomarkers respectively (Figure 4.21 A). The calibration curves showed a linear YES1 and CEA relationship between the oxidation peak currents and the concentrations of YES1 and CEA in the range from 0.01 to 50 ng/mL (Figures 4.21 B and C). The correlation coefficient was 0.9921 for CEA and 0.9900 for YES1 as shown in Figures 4.21 B and C.

The LOD and LOQ values of the immunosensor were calculated from the expressions $LOD = (3X SD/m)$ and $LOQ = (10X SD/m)$ (Armbruster and Pry, 2008), where **SD** is the estimated standard deviation from the points used to construct the calibration curve and **m** is the slope

The limit of detection (LOD) was observed to be 0.0022 and 0.0034 ng/mL for CEA and YES1 respectively while limit of quantification (LOQ) of CEA and YES1 was 0.00732 and 0.01133 ng/mL respectively.

The results obtained in this study showed that the limit of detection was below most of the electrochemical immunosensors for multiplex detection of cancer fabricated so far as shown in Table 4.4. The Table 4.4 shows data on some of the multiplex electrochemical immunosensors which have been fabricated in the literature.(Zhu et al., 2015)

Table 4.4: Multiplexed electrochemical Immunosensors

Electrode	Label	Analyte	Immuno assay	Technique	Linear Range	LOD	Sample	Ref.
GA/Thio Prot G/ AuNPs/ GCE	HRP-AuNPs	CEA YES 1	Sandwich-type; direct detection	DPV	0.01 to 50 ng/mL CEA 0.01 to 50 ng/mL YES 1	0.0022 ng/mL CEA 0.0034 ng/mL YES 1	Human plasma	This work
AuNPs/GCE	PVP/GS/PtPdNPs/HRP/AQ PVP/GS/PtPdNPs/HRP/THI	AFP, APT; DCP, AFP-L3, γ -GT, AFU	Sandwich-type; addition of H ₂ O ₂	DPV	0.2–600 pg·mL ⁻¹ CEA; 0.2–1000 pg·mL ⁻¹ CA125; 0.2–800 pg·mL ⁻¹ PSA; 0.2–800 pg·mL ⁻¹ AFP	0.008 ng·mL ⁻¹ AFP; 0.0082 ng·mL ⁻¹ APT; 0.01UL ⁻¹ DCP; 0.008 ng·mL ⁻¹ AFP-L3; 0.33 UL ⁻¹ γ -GT; 0.4 UL ⁻¹ AFU	Serum	(Yang et al., 2014)
G/Au/GCE	THI (or Co or Fc or AQ)- Strept-Biotin- dsDNA/Strept-Biotin- Ab ₂ /AuNPs/SiO ₂ /Fe ₃ O ₄	CEA, CA125, PSA, AFP	Sandwich-type; direct detection after conjugation	DPV	0.2–600 pg·mL ⁻¹ CEA; 0.2–1000 pg·mL ⁻¹ CA125; 0.2–800 pg·mL ⁻¹ PSA; 0.2–800 pg·mL ⁻¹ AFP	48 fg·mL ⁻¹ CEA; 77 fg·mL ⁻¹ CA125; 60 fg·mL ⁻¹ PSA; 62 fg·mL ⁻¹ AFP	-	(Zhu et al., 2015)
IL/rGO/GCE	PtNPs-Cu ²⁺ PtNPs-Cd ²⁺	AFP CEA	Sandwich-type; reduction	DPV	0.05–200 ng·mL ⁻¹	0.05 ng·mL ⁻¹ AFP 0.002 ng·mL ⁻¹ CEA	serum	(Z. Wang et al., 2014)
GCE (Hg)	PAMAM-CdS (or ZnS, or PbS)	CA125 CA15-3 CA19-9	Sandwich-type; direct detection of Cd, Zn and Ag	SWASV	0.01–50 U·mL ⁻¹	0.005 U·mL ⁻¹	serum	(Tang et al., 2013)
AuNPs/Chit/GCE	CGS-PB; CGS-TB	CEA; AFP	Sandwich-type; direct detection	DPV	0.5–60 ng·mL ⁻¹	0.1 ng·mL ⁻¹ (CEA) 0.05 ng·mL ⁻¹ (AFP)	serum	(Chen et al., 2013)
AuNPs/Chit/GCE	Chit/AuNPs/PB; Chit/AuNPs/Fc	CEA; AFP	Sandwich-type; direct detection	DPV	0.05–100 ng·mL ⁻¹	0.02 ng·mL ⁻¹ (CEA) 0.03 ng·mL ⁻¹ (AFP)	serum	(Chen & Ma, 2014)
HAG/PANI/rGO/GCE	AuNPs/rGO/PB; AuNPs/rGO/PDDA/THI	CEA; AFP	Sandwich-type; direct detection	DPV	0.6–80 ng·mL ⁻¹	0.12 ng·mL ⁻¹ (CEA) 0.08 ng·mL ⁻¹ (AFP)	serum	(Feng et al., 2014)
AuNPs/GCE	Fc/HRP THI/HRP	CEA AFP	Direct assay after addition of H ₂ O ₂	DPV	0.01–50 ng·mL ⁻¹	0.01 ng·mL ⁻¹	serum	(Lai et al., 2012)
AuNPs/G/GCE	THI-HRP-NPG-MnO ₂ Fc-HRP-NPG-MnO ₂	CA-15-3 CA-125	Sandwich-type; addition of H ₂ O ₂	SWV	0.01–50 U·mL ⁻¹	3.5 mU·mL ⁻¹ (CA-153) 4.1 mU·mL ⁻¹ (CA-125)	serum	(Y. Zhang et al., 2013)
PDPMT-Cl-Chit/GCE	THI-Fe ₃ O ₄ NPs Fca-Fe ₃ O ₄ NPs	SCC-Ag CEA	Sandwich; direct detection	DPV	0.01–10 ng·mL ⁻¹	4 pg·mL ⁻¹ (SCC-Ag) 5 pg·mL ⁻¹ (CEA)	serum	(X. Zhang et al., 2014)

AuNPs/AuE	TiO ₂ /NF- Co(dcbpy) ₃ ²⁺ TiO ₂ /NF- MB	CA15-3 CA19-9	Sandwich-type; direct detection	DPV	5-100 U·mL ⁻¹ CA15-3 1-100 U·mL ⁻¹ CA19-9	UmL ⁻¹ CA15-3 1.6 UmL ⁻¹ CA19-9	serum	(G. Wang et al., 2013)
mucin1 (MUC1), GCE	poly(VFc-ATP) AuNPsPOPD/AuNPs	AFP CEA	Sandwich-type; direct detection	DPV	0.01-100 ng·mL ⁻¹	0.003 ng·mL ⁻¹ AFP 0.006 ng·mL ⁻¹ CEA	serum	(Liu et al., 2015)
AuNPs/G/GCE	PS-Cd ²⁺ PS-Fc	IL-6 IL-17	Sandwich-type; direct detection	SWV	1-1000 pg·mL ⁻¹ IL-6 2-1000 pg·mL ⁻¹ IL-17	0.5 pg·mL ⁻¹ 1 pg	serum	(T. Li et al., 2013)
Protein A/Nafion/GCE	GS/AuNPs-THI (or Cobpy) ₃ ³⁺ or Fc)	AFP CEA SS2	Sandwich-type; direct detection	DPV	0.016-50 ng·mL ⁻¹ AFP 0.010-50 ng·mL ⁻¹ CEA 0.012-50 ng·mL ⁻¹ SS2	5.4 pg·mL ⁻¹ AFP 2.8 pg·mL ⁻¹ CEA 4.2 pg·mL ⁻¹ SS2	-	(Zhu et al., 2013)
AuNPs/PEI/PT CA/GCE	Au@PBNPs/O-GS-Strept- AP; Au@NiNPs/O-GS- Strept-AP	fPSA PSA	Sandwich-type; AA-P addition	DPV	0.02-10 ng·mL ⁻¹ fPSA 0.01-50 ng·mL ⁻¹ PSA	6.7 pg·mL ⁻¹ 3.4 pg·mL ⁻¹	serum	(Han et al., 2012)
MWCNTs/GC E	AA liposome UA liposome	NSE ProGRP	Sandwich-type, direct detection	LSV	50-1000 pg·mL ⁻¹	5.0 pg·mL ⁻¹ NSE 100 pg·mL ⁻¹ ProGRP	serum	(Zhong et al., 2011)
AuNPs/ILrGO /GCE	Cd (or Pb or Cu) AlgNBs	AFP CEA PSA	Sandwich-type; direct detection	DPV	0.01-100 ng·mL ⁻¹	0.01 ng·mL ⁻¹ AFP 0.0086 ng·mL ⁻¹ CEA 0.0075 ng·mL ⁻¹ PSA	serum	(Z. Wang et al., 2015)
GCE (Bi)	PLL/AuNPs/Cd-Apo (or Pb-Apo)	AFP CEA	Sandwich-type; direct detection	ASSWV	0.01-50 ng·mL ⁻¹	4 pg·mL ⁻¹	serum	(D. Wang, Li, et al., 2015)
Chit/AuNPs/G CE	GA/Chit/pAA NSs- Cu ²⁺ (or Cd ²⁺ or Zn ²⁺)	CEA CA19-9 CA125 CA242	Sandwich-type; direct detection	SWV	0.1-100 ng·mL ⁻¹ CEA 1-150 U·mL ⁻¹ CA 19-9, CA125,CA242	0.02 ng·mL ⁻¹ CEA 0.4 U·mL ⁻¹ CA19-9 0.3 U·mL ⁻¹ CA125 0.4 U·mL ⁻¹ CA242	serum	(Rong et al., 2016)
SPCE	PEI-AuNPs	MUC1 CA15-3 HER2	Sandwich-type; direct detection	DPV	0.10-100 U mL ⁻¹ CA15-3 0.10-100 ng mL ⁻¹ MUC1 and HER2	0.21 U mL ⁻¹ , CA15-3 0.53 ng mL ⁻¹ MUC1 0.50 ng mL ⁻¹ HER2	-	(Kuntamung et al., 2021)
graphene/meth ylene blue- chitosan/antibo dy	graphene/methylene blue- chitosan/antibody	CEA CA153 CA125	Sandwich-type; direct detection	CV	0.10-1.00 pg mL ⁻¹ CEA, 0.10-2.50 mU mL ⁻¹ CA153, 0.10-2.50 mU mL ⁻¹ CA125,	0.04 pg mL ⁻¹ CEA, 0.04 mU mL ⁻¹ CA153, 0.04 mU mL ⁻¹ CA125.	-	(Cotchim et al., 2020)

rGO/THI (or PB)/AuNPs/ITO	-	CEA AFP	Direct detection of of THI or PB	SWV	0.01–300 ng·mL ⁻¹	0.650 pg·mL ⁻¹ CEA 0.885 pg·mL ⁻¹ AFP	serum	(Jia et al., 2014)
CD/G/GCE	CD/Fc/G CD/THI/G	CEA AFP	Sandwich-type with HRP-Ab ₂ and H ₂ O ₂ detection	DPV	0.003–40 ng·mL ⁻¹ CEA 0.001–60 ng·mL ⁻¹ AFP	0.8 pg·mL ⁻¹ CEA 0.5 pg·mL ⁻¹ AFP	serum	(Q. Li et al., 2014)
orPB)/AuNPs/TCCRMSs/FTO	-	CEA NSE	Direct; detection of TB or PB	SWV	2–25 ng·mL ⁻¹	0.11 ng·mL ⁻¹ CEA 0.08 ng·mL ⁻¹ NSE	serum	(Lu et al., 2015)
HOOC-MBs/SPCE	ACTP/AuNPs ATLP/AuNPs	p53 ¹⁵ , p53 ³⁹²	Sandwich-type; detection of metals	SWV	1–20 ng·mL ⁻¹ (p53 ¹⁵) 0.5–20 ng·mL ⁻¹ (p53 ³⁹²)	0.5 ng·mL ⁻¹ (p53 ¹⁵) 0.2 ng·mL ⁻¹ (p53 ³⁹²)	serum	(Ge et al., 2016)
GCE (Bi)	G/AuNPs-r-Apo-Cd G/AuNPs-r-Apo-Pb	AFP CEA	Sandwich-type; detection of metals	SWASV	0.001–5 ng·mL ⁻¹	0.3 pg·mL ⁻¹ AFP; 0.35 pg·mL ⁻¹ CEA	serum	(D. Wang, Gan, et al., 2015)
rGO	CdSeTe@CdS Ag NCs	Bcl-2 Bax	Sandwich-type; direct detection of Cd and Ag	SWASV	1–250 ng·mL ⁻¹	0.5 fmol	leukemia K562 cells	(Zhou et al., 2016)
Chit/MWCNTs/GCE	OMC-Zn OMC-Cd	AFP HER-2	Sandwich-type; oxidation of metal ions	DPV	0.001–150 ng·mL ⁻¹	0.6 pg·mL ⁻¹ AFP 0.35 pg·mL ⁻¹ HER-2	serum	(Fang et al., 2015)
GCE	Euvison™-CdS (or PbS or AuNPs)	AFP CEA CA19-9	Sandwich-type; detection of metals	DPASV DPCSV	0.001–50 ng·mL ⁻¹ AFP; CEA; 0.005–100 ng·mL ⁻¹ CA19-9	0.02 pg·mL ⁻¹ AFP; 0.05 pg·mL ⁻¹ CEA; 0.3 pg·mL ⁻¹ CA19-9	serum	(D. Wang et al., 2014)
Gln/Chit/AuNPs/AuE	BSA/AuNPs-Pb ²⁺ BSA/AuNPs-Cd ²⁺	CEA AFP	Sandwich-type; reduction of metal ions	DPV	0.01–50 ng·mL ⁻¹	4.6 pg·mL ⁻¹ CEA 3.0 pg·mL ⁻¹ AFP	serum	(Xu et al., 2014)
AuNPs/AuE	AuNPs@MWCNTs-Pb ²⁺ AuNPs@MWCNTs-Cd ²⁺	CEA AFP	Sandwich-type; reduction of metal ions	SWV	0.01–60 ng·mL ⁻¹	3.0 pg·mL ⁻¹ CEA 4.5 pg·mL ⁻¹ AFP	serum	(Feng et al., 2015)
AuNPs/rGO/Chit	AgNPs/THI/CNSs AgNPs/CNSs	CEA AFP	Sandwich-type; direct detection	DPV	0.01–80 ng·mL ⁻¹	2.8 pg·mL ⁻¹ CEA 3.5 pg·mL ⁻¹ AFP	serum	(L. Li et al., 2016)
IL/rGO/PSS/GCE	CGN-THI CGN-DAP CGN-Cd ²⁺	CEA PSA AFP	Sandwich-type; direct detection	SWV	0.01–100 ng·mL ⁻¹	2.7 pg·mL ⁻¹ CEA 4.8 pg·mL ⁻¹ PSA 3.1 pg·mL ⁻¹ AFP	serum	(Xu et al., 2015)

Abbreviations used : Ascorbic acid (AA), Ascorbic acid 2-phosphate (AA-P), Apoferritin templated cadmium phosphates(ATCP), Alpha fetoprotein (AFP), Lens culinaris (LCA)-reactive fraction of AFP, Alpha-L-fucosidase (AFU), Silver nanoclusters (AgNCs), Alginate (Alg), Apoferritin (Apo), Abnormal prothrombin (APT), Apoferritin templated lead phosphates (ATLP), Uric acid (UA), Bcl-2 associated X protein (Bax), B-cell lymphoma (Bcl), Carcinoembryonic antigen (CEA), Chitosan (Chit), Carbon-gold nanocomposite (CGN), Carboxyl graphene Nano sheet (CGS), Carbon nanospheres (CNS), Des-c-carboxyl prothrombin (DCP), Ferrocene (Fc), free-prostate specific antigen (fPSA), Fluorine-doped tin oxide (FTO), Graphene (G), γ -glutamyltranspeptidase (γ -GT), Glassy carbon electrode (GCE), Onion-like graphene sheet (O-

GS), Human epidermal growth factor receptor type-2 (HER-2), Horse-radish peroxidase (HRP), Ionic liquid (IL), Nanoporous gold (NPG), Neuron-specific enolase (NSE), Ordered mesoporous carbon (OMC), Polyacrylic acid (pAA), poly(2-aminothiophenol) (PATP), Prussian blue (PB), Poly(3-(1,1-o-dimethyl-4-piperidine-methylene)thiophene-2,5-diylchloride)(PDPMT-Cl) ,Polyethyleneimine (PEI), Poly-L-lysine (PLL), Poly(o-phenylenediamine) (POPD), Progastrin-releasing peptide (ProGRP), 3,4,9,10-perylenetetracarboxylic acid (PTCA), Streptococcus suis serotype 2 (SS2), Toluidine blue (TB), Tryptophan and caffeic acid-based resin microspheres (TCCMRs), Thionine (THI), Vinyl ferrocene-2-aminothiophenol (VFc-ATP). Cancer antigen 15-3 (CA15-3), Human epidermal growth factor receptor 2 (HER2), Polyethylenimine coated-gold nanoparticles (PEI-AuNPs), Screen-printed carbon electrode (SPCE), Cancer antigen 153 (CA153), and Cancer antigen 125 (CA125).

4.9.1: Evaluation of reproducibility, stability, specificity, and cross-reactivity of the immunosensor.

The reproducibility, stability and specificity of the fabricated immunosensor were evaluated as discussed in the following subsections.

4.9.1.1: Reproducibility

Figure 4.22 shows an evaluation of reproducibility which was done using the peak current of solutions containing 10 ng/mL of a mixture of CEA artificial antigen and YES1. The reproducibility was done by measuring oxidation peak currents using four freshly prepared immunosensors and recording the oxidation peak current obtained. These measurements were repeated two times, and the relative standard deviation measurements calculated.

Evaluation of reproducibility using peak current for solutions containing 10mg/mL of a mixture of CEA artificial antigen and YES1 showed that the relative standard deviation (RSD) of the three measurements for the four electrodes was calculated to be 6.4%, 3.4%, 6.3% and 6.4% (Figure 4.22 A). This indicated that the proposed immunosensor possessed acceptable precision and reproducibility

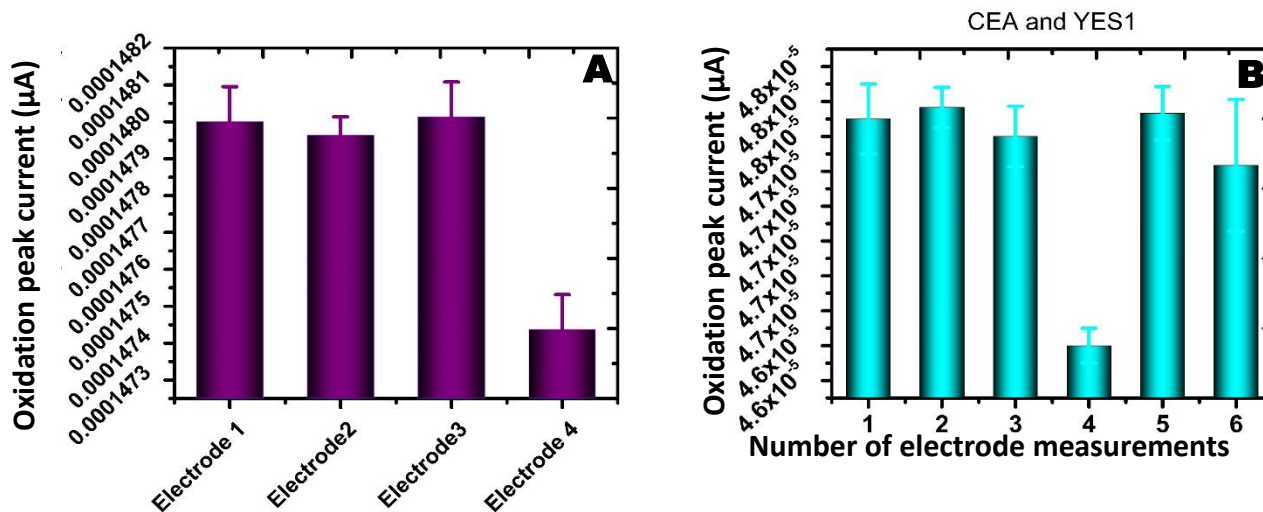


Figure 4.22: measurement of Reproducibility of CEA and YES1(A) using different electrodes. (B) using one electrode. (Error bars represent SD (n = 3)).

Evaluation of reproducibility which was assessed by monitoring the output of 10 ng/mL of a mixture of CEA and YES six times successively using the same immunosensor gave a Relative standard deviation (RSD) value of 1.1 % (Figure 4.22 B). The oxidation peak current was recorded each time for the six successive measurements. Regeneration of the immunosensor was done between each analysis using a solution containing 6mM NaOH and 0.6 % ethanol for 15 minutes in an attempt to break the antibody–antigen linkage and then it was washed three times with tween buffer. The results indicated that the immunosensor can be regenerated and reused, and that it does not need to be prepared afresh with each analysis.

It was observed that peak current in electrode 4 was slightly lower than the rest (Figure 4.22 A and B). This could have been as a result of detachment of the antibodies from the modified electrode to the electrolyte during analysis. The RSD value obtained in this study compared well with the results obtained in the literature. For instance, the relative standard deviation obtained for an immunosensor for sensitive detection of CEA based on Three-Dimensional Porous Nano platinum/Graphene peak current was 5.1% (Jing et al., 2020) while RSD for quantitative detection of breast cancer biomarker UBE2C was 3.11% (Jayanthi et al., 2019). The RSD of the five measurements carried out by Tian et al. (2016a) in Ultrasensitive sandwich-type electrochemical immunosensor for detection of CEA based on Tri metallic nanocomposite for 1 ng/mL CEA was calculated to be 3.2%. Therefore, the proposed immunosensor exhibited apt reproducibility.

4.9.1.2: Stability

Investigation of the stability of the immunosensor using a solution consisting of 5 ng/mL CEA and 5 ng/mL YES1 in which the immunosensor was stored in the refrigerator at 4 °C for two weeks in 0.1 M PBS showed that, at the end of fifteen days, the immunosensor retained 95.3% of the electric signal and had a relative standard deviation (RSD) of 2.2%, (Figure 4.23). The electric signal percentage obtained was slightly lower than results from studies like for the An electrochemical immunosensor for sensitive detection of the tumor marker carcinoembryonic antigen (CEA) based on three-dimensional porous Nanoplatinum/graphene where the electric signal retained was 96% after two weeks (Jing et al., 2020). Results obtained for Ultrasensitive multiplexed immunoassay of autophagic biomarkers based on Au/rGO and Au Nano cages amplifying electrochemical signal showed that the storage stability of the biosensor was 91.5% after two weeks (Wang et al., 2017). The results obtained in this study indicated that, the storage stability of proposed immunosensor was acceptable.

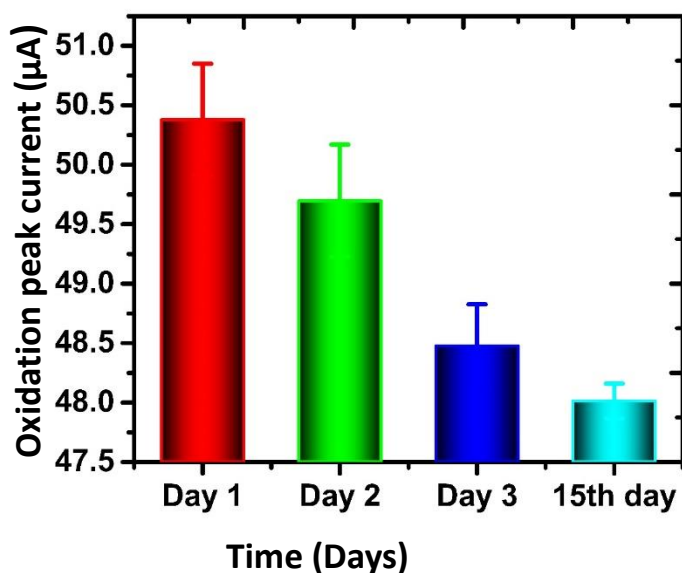


Figure 4.23: Measurement of stability of the biosensor for detecting CEA and YES1, current responses obtained using the initial CEA and YES1 immunosensor and the immunosensor stored for 15 days.

4.9.1.3: Specificity

Evaluation of the specificity of the immunosensor was done. In these sets of experiments, a number of substances such as VEGF, BSA, actin, L- cysteine and Glyceraldehyde-3-phosphate

dehydrogenase (GAPDH) were chosen as possible interfering substances. The objective of this experiment was to establish whether the immunosensor would still pick out the desirable antibodies, even in the presence of these substances. The experiment consisted of mixing 15 ml of 5 ng/mL CEA and 5 ng/mL YES1 with 20 ng/mL each of VEGF, BSA, actin, L- cysteine and GAPDH and the current response of immunosensor recorded. The control consisted of antigens of 5 ng/mL CEA and 5ng/mL YES1 without the interfering substances.

The results obtained indicated that the variation in current of immunosensor caused by the interference substances for CEA and YES1 was 6.8 % and 5.4% respectively when compared to the control (Figure 4.24).

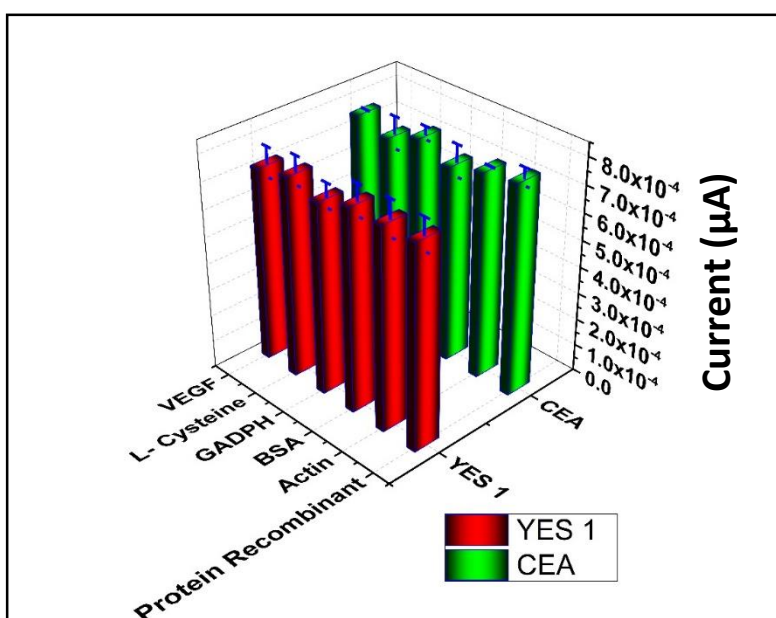


Figure 4.24: Specificity of the immunosensor towards various interfering compounds. Error bars represent SD (n = 3).

These results showed that the immunosensor possesses reliable specificity for CEA and YES1. The immunosensor showed better performance compared to the results previously reported in literature, for instance in the immunosensor for sensitive detection of CEA Based on Three-Dimensional Porous Nano platinum/Graphene change in current caused by interfering compound was less than 5.4% compared to no interference (Jing et al., 2020). The electro catalytic current response was less than 5% of that without the interference in Ultrasensitive sandwich-type

electrochemical immunosensor for detection of CEA based on Tri metallic nanocomposite (Tian et al., 2016).

In summary, we established that the proposed biosensor exhibited low interference, satisfactory specificity, apt reproducibility and good stability.

4.9.2: Evaluation of feasibility and cross- reactivity of the immunosensor

The feasibility and cross-reactivity of the fabricated immunosensor were evaluated as discussed in the following subsections.

4.9.2.1: Evaluation of feasibility

Evaluation of the ability of the immunosensor to detect both CEA and YES1 was investigated and the results obtained were as shown in Figures 4.25 A - D. The immunosensor was incubated with 20 μ L of 5 ng/mL of CEA and YES1 separately for 30 minutes at 37 $^{\circ}$ C and the results obtained are shown in Figures 4.25 A and B. The immunosensors were rinsed with tween buffer to remove unbound YES1 / CEA antigen. After rinsing they were incubated again with polyclonal anti-Rabbit secondary antibody conjugated with horseradish peroxidase (HRP) for 30 minutes at 37 $^{\circ}$ C. The immunosensors were then rinsed with tween buffer X1 to remove any unbound antibodies. Finally, electrochemical measurements were then carried out in 0.1 M PBS (pH 7.2) with 1mM [K₃Fe(CN)₆,] 0.1 M KCl. The electrolyte was bubbled in nitrogen for 5 minutes before measurements were taken.

The results showed that the DPV response for the CEA immunosensor in 0.1 M PBS (pH 7.2) with 1mM [K₃Fe(CN)₆, 0.1 M KCl] solution had an oxidation peak at +0.58 V which was considered as the peak for CEA Figure 4.25 A

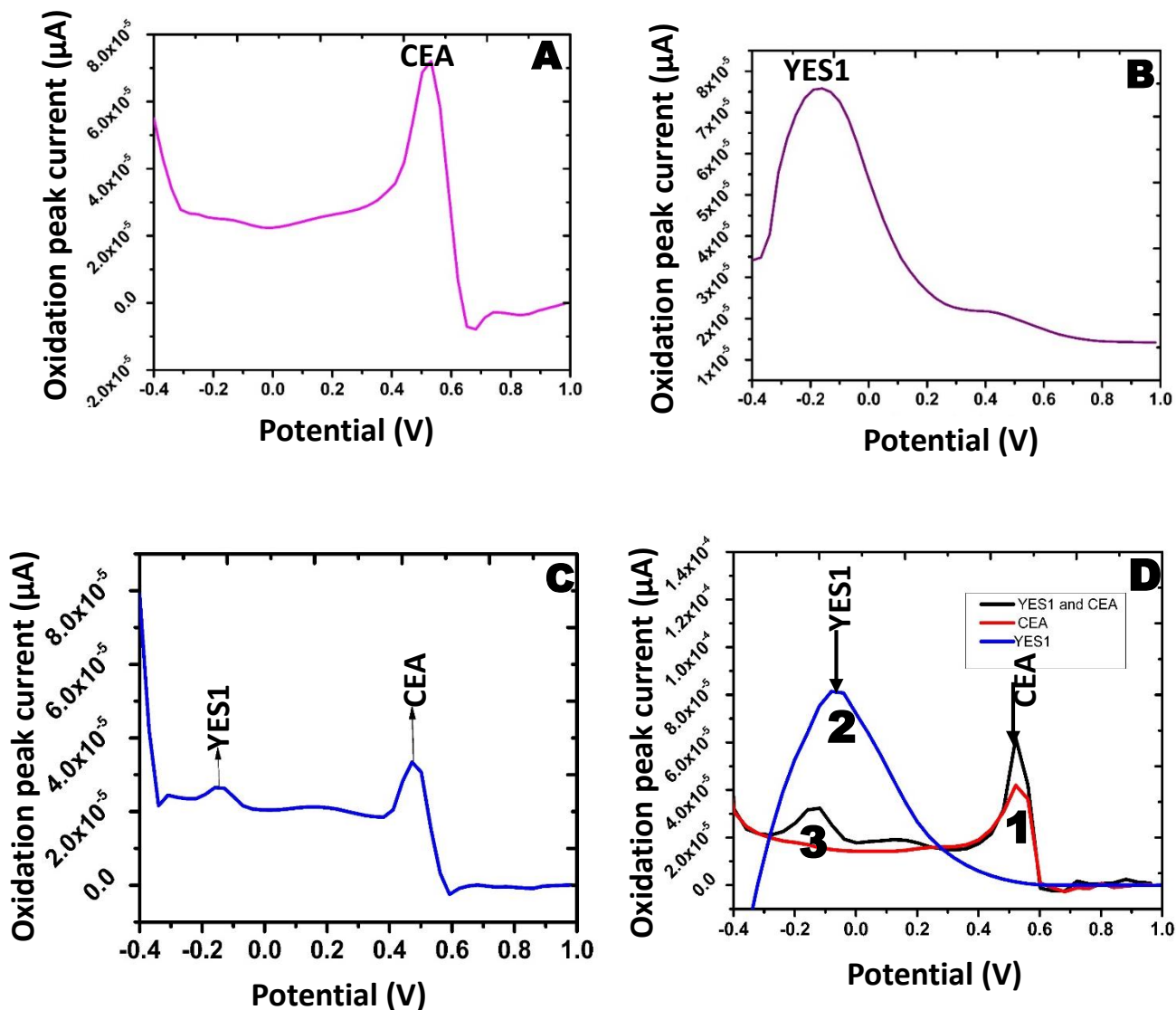


Figure 4.25: DPV of CEA immunosensor (A), YES immunosensor (B), and (C) the immunosensor of both CEA and YES1 in 0.1 M PBS at pH 7.2 (scan rate, 50 mV/s). (D) Simultaneous detection of CEA and YES1

Figure 4.25 B showed the DPV response of the YES1 immunosensor in 0.1 M PBS (pH 7.2) with 1mM $\text{K}_3\text{Fe}(\text{CN})_6$, 0.1 M KCl solution. The peak at - 0.18 V was considered to be the oxidation peak of YES1. When CEA was labeled with gold Nano particles, two oxidation peaks were observed in a single analyte as shown in Figure 4.25 C. The first peak at - 0.18 V observed in

Figure 4.25 C corresponded to the peak obtained in Figure 4.25 C for YES1 while the second peak in Figure 4.25 C corresponded to the peak observed in Figure 4.25 A for CEA. This results showed that the fabricated immunosensor was able to detect both YES1 and CES simultaneously in a single analyte.

4.9.2.2: Cross reactivity tests

Evaluation of cross-reactivity was done by carrying out control tests of the multiplex electrochemical immunosensor under the same experimental conditions. The composite curves Figure 4.25 D, (1), (2) and (3) DPV responses of immunosensor were assessed in the presence of various conditions such as: 0 ng/mL YES1 and 5 ng/mL CEA (1); 5 ng/mL YES and 0 ng/mL CEA (2); 5 ng/mL YES1 and 5 ng/mL CEA (3). Figure 4.25 D (1) showed a peak at +0.58 V which corresponded to the peak for CEA as observed earlier in Figure 4.25 A while Figure 4.25 D (2) showed a peak at - 0.18 V which corresponded to the peak for YES1 as observed earlier in Figure 4.26 B. In Figure 4.25 D (3), two peaks were observed which corresponded to the peaks observed in Figure 4.25 C for both YES1 and CEA. Figure 4.25 (3) showed that, when 5.0 ng/mL CEA and 5.0 ng/mL YES1 were simultaneously monitored the interference of the species with each other was low, meaning that the cross-reactivity was negligible. The results obtained showed that the fabricated immunosensor was able to detect YES1 and CEA biomarkers in a single analyte. Thus, the multiplex immunosensor fabricated for CEA and YES1 could be used as signal reporter to detect two lung cancer biomarkers.

4.9.3: Real sample analysis with the developed immunosensor and validation of the results with ELISA

Evaluation of the feasibility of the fabricated immunosensor for possible clinical application, investigations was done by analyzing human plasma samples from The Center of Applied Medical Research (CIMA) in Spain. The immunoassay for human plasma samples was investigated by analyzing four human plasma samples using the immunosensor and comparing the results with those obtained using the ELISA technique. Each human plasma sample was analyzed in triplicate. The results obtained are tabulated in Table 4.4. The results showed that the relative errors between the two techniques ranged from -4.66 to 6.59 % for CEA and from -7.83 to 1.75 % for YES1 (Table 4.5). When the results obtained from the immunosensor were compared with those obtained from ELISA for the two antibodies, there was no significant difference between the results given

by the two techniques (Figure 4.26). Therefore, the fabricated immunosensor could be applied in the clinical determination of CEA and YES1.

Table 4.5: Assay results in ng/mL of clinical plasma samples using the fabricated immunosensor and the ELISA method.

	Sample no.	1	2	3	4
immunosensor	YES 1	41.667	18.50	27.833	25.667
	CEA	31.740	17.70	21.297	20.193
ELISA	YES 1	40.955	20.071	27.878	26.279
	CEA	32.821	16.606	22.338	20.754
Relative error (%)	YES 1	1.75	-7.83	-0.16	-2.33
	CEA	-3.29	6.59	-4.66	-2.70

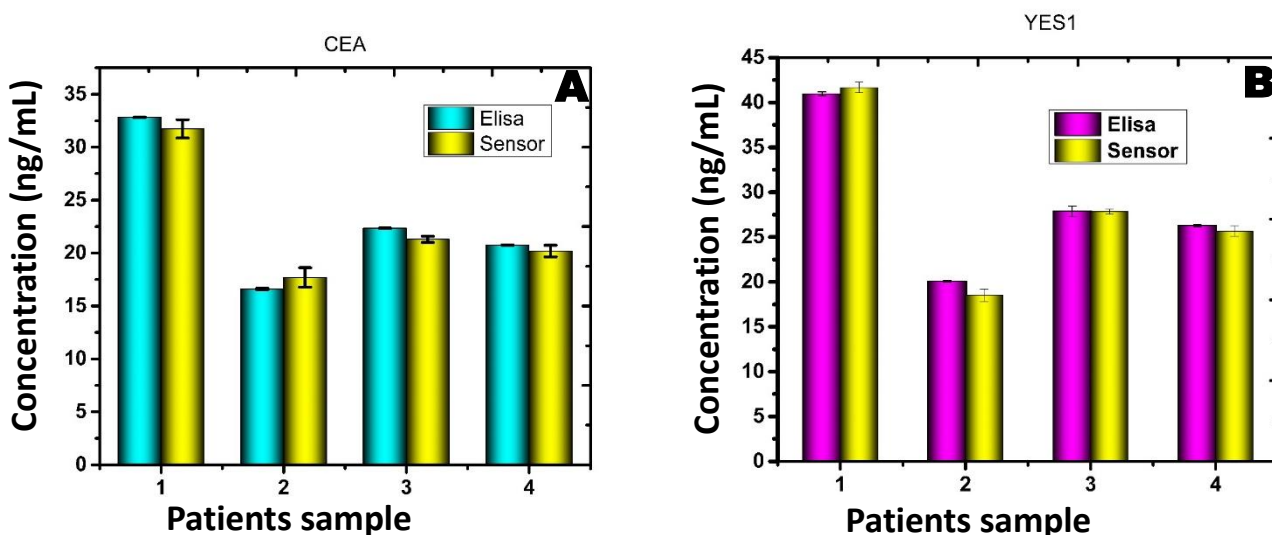


Figure 4.26: Comparison studies of the immunosensor and Elisa for CEA (A) and YES1 (B).

Investigation of the practical application of the proposed immunosensor in the detection of YES1 in biological samples was done in three different samples each containing 20 μ L of human plasma diluted with 20 μ L of 0.1 M phosphate buffer solution (pH 7.2). The samples were spiked with 0.1 ng/mL, 1.0 ng/mL and 10 ng/mL of YES1 recombinant for further detection.

The analytical results and recoveries are presented in Table 4.6. The study showed that the recoveries of the spiked samples varied in the range of 97.5–110% while the relative standard

deviation (RSD) was in the range of 0.35–7.26%. The use of immunosensor in DPV studies for spiked and un spiked human plasma with YES1 recombinant sample were compared and the results are shown in Figure 4.28 and Table 4.6.

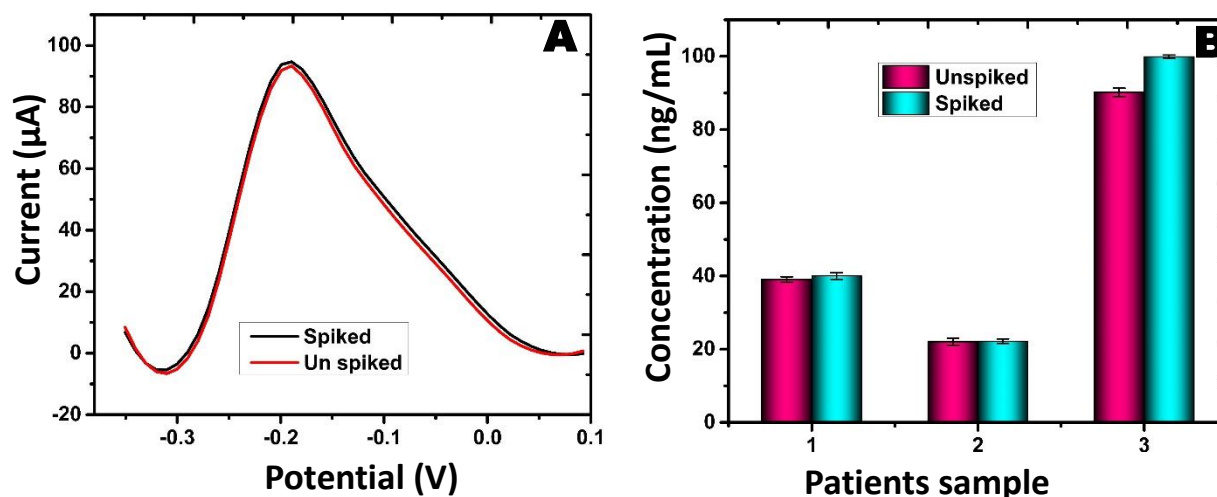


Figure 4.27: Comparison studies of the immunosensor DPV for spiked and un spiked human plasma with YES1 recombinant for 1 sample(A) comparison of spiked and un spiked human plasma (B).

Table 4.6: Assay results of clinical plasma samples spiked with YES1 recombinant.

Sample no.	YES 1 recombinant added(ng/mL)	Amount of YES 1 detected by immunosensor (ng/mL)	Total YES 1 found by Immunosensor	Recovery(%)	RSD (%)
1	0.1	39.02	40.01	99	1.77
2	1.0	22.00	22.11	110	0.35
3	10.0	90.15	99.90	97.5	7.26

The recoveries and RSD obtained in this study compared well with the previously reported studies for example the recovery range for Ultrasensitive multiplexed immunoassay of autophagic biomarkers based on Au/rGO and Au Nano cages amplifying electrochemical signal was in the range of 92-102% (Wang et al., 2017); while the recovery for an Electrochemical Immunosensor

for Sensitive Detection of the Tumor Marker Carcinoembryonic Antigen (CEA) Based on Three-Dimensional Porous Nanoplatinum/Graphene was in the range of 92.29-107%(Jing et al., 2020). The results obtained showed that the fabricated immunosensor had a significant potential to detect YES1 in the human plasma samples

The results obtained for the DPV oxidation peak current showed that the peak current for the spiked human plasma was slightly higher than the unspiked human plasma by 0.625% (Figure 4.27 A). Comparison of the spiked and unspiked for the three patient's samples (Figure 4.27 B) showed that, for the three samples the concentration of YES1 detected by the fabricated immunosensor for the spiked human plasma with YES1 was slightly higher than the unspiked samples. The percentage difference YES1 concentration detected by the immunosensor for the three patient's samples was 2.47%, 0.49% and 9.75% respectively (Figure 4.27 B). The results obtained showed that the fabricated immunosensor had a capacity of detecting different concentrations of YES1 in human plasma and thus potential application in clinical diagnosis.

CHAPTER 5: CONCLUSION AND RECOMMENDATIONS

5.1 Conclusion

Gold nanoparticles were biosynthesized and characterized using UV- Vis, FT-IR and DLS. They were used for modification of the GCE and also for labelling CEA secondary antibodies.

Conjugation of the antibodies was done through covalent bonding using GA as a cross linker. Characterization of the electrochemical immunosensor was done using CV and DPV. Electrochemical multiplexed immunosensor based on GCE/ AuNP/ PTG/ GA/AB CEA- YES1/ BSA was developed for simultaneous detection of CEA and YES1. The developed immunosensor showed reliable performance for CEA and YES1 detection with a remarkable detection limit, acceptable stability, wide linear ranges, and had satisfactory correlation with ELISA results. This immunosensor may hold a great promise for applications in various areas, including clinical diagnostics.

The signal of the fabricated immunosensor was linear from 0.01 to 50 ng/mL YES1 and CEA and had a low detection limit for YES1 and CEA is 0.0022 and 0.0034 ng/mL respectively.

The results obtained showed that the variation in current of immunosensor caused by the interference substances for CEA and YES1 was 6.8 % and 5.4% respectively when compared to the system where there was no interference indicating that the immunosensor possesses acceptable specificity for CEA and YES1. Analysis of stability of the immunosensor for fifteen days showed that it retained 95.3% of the electric signal and had a relative standard deviation (RSD) of 2.2%, indicating that the stability of proposed immunosensor was acceptable.

Evaluation of the kinetics of the biosensor using the Michaeli's Menten model gave a maximum reaction rate of 6.25ng/mL. the results indicated that YES1 binds strongly onto the modified electrode, and that YES1 is a suitable antibody for fabrication of the immunosensor.

The fabricated multiplex immunosensor was tested in human plasma samples for YES1 and CEA and the results obtained by the fabricated immunosensor were compared with those obtained by ELISA method detection and the results showed that the relative errors between the two techniques ranged from -4.66 to 6.59 % for CEA and from -7.83 to 1.75 % for YES1 The attained satisfactory

relative errors of the ultrasensitive multiplex immunosensor designated a potential practical application in clinical diagnostics. The study revealed that the fabricated sensor could be used for simultaneous detection of YES1 and CEA biomarkers.

The main objective of this studies was to develop an immunosensor for early detection of lung cancer that resulted in a patent, number KE/P/2022/4341.

5.2 . Recommendations

The recommendations from this study are:

- Nanofabrication and clinical applications could be adopted to develop low cost novel biosensors
- Further studies be conducted in fabrication of electrochemical transducers that could enhance the stability and reproducibility of the sensing device.
- Biomarker biosensors be commercialized to solve the challenges associated with the miniaturizing of the devices

REFERENCES

- Ankamwar, B. (2010). Biosynthesis of Gold Nanoparticles (Green-gold) Using Leaf Extract of Terminalia Catappa. *E-Journal of Chemistry*, **7**(4), 1334–1339.
- Alexander, B., Checkoway, H., Wechsler, L., Heyer, N., Muhm, J., and O’Keeffe, T. (2015). Lung cancer in chromate-exposed aerospace workers. *occupational environment*, **8**:1253–1258.
- Altintas Z, Fakanya WM, Tothill IE. (2014 b). Cardiovascular disease detection using bio-sensing techniques. *Talanta*, **128**:177-186.
- Altintas, Z., Uludag, Y., Gurbuz, Y. and Tothill, I. E. (2011). Surface plasmon resonance based immunosensor for the detection of the cancer biomarker carcinoembryonic antigen. *Talanta*, **86**:377-383.
- Arya, S. K. and Bhansali, S. (2011). Lung cancer and its early detection using biomarker based biosensors. *Chemical Reviews*, **111**:6783-6809.
- Armbruster, D. A., & Pry, T. (2008). Limit of Blank, Limit of Detection and Limit of Quantitation. *The Clinical Biochemist Reviews*, **29**(Suppl 1), S49–S52.
- Asselin, M., O’Connor, J., Boellaard, R., Thacker, N., & Jackson, A. (2012). Quantifying heterogeneity in human tumours using MRI and PET. *cancer*, **48**:447–455.
- Azri, F. A., Selamat, J., Sukor, R., Yusof, N. A., Ahmad Raston, N. H., Nordin, N., & Jambari, N. N. (2019). Etlingera elatior-Mediated Synthesis of Gold Nanoparticles and Their Application as Electrochemical Current Enhancer. *Molecules*, **24**(17), 3141. <https://doi.org/10.3390/molecules24173141>
- Bard, A. and Faulkner, L. (2001). *Electrochemical methods: fundamentals and applications*, (2nd ed.). Wiley, New York: Chichester: 105-120
- Beets-Tan RG, Beets GL, Vliegen RF. (2001). Accuracy of magnetic resonance imaging in prediction of tumour-free resection margin in rectal cancer surgery. *Lancet*, **357**:497–504.

- Berggren, C., Bjarnason, B. and Johansson, G. (2001). Capacitive biosensors. *Electroanalysis*, **13**:173-180.
- Bermudez V., Farina A., Raghavan V., Tappin I., Hurwitz J. (2011). Studies on human DNA polymerase epsilon and GINS complex and their role in DNA replication. *Biological Chemistry*, **286**: 2896–2897.
- Besaratinia, A., and Pfeifer, G. (2008). Second-hand smoke and human lung cancer. *Lancet Oncology*.2008, **9**: 657–666.
- Bohunicky, B. and Mousa, S. A. (2011). Biosensors: the new wave in cancer diagnosis. *Nanotechnology, Science and Applications*, **4**(1): 1-10.
- Bonel, L., Vidal, J. C., Duato, P., & Castillo, J. R. (2010). *Ochratoxin A nanostructured electrochemical immunosensors based on polyclonal antibodies and gold nanoparticles coupled to the antigen*. 7.
- Bray F, Ferlay J, Soerjomataram I, Siegel RL, Torre LA, Jemal A. (2018). *Global Cancer Statistics, estimates of incidence and mortality worldwide for 36 cancers*. GLOBOCAN ;**9**: 17.
- Bray, F., Ferlay, J., Soerjomataram, I., Siegel, R. L., Torre, L. A., & Jemal, A. (2018). Global cancer statistics 2018: GLOBOCAN estimates of incidence and mortality worldwide for 36 cancers in 185 countries. *CA: A Cancer Journal for Clinicians*, **68**(6), 394–424.
- Brett, C. M. A., & Brett, A. M. (1993). *Electrochemistry: Principles, methods, and applications*. Oxford University Press. 427
- Brown, S. D., Nativo, P., Smith, J.-A., Stirling, D., Edwards, P. R., Venugopal, B., Flint, D. J., Plumb, J. A., Graham, D., & Wheate, N. J. (2010). Gold nanoparticles for the improved

- anticancer drug delivery of the active component of oxaliplatin. *Journal of the American Chemical Society*, **132**(13), 4678–4684.
- Butler, J. (2000). Enzyme-Linked Immunosorbent Assay. *Immunoassay and Immunochemical*, **21**: 165–209.
- Burcham, P. C., & Pyke, S. M. (2006). Hydralazine inhibits rapid acrolein-induced protein oligomerization: Role of aldehyde scavenging and adduct trapping in cross-link blocking and cytoprotection. *Molecular Pharmacology*, **69**(3), 1056–1065.
- Capelozzi. (2009). Role of immunohistochemistry in the diagnosis of lung cancer. *Brasileiro De Pneumologia*, **35**: 375–382.
- Castro-Giner, F., Gkountela, S., Donato, C., Alborelli, I., Quagliata, L., Ng, C. K. Y., Piscuoglio, S., & Aceto, N. (2018). Cancer Diagnosis Using a Liquid Biopsy: Challenges and Expectations. *Diagnostics*, **8**(2), 31.
- Chapman, C.; Murray, A.; Chakrabarti, J.; Thorpe, A.; Woolston, C.; Sahin, U.; Barnes, A.; Robertson, J. (2007). Autoantibodies in breast cancer: Their use as an aid to early diagnosis. *Oncology*, **18**: 868–873.
- Cha, Y. J., Bae, S. J., Kim, D., Ahn, S. G., Jeong, J., Koo, J. S., Yoo, T.-K., Park, W.-C., Lee, A., & Yoon, C. I. (2021). High Nuclear Expression of Yes-Associated Protein 1 Correlates with Metastasis in Patients with Breast Cancer. *Frontiers in Oncology*, **11**, 609-743.
- Chandran, S. P., Chaudhary, M., Pasricha, R., Ahmad, A., & Sastry, M. (2006). Synthesis of gold nanotriangles and silver nanoparticles using Aloe vera plant extract. *Biotechnology Progress*, **22**(2), 577–583.

- Chen, X., Jia, X., Han, J., Ma, J., & Ma, Z. (2013). Electrochemical immunosensor for simultaneous detection of multiplex cancer biomarkers based on graphene nanocomposites. *Biosensors & Bioelectronics*, **50**, 356–361.
- Chen, X., & Ma, Z. (2014). Multiplexed electrochemical immunoassay of biomarkers using chitosan nanocomposites. *Biosensors and Bioelectronics*, **55**, 343–349.
- Cheng, E. S., Egger, S., Hughes, S., Weber, M., Steinberg, J., Rahman, B., Worth, H., Ruano-Ravina, A., Rawstorne, P., & Yu, X. Q. (2021). Systematic review and meta-analysis of residential radon and lung cancer in never-smokers. *European Respiratory Review*, **30**(159). 340-342
- Cheng, B. (2016). Development of a chemiluminescent immunoassay for cancer antigen 15-3. . *Labeled Immunoassay*, **23**: 1348–1351.
- Chiang, H.-C., Wang, Y., Zhang, Q., & Levon, K. (2019a). Optimization of the Electrodeposition of Gold Nanoparticles for the Application of Highly Sensitive, Label-Free Biosensor. *Biosensors*, **9**(2), 50.
- Chiang, C., Chen, Y., Chen, C., You, S., & Lai, M. (2010). Cancer trends in Taiwan. *clinical oncology*, **40**: 897-904.
- Chiang, T. C., Wu, P., Wang, T., Chang, P., Ko, A., Huang, M., and Ko, Y. (2008). Important prognostic factors for the long-term survival of lung cancer subjects in Taiwan. *Biomolecular cancer*, **8**: 324-327
- Chicklore, S., Goh, V., Siddique, M., Roy, A., Marsden, P., and Cook, G. (2013). Quantifying Tumor Heterogeneity in F-18-Fdg Pet/Ct Imaging by Texture Analysis. *Medical Molecular Imaging*, **40**: 133–140.

- Chikkaveeraiah, B. V., Bhirde, A. A., Morgan, N. Y., Eden, H. S., & Chen, X. (2012). Electrochemical Immunosensors for Detection of Cancer Protein Biomarkers. *ACS Nano*, **6**(8), 6546–6561.
- Chung J, Bernhardt R, Pyun J. (2006). Additive assay of cancer marker CA 19-9 by SPR biosensor. *Sens Actuators B Chem*, **118** (10), 28-32.
- Church, T., Black, W., Aberle, D., Berg, C., Clingan, K., Duan, F., Jones, G. (2013). Results of initial low-dose computed tomographic screening for lung cancer. *cancer, England Medical*, **368**: 1980–1991.
- Compton, R. G. and Banks, C. E. (2011). *Understanding voltammetry*. London: Imperial College Press: 86-91
- Costa, B. M. de C., Griveau, S., d'Orlye, F., Bedioui, F., da Silva, J. A. F., & Varenne, A. (2021). Microchip electrophoresis and electrochemical detection: A review on a growing synergistic implementation. *Electrochimica Acta*, **391**, 138928.
- Cotchim, S., Thavarungkul, P., Kanatharana, P., & Limbut, W. (2020). Multiplexed label-free electrochemical immunosensor for breast cancer precision medicine. *Analytica Chimica Acta*, **1130**, 60–71.
- D'Agostino, G., Alberti, G., Biesuz, R., & Pesavento, M. (2006). Potentiometric sensor for atrazine based on a molecular imprinted membrane. *Biosensors & Bioelectronics*, **22**(1), 145–152.
- Daniel, M.-C., & Astruc, D. (2004). Gold Nanoparticles: Assembly, Supramolecular Chemistry, Quantum-Size-Related Properties, and Applications toward Biology, Catalysis, and Nanotechnology. *Chemical Reviews*, **104**(1), 293–346.
- Daniele, S. (2005). VOLTAMMETRY | Anodic Stripping. In P. Worsfold, A. Townshend, & C. Poole (Eds.), *Encyclopedia of Analytical Science (Second Edition)* (pp. 197–203). Elsevier.

- Dekanski, A., Stevanović, J., Stevanović, R., Nikolić, B., & Jovanović, V. (2001). Glassy Carbon Electrodes: I. Characterization and Electrochemical Activation. *Carbon*, **39**, 1195–1205.
- De González AB, Darby S. (2004). Risk of cancer from diagnostic X-rays: estimates for the UK and 14 other countries. *Lancet*, **363**(7), 345–351.
- Diamandis, E., & van der Merwe, D. (2005). Plasma Protein Profiling by Mass Spectrometry for Cancer Diagnosis: Opportunities and Limitations. *Clinical Cancer*, **11**: 963-965.
- Dogan S., Shen R., Ang D., Johnson M., D'Angelo S., Paik P., Brzostowski E., Riely G., Kris M., Zakowski M., et al. (2012). Molecular epidemiology of EGFR and KRAS mutations in 3026 lung adenocarcinomas: Higher susceptibility of women to smoking-related KRAS-mutant cancers. *clinical cancer respiration*, **18**: 6169-77.
- Eissa. S and Shoman.S. (1998). *Tumor markers*. London ; New York.: Chapman & Hall: 120-129
- Ercole, C., Del Gallo, M., Pantalone, M., Santucci, S., Mosiello, L., Laconi, C., & Lepidi, A. (2002). A Biosensor for Escherichia coli Based on a Potentiometric Alternating Biosensing (PAB) Transducer. *Sensors and Actuators B: Chemical*, **83**, 48–52.
- Erden, P. E., Pekyardımcı, Ş., Kılıç, E., & Arslan, F. (2006). An Amperometric Enzyme Electrode for Creatine Determination Prepared by the Immobilization of Creatinase and Sarcosine Oxidase in Poly(vinylferrocenium). *Artificial Cells, Blood Substitutes, and Biotechnology*, **34**(2), 223–239.
- Fang, Y., Huang, X., Zeng, Q., & Wang, L. (2015). Metallic nanocrystallites-incorporated ordered mesoporous carbon as labels for a sensitive simultaneous multianalyte electrochemical immunoassay. *Biosensors and Bioelectronics*, **73**, 71–78.

- Feng, D., Li, L., Han, X., Fang, X., Li, X., & Zhang, Y. (2014). Simultaneous electrochemical detection of multiple tumor markers using functionalized graphene nanocomposites as non-enzymatic labels. *Sensors and Actuators B: Chemical*, **201**, 360–368.
- Feng, D., Li, L., Zhao, J., & Zhang, Y. (2015). Simultaneous electrochemical detection of multiple biomarkers using gold nanoparticles decorated multiwall carbon nanotubes as signal enhancers. *Analytical Biochemistry*, **482**, 48–54.
- Feng X., Lin Z., Liyan W., Quan W. (2015, June 15). Serum neuron specific enolase levels correlate with patient prognosis for advanced lung cancer. *international journal of clinical and experimental medicine*, **8**(6), 9498–9504.
- Felix, F. S., & Angnes, L. (2018). Electrochemical immunosensors—A powerful tool for analytical applications. *Biosensors & Bioelectronics*, **102**, 470–478.
- Foo, Y. Y., Periasamy, V., Kiew, L. V., Kumar, G. G., & Malek, S. N. A. (2017). Curcuma mangga-Mediated Synthesis of Gold Nanoparticles: Characterization, Stability, Cytotoxicity, and Blood Compatibility. *Nanomaterials*, **7**(6), 123.
- Fort, A., Lotti, C., Mugnaini, M., Palombari, R., Rocchi, S., Tondi, L., & Vignoli, V. (2007). A Two Electrode Electrochemical Amperometric Sensor for NO₂ Detection. *Proceedings - 1st IMEKO TC-19 International Symposium on Measurement and Instrumentation for Environmental Monitoring*. **6**(5), 122
- Fowler, J. M., Stuart, M. C., & Wong, D. K. Y. (2007). Self-Assembled Layer of Thiolated Protein G as an Immunosensor Scaffold. *Analytical Chemistry*, **79**(1), 350–354.
- Garmendia, I., Pajares, M. J., Hermida-Prado, F., Ajona, D., Bértolo, C., Sainz, C., Lavín, A., Remírez, A. B., Valencia, K., Moreno, H., Ferrer, I., Behrens, C., Cuadrado, M., Paz-Ares, L., Bustelo, X. R., Gil-Bazo, I., Alameda, D., Lecanda, F., Calvo, A., ... Agorreta,

- J. (2019). YES1 Drives Lung Cancer Growth and Progression and Predicts Sensitivity to Dasatinib. *American Journal of Respiratory and Critical Care Medicine*, **200**(7), 888–899.
- Garmendia, I., Redin, E., Montuenga, L. M., & Calvo, A. (2022). YES1: A Novel Therapeutic Target and Biomarker in Cancer. *Molecular Cancer Therapeutics*, **21**(9), 1371–1380.
- Ghorai, P. Kr., & Glotzer, S. C. (2007). Molecular Dynamics Simulation Study of Self-Assembled Monolayers of Alkanethiol Surfactants on Spherical Gold Nanoparticles. *The Journal of Physical Chemistry C*, **111**(43), 15857–15862.
- Ge, X., Zhang, A., Lin, Y., & Du, D. (2016). Simultaneous immunoassay of phosphorylated proteins based on apoferritin templated metallic phosphates as voltammetrically distinguishable signal reporters. *Biosensors and Bioelectronics*, **80**, 201–207.
- Gerard M, Chaubey A and Malhotra B. (2002). Biosensors for cancer markers diagnosis. *Biosensors and Bioelectronics*, **17**: 345-59.
- Goldsmith, S. (1975). Radioimmunoassay: Review of basic principles. *Seminars of Nuclear Medicine*, **5**: 125–152.
- GsShruthi, S., CvAmitha, A., & Mathew, B. B. (2014). Biosensors: A Modern Day Achievement. *Journal of Instrumentation Technology*, **2**(1), Article 1.
- Hamdan, M. (2007). Cancer biomarkers. In *Analytical techniques for discovery* Wiley: Hoboken. **80**(3) (pp. 651-655).
- Hammarström, S. (1999). The carcinoembryonic antigen (CEA) family: structures, suggested functions and expression in normal and malignant tissues. *Seminars in Cancer Biology*, **9**(2), 67-81.

- Han, J., Zhuo, Y., Chai, Y., Yuan, R., Zhang, W., & Zhu, Q. (2012). Simultaneous electrochemical detection of multiple tumor markers based on dual catalysis amplification of multi-functionalized onion-like mesoporous graphene sheets. *Analytica Chimica Acta*, **746**, 70–76.
- Hara, N., Ichinose, Y., Motohiro, A., Noge, S., Miyake, J., Ohta, M., and Hata, K. (1986). Combination chemotherapy and radiation therapy for small cell carcinoma of the lung. *Gan Kagaku Ryoho Cancer Chemotherapy*, **13**: 80–85.
- Hasan, N., Kumar, R., & Kavuru, M. (2014). Lung cancer screening beyond low-dose computed tomography. The role of novel biomarkers. *Lung cancer*, **192**: 639–648.
- Henschke CI, McCauley DI, Yankelevitz DF, Naidich DP, McGuinness G. (1999). Early Lung Cancer Action Project: overall design and findings from baseline screening. *Lancet*, **354**: 99-105.
- Heurich, M., Kadir, M. K. A. and Tothill, I. E. (2011). An electrochemical sensor based on carboxymethylated dextran modified gold surface for ochratoxin A analysis. *Sensors and Actuators, B: Chemical*, **156**(1), 162-168.
- Hokka D., Maniwa Y., Tane S., Nishio W., Yoshimura M., Okita Y., Ohbayashi C., Sakai Y., Chen X., Hayashi Y. (2013). Psf3 is a prognostic biomarker in lung adenocarcinoma. *Lung Cancer*, **79**: 77–82.
- Ilyas A, Asghar W, Allen PB, Duhon H, Ellington AD. (2012). Electrical detection of cancer biomarker using aptamers with nanogap break-junctions. *Nanotechnology*, **23**(27), 275-375.

- Imyanitov E., Demidova I., Gordiev M., Filipenko M., Kekeyeva T., Moliaka Y., Gervas P., Kozhemyako V., Vodolazhskiy D., Sergeyeva L. (2016). Distribution of EGFR mutations in Russian patients with lung cancer. *Molecular Diagnosis Therapy*, **20**: 401–407
- Indovina P., Marcelli E., Maranta P., Tarro G. (2011). Lung cancer proteomics: Recent advances in biomarker discovery. *International Journal of Proteomics*, **10**: 1155-1160.
- Ippolito, D., Capraro, C., Guerra, L., De Ponti, E., Messa, C., and Sironi, S. (2013). Feasibility of perfusion CT technique integrated into conventional (18) FDG/PET-CT studies in lung cancer patients: Clinical staging and functional information in a single study. *Journal of Molecular Imaging*, **40**: 156-165.
- Ismail, E. H., Saqer, A. M. A., Assirey, E., Naqvi, A., & Okasha, R. M. (2018). Successful Green Synthesis of Gold Nanoparticles using a Corchorus olitorius Extract and Their Antiproliferative Effect in Cancer Cells. *International Journal of Molecular Sciences*, **19**(9), 2612.
- Ivnitski D, Abdel-Hamid I, Atanasov P and Wilkins E. (1999). Classification of biosensors. *Biosensors and Bioelectronics*, **14**: 599-624.
- Jacob, J. A., Biswas, N., Mukherjee, T., & Kapoor, S. (2011). Effect of plant-based phenol derivatives on the formation of Cu and Ag nanoparticles. *Colloids and Surfaces. B, Biointerfaces*, **87**(1), 49–53.
- Jaffrezic-Renault, N., & Dzyadevych, S. V. (2008). Conductometric Microbiosensors for Environmental Monitoring. *Sensors*, **8**(4), 2569–2588.
- Jayanthi, V. S., Das, A. B., & Saxena, U. (2019). Fabrication of an immunosensor for quantitative detection of breast cancer biomarker UBE2C. *RSC Advances*, **9**(29), 16738–16745.

- Jing, A., Xu, Q., Feng, W., & Liang, G. (2020). An Electrochemical Immunosensor for Sensitive Detection of the Tumor Marker Carcinoembryonic Antigen (CEA) Based on Three-Dimensional Porous Nanoplatinum/Graphene. *Micromachines*, **11**(7), E660.
- Jemal, A.; Bray, F.; Center, M.M.; Ferlay, J.; Ward, E.; Forman, D. (2011). Global cancer statistics. *Cancer Journal of Clinical*, **61**: 69–90.
- Jia, X., Liu, Z., Liu, N., & Ma, Z. (2014). A label-free immunosensor based on graphene nanocomposites for simultaneous multiplexed electrochemical determination of tumor markers. *Biosensors and Bioelectronics*, **53**, 160–166.
- Journy, N., Rehel, J., Pointe, H., Lee, C., Brisse, H., Chateil, J., Bernier, M. B. (2015). Are the studies on cancer risk from ct scans biased by indication? Elements of answer from a large-scale cohort study in France. *cancer*, **112**: 1841-1842.
- Kallempudi SS, Altintas Z, Niazi JH, Gurbuz Y. (2012). A new microfluidics system with a hand-operated, on-chip actuator for immunosensor applications. *Sensors and Actuators B Chem*, **163**: 194-201.
- Kaufman, H. L., Hörig, H., Medina, F. A., Golding, S. and Conkright, W. A. (2000). Strategies for cancer therapy using carcinoembryonic antigen vaccines. *Molecular Medicine*, **2**(3), 1-4.
- Kauffmann, J. M., & Guilbault, G. G. (1991). Potentiometric enzyme electrodes. *Bioprocess Technology*, **15**, 63–82.
- Kalpana, V. N., Chakraborty, P., Palanichamy, V., & Rajeswari, V. D. (2016). Synthesis and characterization of copper nanoparticles using *Tridax procumbens* and its application in degradation of bismarck brown. *International Journal of ChemTech Research*, **9**, 498-507.

- Katz, E., & Willner, I. (2005). Switching of Directions of Bioelectrocatalytic Currents and Photocurrents at Electrode Surfaces by Using Hydrophobic Magnetic Nanoparticles. *Angewandte Chemie International Edition*, **44**(30), 4791–4794.
- Kennedy, T. C., Hirsch, F. R., Miller, Y. E., Prindiville, S., Murphy, J. R., Dempsey, E., Proudfoot, S., Bunn, P. A., & Franklin, W. A. (2000). A randomized study of fluorescence bronchoscopy versus white-light bronchoscopy for early detection of lung cancer in high risk patients. *Lung Cancer*, **29**(1), 244–245.
- Khailany, R. A., Aziz, S. A., Najjar, S. M., Safdar, M., & Ozaslan, M. (2020). Genetic biomarkers: Potential roles in cancer diagnosis. *Cellular and Molecular Biology (Noisy-Le-Grand, France)*, **66**(3), 1–7.
- Khan, J. A., Kudgus, R. A., Szabolcs, A., Dutta, S., Wang, E., Cao, S., Curran, G. L., Shah, V., Curley, S., Mukhopadhyay, D., Robertson, J. D., Bhattacharya, R., & Mukherjee, P. (2011). Designing nanoconjugates to effectively target pancreatic cancer cells in vitro and in vivo. *PloS One*, **6**(6), e20347.
- Khalil, I.; Julkapli, N.M.; Yehye, W.A.; Basirun, W.J.; Bhargava, S.K. (2016). Graphene-gold nanoparticles hybrid—Synthesis, functionalization, and application in a electrochemical and surface-enhanced Raman scattering biosensor. *Materials*, **9**: 406.
- Kikuchi T., Hassanein M., Amann J., Liu Q., Slebos R., Rahman S., Kaufman J., Zhang X., Hoeksema M., Harris B. (2012). In-depth proteomic analysis of nonsmall cell lung cancer to discover molecular targets and candidate biomarkers. *Molecular Cell Proteomics*, **11**(10), 916-932.
- Kim N, Kim DK, Cho YJ. (2010). Gold nanoparticle-based signal augmentation of quartz crystal microbalance immunosensor measuring C-reactive protein. *Current Applied Physics*,

10 :1227-1230.

- Kimmel, D. W., Leblanc, G., Meschievitz, M. E. and Cliffel, D. E. (2012). Electrochemical sensors and biosensors. *Analytical Chemistry*, **84**(2), 685-707.
- Kile, B. M., Walsh, P. L., McElligott, Z. A., Bucher, E. S., Guillot, T. S., Salahpour, A., Caron, M. G., & Wightman, R. M. (2012). Optimizing the Temporal Resolution of Fast-Scan Cyclic Voltammetry. *ACS Chemical Neuroscience*, **3**(4), 285–292.
- Kitade, T., Kitamura, K., Konishi, T., Takegami, S., Okuno, T., Ishikawa, M., Wakabayashi, M., Nishikawa, K., & Muramatsu, Y. (2004). Potentiometric immunosensor using artificial antibody based on molecularly imprinted polymers. *Analytical Chemistry*, **76**(22), 6802–6807.
- Kong, T., Chen, Y., Ye, Y., Zhang, K., Wang, Z., & Wang, X. (2009). An amperometric glucose biosensor based on the immobilization of glucose oxidase on the ZnO nanotubes. *Sensors and Actuators B: Chemical*, **138**(1), 344–350.
- Korpan, Y. I., Raushel, F. M., Nazarenko, E. A., Soldatkin, A. P., Jaffrezic-Renault, N., & Martelet, C. (2006). Sensitivity and specificity improvement of an ion sensitive field effect transistors-based biosensor for potato glycoalkaloids detection. *Journal of Agricultural and Food Chemistry*, **54**(3), 707–712.
- Kulkarni, M., Ayachit, N., & Aminabhavi, T. (2022). Biosensors and Microfluidic Biosensors: From Fabrication to Application. *Biosensors*, **12**, 543.
- Kuntamung, K., Jakmune, J., & Ounnunkad, K. (2021). A label-free multiplex electrochemical biosensor for the detection of three breast cancer biomarker proteins employing dye/metal ion-loaded and antibody-conjugated polyethyleneimine-gold nanoparticles. *Journal of Materials Chemistry B*, **9**(33), 6576–6585.

- Ladd, J., Taylor, A., Piliarik, M., Homola, J., & Jiang, S. (2008). Label-free detection of cancer biomarker candidates using surface plasmon resonance imaging. *Analytical and Bioanalytical Chemistry*, **393**, 1157–1163.
- Lates, V., Yang, C., Popescu, I. C., & Marty, J.-L. (2012). Displacement immunoassay for the detection of ochratoxin A using ochratoxin B modified glass beads. *Analytical and Bioanalytical Chemistry*, **402**(9), 2861–2870.
- Laborla, N., Fragoso, A., Kemmner, W., Latta, D., Nilsson, O., Botero, M. L., Drese, K. and O'Sullivan, C. K. (2010). Amperometric immunosensor for carcinoembryonic antigen in colon cancer samples based on monolayers of dendritic bipodal scaffolds. *Analytical Chemistry*, **82** (5), 1712-1719.
- Laboria, N., Fragoso, A., Kemmner, W., Latta, D., Nilsson, O., Luz Botero, M., Drese, K., & O'Sullivan, C. K. (2010). Amperometric immunosensor for carcinoembryonic antigen in colon cancer samples based on monolayers of dendritic bipodal scaffolds. *Analytical Chemistry*, **82**(5), 1712–1719.
- Lai, W., Zhuang, J., Tang, J., Chen, G., & Tang, D. (2012). One-step electrochemical immunosensing for simultaneous detection of two biomarkers using thionine and ferrocene as distinguishable signal tags. *Microchimica Acta*, **178**(3), 357–365.
- Lakshmanan I., Ponnusamy M., Macha M., Haridas D., Majhi P., Kaur S., Jain M., Batra S., Ganti A. (2015). Mucins in lung cancer diagnostic, prognostic, and therapeutic implications. *Thoracic Oncology*, **10**: 19-27.
- Lardinois D, Weder W, Hany TF. (2003). Staging of non–small-cell lung cancer with integrated positron-emission tomography and computed tomography. *England Journal of Medicine*, **348**(13), 2500–2507.

- Laviron, E. (1979). General expression of the linear potential sweep voltammogram in the case of diffusionless electrochemical systems. *Electroanalytical Chemistry and Interfacial Electrochemistry*, **101**(1), 19-28.
- Leach MO, Boggis CR, Dixon AK. (2005). MARIBS Study Group. Screening with magnetic resonance imaging and mammography of a UK population at high familial risk of breast cancer: a prospective multicentre cohort study (MARIBS). *Lancet*, **365**(12), 1769–1778.
- Lee MH, Lee DH, Jung SW, Lee KN, Park YS. (2010). Measurements of serum C-reactive protein levels in patients with gastric cancer and quantification using silicon nanowire arrays. *Nanomedical and Nanotechnology*, **6**(1), 78-83.
- Lee, H., Jin, G., Han, Y., Chung, G., Lee, Y., Kwon, K., and Lynch, D. (2012). Comparison of survival rate in primary non-small-cell lung cancer among elderly patients treated with radiofrequency ablation, surgery, or chemotherapy. *Cardiovasc Radiology*, **35**: 343-350.
- Lee, J. M., Park, H. K., Jung, Y., Kim, J. K., Jung, S. O., & Chung, B. H. (2007). Direct Immobilization of Protein G Variants with Various Numbers of Cysteine Residues on a Gold Surface. *Analytical Chemistry*, **79**(7), 2680–2687
- Lether, F. G., & Wenston, P. R. (1987). An algorithm for the numerical evaluation of the reversible Randles-Sevcik function. *Computers & Chemistry*, **11**(3), 179–183.
- Lone, S. N., Nisar, S., Masoodi, T., Singh, M., Rizwan, A., Hashem, S., El-Rifai, W., Bedognetti, D., Batra, S. K., Haris, M., Bhat, A. A., & Macha, M. A. (2022). Liquid biopsy: A step closer to transform diagnosis, prognosis and future of cancer treatments. *Molecular Cancer*, **21**(1), 79.

- Liang, Y., Xu, Y., Tong, Y., Chen, Y., Chen, X., & Wu, S. (2022). Graphene-Based Electrochemical Sensor for Detection of Hepatocellular Carcinoma Markers. *Frontiers in Chemistry*, **10**, 627
- Li, L., Feng, D., & Zhang, Y. (2016). Simultaneous detection of two tumor markers using silver and gold nanoparticles decorated carbon nanospheres as labels. *Analytical Biochemistry*, **505**, 59–65.
- Li, Q., Tang, D., Lou, F., Yang, X., & Chen, G. (2014). Simultaneous Electrochemical Multiplexed Immunoassay of Biomarkers Based on Multifunctionalized Graphene Nanotags. *ChemElectroChem*, **1**(2), 441–447.
- Li, T., Shu, B., Jiang, B., Ding, L., Qi, H., Yang, M., & Qu, F. (2013). Ultrasensitive multiplexed protein biomarker detection based on electrochemical tag incorporated polystyrene spheres as label. *Sensors and Actuators B: Chemical*, **186**, 768–773.
- Liu, Z., Rong, Q., Ma, Z., & Han, H. (2015). One-step synthesis of redox-active polymer/AU nanocomposites for electrochemical immunoassay of multiplexed tumor markers. *Biosensors and Bioelectronics*, **65**, 307–313.
- Li H, Wei Q, Wang G, Yang M, Qu F. (2011). Sensitive electrochemical immunosensor for cancer biomarker with signal enhancement based on nitrodopamine-functionalized iron oxide nanoparticles. *Biosensors and Bioelectronics*, **26**(6), 3044-3049.
- Lu, W., Tao, L., Wang, Y., Cao, X., Ge, J., Dong, J., & Qian, W. (2015). An electrochemical immunosensor for simultaneous multiplexed detection of two lung cancer biomarkers using Au nanoparticles coated resin microspheres composed of L-tryptophan and caffeic acid. *Ionics*, **21**(4), 1141–1152.

- Macero, D. J., & Rulfs, C. L. (1959). Calibrated Cottrell Diffusion Measurements1. *Journal of the American Chemical Society*, **81**(12), 2942–2944.
- Macharia, L. W., Mureithi, M. W., & Anzala, O. (2019). Cancer in Kenya: Types and infection-attributable. Data from the adult population of two National referral hospitals (2008-2012). *AAS Open Research*, **1**, 25.
- Marzouk, S. A. M., Ashraf, S. S., & Tayyari, K. A. A. (2007). Prototype amperometric biosensor for sialic acid determination. *Analytical Chemistry*, **79**(4), 1668–1674.
- Macieira-Coelho, A., & Avrameas, S. (1973). CHAPTER 4—Protein Polymers as a Substratum for the Modulation of Cell Proliferation in Vitro. In P. F. Kruse & M. K. Patterson (Eds.), *Tissue Culture* (pp. 379–383). Academic Press.
- Mallesha, L., Vinay, G., & Rekha, N. (2018). Synthesis of metal nanoparticles using *Heliconia rostrata* leaf extract and their antiproliferative and apoptotic property. *Current Chemistry Letters*, **7**(2), 65–72.
- Makino T., Mikami T., Hata Y., Otsuka H., Koezuka S., Isobe K., Tochigi N., Shibuya K., Homma S., Iyoda A. (2016). Comprehensive biomarkers for personalized treatment in pulmonary large cell neuroendocrine carcinoma: A comparative analysis with adenocarcinoma. *Lung cancer*, **102**: 1694-1701.
- Marshall H., Bowman R., Yang I., Fong K., Berg C. (2013). Screening for lung cancer with low-dose computed tomography: A review of current status. *cancer cytopathology*, **5**: 524-539.
- Melonie Heron, Donna L. Hoyert, Sherry L. Murphy, Jiaquan Xu, M.D.; Kenneth D. Kochanek, M.A.; and Betzaida Tejada-Vera. (2006, April 19). Division of Vital Statistics. *National Vital Statistics Reports*, **57**(14), 4-15.
- Midthun, D. E. (2016). Early detection of lung cancer. *F1000Research*, **5**, 739.

- Montani F., Marzi M., Dezi F., Dama E., Carletti R., Bonizzi G., Bertolotti R., Bellomi M., Rampinelli C., Maisonneuve P. (2015). Mir-test: A blood test for lung cancer early detection. *Lung Cancer*, **75**: 1538-1573.
- Moulton, S. E., Barisci, J. N., Bath, A., Stella, R., & Wallace, G. G. (2003). Investigation of protein adsorption and electrochemical behavior at a gold electrode. *Journal of Colloid and Interface Science*, **261**(2), 312–319.
- Moyano, D. F., & Rotello, V. M. (2011). Nano meets biology: Structure and function at the nanoparticle interface. *Langmuir: The ACS Journal of Surfaces and Colloids*, **27**(17), 10376–10385.
- Mukherjee, P., Bhattacharya, R., Bone, N., Lee, Y. K., Patra, C. R., Wang, S., Lu, L., Secreto, C., Banerjee, P. C., Yaszemski, M. J., Kay, N. E., & Mukhopadhyay, D. (2007). Potential therapeutic application of gold nanoparticles in B-chronic lymphocytic leukemia (BCLL): Enhancing apoptosis. *Journal of Nanobiotechnology*, **5**, 4.
- Muller, K. (1984). Histological classification and histogenesis of lung-cancer. *lung-cancer*, **65**: 4–19.
- Mulshine JL. (2005). Current issues in lung cancer screening. *Oncology*, **19**: 1724-1730.
- Muralikrishna, T., Malothu, R., Pattanayak, M., & Nayak, P. L. (2014a). *Green Synthesis of Gold Nanoparticles Using Mangifera Indica (Mango Leaves) Aqueous Extract*, **3**(2): 66-73.
- Nagalingam, Nagarajan, K., Rajeswari, D., & Panneerselvam, A. (2018). Biosynthesis, characterization, and evaluation of bioactivities of leaf extract-mediated biocompatible gold nanoparticles from *Alternanthera bettzickiana*. *Biotechnology Reports*, **19**, e00268.

- Nna, E., Tothill, I. E., Ludeman, L. and Bailey, T. (2010). Endogenous control genes in prostate cells: evaluation of gene expression using 'real-time' quantitative polymerase chain reaction. *Medical Principles and Practice*, **19**(6), 433-439.
- Nooreldeen, R., & Bach, H. (2021). Current and Future Development in Lung Cancer Diagnosis. *International Journal of Molecular Sciences*, **22**(16), 8661.
- Nikolelis, D. P., Varzakas, T., Erdem, A., & Nikoleli, G.-P. (2013). *Portable Biosensing of Food Toxicants and Environmental Pollutants*. CRC Press. Boca Raton, 832
- Ogendo SW, Othieno-Abinya, Nyongesa CN, Musibi AM, Waweru W. (2013). *National guidelines for cancer management*. Nairobi: Ministry of Health: 270
- Ohnuki, H., Saiki, T., Kusakari, A., Endo, H., Ichihara, M., & Izumi, M. (2007). Incorporation of glucose oxidase into Langmuir-Blodgett films based on Prussian blue applied to amperometric glucose biosensor. *Langmuir: The ACS Journal of Surfaces and Colloids*, **23**(8), 4675–4681.
- Ojeda, I., López-Montero, J., Moreno-Guzmán, M., Janegitz, B., González-Cortés, A., Nez-Sed, P., No, & Pingarrón, J. (2012). Electrochemical immunosensor for rapid and sensitive determination of estradiol. *Analytica Chimica Acta*, **743**, 117–124.
- Okamura K., Takayama K., Izumi M., Harada T., Furuyama K., Nakanishi Y. (2013). Diagnostic value of CEA and CYFRA 21-1 tumor markers in primary lung cancer. *Lung Cancer*, **80**: 45–49.
- Palmisano WA, Divine KK, Saccomanno G. (2000). Predicting lung cancer by detecting aberrant promoter methylation in sputum. *Cancer Research*, **60**(5), 5954–5958.
- Papadopoulos E., Petraki C., Gregorakis A., Chra E., Fragoulis E., Scorilas A. (2015). L-Dopa decarboxylase mRNA levels provide high diagnostic accuracy and discrimination between

- clear cell and non-clear cell subtypes in renal cell carcinoma. . *Clinical Biochemistry* , **48**: 590-595.
- Park, S. Y., Yi, E. H., Kim, Y., & Park, G. (2019). Anti-neuroinflammatory effects of Ephedra sinica Stapf extract-capped gold nanoparticles in microglia. *International Journal of Nanomedicine*, **14**, 2861–2877.
- Palmirotta, R., Lovero, D., Cafforio, P., Felici, C., Mannavola, F., Pellè, E., Quaresmini, D., Tucci, M., & Silvestris, F. (2018). Liquid biopsy of cancer: A multimodal diagnostic tool in clinical oncology. *Therapeutic Advances in Medical Oncology*, **10**, 175.
- Parker, C. O., Lanyon, Y. H., Manning, M., Arrigan, D. W. M. and Tothill, I. E. (2009). Electrochemical immunochip sensor for aflatoxin M1 detection. *Analytical Chemistry*, **81**(13), 5291-5298.
- Peng, G., Hakim, M., Broza, Y., Billan, S., Abdah-Bortnyak, R., Kuten, A., Haick, H. .. (2010). Detection of lung, breast, colorectal, and prostate cancers from exhaled breath using a single array of nanosensors. *cancer*, **103**:542–551.
- Ponomaryova, A. A., Rykova, E. Y., Cherdyntseva, N. V., Choinzonov, E. L., Laktionov, P. P. and Vlassov, V. (2011). Molecular genetic markers in diagnosis of lung cancer. *Molecular Biology*, **45**(2), 175-189.
- Pragati Malik, S. G. (2013). Quantum dots for diagnosis of cancers. *American Chemical Society*, **4**(11), 811-822.
- Quershi A, Gurbuz Y, Kang W, Davidson JL. (2009). A novel interdigitated capacitor based biosensor for detection of cardiovascular risk marker. *Biosens Bioelectron*, **25**(4), 877-882.
- Radjenovic-Petkovic, T., Pejcic, T., Nastasijević-Borovac, D., Rancic, M., Radojkovic, D., Radojkovic, M. and Djordjevic, I. (2009). Diagnostic value of CEA in pleural fluid for

- differential diagnosis of benign and malign pleural effusion. *Medicinski Arhiv*, **63**(3), 141-142. .
- Rajangam, B., Daniel, D. K., & Krastanov, A. I. (2017). Progress in enzyme inhibition based detection of pesticides. *Engineering in Life Sciences*, **18**(1), 4–19.
- Ramaley, Louis., & Krause, M. S. (1969). Theory of square wave voltammetry. *Analytical Chemistry*, **41**(11), 1362–1365.
- Rao, S. V., Anderson, K. W., & Bachas, L. G. (1998). Oriented immobilization of proteins. *Microchimica Acta*, **128**(3), 127–143.
- Rasooly, A. and Herold, K. (2008). *Biosensors and biodetection: methods and protocols*. New York: Humana Press: 178-188
- Reddy, C., Chilla, D., and Boltax, J. (2011). Lung cancer screening: A review of available data and current guidelines. *Hospital Practice*, **39**: 107–112.
- Redin, E., Garmendia, I., Lozano, T., Serrano, D., Senent, Y., Redrado, M., Villalba, M., De Andrea, C. E., Exposito, F., Ajona, D., Ortiz-Espinosa, S., Ramirez, A., Bertolo, C., Sainz, C., Garcia-Pedrero, J., Pio, R., Lasarte, J., Agorreta, J., Montuenga, L. M., & Calvo, A. (2021). SRC family kinase (SFK) inhibitor dasatinib improves the antitumor activity of anti-PD-1 in NSCLC models by inhibiting Treg cell conversion and proliferation. *Journal for Immunotherapy of Cancer*, **9**(3), e001496.
- Reed, M., Molloy, M., Dalton, E., and Howington, J. (2004). Survival after resection for lung cancer is the outcome that matters. *American journal of surgical*, **188**: 598–602.
- Rodríguez-León, E., Rodríguez-Vázquez, B. E., Martínez-Higuera, A., Rodríguez-Beas, C., Larios-Rodríguez, E., Navarro, R. E., López-Esparza, R., & Iñiguez-Palomares, R. A.

- (2019). Synthesis of Gold Nanoparticles Using Mimosa tenuiflora Extract, Assessments of Cytotoxicity, Cellular Uptake, and Catalysis. *Nanoscale Research Letters*, **14**(1), 334.
- Rong, Q., Feng, F., & Ma, Z. (2016). Metal ions doped chitosan–poly (acrylic acid) nanospheres: Synthesis and their application in simultaneously electrochemical detection of four markers of pancreatic cancer. *Biosensors and Bioelectronics*, **75**, 148–154.
- Ronkainen, N. J., & Okon, S. L. (2014). Nanomaterial-Based Electrochemical Immunosensors for Clinically Significant Biomarkers. *Materials*, **7**(6), 4669–4709.
- Sassolas, A., Blum, L., & Leca-Bouvier, B. (2011). Immobilization strategies to develop enzymatic biosensors. *Biotechnology Advances*, **30**, 489–511.
- Sassolas, A., Blum, L. J. and Leca-Bouvier, B. D. (2012). Immobilization strategies to develop enzymatic biosensors. *Biotechnology Advances*, **30**(3), 489-511.
- Sato Y, Fujimoto K, Kawaguchi H. (2003). Detection of a K-ras point mutation employing peptide nucleic acid at the surface of a SPR biosensor. *Colloids Surface and Biointerfaces*, **27**: 23-31.
- Schramm, W., Paek, S.-H., & Voss, G. (1993a). Strategies for the Immobilization of Antibodies. *ImmunoMethods*, **3**(2), 93–103.
- Schramm, W., Paek, S.-H., & Voss, G. (1993b). Strategies for the Immobilization of Antibodies. *ImmunoMethods*, **3**(2), 93–103.
- Scholz, F. (2015). Voltammetric techniques of analysis: The essentials. *ChemTexts*, **1**(4), 17.
- Schnabel. P and Junker. K. (2015). Pulmonary neuroendocrine tumors in the new WHO 2015 classification. Start of breaking new grounds? *Pathologe*, **36**: 283–292.

- Sengani, M., & V, D. R. (2017). Identification of potential antioxidant indices by biogenic gold nanoparticles in hyperglycemic Wistar rats. *Environmental Toxicology and Pharmacology*, **50**, 11–19.
- Serp, P. (2013). 7.13—Carbon. In J. Reedijk & K. Poeppelmeier (Eds.), *Comprehensive Inorganic Chemistry II (Second Edition)* (pp. 323–369). Elsevier
- Sett, A., Gadewar, M., Sharma, P., Deka, M., & Bora, U. (2016). Green synthesis of gold nanoparticles using aqueous extract of *Dillenia indica*. *Advances in Natural Sciences: Nanoscience and Nanotechnology*, **7**(2), 025005.
- Ševčík, A. (1948). Oscillographic polarography with periodical triangular voltage. *Collection of Czechoslovak Chemical Communications*, **13**, 349–377.
- Sojinrin, T., Liu, K., Wang, K., Cui, D., J. Byrne, H., Curtin, J. F., & Tian, F. (2019). Developing Gold Nanoparticles-Conjugated Aflatoxin B1 Antifungal Strips. *International Journal of Molecular Sciences*, **20**(24), 6260.
- Sung, H., Ferlay, J., Siegel, R. L., Laversanne, M., Soerjomataram, I., Jemal, A., & Bray, F. (2021). Global Cancer Statistics 2020: GLOBOCAN Estimates of Incidence and Mortality Worldwide for 36 Cancers in 185 Countries. *CA: A Cancer Journal for Clinicians*, **71**(3), 209–249.
- Susmel, S., Toniolo, R., Pizzariello, A., Dossi, N., & Bontempelli, G. (2005). A piezoelectric immunosensor based on antibody entrapment within a non-totally rigid polymeric film. *Sensors and Actuators B: Chemical*, **111–112**, 331–338.

- Shahrokhian, S., and Saeed R. (2007). Differential Pulse Voltammetric Determination of Propylthiouracil and Methylthiouracil Using their Catalytic Effects on the Electrochemical Oxidation of Catechol. *Electrochemical science*, **45**(2), 166-7.
- Shah, K. A., Patel, M. B., Patel, R. J., & Parmar, P. K. (2010). *Mangifera Indica* (Mango). *Pharmacognosy Reviews*, **4**(7), 42–48.
- Sharma, R., Hebbal, M., Ankola, A. V., Murugaboopathy, V., & Shetty, S. J. (2014). Effect of Two Herbal Mouthwashes on Gingival Health of School Children. *Journal of Traditional and Complementary Medicine*, **4**(4), 272–278.
- Shen, M., Rusling, J., & Dixit, C. K. (2017). Site-Selective Orientated Immobilization of Antibodies and Conjugates for Immunodiagnostics Development. *Methods (San Diego, Calif.)*, **116**, 95–111.
- Sholl, L. (2015). Biomarkers in lung adenocarcinoma a decade of progress. *Pathology*, **139**: 469–480.
- Simões, F. R., & Xavier, M. G. (2017). 6—Electrochemical Sensors. In A. L. Da Róz, M. Ferreira, F. de Lima Leite, & O. N. Oliveira (Eds.), *Nanoscience and its Applications* (pp. 155–178). William Andrew Publishing.
- Simon, E. (2010). Biological and chemical sensors for cancer diagnosis. *Measurement Science and Technology*, **21**(11), 615-625.
- Simons, B. L., King, M. C., Cyr, T., Hefford, M. A., & Kaplan, H. (2002). Covalent cross-linking of proteins without chemical reagents. *Protein Science: A Publication of the Protein Society*, **11**(6), 1558–1564.
- Soper, S. A., Brown, K., Ellington, A., Frazier, B., Garcia-Manero, G., Gau, V., Gutman, S. I., Hayes, D. F., Korte, B., Landers, J. L., Larson, D., Ligler, F., Majumdar, A., Mascini, M.,

- Nolte, D., Rosenzweig, Z., Wang, J. and Wilson, D. (2006). Point-of-care biosensorsystems for cancer diagnostics/prognostics. *Biosensors and Bioelectronics*, **21**(10), 1932-1942.
- Song, Y., Li, X., Wang, L., Rojanasakul, Y., Castranova, V., Li, H., & Ma, J. (2011). Nanomaterials in Humans: Identification, Characteristics, and Potential Damage. *Toxicologic Pathology*, **39**(5), 841–849.
- Soriano, M. C. H. (2014). *Environmental Risk Assessment of Soil Contamination*. BoD – Books on Demand. 922
- Štěpánková, Š., & Vorčáková, K. (2016). Cholinesterase-based biosensors. *Journal of Enzyme Inhibition and Medicinal Chemistry*, **31**(sup3), 180–193.
- Stamatis, G., Eberhard, W., and Pöttgen, C. (2004). Surgery after multimodality treatment for non-small-cell lung cancer. *Lung Cancer* **45**: 107-112.
- Stieber P., Dienemann H., Hasholzner U., Muller C., Poley S., Hofmann K., Fatehmoghadam A. . (1993). Comparison of cytokeratin fragment 19 (CYFRA 21-1), tissue polypeptide antigen (TPA) and tissue polypeptide specific antigen (TPS) as tumor-markers in lung-cancer. *clinical Biochemistry*, **31**: 689-694.
- Stovold R., Blackhall F., Meredith S., Hou J., Dive C., White A. (2012). Biomarkers for small cell lung cancer: Neuroendocrine, epithelial and circulating tumour cells. *Lung Cancer*, **76**: 263–268.
- Su, F., Xu, C., Taya, M., Murayama, K., Shinohara, Y. and Nishimura, S. I. (2008). Detection of carcinoembryonic antigens using a surface plasmon resonance biosensor. *Sensors*, **8**(7), 4282-4295.

- Sullivan, I., Salazar, J., Arqueros, C., Andrés, M., Sebio, A., Majem, M., . López-Pousa, A. (2017). genetic variant as a prognostic factor for recurrence in resectable non-small cell lung cancer. *Clinical Translation Oncology*, **19**: 884-890.
- Suminami Y., Nawata S., Kato H. (1998). Biological role of SCC antigen. *Tumor Biology*, **19**: 488–493.
- Sun, X., Zhu, Y., & Wang, X. (2011). Amperometric Immunosensor Based on a Protein A/Deposited Gold Nanocrystals Modified Electrode for Carbofuran Detection. *Sensors (Basel, Switzerland)*, **11**(12), 11679–11691.
- Sung, H., Ferlay, J., Siegel, R. L., Laversanne, M., Soerjomataram, I., Jemal, A., & Bray, F. (2021). Global Cancer Statistics 2020: GLOBOCAN Estimates of Incidence and Mortality Worldwide for 36 Cancers in 185 Countries. *CA: A Cancer Journal for Clinicians*, **71**(3), 209–249.
- Sung, H. J. and Cho, J. Y. (2008). Biomarkers for the lung cancer diagnosis and their advances in proteomics. *Biochemistry and Molecular Biology*, **41**(9), 615-625.
- Susana Campuzano, S.; Yáñez-Sedeño, P.; Pingarrón, J. (2017). Electrochemical Genosensing of Circulating Biomarkers. *Sensors*, **17**: 866-870
- Takeda, T., Yamamoto, H., Kanzaki, H., Suzawa, K., Yoshioka, T., Tomida, S., Cui, X., Murali, R., Namba, K., Sato, H., Torigoe, H., Watanabe, M., Shien, K., Soh, J., Asano, H., Tsukuda, K., Kitamura, Y., Miyoshi, S., Sendo, T., & Toyooka, S. (2017). Yes1 signaling mediates the resistance to Trastuzumab/Lapatinib in breast cancer. *PLoS ONE*, **12**(2), e0171356.

- Tang, D., Hou, L., Niessner, R., Xu, M., Gao, Z., & Knopp, D. (2013). Multiplexed electrochemical immunoassay of biomarkers using metal sulfide quantum dot nanolabels and trifunctionalized magnetic beads. *Biosensors and Bioelectronics*, **46**, 37–43.
- Tang J, Huang J, Su B, Chen H, Tang D. (2011). Sandwich-type conductometric immunoassay of alpha-fetoprotein in human serum using carbon nanoparticles as labels. *Biochemical engeneering*, **53**(6), 223-228.
- Tauchi S., Sakai Y., Fujimoto S., Ogawa H., Tane S., Hokka D., Tanaka Y., Nishio W., Yoshimura M., Yanagita E. (2016). Psf3 is a prognostic biomarker in lung adenocarcinoma: A larger trial using tissue microarrays of 864 consecutive resections. *Cardio Thoracic Surgery*, **50**: 758-764.
- Tansil, N. C., Xie, F., Xie, H., & Gao, Z. (2005). An ultrasensitive nucleic acid biosensor based on the catalytic oxidation of guanine by a novel redox threading intercalator. *Chemical Communications (Cambridge, England)*, **8**, 1064–1066.
- Thévenot, D. R., Toth, K., Durst, R. A., & Wilson, G. S. (2001). Electrochemical Biosensors: Recommended Definitions and Classification*. *Analytical Letters*, **34**(5), 635–659.
- Tian, L., Liu, L., Li, Y., Wei, Q., & Cao, W. (2016). Ultrasensitive sandwich-type electrochemical immunosensor based on trimetallic nanocomposite signal amplification strategy for the ultrasensitive detection of CEA. *Scientific Reports*, **6**, 30849.
- Tibor . p., M. K. (2017, August). Carbon Nanomaterial Based Biosensors forNon-Invasive Detection of Cancer and Disease Biomarkers for Clinical Diagnosis. *Sensors*, **17**: 1919-23.
- Tiwari, J.N.; Vij, V.; Kemp, K.C.; Kim, K.S. (2016). Engineered Carbon-Nanomaterial-Based Electrochemical Sensors for Biomolecules. *Nanomaterials* , **10**: 46-80.

- Timur, S., & Telefoncu, A. (2004). Acetylcholinesterase (AChE) Electrodes Based on Gelatin and Chitosan Matrices for the Pesticide Detection. *Artificial Cells, Blood Substitutes, and Biotechnology*, **32**(3), 427–442.
- Tothill, I. E. (2009). Biosensors for cancer markers diagnosis. *Cell and Developmental Biology*, **20**(1), 55-62.
- Tothill, I. E., Heurich, M., Kadir, M. K. A. (2011). An electrochemical sensor based on carboxymethylated dextran modified gold surface for ochratoxin A analysis. *Sensors and Actuators, B: Chemical*, **156**(1), 162-168.
- Travis, W. (2012). Update on small cell carcinoma and its differentiation from squamous cell carcinoma and other non-small cell carcinomas. *Mod. Pathology*, **25**: 18–30.
- Tripathi, K.M.; Kim, T.Y.; Losic, D.; Tung, T. (2016). Recent advances in engineered graphene and composites for detection of volatile organic compounds (VOCs) and non-invasive diseases diagnosis. *Carbon*, **110**: 97–129.
- Triroj N, Jaroenapibal P, Shi H, Yeh JI, Beresford R. (2011). Microfluidic chip-based nanoelectrode array as miniaturized biochemical sensing platform for prostate specific antigen detection. *Biosensors and Bioelectronics*, **26**(6), 2927-2933.
- Turner, A., Karube, I., & Wilson, G. S. (1987). *Biosensors: Fundamentals and Applications*. Oxford University Press. <http://urn.kb.se/resolve?urn=urn:nbn:se:liu:diva-720>
- Uehara, N. (2010). Polymer-functionalized gold nanoparticles as versatile sensing materials. *Analytical Sciences: The International Journal of the Japan Society for Analytical Chemistry*, **26**(12), 1219–1228.
- Van der Linden, W. E., & Dieker, J. W. (1980). Glassy carbon as electrode material in electro-analytical chemistry. *Analytica Chimica Acta*, **119**(1), 1–24.

- Vazquez M., Koizurni J., Henschke C., Yankelevitz D. (2007). Reliability of cytologic diagnosis of early lung cancer. *Cancer Cytopathology*, **111**: 252–258.
- Velusamy, V., Arshak, K., Korostynska, O., Oliwa, K., & Adley, C. (2009). An overview of foodborne pathogen detection: In the perspective of biosensors. *Biotechnology Advances*, **28**, 232–254.
- Wambalaba, F. W., Son, B., Wambalaba, A. E., Nyong'o, D., & Nyong'o, A. (2019). Prevalence and Capacity of Cancer Diagnostics and Treatment: A Demand and Supply Survey of Health-Care Facilities in Kenya. *Cancer Control : Journal of the Moffitt Cancer Center*, **26**(1), 1073274819886930.
- Wang, D., Gan, N., Zhang, H., Li, T., Qiao, L., Cao, Y., Su, X., & Jiang, S. (2015). Simultaneous electrochemical immunoassay using graphene–Au grafted recombinant apoferritin-encoded metallic labels as signal tags and dual-template magnetic molecular imprinted polymer as capture probes. *Biosensors and Bioelectronics*, **65**, 78–82.
- Wang, D., Gan, N., Zhou, J., Xiong, P., Cao, Y., Li, T., Pan, D., & Jiang, S. (2014). Signal amplification for multianalyte electrochemical immunoassay with bidirectional stripping voltammetry using metal-enriched polymer nanolabels. *Sensors and Actuators B: Chemical*, **197**, 244–253.
- Wang, D., Li, T., Gan, N., Zhang, H., Long, N., Hu, F., Cao, Y., Jiang, Q., & Jiang, S. (2015). Electrochemical coding for multiplexed immunoassays of biomarkers based on bio-based polymer-nanotags. *Electrochimica Acta*, **163**, 238–245.

- Wang, G., Qing, Y., Shan, J., Jin, F., Yuan, R., & Wang, D. (2013). Cation-exchange antibody labeling for simultaneous electrochemical detection of tumor markers CA15-3 and CA19-9. *Microchimica Acta*, **180**(7), 651–657.
- Wang, Z., Liu, N., Feng, F., & Ma, Z. (2015). Synthesis of cadmium, lead and copper alginate nanobeads as immunosensing probes for the detection of AFP, CEA and PSA. *Biosensors and Bioelectronics*, **70**, 98–105.
- Wang, Z., Liu, N., & Ma, Z. (2014). Platinum porous nanoparticles hybrid with metal ions as probes for simultaneous detection of multiplex cancer biomarkers. *Biosensors and Bioelectronics*, **53**, 324–329.
- Wang J., Yi Y., Li B., Wang Z., Sun H., Zhang P., Huang W. (2010). CYFRA 21-1 can predict the sensitivity to chemoradiotherapy of non-small-cell lung carcinoma. *Biomarkers*, **15**: 594–601.
- Wang L, Xiong Q, Xiao F, Duan H . (2017). 2D nanomaterials based electrochemical biosensors for cancer diagnosis. *Biosensors and Bioelectronics*, **89**(1), 136-151.
- Wang, J. (1999). Electrochemical biosensors. *Analytical chemistry*, **19**: 47-53.
- Wang, J. (2006). *Analytical electrochemistry* (3rd ed.). New York: Wiley: 1890-1899
- Wang, J. (2006a). Electrochemical biosensors: towards point-of-care cancer diagnostics. *Biosensors and Bioelectronics*, **21**(10), 1887-1892.
- Wang, L. (2017). Early Diagnosis of Breast Cancer. *Sensor*, **17**: 1572-1578
- Watt I, Stewart I, Anderson D, Bell G, Anderson JR. (1989). Laparoscopy, ultrasound and computed tomography in cancer of the oesophagus and gastric cardia: a prospective comparison for detecting intra-abdominal metastases. *British Journal of Surgery*, **76**(2), 1036–1039.

- Wang, J., Wang, L., Di, J., & Tu, Y. (2008). Disposable biosensor based on immobilization of glucose oxidase at gold nanoparticles electrodeposited on indium tin oxide electrode. *Sensors and Actuators B: Chemical*, **135**(1), 283–288.
- Wang, Y., Deng, J., Di, J., & Tu, Y. (2009). Electrodeposition of large size gold nanoparticles on indium tin oxide glass and application as refractive index sensor. *Electrochemistry Communications*, **11**(5), 1034–1037.
- Wang, Y., Wu, X., Sun, J., Wang, C., Zhu, G., Bai, L.-P., Jiang, Z.-H., & Zhang, W. (2022). Stripping voltammetric determination of cadmium and lead ions based on a bismuth oxide surface-decorated nanoporous bismuth electrode. *Electrochemistry Communications*, **136**, 107233.
- Wei Q, Mao K, Wu D, Dai Y, Yang J. (2010). A novel label-free electrochemical immunosensor based on graphene and thionine nanocomposite. *Sensors Actuators B: Chem*, **149**(5), 314-318.
- Weynants P., H. (1990). Biology of small-cell lung-cancer. *Eur. Respir.*, **3**, 699–714.
- Widjoatmodjo, M., Fluit, A., Torensma, R., Verdonk, G., and Verhoef, J. (1992). The magnetic immuno polymerase chain reaction assay for direct detection of salmonellae in fecal samples. *Clinical Microbiology*, **30**: 3195–3199.
- Wilson, M. (2005). Electrochemical Immunosensors for the Simultaneous Detection of Two Tumor Markers. *Analytical Chemistry*, **77**, 1496–1502.
- Woolner LB, McDonald JR. (1952). Biopsy in cancer diagnosis. *Plastic Reconstruction Surgery*., **9**(6), 388- 389.

- Xin Lee, K., Shameli, K., Miyake, M., Kuwano, N., Bt Ahmad Khairudin, N. B., Bt Mohamad, S. E., & Yew, Y. P. (2016). Green Synthesis of Gold Nanoparticles Using Aqueous Extract of *Garcinia mangostana* Fruit Peels. *Journal of Nanomaterials*, **2016**, e8489094.
- Xu, T., Jia, X., Chen, X., & Ma, Z. (2014). Simultaneous electrochemical detection of multiple tumor markers using metal ions tagged immunocolloidal gold. *Biosensors and Bioelectronics*, **56**, 174–179.
- Xu, T., Liu, N., Yuan, J., & Ma, Z. (2015). Triple tumor markers assay based on carbon–gold nanocomposite. *Biosensors and Bioelectronics*, **70**, 161–166.
- Yang, Z.-H., Zhuo, Y., Chai, Y.-Q., & Yuan, R. (2014). High throughput immunosensor based on multi-label strategy and a novel array electrode. *Scientific Reports*, **4**(1), 4747.
- Ye, J., Liu, H., Xu, Z., Zheng, L., & Liu, R. (2019). Identification of a multidimensional transcriptome prognostic signature for lung adenocarcinoma. *Journal of Clinical Laboratory Analysis*, **33**(9), e22990.
- Yu Z., Chen X., Cui L., Si H., Lu H., Liu S. (2014). Prediction of lung cancer based on serum biomarkers by gene expression programming methods. *Asian Pac. Cancer Preview*, **15**: 9367–9373.
- Yu, H., Yan, F., Dai, Z., & Ju, H. (2004). A disposable amperometric immunosensor for α -1-fetoprotein based on enzyme-labeled antibody/chitosan-membrane-modified screen-printed carbon electrode. *Analytical Biochemistry*, **331**(1), 98–105.
- Yuan, Y. R., Yuan, R., Chai, Y. Q., Zhuo, Y. and Miao, X. M. (2009). Electrochemical amperometric immunoassay for carcinoembryonic antigen based on bi-layer nano-Au and nickel hexacyanoferrates nanoparticles modified glassy carbon electrode. *Electroanalytical Chemistry*, **626** (1-2), 6-13.

- Yoshinobu, T., Iwasaki, H., Ui, Y., Furuichi, K., Ermolenko, Yu., Mourzina, Yu., Wagner, T., Näther, N., & Schöning, M. J. (2005). The light-addressable potentiometric sensor for multi-ion sensing and imaging. *Methods*, **37**(1), 94–102.
- You, C.-C., Arvizo, R. R., & Rotello, V. M. (2006). Regulation of alpha-chymotrypsin activity on the surface of substrate-functionalized gold nanoparticles. *Chemical Communications (Cambridge, England)*, **27**, 2905–2907.
- Zamay G., Kolovskaya O., Zamay T., Glazyrin Y., Krat A., Zubkova O., Spivak E., Wehbe M., Gargaun A., Muharemagic D. (2015). Aptamers selected to postoperative lung adenocarcinoma detect circulating tumor cells in human blood. *Molecular Therapy*, **23**: 1486-1496.
- Zamay G.S., Ivanchenko T., Zamay T.N., Grigorieva V.L., Glazyrin Y.E., Kolovskaya O.S., Garanzha I., Barinov A., Krat A.V., Mironov G. (2016). DNA-aptamers for characterization of histological structure of lung adenocarcinoma. *Molecular Therapy Nucleic Acid*, **6**(10), 150-162.
- Zhang, G.; Xiaobo, M.A.; Liyi, H.U.; Zang, J.; Zhang, G.; Qinglei, X.U. (2013). The application significance of serum cyfra21-1 change in therapeutic efficacy monitoring of advanced stage NSCLC. *Biomedical*, **28**: 124–127.
- Zhang, Y.; Yang, D.; Weng, L.; Wang, L. (2013). Early lung cancer diagnosis by biosensors. *Internatinal Journal of Molecular Science*, **14**: 15479–15509.
- Zhang, X., Ren, X., Cao, W., Li, Y., Du, B., & Wei, Q. (2014). Simultaneous electrochemical immunosensor based on water-soluble polythiophene derivative and functionalized magnetic material. *Analytica Chimica Acta*, **845**, 85–91.

- Zhang, Y., Li, L., Lu, J., Ge, L., Ge, S., Yan, M., Song, X., & Yu, J. (2013). Triple catalysis amplification strategy for simultaneous multiplexed electrochemical immunoassays based on cactus-like MnO₂ functionalized nanoporous gold. *Sensors and Actuators B: Chemical*, **186**, 545–549.
- Zhao, Y., Wu, Y., Zhang, Y., Chen, Z., Cao, X., Di, J., & Yang, J. (2009). Electrocatalytic Behavior and Amperometric Detection of Morphine on ITO Electrode Modified with Directly Electrodeposited Gold Nanoparticles. *Electroanalysis*, **21**(8), 939–943.
- Zhu, Q., Chai, Y., Zhuo, Y., & Yuan, R. (2015). Ultrasensitive simultaneous detection of four biomarkers based on hybridization chain reaction and biotin–streptavidin signal amplification strategy. *Biosensors and Bioelectronics*, **68**, 42–48.
- Zhuo, Y., Yuan, P.-X., Yuan, R., Chai, Y.-Q., & Hong, C.-L. (2008). Nanostructured conductive material containing ferrocenyl for reagentless amperometric immunosensors. *Biomaterials*, **29**(10), 1501–1508.
- Zhong, L., Coe, S., Stromberg, A., Khattar, N., Jett, J., and Hirschowitz, E. (2006). Profiling tumor-associated antibodies for early detection of non-small cell lung cancer. *Thoracic Oncology*, **1**: 513–519.
- Zhong, Z., Peng, N., Qing, Y., Shan, J., Li, M., Guan, W., Dai, N., Gu, X., & Wang, D. (2011). An electrochemical immunosensor for simultaneous multiplexed detection of neuron-specific enolase and pro-gastrin-releasing peptide using liposomes as enhancer. *Electrochimica Acta*, **56**(16), 5624–5629.
- Zhou, S., Wang, Y., & Zhu, J.-J. (2016). Simultaneous Detection of Tumor Cell Apoptosis Regulators Bcl-2 and Bax through a Dual-Signal-Marked Electrochemical Immunosensor. *ACS Applied Materials & Interfaces*, **8**(12), 7674–7682.

Zhu, Q., Chai, Y., Yuan, R., Zhuo, Y., Han, J., Li, Y., & Liao, N. (2013). Amperometric immunosensor for simultaneous detection of three analytes in one interface using dual functionalized graphene sheets integrated with redox-probes as tracer matrixes. *Biosensors and Bioelectronics*, **43**, 440–445.

Internet sources

KEMRI. (2016). *mercystepsprogram.org*. Retrieved 2016, from www.mercystepsprogram.org/english/cancer_sit_kenya.html

Rooprai, P. J., HOPE CRAIG, CHANDRAKANTH ARE, Gurpreet. (2021.). *Cancer on the Global Stage: Incidence and Cancer-Related Mortality in Kenya - The ASCO Post*. Retrieved December 18, 2022, from <https://ascopost.com/issues/february-25-2021/cancer-on-the-global-stage-incidence-and-cancer-related-mortality-in-kenya/>

World Health Organization. (2017, September 22). *Cancer Fact Sheet*. Retrieved from <http://www.who.int/mediacentre/factsheets/fs297/en/>.

World Health Organization. (2018, February 1). *Key facts about cancer*. Retrieved from <http://www.who.int/en/news-room/fact-sheets/detail/cancer>.

Administrator. (2013, November 14). *Linear Sweep and Cyclic Voltametry: The Principles* <https://www.ceb.cam.ac.uk/research/groups/rg-eme/Edu/linear-sweep-and-cyclic-voltametry-the-principles>

Vimalraj, S., Ashokkumar, T., & Saravanan, S. (2018). Biogenic gold nanoparticles synthesis mediated by *Mangifera indica* seed aqueous extracts exhibits antibacterial, anticancer and anti-angiogenic properties. *Biomedicine & Pharmacotherapy = Biomedecine & Pharmacotherapie*. <https://doi.org/10.1016/j.biopha.2018.05.151>

APPENDICES

APPENDIX 1: BUFFERS USED

RIPA (Radio immunoprecipitation Assay) lysis buffer

150 mM NaCl

1% NP-40 or Triton X-100

0.5% sodium deoxycholate

0.1% SDS

50 mM Tris, pH 8.0

Tris-HCl

20 mM Tris-Hcl, pH 7.5

1X PBS

137 mM NaCl

2.7 mM KCl

4.3 mM Na₂HPO₄

1.47 mM KH₂PO₄

Adjust pH to 7.4

2X Laemmli loading Buffer

4% SDS

5% β-mercaptoethanol or 100 mM DTT

20% glycerol

0.004% bromophenol blue

0.125 M Tris HCl, pH 6.8

Running Buffer (X1 mops)

25 mM Tris base

192 mM glycine

0.1% SDS

Adjust to pH 8.3

1X Transfer Buffer (wet)

25 mM Tris base

192 mM glycine

20 % methanol

Adjust to pH to 8.3

1X TBST (Tris-buffered saline, 0.1% Tween)

20 mM Tris base

150 mM NaCl

0.1% Tween-20

APPENDIX 2:PROTOCOL FOR PROTEIN QUANTIFICATION

The dilution Table is as shown below.

BSA stock of 2mg/ml

Concentration (ug/ml)	BSA (KIT) uL	Dilutant (H ₂ O/PBS)
2000	50	0
1500	37.5	12.5
1000	25	25
750	18.75	31.25
500	12.5	37.5
250	6.25	43.75
125	3.125	
0	0	

In 96 well plate put 10 ul of samples

Do in triplicate

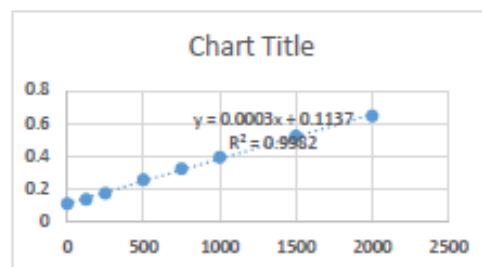
Prepare reagent A and B as (Prepared in ratio 50:1)

Incubate for 30 minutes at 37 °c and read the absorbance at 562nm

APPENDIX 3: PROTEIN QUANTIFICATION RESULTS

User: USER												
Path: C:\Program Files (x86)\BMG\SPECTROstar Nano\User\Data\												
Test ID: 14153												
Test Name: Lk supas n lysates												
Date: 24/03/2022												
Time: 10:57:55												
ID1: LK supas n lysates												
Absorbance	Absorbance values are displayed as OD											
Raw Data (590)												
	1	2	3	4	5	6	7	8	9	10	11	12
A	0.652	0.527	0.406	0.331	0.264	0.173	0.138	0.11	0.05	0.051	0.051	0.052
B	0.642	0.521	0.393	0.32	0.253	0.178	0.135	0.106	0.051	0.05	0.053	0.047
C	0.639	0.518	0.381	0.319	0.256	0.37	0.141	0.119	0.054	0.052	0.053	0.054
D	0.194	0.267	0.219	0.2	0.132	0.291	0.195	0.272	0.05	0.064	0.049	0.058
E	0.188	0.289	0.178	0.202	0.134	0.296	0.198	0.276	0.055	0.055	0.055	0.054
F	0.191	0.295	0.18	0.2	0.134	0.289	0.198	0.272	0.054	0.05	0.051	0.05
G	0.05	0.052	0.052	0.055	0.053	0.055	0.053	0.05	0.1	0.053	0.055	0.047
H	0.048	0.055	0.054	0.053	0.051	0.052	0.05	0.064	0.071	0.071	0.057	0.049
	calibration											
	2000	1500	1000	750	500	250	125	0				
	0.652	0.527	0.406	0.331	0.264	0.173	0.138	0.11				
	0.642	0.521	0.393	0.32	0.253	0.178	0.135	0.106				
	0.639	0.518	0.381	0.319	0.256		0.141	0.119				
Abs	0.64433333	0.522	0.39333333	0.32333333	0.25766667	0.1755	0.138	0.11166667				

		0	0.11166667
		125	0.138
		250	0.1755
		500	0.25766667
		750	0.32333333
		1000	0.39333333
		1500	0.522
		2000	0.64433333

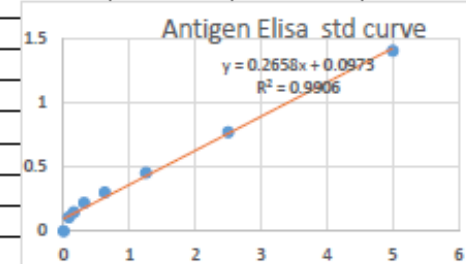


	supernatants				lysates				
	H2009	A549	H23	H2170	H2009	A549	H23	H2170	
	0.194	0.267	0.219	0.2	0.132	0.291	0.195	0.272	
	0.188	0.289	0.178	0.202	0.134	0.296	0.198	0.276	
	0.191	0.295	0.18	0.2	0.134	0.289	0.198	0.272	
AV	0.191	0.28366667	0.19233333	0.20066667	0.13333333	0.292	0.197	0.27333333	
CONC	257.666667	566.555556	262.111111	289.888889	65.444444	594.333333	277.666667	532.111111	
DIL *10	2576.66667	5665.55556	2621.11111	2898.88889	654.44444	5943.33333	2776.66667	5321.11111	mg/ml
30mg/ml	11.6429495	5.29515591	11.4455278	10.3487926	45.8404075	5.04767246	10.8043217	5.63792023	
50mg/ml	19.4049159	8.82525985	19.0758796	17.2479877	76.4006791	8.41278744	18.0072029	9.39653372	
60	23.2858991	10.5903118	22.8910555	20.6975853	91.6808149	10.0953449	21.6086435	11.2758405	
	Western blotting Loading sample preparation								
				B-mercaptoethanol					
Sample	protein	water	LSD		TV				
H2009 SFM	11.64	12.86	4	1.5	30				
A549 SFM	5.3	19.2	4	1.5	30				
H23 SFM	11.45	13.05	4	1.5	30				
H2170 SFM	10.35	14.15	4	1.5	30				
H2009 LYS	24.5	0	4	1.5	30				
A549S LYS	5.05	19.45	4	1.5	30				
H23 LYS	10.8	13.7	4	1.5	30				
2170 LYS	5.64	18.86	4	1.5	30				

APPENDIX 4: ELISA DATA AND STANDARD CURVE

User: USER											
Path: C:\Program Files (x86)\BMG\SPECTROstar Nano\User\Data\											
Test ID: 14434											
Test Name: 450 Elisa Lucy K											
Date: 08/04/2022											
Time: 16:00:06											
ID1: Elisa											
Absorbance	Absorbance values are displayed as OD										
	Raw Data (450)										
	1	2	3	4	5	6	7	8	9	10	11
A	0.061	0.04	1.455	1.449	0.046	0.045	0.047	0.046	0.048	0.047	0.047
B	0.376	0.345	0.803	0.834	0.044	0.045	0.046	0.049	0.053	0.047	0.066
C	0.263	0.236	0.501	0.502	0.047	0.044	0.046	0.046	0.047	0.048	0.047
D	0.287	0.295	0.368	0.328	0.071	0.046	0.043	0.045	0.045	0.046	0.046
E	0.273	0.292	0.273	0.261	0.059	0.146	0.049	0.05	0.047	0.046	0.048
F	0.049	0.049	0.195	0.192	0.051	0.05	0.047	0.045	0.074	0.05	0.049
G	0.048	0.048	0.152	0.155	0.089	0.069	0.048	0.045	0.048	0.047	0.048
H	0.049	0.049	0.045	0.046	0.054	0.05	0.046	0.047	0.045	0.047	0.046
	Average blank	0.0455	(values blank subtracted)								
			standards								
	0.0155	-0.0055	1.4095	1.4035	0.0005	-0.0005	0.0015	0.0005	0.0025	0.0015	0.0015
	0.3305	0.2995	0.7575	0.7885	-0.0015	-0.0005	0.0005	0.0035	0.0075	0.0015	0.0205
samples	0.2175	0.1905	0.4555	0.4565	0.0015	-0.0015	0.0005	0.0005	0.0015	0.0025	0.0015
	0.2415	0.2495	0.3225	0.2825	0.0255	0.0005	-0.0025	-0.0005	-0.0005	0.0005	0.0005
	0.2275	0.2465	0.2275	0.2155	0.0135	0.1005	0.0035	0.0045	0.0015	0.0005	0.0025
	0.0035	0.0035	0.1495	0.1465	0.0055	0.0045	0.0015	-0.0005	0.0285	0.0045	0.0035
	0.0025	0.0025	0.1065	0.1095	0.0435	0.0235	0.0025	-0.0005	0.0025	0.0015	0.0025
	0.0035	0.0035	-0.0005	0.0005	0.0085	0.0045	0.0005	0.0015	-0.0005	0.0015	0.0005

conc (ng/mL)			avg		conc	ABS			
5	1.4095	1.4035	1.4065		5	1.4065			
2.5	0.7575	0.7885	0.773		2.5	0.773			
1.25	0.4555	0.4565	0.456		1.25	0.456			
0.625	0.3225	0.2825	0.3025		0.625	0.3025			
0.3125	0.2275	0.2155	0.2215		0.3125	0.2215			
0.15625	0.1495	0.1465	0.148		0.15625	0.148			
0.078125	0.1065	0.1095	0.108		0.078125	0.108			
0	-0.0005	0.0005	0		0	0			
			avg						
samples 1	0.3305	0.2995	0.315						
2	0.2175	0.1905	0.204						
3	0.2415	0.2495	0.2455						
4	0.2275	0.2465	0.237						
									Concentration
	concentration of the samples	ng/mL	*50 (dil factor)ng/mL in the sample						
	1	0.315	0.81903687	40.9518435					
	2	0.204	0.40142965	20.0714823			LOD	0.56489842	
	3	0.2455	0.55756208	27.8781038			LOQ		
	4	0.237	0.52558315	26.2791573					



APPENDIX 5: REPRODUCIBILITY OF CEA AND YES1 DIFFERENT ELECTRODES

	1st plot	2nd plot	3rd plot	AV	SD	
Electrode 1	0.000148	0.000148	0.000148	0.000148	9.5394E-08	9.539E-06
Electrode2	0.000148	0.000148	0.000148	0.000148	5.0332E-08	5.0332E-06
Electrode3	0.000148	0.000148	0.000148	0.000148	9.4516E-08	9.4516E-06
Electrode 4	0.000147	0.000147	0.000148	0.000147	9.5044E-08	9.5044E-06
mean of all				0.000148	2.7858E-07	
				RSD	0.188417166	RSD= (S/ab
					0.19	

APPENDIX 6: REPRODUCIBILITY OF CEA AND YES1 SAME ELECTRODES

	1st plot	2nd plot	3rd plot	avg	sdv	RSD
1	0.0000477	0.0000475	0.0000479	4.77E-05	2E-07	0.419287
2	0.0000477	0.0000479	0.0000477	4.78E-05	1.15E-07	0.241738
3	0.0000475	0.0000475	0.0000478	4.76E-05	1.73E-07	0.363876
4	0.0000465	0.0000463	0.0000464	4.64E-05	1E-07	0.215517
5	0.0000476	0.0000479	0.0000477	4.77E-05	1.53E-07	0.320012
6	0.0000476	0.0000477	0.000047	4.74E-05	3.79E-07	0.79816
total mean				4.74E-05	5.23E-07	1.10245

APPENDIX 7: STABILITY OF CEA AND YES1

	1st plot	2nd plot	3rd plot	avg	sdv	RSD
Day 1	50.16	50.06	50.92	50.38	0.470319	0.933543
Day 2	49.16	49.88	50.05	49.69667	0.472476	0.950719
Day 3	48.45	48.14	48.84	48.47667	0.350761	0.723567
15th day	47.91	48.18	47.95	48.01333	0.145717	0.303492
total mean				49.14167	1.088861	2.215759 RSD 2.2%